Chelating phosphine complexes of ruthenium for the co-ordination and activation of small molecules

Ledger, Araminta

Award date:
2011

Awarding institution:
University of Bath

CHELATING PHOSPHINE COMPLEXES OF RUTHENIUM FOR THE COORDINATION AND ACTIVATION OF SMALL MOLECULES

Araminta Elizabeth Walton Ledger

A thesis submitted in partial fulfilment of the requirements for the degree of

Doctor of Philosophy

University of Bath

Department of Chemistry

April 2011

CONTENTS

ACKNOWLEDGEMENTS

There are a number of people that I would like to thank now that this PhD is finally finished. First on the list is Dr Mike Whittlesey, the one and only beard-of-wisdom and supervisor extraordinaire for all his help and advice over the last five years. He has answered far more than his fair share of questions, and broadened my musical knowledge no end.*

I would also like to thank Prof. Jon Williams for his valuable advice and supervision, as well as forming an integral part of Team Samarium. Thanks also to Dr John Lowe for all the NMR support and for patiently enduring my badgering, and to Dr Mary Mahon for all the X-ray crystallography – here I should also thank Charlie 'Crystal-Fingers' Ellul.

A number of external collaborators have contributed to the work contained in this thesis. These include Prof. Paul Pregosin for various $^{15}N_2$ labelled NMR experiments, Prof. Bob Morris for valuable discussions, and Prof. Piet van Leeuwen for the donation of a number of xanthene ligands.

In particular, a series of post-docs have helped to make the last few years thoroughly enjoyable. These include Dr Paul Slatford and Dr Suz Burling who both had the dubious pleasure of seeing me through my MChem project, Dr Tracy 'the Beaker' Nixon for acting as my organic guru, our token Australian, Dr Mike Page, or Baron Pagius as he likes to be known, and of course Dr Elena Mas-Marzá for providing her very own Spanish soundtrack to my PhD.

I would also like to thank my labmates and friends for some great times: Steve Reade, Olly Saker, Sarah Chatwin, Tom Martin, Charlie Ellul, Lucy Hackshaw, Keely Gunson, Caroline Davies and Nicola Bramananthan (and now Becs Poulten to carry the Whittlesey flag!). This PhD has been brought to you by the magical liopleurodon, cheeky Thursdays, the Pointer Sisters, unhealthy amounts of Gray's Anatomy, Mussolini, BOTTY time, the Rue de Soif and, of course, the big C.

Thanks must also go to my parents for their continuing love, support and encouragement. I'm afraid I still won't be able to keep you in the manner to which you'd like to become accustomed though! Thanks also to the Chamorro family for adopting me into their particular brand of madness, and finally to Alex Chamorro, master of the catchphrase (and Photoshop!) and most definitely plural; here's to you for putting up with me and being generally wonderful.

* An interesting debate: Should Metallica be classed as music?

ABSTRACT

This thesis describes the development of ruthenium(P-P) and ruthenium(POP) complexes for the coordination and activation of small molecules, and examines their catalytic applications. The catalytic behaviour of both [Ru(xantphos)(PPh_3)(CO)H_2] (**2**) and [Ru(dppp)(PPh_3)(CO)H_2] (**3**) in the Knoevenagel reaction was investigated by stoichiometric reaction of each complex with benzyl alcohol. Whilst **3** demonstrates no activity, **2** is shown to decarbonylate a range of primary alcohols to generate [Ru(xantphos)$(CO)_2H_2$] (**4**), [Ru(xantphos)(PPh_3)$(CO)_2$] (**5**) and [Ru(xantphos)$(CO)_3$] (**6**), all of which are less catalytically active than **2** for Knoevenagel chemistry.

Reaction of **2** with various NHC ligands (NHC = N-heterocyclic carbene) resulted in a series of [Ru(xantphos)(NHC)'(CO)H] complexes (NHC = IEt_2Me_2 (**8**), $I^iPr_2Me_2$ (**9**) and IMes (**10**)), all of which exhibited spontaneous C-H activation of the carbene N-substituents. The synthesis and subsequent treatment of [Ru(xantphos)(ICy)(CO)H_2] (**12**) with the hydrogen acceptor, $H_2C{=}CH_2SiMe_3$, was able to induce C-H activation in the normally inert ICy ligand, resulting in formation of [Ru(xantphos)(ICy)'(CO)H] (**13**). Complexes **8-10** and **13** were found to be less catalytically active for Knoevenagel chemistry than [Ru(xantphos)(PPh_3)(CO)H_2] (**2**). [Ru(xantphos)(IEt_2Me_2)(CO)H_2] (**11**) and **12** were investigated as potential precatalysts for the hydrodefluorination (HDF) of C_6F_6, but proved catalytically inactive since intramolecular C-H activation was preferred over intermolecular C-F activation. Substitution of the xantphos ligand for the ferrocenyl diphosphine ligand dppf resulted in the synthesis of [Ru(dppf)(ICy)(CO)H_2] (**21**) and [Ru(dppf)(ICy)(CO)HF] (**22**), but these complexes also proved ineffective for catalytic HDF.

The reaction between [Ru$(PPh_3)_3$HCl] (**23**) and the chelating POP ligands, xantphos, DPEphos and $(Ph_2CH_2CH_2)_2O$ resulted in the formation of [Ru(POP)(PPh_3)HCl] precursors (**24a-c**) which all exhibited tridentate coordination of the POP ligand. Abstraction of the chloride ligand with $NaBAr_4^F$ or AgOTf formed the cationic complexes $[Ru(POP)(PPh_3)(OH_2)H]^+$ (**25a-c**). These all possessed a highly labile H_2O ligand, which could be readily displaced by O_2, N_2 or H_2. Contrasting reactivity was demonstrated by [Ru(dppf)(PPh_3)HCl] (**31**) which formed an unusual η^6-aryl phosphine complex, [Ru(dppf)($\{\eta^6$-$C_6H_5\}PPh_2$)H]BAr_4^F (**32**) on chloride abstraction.

The reactivity of **25a** towards a range of amine-boranes was investigated, and resulted in the synthesis and characterisation of the η^1-H-B coordinated complexes [Ru(xantphos)(PPh_3)($H_3B{\cdot}N^tBuH_2$)H]BAr_4^F (**35**) and [Ru(xantphos)(PPh_3)($H_3B{\cdot}NH_3$)H]BPh_4 (**38**). In contrast, reaction of **25a** with the phosphine-borane, $H_3B{\cdot}PPh_2H$, led to P-B cleavage to afford a *bis* secondary phosphine complex [Ru(xantphos)$(PPh_2H)_2$H]BAr_4^F (**41**) as the ultimate product of the reaction. The ruthenium-xantphos complexes **24a**, **25a**, **38** and **41** proved inactive for the

catalytic dehydrocoupling of $H_3B{\cdot}NMe_2H$, whereas the ruthenium-dppf complexes **31** and **32** were able to catalyse the dehydrogenation of $H_3B{\cdot}NMe_2H$ to form the dimeric species $[H_2B\text{-}NMe_2]_2$. Treatment of [Ru(dppf)(PPh_3)HCl] (**31**) with the NHC ligands ICy and IAd generated [Ru(dppf)(ICy)HCl] (**43**), a highly active catalyst for the dehydrocoupling of $H_3B{\cdot}NMe_2H$ (TOF = 75 h^{-1}), and [Ru(dppf)(IAd)HCl] (**44**), which proved to be catalytically inactive.

ABBREVIATIONS – SPECTROSCOPIC

ap	Apical
ax	Axial
br	Broad
COSY	Correlation Spectroscopy
d	Doublet
δ	NMR chemical shift
DFT	Density Functional Theory
ESI-TOF MS	Electrospray Ionisation-Time of Flight Mass Spectrometry
eq	Equatorial
EXSY	Exchange Spectroscopy
HMBC	Heteronuclear Multiple Bond Correlation
HMQC	Heteronuclear Multiple Quantum Coherence
HSQC	Heteronuclear Single Quantum Coherence
IR	Infrared
$^{x}J_{YZ}$	Coupling constant of Y to Z across x bonds
m	Multiplet
NMR	Nuclear Magnetic Resonance Spectroscopy
q	Quartet
quin	Quintet
s	Singlet
sept	Septet
t	Triplet
ν(XY)	IR shift of XY bond
VT	Variable Temperature

ABBREVIATIONS – UNITS

atm.	Atmosphere
cm^{-1}	Wavenumber
eq.	Equivalents
g	Gram
h	Hour(s)
Hz	Hertz

K	Kelvin
kcal	Kilocalorie
kJ	Kilojoule
mg	Milligram
MHz	MegaHertz
min	Minute(s)
mL	Millilitre
mmol	Millimole
mol	Mole
ms	Milliseconds
ppm	Parts per million
s	Second(s)
Å	Angström
µL	Microlitre

ABBREVIATIONS – CHEMICAL

Ar	Aryl group
Arphos	1-diphenylphosphino-2-diphenylarsinoethane
BAr_4^F	$B(3,5\text{-}C_6H_3(CF_3)_2)_4$
Bn	Benzyl group (CH_2Ph)
COD	Cycloocta-1,5-diene
COE	Cyclooctene
Cp	Cyclopentadienyl
Cp*	1,2,3,4,5-pentamethylcyclopentadienyl
Cy	Cyclohexyl
Cyp	Cyclopentene
DPEphos	(Oxydi-2,1-phenylene)*bis*-(diphenylphosphine)
dppf	1,1'-*bis*(diphenylphosphino)ferrocene
dppp	1,3-*bis*(diphenylphosphino)propane
IAd	1,3-*bis*(1-adamantyl)imidazol-2-ylidene
ICy	1,3-dicyclohexylimidazol-2-ylidene
IEt_2Me_2	1,3-diethyl-4,5-dimethylimidazol-2-ylidene
I^iPr_2Me2	1,3-diisopropyl-4,5-dimethylimidazol-2-ylidene
IMe_4	1,3,4,5-tetramethylimidazol-2-ylidene

IMes	1,3-*bis*(2,4,6-trimethylphenyl)imidazol-2-ylidene
IPr	1,3-*bis*(2,6-diisopropylphenyl)imidazol-2-ylidene
I^{t}Bu	1,3-*bis*(*tert*-butyl)imidazol-2-ylidene
i-	*Ipso*
L	Ligand
(L)'	Denotes a C-H activated ligand with M-C coordination
m-	*Meta*
NHC	N-heterocyclic carbene
o-	*Ortho*
OTf	Triflate (O_3SCF_3)
p-	*Para*
PipOAc	Piperidinium acetate
Py	Pyridene
R	Alkyl or aryl group
SIMes	1,3-*bis*(2,4,6-trimethylphenyl)imidazolin-2-ylidene
TOF	Turnover frequency (TON / h)
TON	Turnover number (moles of product / moles of catalyst)
X	Halide or heteroatom
Xantphos	4,5-bis(diphenylphosphino)-9,9-dimethylxanthene
μ-L	Bridging ligand
η^{n}-L	Ligand hapticity (of number, n)
3c-2e	3 centre-2 electron

1. CHAPTER 1

1.1 Bidentate Phosphine Ligands

It is well known that the activity of a transition metal centre is strongly influenced by the surrounding ligand set. As such, research into the effects of various ligands upon both structure and catalytic activity is integral to organometallic research.

Phosphine ligands in particular have had a large impact on catalysis, being present in a wide variety of metal precatalysts for use in reactions from hydroformylation and hydrocyanation, to amination. Wilkinson's hydrogenation catalyst, $[RhCl(PPh_3)_3]$ *(see Figure 1)*, discovered in 1965, provided one of the first examples of the effect of phosphine ligands on reactivity.[1]

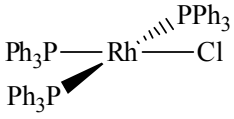

Figure 1: Wilkinson's catalyst.

Functionalised phosphines are an attractive class of ligands to create stable water-soluble transition metal complexes for catalytic (and biomedical) applications, since specific polar groups, like sulfonates, can be introduced to a phosphine ligand to render it water-soluble. They are also able to stabilise metal centres, even those with high and unusual oxidation states, via their neutral donating ability. The versatile co-ordination chemistry associated with phosphines can also be readily utilised in complex design.[2]

By the early 1960s, bidentate phosphine ligands appeared in patents, but showed little catalytic advantage over their monodentate counterparts. Slow rates of activity with the dppe ligand in reactions such as cobalt-catalysed hydroformylation[3] and the hydrogenation of styrene[4] led many researchers to believe that the strong chelating power of diphosphines formed more stable complexes and therefore discouraged catalytic processes. Since Wilkinson's catalyst relies upon the dissociation of one monophosphine ligand, initial experimentation with bidentate phosphines actually inhibited the catalysis.[5]

A superior understanding of various reaction mechanisms had to be attained before the use of chelating diphosphines in catalysis became more prevalent. The seminal work of Thorn and Hoffmann[6] outlined the effect of a geometrical restriction on the activity of a metal complex. Their calculations predicted that a bidentate phosphine ligand would attempt to enlarge the P-M-P angle during migration in order to 'pursue' the migrating ligand. It was surmised that a diphosphine possessing a wide P-M-P angle would accelerate the rate of a migration reaction by mimicking the

transition state. Increasing migration rates were indeed found in palladium complexes using diphosphine ligands with larger bite angles.[7] Conversely, a diphosphine with a small bite angle, like dppe, would constrain the P-M-P angle and therefore hinder the migration reaction.

The influence of the steric and electronic properties of these ligands in catalyst activity and reaction selectivity is now well-known. More recently, it has also been recognised that the orientation of ligands around the metal centre can influence the progress of a reaction.[8] However, specific effects are difficult to pinpoint and rationalise, often due to a lack of information regarding the reaction mechanism and rate determining steps in the catalytic cycle. Many breakthroughs in this field have arisen through chance or *via* experimentation with ligands possessing unusual properties.[9]

In order to develop better catalysts, researchers have recognised the need to rationalise the steric and electronic effects of these ligands. To this end, many experimental and theoretical studies have attempted to develop parameters that are effective in describing ligand properties without being prohibitively complicated to calculate. Of course, relating these parameters directly to catalyst performance is the crux of the problem, and one that is far more difficult.

Early work was able to relate the IR stretching frequencies of metal carbonyl complexes to the electronic properties of the ancillary ligands.[10] The system developed by Tolman became a standard method to evaluate steric and electronic ligand effects, and has proved very useful for monophosphines.[11] The system describes the steric bulk of a phosphine as a cylindrical cone *(see Figure 2)*. A parameter θ is defined as the apex angle of this cone, centred on the metal and set 2.28 Å from the central phosphorus atom, which connects with the most distant atoms of the phosphine substituents. An electronic parameter, χ, is derived from the IR carbonyl stretching frequencies of $[Ni(CO)_3L]$ (L = PR_3) in comparison with those of a reference compound, $[Ni(CO)_3(P\text{-}^tBu_3)]$.[12]

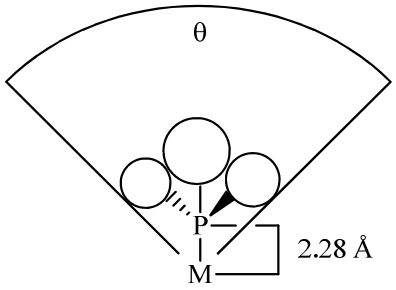

Figure 2: Calculation of the Tolman cone angle, θ.[11]

The extension of the Tolman model to bidentate phosphines has proved more complicated, particularly for those diphosphines that incorporate a rigid backbone. A number of ideas have been suggested, including the concepts of *repulsive energy*,[13] *solid angle* (Ω),[14] *pocket angle*,[15] and the

accessible molecular surface.[16] Unfortunately, these closely linked parameters require extensive use of molecular mechanics in order to calculate them. Instead, the favoured chelation mode of bidentate ligands can be more simply described by the concepts of *natural bite angle*, β_n, and *flexibility range*. These parameters were introduced by Casey and Whiteker in 1990, and have seen widespread use.[8] The *natural bite angle* is described as the favoured chelation angle set by the ligand backbone only and not by any metal valence angles. Calculation of this first parameter provides an energetic minimum. The *flexibility range* is then derived from the series of bite angles achievable within 3 kcal mol^{-1} of this value. The development of this widely adopted system has given researchers a standard model to evaluate bite angle effects.

1.2 Wide Bite Angle Diphosphines

With a standard model to gauge the effect of bite angle on a reaction, the result of changing the diphosphine bite angle could be analysed experimentally for a wide range of catalytic systems.[5, 9, 12, 17] For instance, the inflexible aromatic backbone of the transphos ligand was designed to impose *trans* chelation *(see Figure 3)*.[18] In general though, the difficulty was to find a range of ligands where small structural changes could finely tune the bite angle without significantly altering the overall steric and electronic properties.

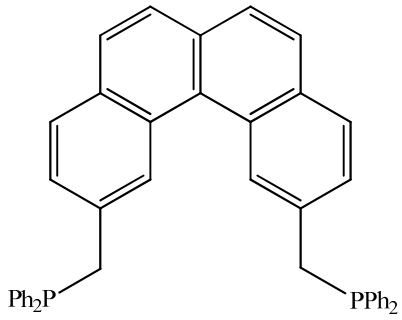

Figure 3: The transphos ligand, used to enforce *trans* conformation.

Promising structural features were identified by van Leeuwen *et al*. in a series of rigid aromatic xanthene heterocycles *(see Figure 4)*.[17] These could be simply converted into bidentate phosphine ligands by two-fold ortholithiation followed by treatment with a disubstituted chlorophosphine.[19] The rigid backbone provides an identical ligand scaffold across the series and the ability to impose a particular geometry upon coordination to a metal centre. Variation at the 9-position along the ligand backbone could induce small alterations to the bite angle which was enough to induce *trans* coordination over *cis* if so desired. Of this series, the xantphos ligand is by

far the most commonly used in catalysis and is commercially available.[20] The natural bite angle of xantphos has been calculated at 111° *(see Figure 4)*, with a flexibility range between 97° and 133°.[21]

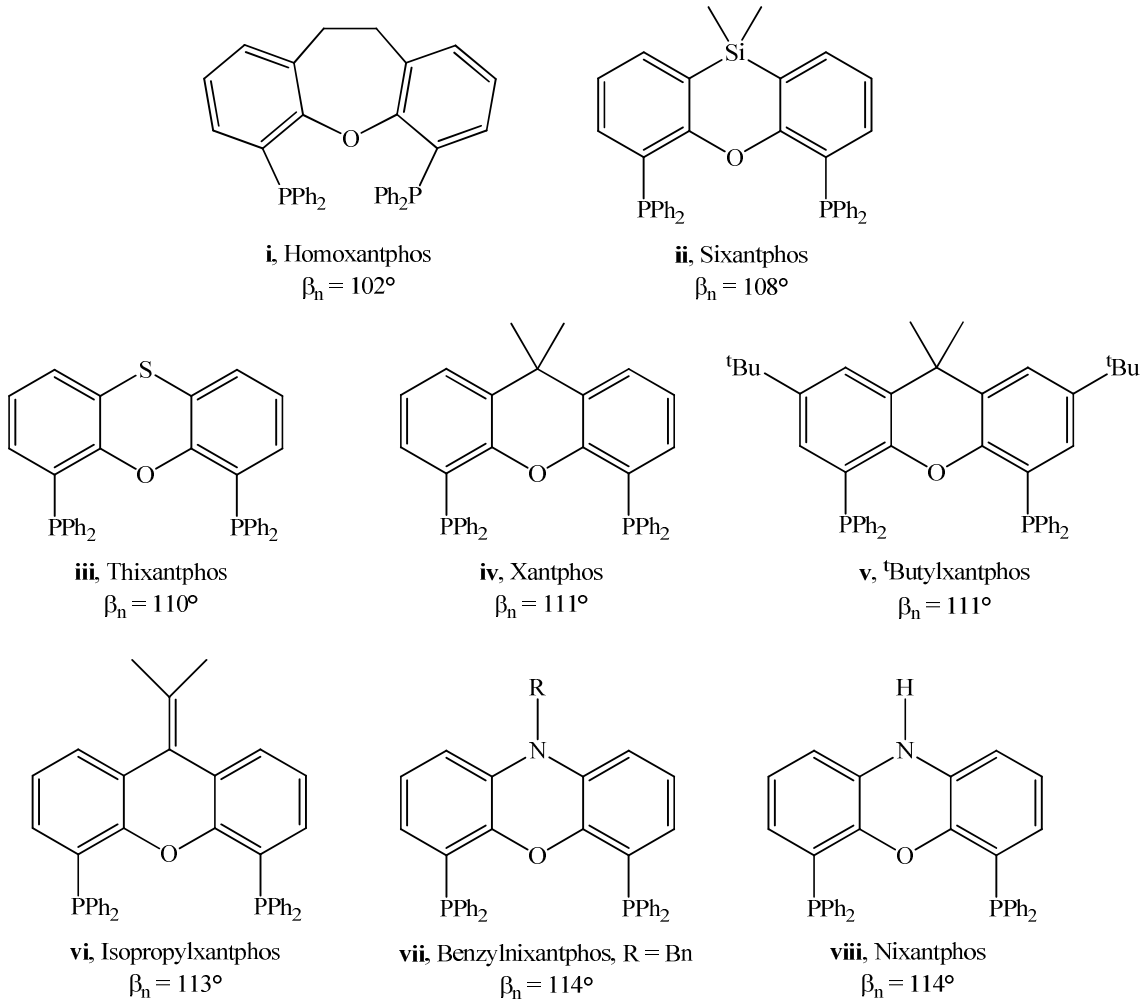

Figure 4: The xantphos series of diphosphine ligands with their corresponding bite angles, β_n.

In general, xantphos coordinates in a *cis* fashion, a conformation which has been observed in varying coordination geometries.[12] Xantphos-palladium complexes have been widely used in cross-coupling reactions, with the xantphos ligand occupying the *cis* positions on a square-planar complex, [Pd(xantphos)Cl_2].[22] Copper (I) halide chelates with xantphos and various heterocyclic thiones have a tetrahedral structure *(see Figure 5)*.[23]

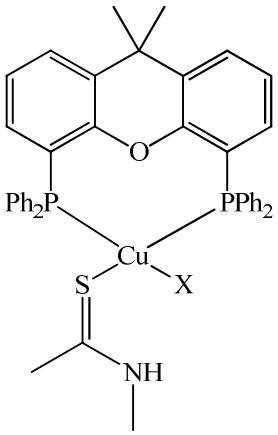

Figure 5: Tetrahedral structure of *cis*-[Cu(X)(xantphos)(thione)].[23]

Homoxantphos, thixantphos and sixantphos *(see Figure 4)* have been used to prepare octahedral *cis*-[Ru(P-P)$_2$H$_2$] complexes.[24] On protonation with HBF_4 or CF_3COOH, the cationic dihydrogen hydride *cis*-[Ru(P-P)$_2$(η^2-H$_2$)H]$^+$ complexes are formed. These species demonstrate facile hydrogen atom exchange between the dihydrogen ligand and the terminal hydride even at temperatures as low as 193 K, and thermally decompose to give solvent stabilised cationic monohydride complexes, [Ru(P-P)$_2$H]$^+$ *(see Figure 6)*.

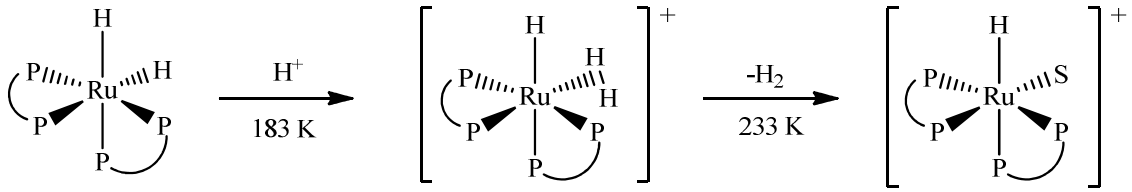

Figure 6: Protonation of neutral dihydrides to give dihydrogen complexes and loss of dihydrogen (P-P = homoxantphos, thixantphos and sixantphos).

Whilst the vast majority of investigations using the xantphos series of ligands observe *cis* coordination, they have also been known to coordinate in a *trans* fashion. A palladium (II) complex, [Pd(xantphos)(4-cyanophenyl)(Br)], was found to be an active catalyst for the amidation of aryl halides.[25] Unusually the xantphos ligand was found in *trans* coordination, spanning the square planar complex with a large P-Pd-P angle of 150.7˚. Since the flexibility range of xantphos extends to only 133˚, this type of co-ordination is unusual. A weak interaction between the oxygen atom and the palladium centre was also noted (Pd-O distance = 2.697 Å) and invoked as an explanation for the larger than expected bite angle.

The interaction of the oxygen atom on the xantphos ligand with the metal centre has also been detected in other studies. The X-ray crystal structures of square-planar [Pd(P-P)(4-cyanophenyl)Br] complexes revealed the *trans* coordination of various xanthene ligands. The

electron withdrawing cyanophenyl group was thought to strengthen the Pd-O interaction by lowering electron density at the palladium centre and encouraging *trans* coordination. In addition, a π-π interaction between the phenyl substituents on the phosphorus and the cyanophenyl group could stabilize the *trans* complex in relation to the *cis* complex, since *cis* orientation of the rigid ligand would prevent alignment of the phenyl groups in this way. In solution, interconversion between the *cis* and *trans* isomers was also facilitated by interaction of the oxygen since its close proximity to the palladium centre was thought to stabilise a four-coordinate ionic intermediate formed during the *cis-trans* isomerisation *(see Figure 7)*.[26]

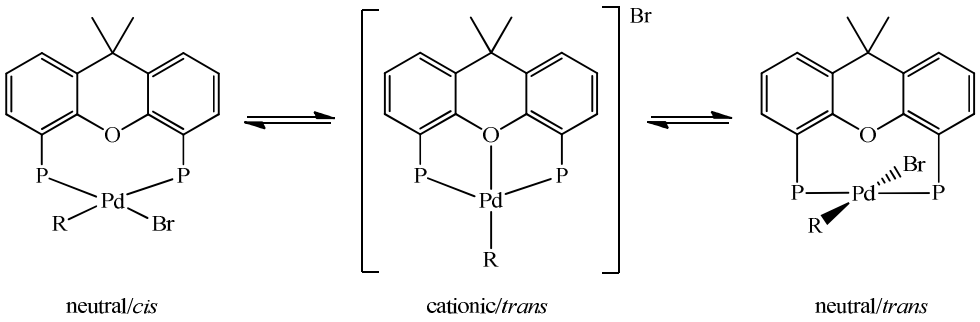

Figure 7: Possible pathway for *cis-trans* isomerisation, R = cyanophenyl group.[26]

Perhaps even more unusually, the *trans* and also tridentate P-O-P coordination of xantphos has also been observed in a ruthenium benzylidene complex, resulting in a distorted octahedral environment *(see Figure 8)*. The Ru-O bond distance of 2.3314(12) Å in this complex was significantly longer than the average Ru-O distance (2.0 – 2.2 Å), and this observation, coupled with the non-planarity of the xanthene backbone, led the researchers to conclude that the Ru-O interaction was compelled on coordination of the diphosphine.[27]

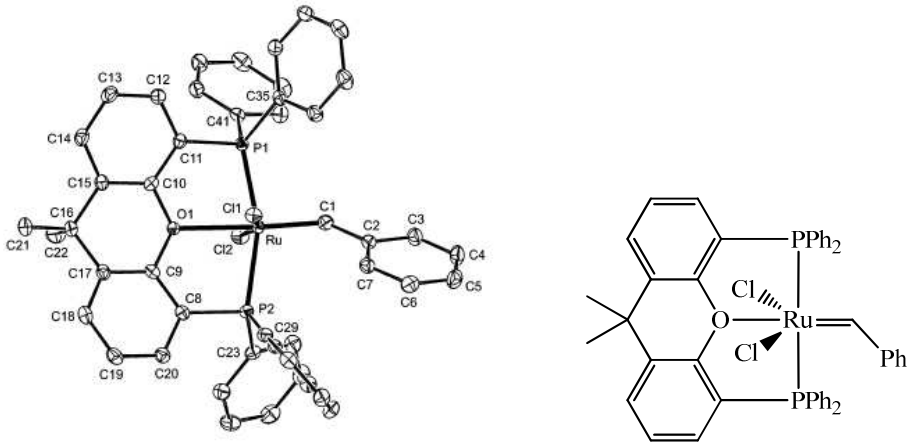

Figure 8: X-ray crystal structure and schematic of a *trans*-chelating Ru-xantphos complex.[27]

It should be mentioned that the P-M-P angle determined from crystal structures is a compromise between the bite angle of the free ligand and that imposed by the metal centre. As referred to previously, the preferred ligand bite angle is generally determined by alterations to the ligand backbone and any steric repulsion present between the backbone and the phosphorus substituents. However, the bite angle preferred by the metal centre is mainly a consequence of electronic effects and is dependent on transition metal, charge and ligand environment. All of these factors will affect the metal *d*-orbital participation in the bonding molecular orbitals, and also influence the electronic effects more indirectly by altering the metal-phosphorus bond length.[17] Tuning the P-M-P angle can therefore be a difficult enterprise, as changes to the bite angle of the free ligand do not necessarily translate once the ligand is co-ordinated to a metal centre.

In addition, when dealing with wide bite angle ligands like the xantphos series, the bite angle can enforce two different effects on a catalytic cycle. The first is derived from the steric interactions between the ligand and the metal or the ligand and other substituents. This is termed a *steric bite angle effect*, and is induced when the backbone of the xantphos ligand is modified to change the bite angle, whilst the remaining ligand environment is kept constant. This can influence the energies of the catalyst resting state and subsequent transition states, changing the overall selectivity and activity of the reaction. However, there are also electronic changes associated with an increase or decrease in the bite angle, leading to an *electronic bite angle effect*. This can be thought of as an orbital effect since modifying the angle of chelation alters the metal hybridisation, changing the overlap between the metal and ligand orbitals. This can affect the stability of the initial, final or transition states of a catalytic profile.

Unfortunately, for most experimental purposes, the two effects are virtually indistinguishable and are concomitant.[9] However, much research into the use of wide bite angle xanthene ligands has concentrated on the important industrial processes of hydroformylation and hydrocyanation. In these cases, the different *steric* and *electronic bite angle effects* alter the activity of the reaction in distinct ways, and since changes to the catalytic system are attributable to one effect over the other, researchers have been able to optimise the catalysis.

1.3 Hydroformylation

The rhodium-catalysed hydroformylation of alkenes to form aldehydes is a well established and widely used industrial process. Much research has focused on the development of catalytic systems that have improved regioselectivity towards the linear rather than the branched aldehyde. Traditionally, $[Rh(PPh_3)_3(CO)H]$ was used as the catalyst precursor, and investigation of the reaction mechanism identified the active catalytic species as a trigonal bipyramidal rhodium

hydride complex incorporating two phosphine ligands.[28] Further mechanistic work suggested that formation of the linear aldehyde was favoured by an intermediate in which the two phosphine ligands were *cis* to one another, but both occupying equatorial positions (ee) over an equatorial-apical conformation (ea).[29] It was hoped that bidentate phosphine ligands could impose equatorial-equatorial chelation and positively influence the selectivity of the reaction towards the linear product. Indeed, use of the chelating ligand, BISBI, achieved very high regioselectivity for the formation of straight chain aldehydes *(see Figure 9)*. The complex [Rh(BISBI)(PPh_3)(CO)H] was patented by Kodak in 1987.[30]

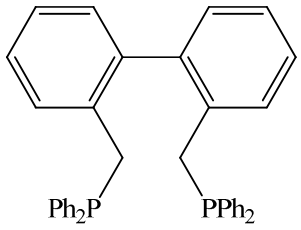

Figure 9: The chelating diphosphine ligand, BISBI.

One of the first literature references utilising xantphos described the synthesis of the trigonal bipyramidal complex, [Rh(xantphos)(PPh_3)(CO)H], for use in the hydroformylation of 1-octene, which increased the regioselectivity to the linear product, producing over 98% of the *n*-aldehyde at just 313 K.[31] In later work, van Leeuwen *et al.* extended this research and used the entire series of xanthene ligands to synthesise a range of these hydroformylation catalysts, all of which achieved high regioselectivities. This challenged the initial hypothesis that the ee isomer led to higher selectivity for the linear aldehyde, since the ratios of ee:ea isomer varied widely across all the highly selective reactions. Differences in the observed regioselectivities were instead attributed to a *steric bite angle effect.* The researchers argued that steric congestion around the metal centre was exaggerated with larger bite angles. Given that the least sterically demanding transition states correspond to production of the linear aldehyde, better regioselectivity is observed as the bite angle is increased. This observation has now been quantified with the use of an integrated molecular orbital/molecular mechanics approach. When only small variations in bite angle are induced, the observed regioselectivity is determined by the steric repulsion between the phosphine substituents and the substrate itself.[32]

An increase in the rate of hydroformylation was also found with increasing bite angle. This relationship between activity and bite angle can be attributed to electronic effects. It is thought that a wider bite angle will stabilise the unsaturated four-coordinate intermediate [Rh(P-P)(CO)H], thereby increasing its concentration and the associated rate of reaction.[9] Migration reactions are

likely to be accelerated by widening the bite angle of a *bis*-equatorial ligand, assuming a similar effect to increasing the bite angle of a *cis* bidentate ligand in a square planar complex.[33]

1.4 Hydrocyanation

Hydrocyanation comprises the addition of HCN to alkenes, and is of particular importance industrially due to the DuPont production of adiponitrile using nickel-phosphite catalysts. Kinetic studies have identified the rate determining step as the reductive elimination of the alkyl cyanide, RCN, from the square planar Ni(II) species to yield a tetrahedral Ni(0) complex.[34] This step is favoured by electron withdrawing ligands, since formation of the electron rich d^{10} centre is stabilised by back donation from the nickel centre into the empty ligand orbitals. Historically, the incorporation of phosphite and phosphinite ligands has therefore generated very active catalysts, whilst the use of more basic phosphine ligands results in little activity.

However, it has now been shown that the introduction of chelating diphosphines produces highly active catalysts that are very sensitive to changes in the bite angle.[35] The use of wide bite angle diphosphines in particular help to stabilise the tetrahedral geometries that result upon reductive elimination *(see Figure 10)*, thus increasing the rate of this process. For instance, the hydrocyanation of styrene with nickel catalysts containing xanthene ligands is very successful, particularly with sixantphos, giving yields of 95% and selectivities for the desired branched product of over 97%.[36]

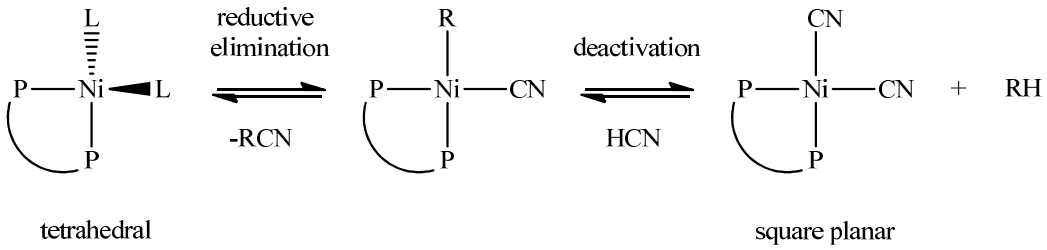

Figure 10: Competitive reductive elimination and deactivation pathways for a typical nickel hydrocyanation catalyst.

The presence of a chelating diphosphine ligand can also arrest the facile deactivation of the catalyst *(see Figure 10)*. The presence of excess HCN leads to the production of the square planar complex [Ni(diphosphine)$(CN)_2$], which is completely inactive. The formation of this species then competes with the reductive elimination step and inhibits the catalytic activity. The natural bite angles of some common bidentate phosphines like dppp are small enough to stabilize the square planar Ni(II) geometries, favouring the formation of [Ni(diphosphine)$(CN)_2$] and thus exacerbating

the problem of deactivation. However, wide bite angle ligands have the opposite effect, discouraging the formation of square planar geometries in favour of tetrahedral Ni(0) complexes. This 'negative' *electronic bite angle effect* produces catalysts that are more resistant to deactivation.[9]

1.5 C-C Bond Formation from Alcohols

Carbon-carbon bond formation is one of the most important synthetic goals in organic chemistry, in particular, allowing the alkylation of various compounds, including nitriles and ketones. The more traditional process uses electrophiles such as alkyl halides to act as the alkylating agents, but this method has various disadvantages from an economic and environmental outlook. In particular, many alkylating agents are toxic and frequently mutagenic, and necessitate a further reaction step requiring the use of LDA, $LiN(^iPr)_2$. The stoichiometric use of high molecular weight inorganic bases and the loss of the electrophile leaving group also translate into low atom efficiency *(see Figure 11)*. These problems, together with waste disposal issues and the production of inorganic salts, can make industrial scale alkylation an impractical option.[37]

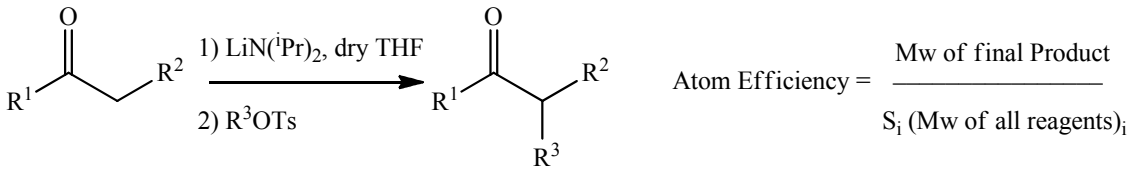

Figure 11: The α-alkylation of ketones via the use of alkyl halides.

An ideal system would replace the highly reactive alkylating agents with a more moderate agent, but this would require a different method of activation. Transition metal catalysis has therefore been investigated as a new route to the formation of C-C bonds from alcohols.[38] Such a process would provide an attractive alternative to the use of alkyl halides, giving water as the only waste product. Alcohols are not generally used as alkylating agents due to the strength of the C-O bond, which is only increased by deprotonation under basic conditions.[39] Hydrogen transfer (also known as 'hydrogen auto-transfer'[37, 40]) by an organometallic catalyst can provide an efficient strategy for their use in alkylation reactions.

Research from the Williams group has identified a route for this system in which no net oxidation or reduction need occur.[41] Instead, the nucleophilic alcohol is temporarily oxidised by catalytic removal of hydrogen to yield a highly electrophilic aldehyde intermediate. This intermediate is then converted into an alkene on attack by a nucleophile, and then subsequently

reduced to give the final product, a longer chain alkane *(see Figure 12)*. The key to this catalytic system is therefore the borrowing of hydrogen by the catalyst – the hydrogen released on oxidation of the alcohol must be stored by the catalyst and then returned in order to hydrogenate the alkene. The catalyst therefore needs to exhibit facile hydrogen transfer properties, preferably under moderate conditions.[42]

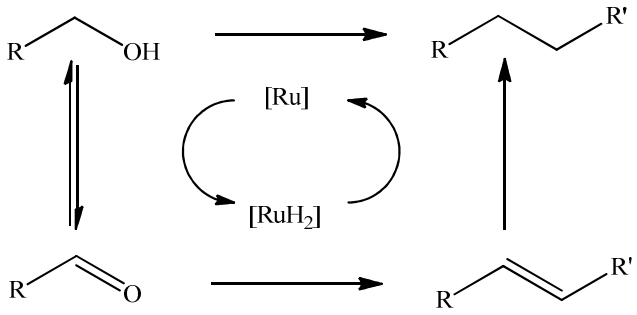

Figure 12: Borrowing hydrogen in the alkylation of alcohols.

Previously, the group has concentrated on using an indirect Wittig reaction to facilitate formation of the alkane by reaction of the intermediate aldehyde with an activated benzyl ester ylide *(see Figure 13)*. This indirect Wittig chemistry has been demonstrated with both iridium and ruthenium phosphine based catalysts. $[Ru(PPh_3)_3(CO)H_2]$ (**1**) at a catalyst loading of 5 mol% was able to complete the reaction to form the longer chain alkane in 48 h at 353 K *(see **x**, Figure 13)*.[42] This was an improvement upon the iridium system, where a combination of $[\{Ir(COD)Cl\}_2]$, the chelating ligand dppp and Cs_2CO_3, was only able to achieve yields of 47-71% even under the forcing conditions of 72 h at 423 K and at the same catalyst loading *(see **ix**, Figure 13)*.[43]

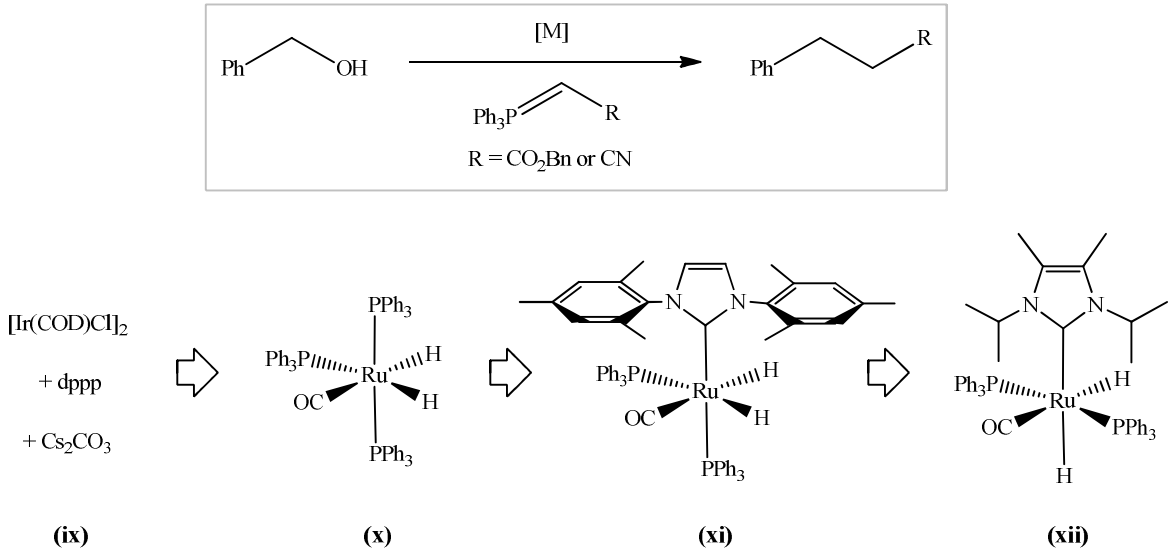

Figure 13: Catalyst development for the indirect Wittig reaction to form alkylated product.

Significant catalytic improvements were made on substitution of PPh_3 for various N-heterocyclic carbene (NHC) ligands. The ruthenium system, $[Ru(PPh_3)_2(IMes)(CO)H_2]$, was able to give good isolated yields of 70-84% within 24 h at only 353 K, and at a catalyst loading of 1 mol% *(see **xi**, Figure 13)*.[42] Subsequent work with catalysts such as the C-H activated complex $[Ru(PPh_3)_2(I^iPr_2Me_2)'(CO)H]$ and an activated cyano ylide has given better yields in only 2 h at 343 K although with a higher catalyst loading of 5 mol% *(see **xii**, Figure 13)*.[44]

Similar hydrogen borrowing approaches have been used to alkylate ketones. A combination of $[Ir(COD)Cl]_2$, PPh_3 and KOH was able to complete an alkylation reaction in only 4 h without solvent, but again, needed a high temperature of 383 K.[45] $[Ru(DMSO)_4Cl_2]$ has been used by Yus *et al.* to alkylate ketones, with the advantage of high yields at only 353 K[39] whilst another ruthenium system, $[Ru(PPh_3)_3Cl_2]$ with KOH, has been effective for the alkylation of secondary alcohols at the same temperature, although 1-dodecene was needed as a sacrificial hydrogen acceptor to generate the coupled secondary alcohols.[46] More recently, Krische *et al*. have applied the hydrogen transfer methodology to the C-C bond forming reactions between primary alcohols and a range of substrates including dienes and enynes with iridium and ruthenium catalysts *(see Figure 14)*.[47]

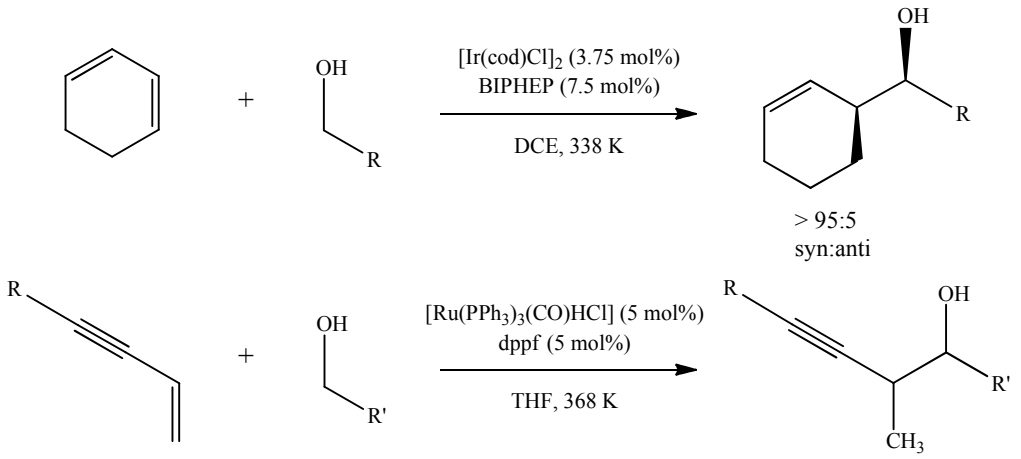

Figure 14: C-C bond forming reactions developed by Krische *et al*. using $[Ir(cod)Cl]_2$/BIPHEP and $[Ru(PPh_3)_3(CO)HCl]$/dppf to catalyse the reaction between primary alcohols and dienes and enynes respectively.

The hydrogen transfer strategy was applied to the alkylation of nitriles with alcohols in a homogeneous process as early as 1981, when $[Ru(PPh_3)_4H_2]$ was shown to be an effective catalyst by Grigg *et al*. Moderate yields were achieved although stoichiometric amounts of Na_2CO_3 were still needed.[48] Fujita and Yamaguchi initially showed that the iridium complex $[Cp^*IrCl_2]_2$ could be used as a catalyst for the oxidation of both primary and secondary alcohols when the reaction was conducted in acetone with K_2CO_3. Use of this catalyst was then extended to N-alkylation reactions,

with the system able to alkylate a wide range of primary and secondary amines with a series of different alcohols. Catalytic amounts of K_2CO_3 were still needed to initially activate the catalyst.[49] The Whittlesey and Williams collaboration has also achieved the iridium catalysed alkylation of alcohols with malonates and nitroalkanes *(see Figure 15)*.[50]

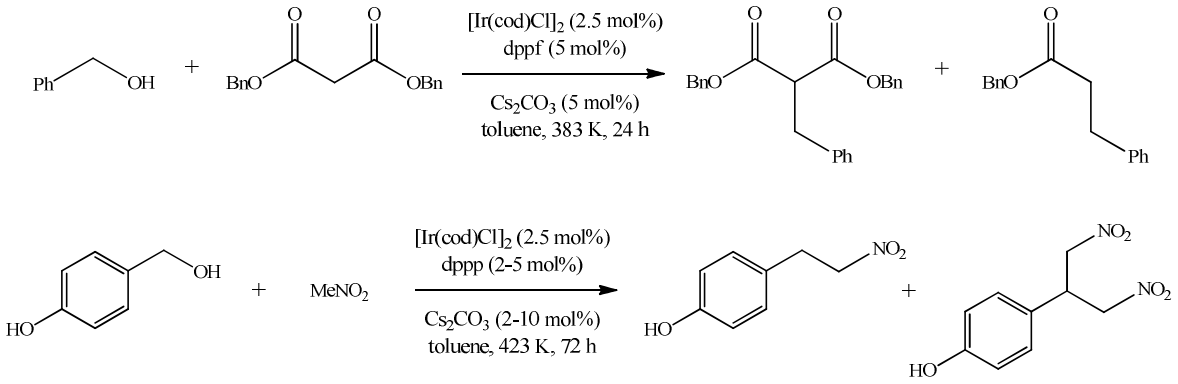

Figure 15: The iridium catalysed alkylation of alcohols with malonates and nitroalkanes.

The direct alkylation of nitriles by alcohols has also been achieved with a heterogenous system, using a ruthenium-grafted hydrotalcite catalyst.[51] The hydrotalcite is an inorganic crystal with consecutive cationic and anionic layers which possesses tunable surface basicity. It was hoped that these properties would allow the reaction to occur without the need for an inorganic base and under milder conditions. However, whilst the crystal was able to perform the function of hydrogen transfer to give high yields, the reaction still required the forcing conditions of 20 h at 473 K. A homogeneous ruthenium system for the N-alkylation of secondary alcohols was developed by Beller and co-workers. $Ru_3(CO)_{12}$ was used in combination with the bulky monophosphine ligand P(*o*-tolyl)$_3$ to effect the quantitative amination of 1-phenylethanol with *n*-hexylamine without solvent and at the lower temperature of 383 K *(see Figure 16)*.[52]

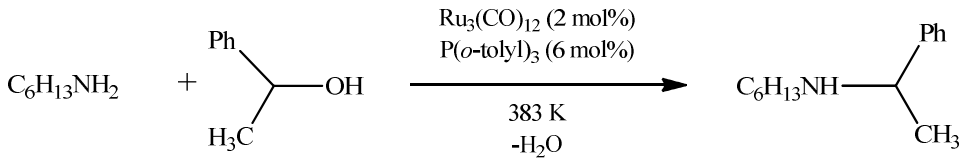

Figure 16: The N-alkylation of 1-phenylethanol with *n*-hexylamine.

Milstein *et al.* have developed a ruthenium catalyst incorporating a dearomatised PNN-type pincer ligand. In an unprecedented reaction, the direct acylation of primary amines was achieved in a 1:1 reaction with alcohol to give amides and H_2 as the sole products.[53] Refluxing the reactants together in toluene for approximately 7 h with a catalyst loading of 0.1 mol% produces a range of

amides with isolated yields of over 95%. If the reaction is carried out in a closed system the generated H_2 gas is unable to escape, inhibiting product formation. This reaction is a very neat example of hydrogen transfer – an environmentally benign process with high atom economy that can occur with a wide range of simple amine and alcohol substrates.

The mechanism of the amide-forming reaction is believed to proceed via the reaction of the amine with an intermediate aldehyde, which in this case generates a hemiaminal *(see Figure 17)*. Reaction of the hemiaminal with the catalyst leads to the aromatic complex **(xv)**. The desired amide product is formed via β-hydride elimination to give the *trans* dihydride complex **(xvi)**, which was described in a separate communication.[54] The elimination of H_2 from this complex regenerates the original catalyst **(xiii)**.

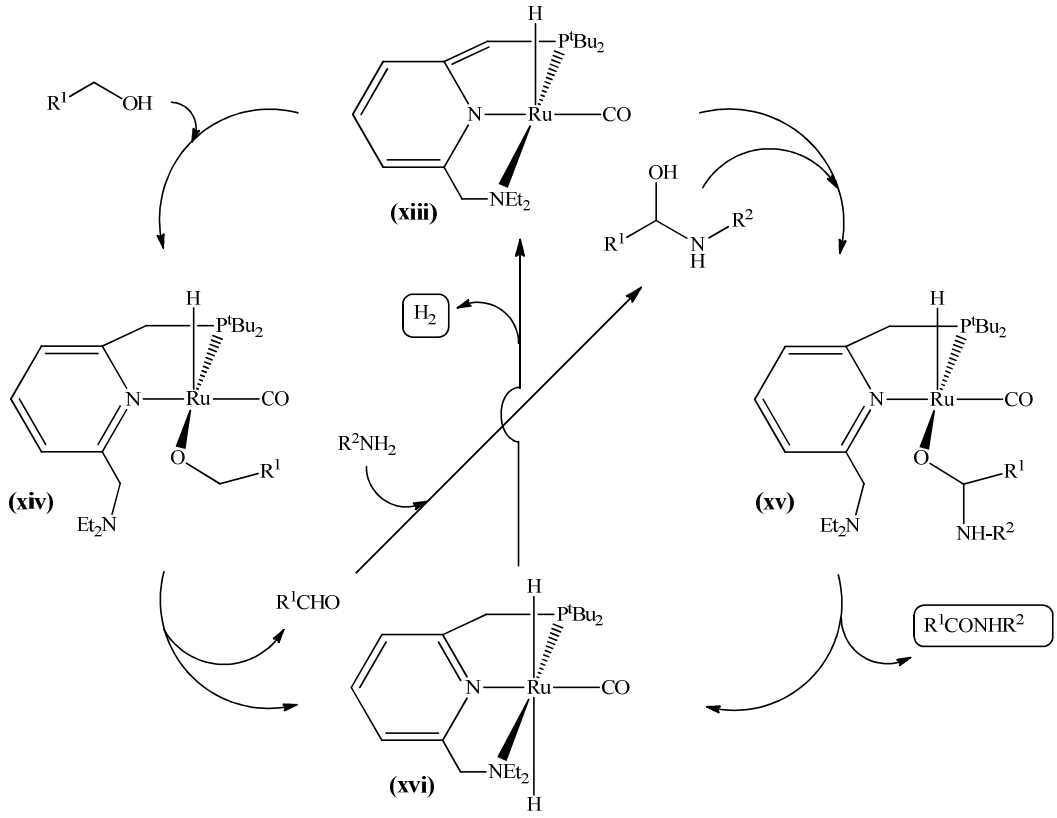

Figure 17: The proposed mechanism for the direct acylation of amines by alcohols catalysed by a [Ru(PNN)(CO)H] complex.

The Whittlesey and Williams' group collaboration have also extended the hydrogen transfer methodology to an oxidation-Knoevenagel-reduction reaction between benzyl alcohol and *tert*-butyl-ketonitrile. This approach improved on the previous Wittig chemistry by avoiding the formation of triphenyl phosphine oxide in the reaction mixture. Experimentation with various catalyst systems identified $[Ru(PPh_3)_3(CO)H_2]$(**1**)/xantphos as the most effective. One equivalent of

each of the substrates with 5 mol% piperidinium acetate and 0.5 mol% **1**/xantphos gave complete conversion to alkylated product within 3 h at 393 K *(see Figure 18)*.[55]

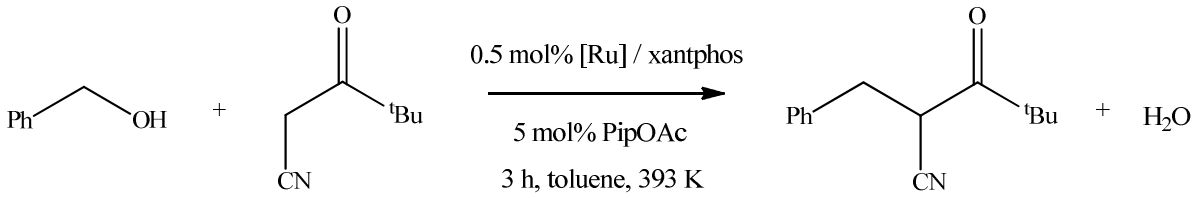

Figure 18: Reaction of benzyl alcohol with ^{t}butyl-ketonitrile to give alkylated product.[55]

The success of a wide bite angle ligand such as xantphos prompted an investigation into the use of other xanthene ligands.[56] A total of eight xanthene ligands were tested *in situ* with $[Ru(PPh_3)_3(CO)H_2]$ (**1**) to form a catalytic system for the oxidation-Knoevenagel-reduction reaction under standard conditions (*see Table 1 & Experimental 5.3.5*). In contrast to other reactions that have seen a correlation between bite angle and performance,[5, 17] this system shows no obvious relationship between the two parameters. Although two of the ligands, **ii** and **vi** out-performed the xantphos ligand itself, the commercial availability of xantphos ensured its continued use in this system.

Table 1: Activity of added xanthene ligands for the reaction in *Figure 18*

Ligand[57]	Bite Angle, β_n (°)[5, 12]	Conversion (%)
Homoxantphos, **i**	102	46
Sixantphos, **ii**	108	98
Thixantphos, **iii**	110	77
Xantphos, **iv**	111	81
^{t}Butylxantphos, **v**	111	1
Isopropylxantphos, **vi**	113	92
Benzylnixantphos, **vii**	114	4
Nixantphos, **viii**	114	3

Reaction conditions: 2 mmol benzyl alcohol, 2 mmol tert-butyl ketonitrile, 5 mol% piperidinium acetate, 0.5 mol% [Ru], 0.5 mol% xanthene ligand, toluene, 383 K, 3.5 h.

The scope of the **1**/xantphos system has been increased with further experimentation. The system has proved effective for the conversion of a range oxime ethers into their corresponding nitriles *via* the elimination of methanol *(see Reaction **a**, Figure 19)*.[58] Methyl esters can be

produced simply from methanol and the corresponding aldehydes when crotonitrile is used as a sacrificial hydrogen acceptor *(see Reaction **b**, Figure 19)*.[59] Alkyne-1,4-diols can also be utilised as hydrogen transfer substrates; initial isomerisation to 1,4-diketones is promoted by the **1**/xantphos system with subsequent *in situ* cyclisation forming 2,5-disubstituted furans *(see Reaction **c**, Figure 19)*.[60] If the reaction is carried out in the presence of amines or hydrazines, the methodology can be further extended to the formation of pyrroles or pyridazines respectively *(see Reactions **d** & **e**, Figure 19)*.[61]

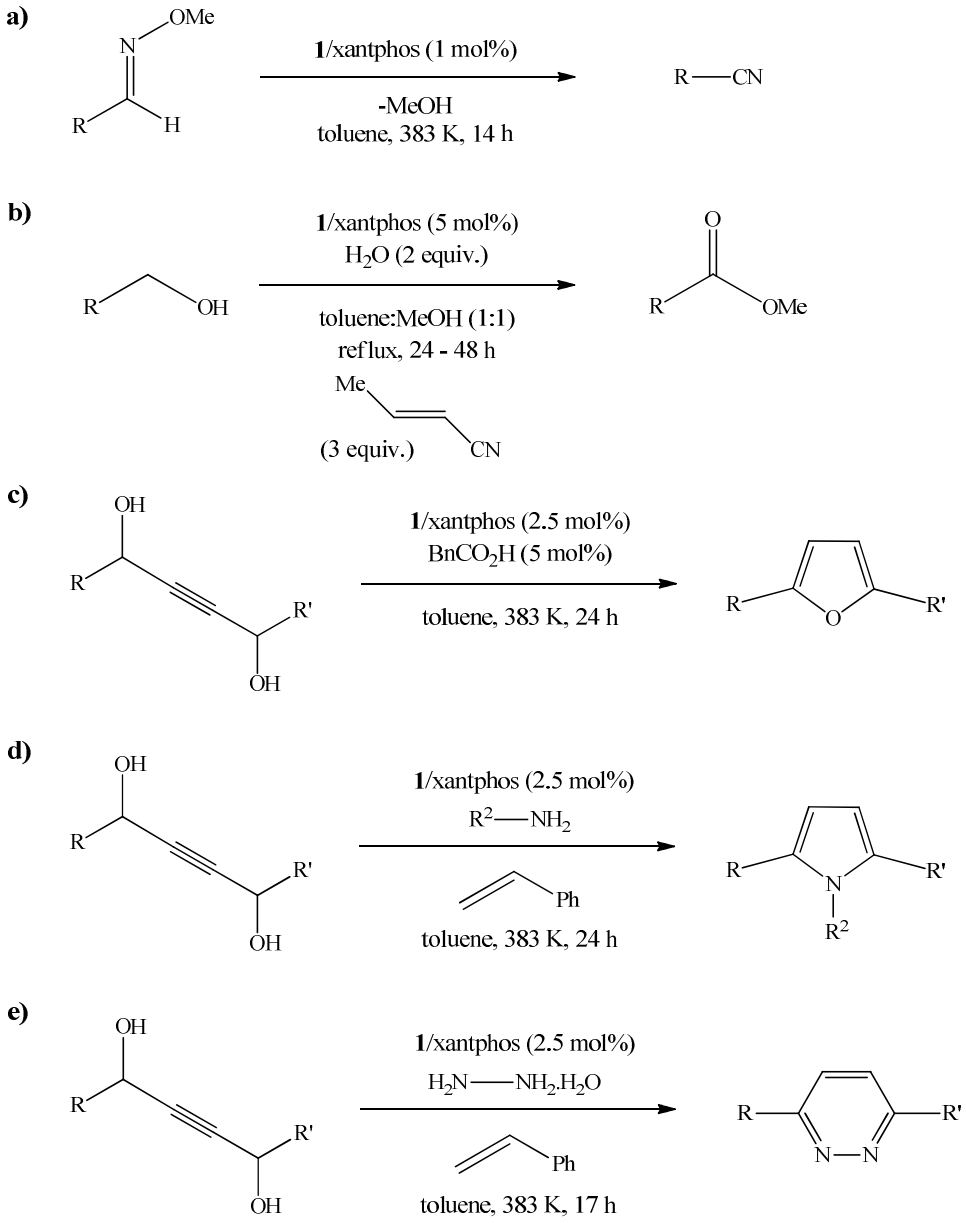

Figure 19: Reactions and reaction conditions for a range or organic transformations using **1**/xantphos as the catalyst system.

The incorporation of the xantphos ligand evidently confers a marked catalytic improvement on **1** and proves crucial to the high reactivity of the ruthenium catalyst. To enhance the catalytic activity of this system, the mechanism of the reaction and the intermediates formed warranted further investigation. This began with fundamental studies of the isolated complex [Ru(xantphos)(PPh_3)(CO)H_2] (**2**) in comparison with the catalytically inactive complex [Ru(dppp)(PPh_3)(CO)H_2] (**3**).

1.6 Synthesis and Characterisation of [Ru(P-P)(PPh_3)(CO)H_2] Precursors

Reaction of **1** with 1.2 equivalents xantphos for 3 h in refluxing toluene resulted in the formation of [Ru(xantphos)(PPh_3)(CO)H_2] (**2**). [Ru(dppp)(PPh_3)(CO)H_2] (**3**) was prepared *via* literature methods.[62] Whilst the $^{31}P\{^1H\}$ NMR spectrum of **3** displayed the three sharp ^{31}P resonances as expected, that of **2** revealed some fluxionality at 298 K. A sharply defined doublet of doublets was observed at δ 58.5 displaying both a *trans* coupling and a *cis* coupling to ^{31}P ($^2J_{PP}$ = 237.2 Hz, 15.5 Hz). This resonance was assigned as the PPh_3 ligand on the basis of work performed by Jung and Garrou.[62a] Two other broad signals in the $^{31}P\{^1H\}$ NMR spectrum at δ 45.2 and 30.5 resulted from the xantphos ligand. On cooling to 199 K, the resonance at δ 45.2 resolved into a doublet of doublets with a large *trans* $^2J_{PP}$ coupling of 237.2 Hz identifying this signal as that *trans* to the PPh_3 ligand. The room temperature ^1H NMR spectrum of **2** revealed two hydride resonances that remained somewhat broad even upon cooling to 199 K, precluding determination of $^2J_{HP}$ and $^2J_{HH}$. Instead, simulation by g-NMR[63] *(see Figure 20)* was used to elucidate the coupling constants. In an attempt to further explain the broadening of the xantphos resonances, **2** was heated with 3 equivalents of P(p-tolyl)$_3$ at 343 K for 15 h, although no evidence for phosphine exchange was observed. Despite this, the implied fluxionality of the xantphos ligand in this research is supported by a number of other studies.[24, 26]

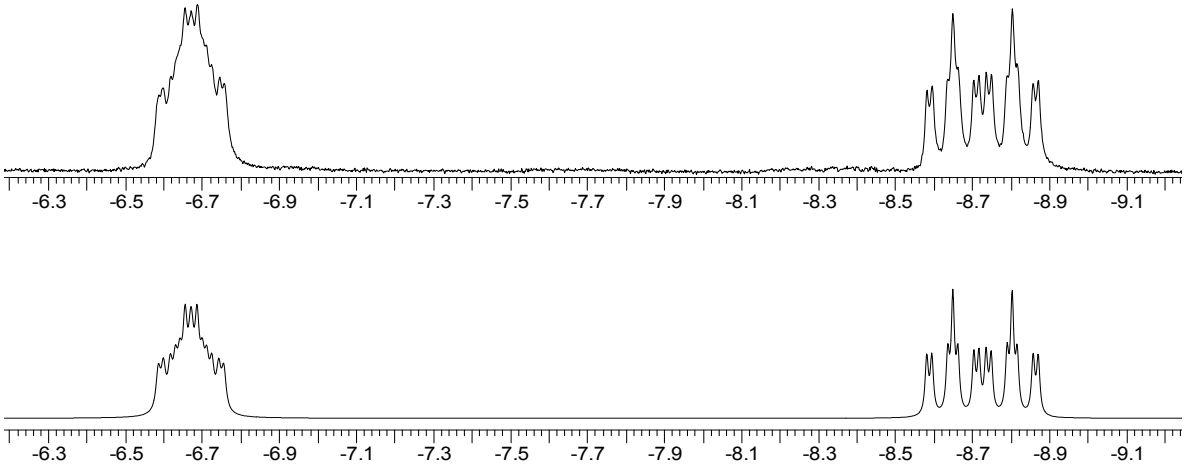

Figure 20: Experimental *(upper)* ^{1}H NMR spectrum of [Ru(xantphos)(PPh_3)(CO)H_2] (**2**) ([D_8]-toluene, 500 MHz, 298 K) against simulated[63] *(lower)* ^{1}H NMR spectrum. See *Experimental* for calculated chemical shifts (ppm) and coupling constants (Hz).

The molecular structure of **2** was confirmed by an X-ray crystal structure *(see Figure 21)*.[64] The xantphos ligand coordinates in a *cis* fashion to the ruthenium centre, occupying both an axial and an equatorial position. As predicted, the larger bite angle enforces a greater P_{transP}-Ru-P_{transH} angle at ruthenium than in the dppp analogue (102.76(2)˚ *vs*. 92.14(9)˚ respectively) *(see Table 2)*.[62b] As a result, the octahedral geometry of **2** suffers a greater distortion than that of **3**. This effect is particularly noticeable when comparing the P_{transP}-Ru-PPh_3 angles: the dppp analogue **3** is able to maintain an angle closer to the linear ideal at 160.67(9)˚ than in the more strongly distorted structure of **2** (P_{transP}-Ru-PPh_3 = 145.06(2)˚).

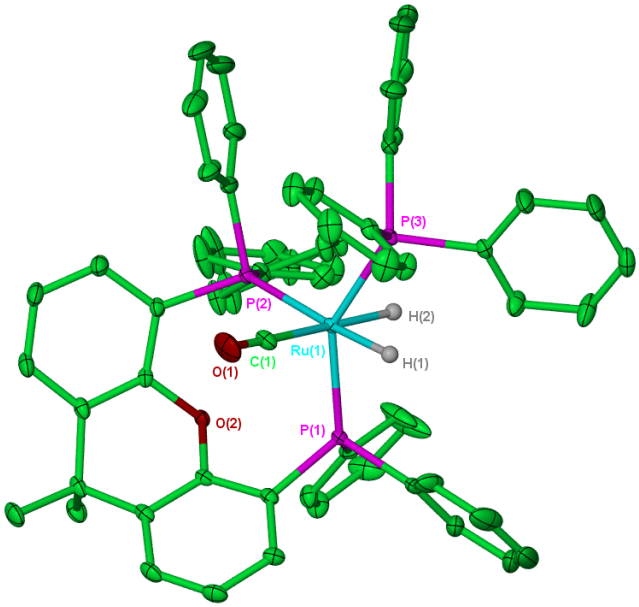

Figure 21: Molecular structure of [Ru(xantphos)(PPh_3)(CO)H_2] (**2**). All hydrogen atoms except Ru-H are omitted. Thermal ellipsoids are shown at the 30% probability level.

Table 2: Selected bond lengths [Å] and angles [°] for [Ru(xantphos)(PPh_3)(CO)H_2] (**2**) and [Ru(dppp)(PPh_3)(CO)H_2][62b] (**3**)

	2	**3**
Ru-P_{transP}	2.3283(6)	2.309(3)
Ru-P_{transH}	2.3950(6)	2.363(2)
Ru-PPh_3	2.2973(6)	2.326(3)
Ru-CO	1.897(3)	1.930(1)
P_{transP}-Ru-P_{transH}	102.76(2)	92.14(9)
P_{transP}-Ru-PPh_3	145.06(2)	160.67(9)
P_{transH}-Ru-PPh_3	107.16(2)	102.11(9)

1.7 Stoichiometric Reactivity of Benzyl Alcohol with 2 and 3

The isolated complexes, [Ru(xantphos)(PPh_3)(CO)H_2], **2**, and [Ru(dppp)(PPh_3)(CO)H_2], **3**, were reacted with benzyl alcohol under stoichiometric conditions. Heating the two complexes with 10 equivalents of $PhCH_2OH$ in toluene at 393 K resulted in very different behaviour. After 2 h, only unreacted starting material was observed by ^{1}H NMR spectroscopy in the case of **3**. However,

the equivalent reaction with the xantphos analogue showed that **2** had been converted into a mixture of [Ru(xantphos)$(CO)_2H_2$] (**4**) and [Ru(xantphos)$(PPh_3)(CO)_2$] (**5**) in a 2:1 ratio *(see Figure 22)*. Also present in the ^{1}H NMR spectrum were PhCHO, benzene and H_2.

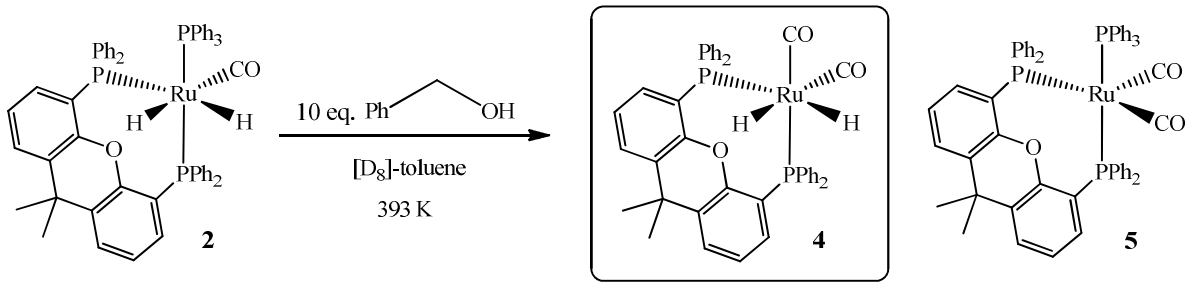

Figure 22: Reactivity of [Ru(xantphos)$(PPh_3)(CO)H_2$] (**2**) with benzyl alcohol.

[Ru(xantphos)$(PPh_3)(CO)_2$] (**5**) was prepared by an independent synthesis using a modification of a literature preparation for [Ru(P-P)$(PPh_3)(CO)_2$] complexes.[65] The complex was isolated in 26% yield as an orange solid which gave rise to the expected spectroscopic data *(see Experimental)*.

[Ru(xantphos)$(CO)_2H_2$] (**4**) was accessed by the initial synthesis of [Ru(xantphos)$(CO)_3$] (**6**) *via* a modified literature preparation.[66] [$Ru_3(CO)_{12}$] and 3 equivalents of xantphos were heated together in toluene at 373 K under 25 atm. CO for 72 h to give **6** in 70% yield. $^{31}P\{^1H\}$ NMR spectroscopy of **6** revealed one singlet resonance at δ 27.9, the two phosphorus atoms clearly in equivalent positions. The $^{13}C\{^1H\}$ NMR spectrum exhibited a single carbonyl resonance split by the phosphorus nuclei of the xantphos ligand at δ 215.4 (t, $^2J_{CP}$ = 3.6 Hz). IR spectroscopy revealed three carbonyl signals at 2007, 1921 and 1920 cm^{-1} consistent with other reported [Ru(P-P)$(CO)_3$] complexes.[66] An X-ray crystal structure of compound **6**[67] *(see Figure 23)* revealed a distorted square pyramidal structure, with the apical position occupied by one arm of the xantphos ligand. The four base positions of the pyramid are pushed out of alignment away from the apex, with the xantphos ligand adopting a bite angle of 101.80(2)° *(see Table 3)*.

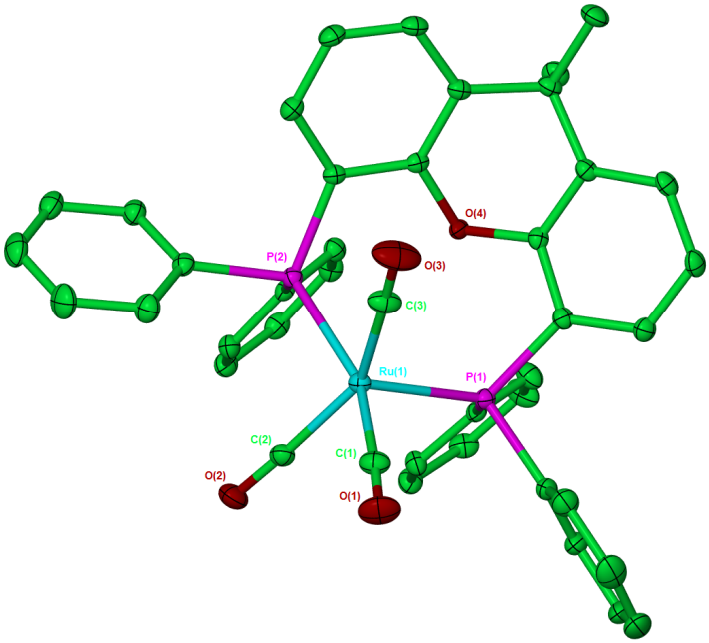

Figure 23: Molecular structure of **6**. All hydrogen atoms are omitted. Thermal ellipsoids are shown at the 30% probability level.

Table 3: Selected bond lengths [Å] and angles [°] for [Ru(xantphos)$(CO)_3$] (**6**)

Ru-P_{apical}	2.4034(6)
Ru-$P_{equatorial}$	2.3975(6)
P_{apical}-Ru-$P_{equatorial}$	101.80(2)
$C_{(1)}$-Ru-P_{apical}	100.63(9)
$C_{(1)}$-Ru-$C_{(2)}$	88.10(11)

[Ru(xantphos)$(CO)_2H_2$] (**4**) was synthesised by the photolysis of a THF solution of **6** under a purge of H_2 at 273 K for 0.5 h and isolated in 76% yield. Complex **4** displayed two hydride resonances in the ^{1}H NMR spectrum at δ -6.13 and δ -7.65, both with a doublet of doublet of doublets splitting pattern. The lower frequency signal was identified as that arising from the hydride *trans* to a phosphorus by the large $^2J_{HP}$ value of 83 Hz. As expected the $^{31}P\{^1H\}$ NMR spectrum showed two doublets at δ 24.6 and 35.1, with a $^2J_{PP}$ value of 21.5 Hz, confirming a *cis* configuration of the xantphos ligand. The $^{13}C\{^1H\}$ NMR spectrum displayed the carbonyl signals as two doublet of doublets at δ 203.3 ($^2J_{(CP)}$ = 81.9 Hz, 7.1 Hz) and 201.5 ($^2J_{(CP)}$ = 11.2 Hz, 8.5 Hz),

the coupling constants revealing one carbonyl as *cis* to both phosphorus atoms, and the other as *trans* to one phosphorus atom and *cis* to the other.

A small amount of a second species was always detected in the formation of **4**. This displayed a doublet hydride resonance at δ -7.63 ($^2J_{HP}$ = 45.7 Hz) and a singlet ^{31}P resonance at δ 29.2. The multiplicity of the hydride reduced to a singlet upon ^{31}P decoupling indicating a single hydride, or equivalent *trans* dihydrides, whilst the singlet ^{31}P resonance, and the lack of free xantphos in the ^{31}P{^{1}H} NMR spectrum, suggests that the phosphorus atoms of the xantphos ligand are occupying equivalent positions. Efforts to generate this complex in higher yields or to separate it were unsuccessful, but the acquisition of an accurate elemental analysis led us to tentatively assign this species as an isomer of **4** where the hydrides lie *trans* to one another.

The IR spectrum of **4** revealed two CO bands of equal intensity at 2007 and 1960 cm^{-1}, suggesting a *cis* conformation of the carbonyl ligands, as found in other reported [Ru(P-P)(CO)$_2$H$_2$] complexes.[68] This was confirmed by the X-ray crystal structure of the complex *(see Figure 24)* which showed a distorted octahedral structure, very similar to that of [Ru(xantphos)(PPh$_3$)(CO)H$_2$] (**2**) A comparison of the two complexes revealed a lengthening of the Ru-xantphos and Ru-CO distances in **4** as well as a widening of the *trans*-P-Ru-L angle from 145.16(2)˚ (L = PPh$_3$) to 156.18(10)˚ (L = CO) *(see Table 4)*.

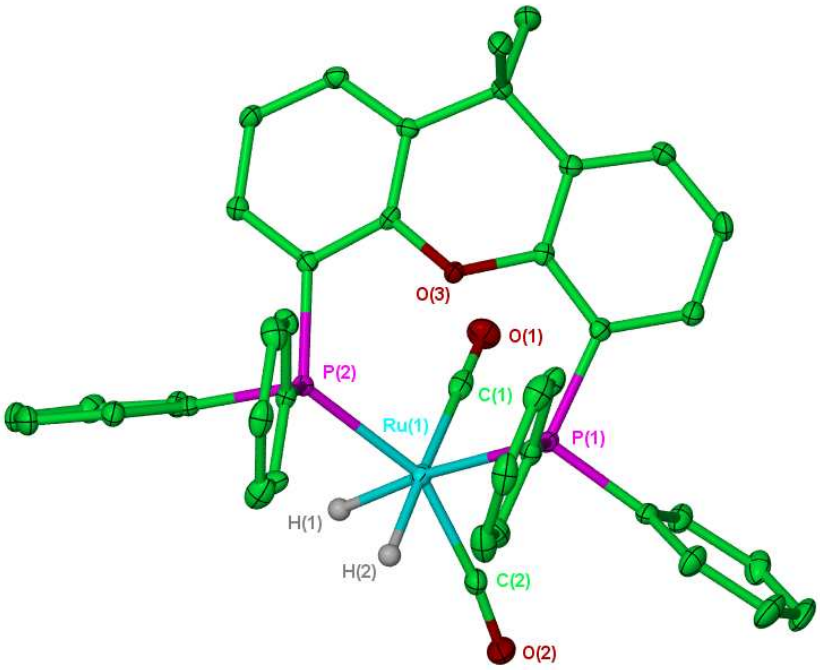

Figure 24: Molecular structure of [Ru(xantphos)(CO)$_2$H$_2$] (**4**). All hydrogen atoms except Ru-H are omitted. Thermal ellipsoids are shown at the 30% probability level.

Table 4: Selected bond lengths [Å] and angles [˚] for [Ru(xantphos)$(CO)_2H_2$] (**4**) and [Ru(xantphos)$(PPh_3)(CO)H_2$] (**2**)

	4	**2**
Ru-P_{transH}	2.4146(8)	2.3950(6)
Ru-$P_{transCO/P}$	2.3805(9)	2.3283(6)
P_{transH}-Ru-$P_{transCO/P}$	102.20(3)	102.76(2)
CO_{transH}-Ru-CO_{transP}	101.92(15)	-
CO_{transP}-Ru-$H_{transCO}$	74.2(13)	-
$P_{transCO}$-Ru-CO_{transP}/PPh_3	156.18(10)	145.16(2)

The formation of PhCHO from the stoichiometric reaction between [Ru(xantphos)$(PPh_3)(CO)H_2$] (**2**) and $PhCH_2OH$ would appear consistent with the initial oxidation step required of a catalyst for the Knoevenagel reaction. However, the formation of [Ru(xantphos)$(CO)_2H_2$] (**4**) and [Ru(xantphos)$(PPh_3)(CO)_2$] (**5**), as well as benzene and H_2, indicate that **2** is capable of decarbonylating the primary alcohol under the same conditions. Indeed, reaction of **2** with $Ph^{13}CH_2OH$ in toluene at 393 K gave rise to both [Ru(xantphos)$(^{13}CO)(CO)H_2$] and [Ru(xantphos)$(^{13}CO)_2H_2$] (and also some ^{13}CO labelled **2** and $Ph^{13}CHO$). When **4** itself was reacted with 5 eq. $PhCH_2OH$ at 393 K, the rapid formation of [Ru(xantphos)$(CO)_3$] (**6**) was observed, again *via* decarbonylation of the alcohol, as well as production of PhCHO and H_2. Further reaction of **6** with 5 eq. $PhCH_2OH$ gave small amounts of PhCHO and H_2, but no new ruthenium products could be detected in the NMR spectra even after 3 h at 393 K.

The catalytic activities of complexes **4-6** were assessed relative to the performance of [Ru(xantphos)$(PPh_3)(CO)H_2$] (**2**) in the oxidation-Knoevenagel-reduction reaction *(see Table 5)*.

Table 5: Catalytic activity of xantphos complexes in oxidation-Knoevenagel-reduction chemistry

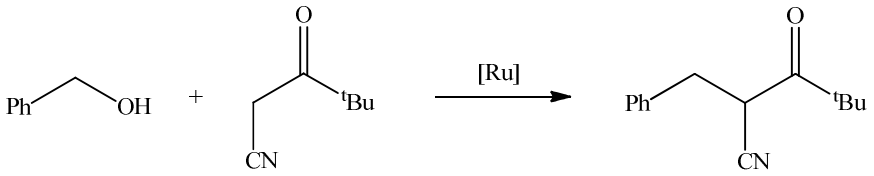

Reaction conditions: *Alcohol (1 eq.), ketonitrile (1 eq.), piperidinium acetate (5 mol%), refluxing toluene, 3 h.*

Catalyst	**Loading (mol%)**	**Time (h)**	**Conversion (%)**
[Ru(xantphos)(PPh_3)(CO)H_2] (**2**)	0.5	0.5	80
[Ru(xantphos)$(CO)_2H_2$] (**4**)	0.5	0.5	55
[Ru(xantphos)$(CO)_3$] (**6**)	0.5	0.5	30
[Ru(xantphos)(PPh_3)$(CO)_2$] (**5**)	0.5	0.5	4

Although **4** did prove to be catalytically active, after 0.5 h its performance still fell behind that of **2**, whilst **5** and **6** proved even less reactive. The poor performance of complexes **4-6** indicates that none of these ruthenium complexes can be associated with the catalytic activity of **2** in the Knoevenagel reaction. Instead, the formation of these less active species represent facile deactivation pathways for the catalyst *(see Figure 25)*. The production of the two Ru(0) complexes [Ru(xantphos)(PPh_3)$(CO)_2$] (**5**) and [Ru(xantphos)$(CO)_3$] (**6**) would appear to approach the endpoint for this deactivation.

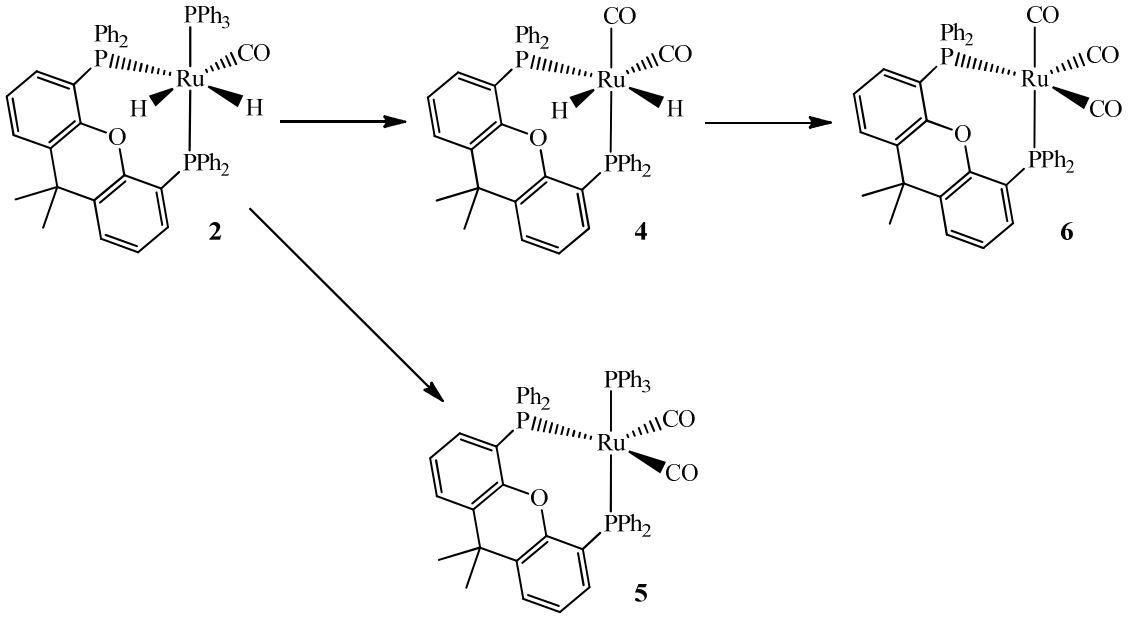

Figure 25: A simplified representation of the deactivation pathway available to [Ru(xantphos)(PPh_3)(CO)H_2] (**2**).

1.8 Decarbonylation Studies

The deactivation of organometallic catalysts by decarbonylation is a common phenomenon, frequently occurring when primary alcohols like ethanol or methanol are used as the solvents for a reaction.[38] In many cases, the presence of base is needed for decarbonylation to occur.[69] For hydroacylation reactions, where one of the substrates is a highly reactive aldehyde, decarbonylation actively competes with the reaction pathway and several strategies have been developed to inhibit this process.[70] Heteroatoms or chelation auxiliaries attached to the aldehyde moiety can temporarily co-ordinate to the metal centre where they block the vacant site needed for the acyl hydride to decarbonylate. Often masked forms of the aldehyde like aldimines or allylamines are used in preference to problematic aldehydes.

The decarbonylation process identified *via* the isolation of the ruthenium-xantphos complexes was further investigated. Studies showed that [Ru(xantphos)(PPh_3)(CO)H_2] (**2**) could decarbonylate a range of primary aromatic alcohols, including $Ph(CH_2)_nOH$ (n = 1, 2, 3) and 1,2-$C_6H_4(CH_2OH)_2$, although yields were always poor. For instance, the conversion of 3-phenylpropanol to ethylbenzene revealed a 6% conversion to product after 3 h at 393 K. This implied that the decarbonylation observed was a stoichiometric rather than a catalytic process.

To exploit the decarbonylation process catalytically, the transformation of **2** through to [Ru(xantphos)(PPh_3)$(CO)_2$] (**5**) and [Ru(xantphos)$(CO)_3$] (**6**) would need to be reversible. To this end, attempts were made to inhibit the formation of these end products. **2** and 5 eq. of $Ph(CH_2)_3OH$ were reacted together in refluxing toluene under three sets of conditions – one reaction under vacuum to encourage the removal of CO, another with the addition of PPh_3, and the last with the addition of PPh_3 under a H_2 atmosphere. All three systems successfully reduced the formation of **4-6** but were also accompanied by a concomitant decrease in the amount of decarbonylation of the alcohol.

Although catalytic decarbonylation was not possible, it was hoped that the above methods to inhibit decarbonylation could be applied to the oxidation-Knoevenagel-reduction reaction to prevent what is, for this system, an unwanted deactivation pathway. Two Knoevenagel reactions were run, one under standard conditions,[71] and the other in the presence of 3 eq. of PPh_3 under a H_2 atmosphere. The standard system achieved 81% conversion to alkylated product after 0.5 h in refluxing toluene, whilst the modified system only achieved 77% within the same time. It appears that the addition of PPh_3 and H_2 also blocks the initial co-ordination of alcohol to the catalyst as well as inhibiting the deactivation pathway.

1.9 Stoichiometric Reactivity of Benzaldehyde with 2 and 3

An investigation was prompted into the reaction of [Ru(xantphos)(PPh_3)$(CO)H_2$] (**2**) with benzaldehyde itself, since free benzaldehyde was observed as a product of the reaction between **2** and $PhCH_2OH$. Heating **2** with 5 equivalents PhCHO for 1 h in refluxing toluene led to a mixture of products *(see Figure 26)*. $PhCH_2OH$ and benzene were identified in the ^1H NMR spectrum, whilst the $^{31}P\{^1H\}$ NMR spectrum revealed the formation of large amounts of [Ru(xantphos)$(CO)_3$] (**6**), a small amount of [Ru(xantphos)(PPh_3)$(CO)_2$] (**5**), and a small amount of an unknown compound (**7**). This new complex possessed a single hydride resonance, which appeared at δ -6.14 in the ^1H NMR spectrum, displaying both a *trans* coupling and a *cis* coupling to phosphorus ($^2J_{HP}$ = 121.3 Hz, $^2J_{HP}$ = 25.8 Hz). Two doublets in the $^{31}P\{^1H\}$ NMR spectrum were identified *via* a ^1H-$^{31}P\{^1H\}$ HMQC experiment, the $^2J_{PP}$ value of 21.5 Hz indicating *cis* coordination of the xantphos ligand. $^{13}C\{^1H\}$ NMR spectroscopy revealed two carbonyl resonances, but the remaining sixth ligand could not be identified. An acyl group (COPh) was excluded as a high frequency ^{13}C resonance could not be detected, even upon reaction with $Ph^{13}CHO$.[72] Instead, it was postulated that **7** corresponded to the phenyl hydride complex [Ru(xantphos)$(CO)_2$(Ph)H], an intermediate formed from the facile decarbonylation of benzaldehyde. This was supported by the presence of

benzene and large amounts of the tricarbonyl complex **6** in the reaction mixture. We were unable to find any conditions that allowed **7** to be isolated.

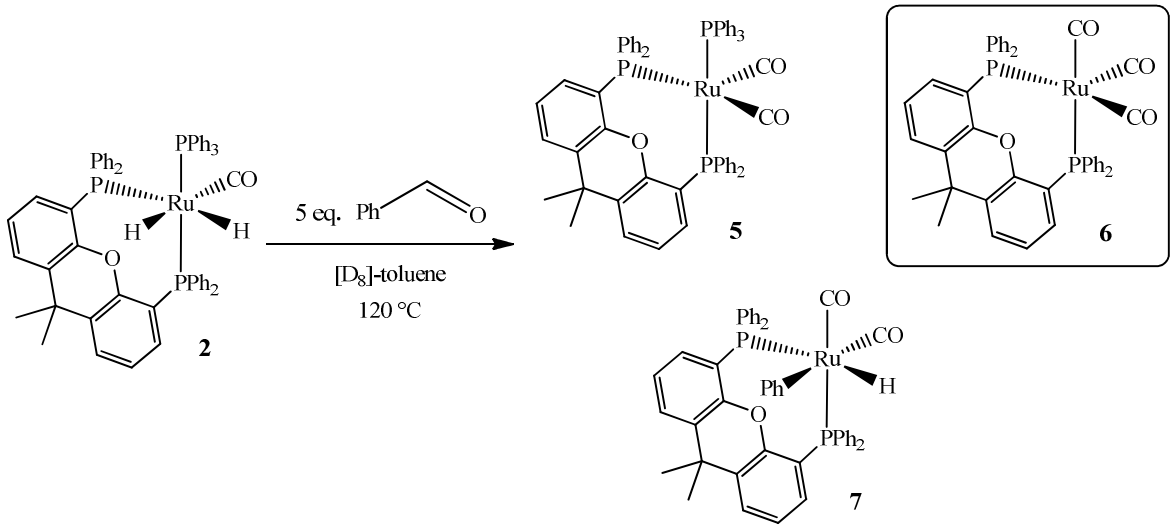

Figure 26: Reactivity of [Ru(xantphos)(PPh_3)(CO)H_2] (**2**) with benzaldehyde.

. The equivalent reaction of [Ru(dppp)(PPh_3)(CO)H_2] (**3**) with benzaldehyde gave rise to a large number of low intensity species in both the $^{31}P\{^1H\}$ NMR and ^1H NMR spectra, as well as production of $PhCH_2OH$ and a large amount of free PPh_3.

1.10 Proposed Mechanism for the Catalyst Action of 2 in the Knoevenagel Reaction

A plausible mechanism for the action of [Ru(xantphos)(PPh_3)(CO)H_2] (**2**) in the Knoevenagel reaction is shown in *Figure 27*. Loss of H_2 from **2** at the reflux temperatures employed is the most likely method of activation for the catalyst precursor. Indeed, on reaction of **2** with D_2 (1 atm. D_2, 323 K, 0.5 h), facile HD exchange was observed between the hydrides and D_2 by ^1H NMR spectroscopy. Coordination of benzyl alcohol would yield intermediate **xvii** by oxidative addition of the O-H bond, followed by β-hydride elimination to afford complex **xviii**, which could eliminate PhCHO. This process requires temporary loss of the PPh_3 ligand. Evidently [Ru(dppp)(PPh_3)(CO)H_2] (**3**) is unable to coordinate benzyl alcohol to complete this first part of the catalytic cycle.

Under stoichiometric conditions in the absence of ketonitrile, decarbonylation chemistry appears to be the dominant pathway for the reaction of the ruthenium centre in complex **b** with benzaldehyde. Loss of hydrogen from intermediate **xviii** is followed by oxidative addition of the C-H bond of the aldehyde, resulting in decarbonylation and the formation of the phenyl hydride

complex **7**. On this deactivation pathway, benzene is eliminated and hydrogen can then recombine to form the dicarbonyl dihydride complex, **4**. Interestingly, the formation of [Ru(xantphos)(PPh_3)($CO)_2$] (**5**) implies the existence of a pathway that involves reversible dechelation of the xantphos ligand, since this would be needed to retain the PPh_3 ligand whilst affording a Ru (0) oxidation state. Similarly, formation of [Ru(xantphos)($CO)_3$] (**6**) as the ultimate product of this decarbonylation process would also require dechelation of the xantphos ligand.[73]

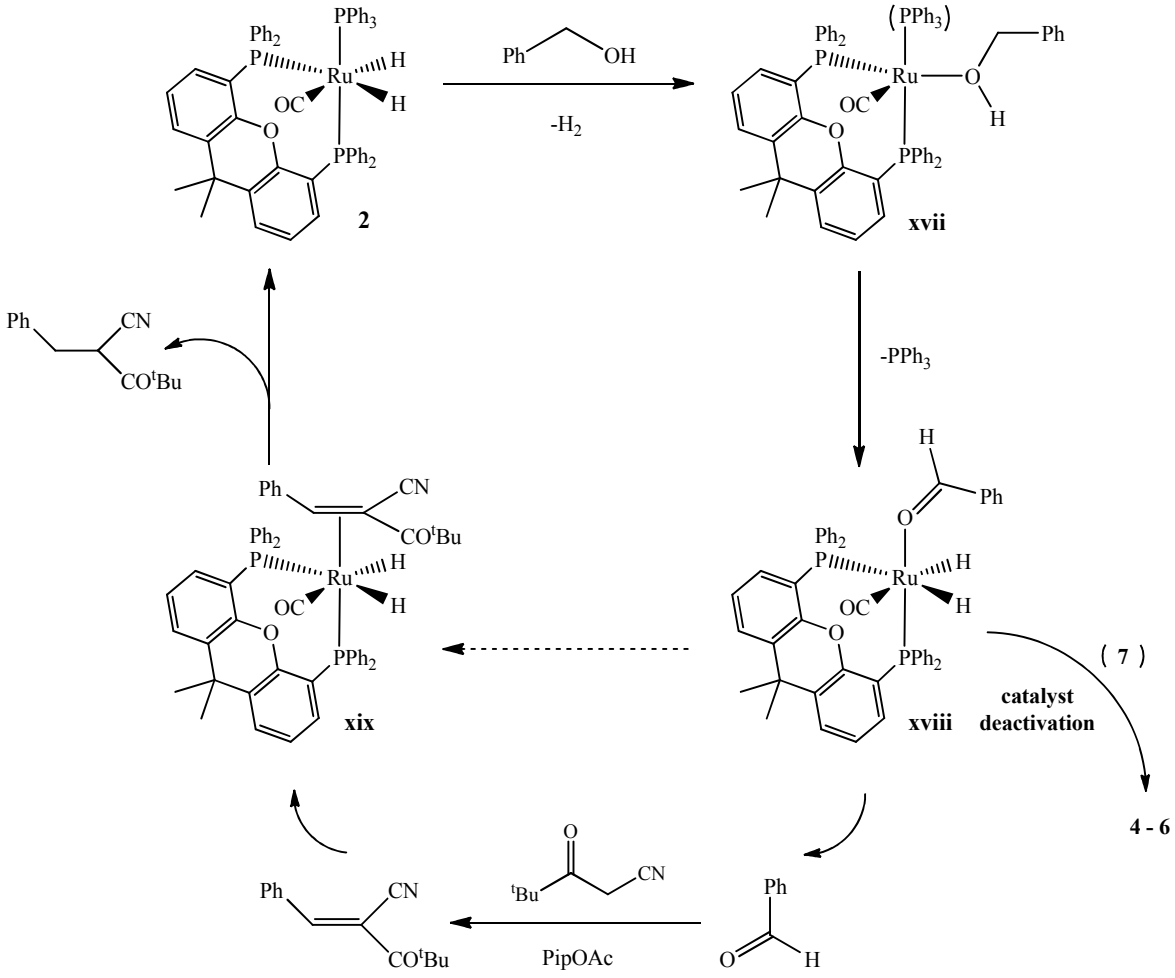

Figure 27: Proposed reaction pathways of [Ru(xantphos)(PPh_3)(CO)H_2] (**2**) for catalytic Knoevenagel chemistry and stoichiometric decarbonylation.

However, in the Knoevenagel chemistry, the complex must remain active throughout the process. In this situation, reaction of the intermediate aldehyde with the excess ketonitrile must be more facile than decarbonylation of the aldehyde by the metal centre. It also seems likely that the alkylation reaction between the aldehyde and the ketonitrile to yield the intermediate alkene occurs without involvement of the ruthenium centre, since piperidinium acetate is needed for this

transformation. Once the alkene has been generated, it can then return to the ruthenium centre to form the intermediate complex **xix**, undergoing hydrogenation to yield the desired alkylation product and reforming the catalytically active complex **2** on recombination of the PPh_3 ligand.
Although the decarbonylation chemistry displayed by **2** under stoichiometric reaction with benzyl alcohol reveals a deactivation pathway for the catalyst, it contrasts sharply with the inactivity of **3** under the same conditions. This would appear to suggest that the ability of a catalyst for alcohol activation can be linked to its affinity for decarbonylation. Indeed, $[Ir(COD)Cl]_2$ is used as the precursor for transfer hydrogenation catalysts, and will also decarbonylate aldehydes under similar conditions to this study (5 mol% Ir, refluxing dioxane).[74] Other ruthenium phosphine hydride complexes, such as $[Ru(PPh_3)_3(\eta^2\text{-}H_2)H_2]$, have also been shown to decarbonylate primary alcohols under mild conditions.[75] Thus, the decarbonylation of primary alcohols could provide us with an indication of probable catalytic activity in these systems.

1.11 CHAPTER SUMMARY

$[Ru(xantphos)(PPh_3)(CO)H_2]$ (**2**) and $[Ru(dppp)(PPh_3)(CO)H_2]$ (**3**) exhibit markedly different catalytic behaviour in the Knoevenagel reaction, echoed by the different outcomes of their stoichiometric reactions with benzyl alcohol.

The catalytically inactive complex **3** demonstrates no activity upon reaction with benzyl alcohol. In contrast, **2** will decarbonylate primary alcohols, leading ultimately to the deactivation of the catalyst by the formation of complexes **4-6**.

Whilst the deactivation pathway revealed by reaction of **2** with benzyl alcohol is not directly associated with the activity of the catalyst in the Knoevenagel reaction, it is suggested that the observed decarbonylation chemistry provides a ‘marker’ for catalytic activity in these systems.

References

1. Young, J. F., Osborn, J. A., Jardine, F. H.; Wilkinson.G; *J. Chem. Soc., Chem. Commun.*; **1965**; (7); 131-132
2. Katti, K. V., Gali, H., Smith, C. J.; Berning, D. E.; *Acc. Chem. Res.*; **1999**; *32*; (1); 9-17
3. Cannel, L. G., Slaugh, L. H.; Mullineaux, R. D.; *Chem. Abstr.*; **1965**; *62*; 16054
4. Knowles, W. S., Sabacky, M. J., Vineyard, B. D.; Weinkauff, D. J.; *J. Am. Chem. Soc.*; **1975**; *97*; (9); 2567-2568
5. van Leeuwen, P. W. N. M., Kamer, P. C. J., Reek, J. N. H.; Dierkes, P.; *Chem. Rev.*; **2000**; *100*; (8); 2741-2769
6. Thorn, D. L.; Hoffmann, R.; *J. Am. Chem. Soc.*; **1978**; *100*; (7); 2079-2090
7. Dekker, G. P. C. M., Elsevier, C. J., Vrieze, K., van Leeuwen, P. W. N. M.; Roobeek, C. F.; *J. Organomet. Chem.*; **1992**; *430*; (3); 357-372
8. Casey, C. P.; Whiteker, G. T.; *Isr. J. Chem.*; **1990**; *30*; 299-304
9. Freixa, Z.; van Leeuwen, P. W. N. M.; *Dalton Trans.*; **2003**; (10); 1890-1901
10. Strohmeier, W.; Müller, F. J.; *Chem. Ber.*; **1967**; *100*; (9); 2812-2821
11. Tolman, C. A.; *Chem. Rev.*; **1977**; *77*; (3); 313-348
12. Kamer, P. C. J., van Leeuwen, P. W. N.; Reek, J. N. H.; *Acc. Chem. Res.*; **2001**; *34*; (11); 895-904
13. (a) Brown, T. L.; *Inorg. Chem.*; **1992**; *31*; (7); 1286-1294; (b) Brown, T. L.; Lee, K. J.; *Coord. Chem. Rev.*; **1993**; *128*; (1-2); 89-116; (c) Choi, M. G., White, D.; Brown, T. L.; *Inorg. Chem.*; **1994**; *33*; (24); 5591-5594
14. (a) Hirota, M., Sakakibara, K., Komatsuzaki, T.; Akai, I.; *Comput. Chem.*; **1991**; *15*; (3); 241-248; (b) White, D., Tavener, B. C., Leach, P. G. L.; Coville, N. J.; *J. Organomet. Chem.*; **1994**; *478*; (1-2); 205-211; (c) White, D., Taverner, B. C., Coville, N. J.; Wade, P. W.; *J. Organomet. Chem.*; **1995**; *495*; (1-2); 41-51
15. Koide, Y., Bott, S. G.; Barron, A. R.; *Organometallics*; **1996**; *15*; (9); 2213-2226
16. Angermund, K., Baumann, W., Dinjus, E., Fornika, R., Gorls, H., Kessler, M., Kruger, C., Leitner, W.; Lutz, F.; *Chem. Eur. J.*; **1997**; *3*; (5); 755-764
17. Dierkes, P.; van Leeuwen, P. W. N. M.; *J. Chem. Soc., Dalton Trans.*; **1999**; (10); 1519-1529
18. Destefano, N. J., Johnson, D. K.; Venanzi, L. M.; *Angew. Chem. Int. Ed.*; **1974**; *13*; (2); 133-134
19. Hillebrand, S., Bruckmann, J., Kruger, C.; Haenel, M. W.; *Tetrahedron Lett.*; **1995**; *36*; (1); 75-78
20. The xantphos ligand is available from a range of suppliers, including Sigma-Aldrich and Acros Organics.
21. van der Veen, L. A., Keeven, P. H., Schoemaker, G. C., Reek, J. N. H., Kamer, P. C. J., van Leeuwen, P. W. N. M., Lutz, M.; Spek, A. L.; *Organometallics*; **2000**; *19*; (5); 872-883
22. Kranenburg, M., Kamer, P. C. J.; van Leeuwen, P. W. N. M.; *Eur. J. Inorg. Chem.*; **1998**; (2); 155-157
23. Cox, P. J., Kaltzoglou, A.; Aslanidis, P.; *Inorg. Chim. Acta*; **2006**; *359*; (10); 3183-3190
24. Lenero, K. A., Kranenburg, M., Guari, Y., Kamer, P. C. J., van Leeuwen, P. W. N. M., Sabo-Etienne, S.; Chaudret, B.; *Inorg. Chem.*; **2003**; *42*; (9); 2859-2866
25. Yin, J. J.; Buchwald, S. L.; *J. Am. Chem. Soc.*; **2002**; *124*; (21); 6043-6048
26. Zuideveld, M. A., Swennenhuis, B. H. G., Boele, M. D. K., Guari, Y., van Strijdonck, G. P. F., Reek, J. N. H., Kamer, P. C. J., Goubitz, K., Fraanje, J., Lutz, M., Spek, A. L.; van Leeuwen, P. W. N. M.; *J. Chem. Soc., Dalton Trans.*; **2002**; (11); 2308-2317
27. Nieczypor, P., van Leeuwen, P. W. N. M., Mol, J. C., Lutz, M.; Spek, A. L.; *J. Organomet. Chem.*; **2001**; *625*; (1); 58-66
28. (a) Heck, R. F.; Breslow, D. S.; *J. Am. Chem. Soc.*; **1961**; *83*; (19); 4023-4027; (b) Heck, R. F.; Breslow, D. S.; *J. Am. Chem. Soc.*; **1962**; *84*; (13); 2499-2502; (c) Evans, D., Osborn, J. A.; Wilkinson.G; *J. Chem. Soc. A*; **1968**; (12); 3133-3142

29. Brown, J. M.; Kent, A. G.; *J. Chem. Soc., Perkin Trans. 2*; **1987**; (11); 1597-1607
30. Devon, T. J., Whiteker, G. T., Puckette, T. A., Stavinoha, J. L.; Vanderbilt, J. J.; *US Patent 4,694,109*;
31. Kranenburg, M., Vanderburgt, Y. E. M., Kamer, P. C. J., van Leeuwen, P. W. N. M., Goubitz, K.; Fraanje, J.; *Organometallics*; **1995**; *14*; (6); 3081-3089
32. Carbo, J. J., Maseras, F., Bo, C.; van Leeuwen, P. W. N. M.; *J. Am. Chem. Soc.*; **2001**; *123*; (31); 7630-7637
33. van der Veen, L. A., Kamer, P. C. J.; van Leeuwen, P. W. N. M.; *Angew. Chem. Int. Ed.*; **1999**; *38*; (3); 336-338
34. (a) Goertz, W., Keim, W., Vogt, D., Englert, U., Boele, M. D. K., van der Veen, L. A., Kamer, P. C. J.; van Leeuwen, P. W. N. M.; *J. Chem. Soc., Dalton Trans.*; **1998**; (18); 2981-2988; (b) Casalnuovo, A. L., Rajanbabu, T. V., Ayers, T. A.; Warren, T. H.; *J. Am. Chem. Soc.*; **1994**; *116*; (22); 9869-9882
35. Marcone, J. E.; Moloy, K. G.; *J. Am. Chem. Soc.*; **1998**; *120*; (33); 8527-8528
36. Kranenburg, M., Kamer, P. C. J., Vanleeuwen, P. W. N. M., Vogt, D.; Keim, W.; *J. Chem. Soc., Chem. Commun.*; **1995**; (21); 2177-2178
37. Guillena, G., Ramon, D. J.; Yus, M.; *Angew. Chem. Int. Ed.*; **2007**; *46*; (14); 2358-2364
38. Dobereiner, G. E.; Crabtree, R. H.; *Chem. Rev.*; **2010**; *110*; (2); 681-703
39. Martinez, R., Brand, G. J., Ramon, D. J.; Yus, M.; *Tetrahedron Lett.*; **2005**; *46*; (21); 3683-3686
40. Guillena, G., Ramon, D. J.; Yus, M.; *Chem. Rev.*; **2010**; *110*; (3); 1611-1641
41. Nixon, T. D., Whittlesey, M. K.; Williams, J. M. J.; *Dalton Trans.*; **2009**; (5); 753-762
42. Edwards, M. G., Jazzar, R. F. R., Paine, B. M., Shermer, D. J., Whittlesey, M. K., Williams, J. M. J.; Edney, D. D.; *Chem. Commun.*; **2004**; (1); 90-91
43. Edwards, M. G.; Williams, J. M. J.; *Angew. Chem. Int. Ed.*; **2002**; *41*; (24); 4740-4743
44. Burling, S., Paine, B. M., Nama, D., Brown, V. S., Mahon, M. F., Prior, T. J., Pregosin, P. S., Whittlesey, M. K.; Williams, J. M. J.; *J. Am. Chem. Soc.*; **2007**; *129*; (7); 1987-1995
45. Taguchi, K., Nakagawa, H., Hirabayashi, T., Sakaguchi, S.; Ishii, Y.; *J. Am. Chem. Soc.*; **2004**; *126*; (1); 72-73
46. (a) Cho, C. S., Kim, B. T., Kim, T. J.; Shim, S. C.; *Tetrahedron Lett.*; **2002**; *43*; (44); 7987-7989; (b) Cho, C. S., Kim, B. T., Kim, T. J.; Shim, S. C.; *J. Org. Chem.*; **2001**; *66*; (26); 9020-9022
47. (a) Bower, J. F., Patman, R. L.; Krische, M. J.; *Org. Lett.*; **2008**; *10*; (5); 1033-1035; (b) Patman, R. L., Williams, V. M., Bower, J. F.; Krische, M. J.; *Angew. Chem. Int. Ed.*; **2008**; *47*; (28); 5220-5223
48. Grigg, R., Mitchell, T. R. B., Sutthivaiyakit, S.; Tongpenyai, N.; *Tetrahedron Lett.*; **1981**; *22*; (41); 4107-4110
49. Fujita, K., Li, Z. Z., Ozeki, N.; Yamaguchi, R.; *Tetrahedron Lett.*; **2003**; *44*; (13); 2687-2690
50. Black, P. J., Cami-Kobeci, G., Edwards, M. G., Slatford, P. A., Whittlesey, M. K.; Williams, J. M. J.; *Org. Biomol. Chem.*; **2006**; *4*; (1); 116-125
51. Motokura, K., Nishimura, D., Mori, K., Mizugaki, T., Ebitani, K.; Kaneda, K.; *J. Am. Chem. Soc.*; **2004**; *126*; (18); 5662-5663
52. Tillack, A., Hollmann, D., Michalik, D.; Beller, M.; *Tetrahedron Lett.*; **2006**; *47*; (50); 8881-8885
53. Gunanathan, C., Ben-David, Y.; Milstein, D.; *Science*; **2007**; *317*; (5839); 790-792
54. (a) Zhang, J., Leitus, G., Ben-David, Y.; Milstein, D.; *J. Am. Chem. Soc.*; **2005**; *127*; (31); 10840-10841; (b) Zhang, J., Leitus, G., Ben-David, Y.; Milstein, D.; *Angew. Chem. Int. Ed.*; **2006**; *45*; (7); 1113-1115
55. Slatford, P. A., Whittlesey, M. K.; Williams, J. M. J.; *Tetrahedron Lett.*; **2006**; *47*; (38); 6787-6789
56. Ledger, A. E. W., Slatford, P. A., Lowe, J. P., Mahon, M. F., Whittlesey, M. K.; Williams, J. M. J.; *Dalton Trans.*; **2009**; (4); 716-722

57. Ligands **i-iii**, **v-vi** were kindly donated by Professor P. W. N. M. Leeuwen.
58. Anand, N., Owston, N. A., Parker, A. J., Slatford, P. A.; Williams, J. M. J.; *Tetrahedron Lett.*; **2007**; *48*; (44); 7761-7763
59. Owston, N. A., Nixon, T. D., Parker, A. J., Whittlesey, M. K.; Williams, J. M. J.; *Synthesis*; **2009**; (9); 1578-1581
60. Pridmore, S. J., Slatford, P. A.; Williams, J. M. J.; *Tetrahedron Lett.*; **2007**; *48*; (29); 5111-5114
61. Pridmore, S. J., Slatford, P. A., Taylor, J. E., Whittlesey, M. K.; Williams, J. M. J.; *Tetrahedron*; **2009**; *65*; (44); 8981-8986
62. (a) Jung, C. W.; Garrou, P. E.; *Organometallics*; **1982**; *1*; (4); 658-666; (b) Kawano, H., Tanaka, R., Fujikawa, T., Hiraki, K.; Onishi, M.; *Chem. Lett.*; **1999**; (5); 401-402
63. Budzelaar, P. H. M.; *Cherwell Scientific Publishing Ltd., Oxford, UK*; **1995-1997**;
64. Obtained previously by Dr P. A Slatford.
65. Blazina, D., Dunne, J. P., Aiken, S., Duckett, S. B., Elkington, C., McGrady, J. E., Poli, R., Walton, S. J., Anwar, M. S., Jones, J. A.; Carteret, H. A.; *Dalton Trans.*; **2006**; (17); 2072-2080
66. Sanchez-Delgado, R. A., Bradley, J. S.; Wilkinson, G.; *J. Chem. Soc., Dalton Trans.*; **1976**; (5); 399-404
67. Obtained previously by Dr P. A. Slatford.
68. (a) Whittlesey, M. K., Perutz, R. N.; Moore, M. H.; *Organometallics*; **1996**; *15*; (24); 5166-5169; (b) Gottschalk-Gaudig, T., Folting, K.; Caulton, K. G.; *Inorg. Chem.*; **1999**; *38*; (23); 5241-5245; (c) Schott, D., Sleigh, C. J., Lowe, J. P., Duckett, S. B., Mawby, R. J.; Partridge, M. G.; *Inorg. Chem.*; **2002**; *41*; (11); 2960-2970; (d) Schott, D., Callaghan, P., Dunne, J., Duckett, S. B., Godard, C., Goicoechea, J. M., Harvey, J. N., Lowe, J. P., Mawby, R. J., Muller, G., Perutz, R. N., Poli, R.; Whittlesey, M. K.; *Dalton Trans.*; **2004**; (20); 3218-3224; (e) Whittlesey, M. K., Perutz, R. N., Virrels, I. G.; George, M. W.; *Organometallics*; **1997**; *16*; (2); 268-274
69. Chen, Y. Z., Chan, W. C., Lau, C. P., Chu, H. S., Lee, H. L.; Jia, G. C.; *Organometallics*; **1997**; *16*; (6); 1241-1246
70. Jun, C. H., Jo, E. A.; Park, J. W.; *Eur. J. Org. Chem.*; **2007**; (12); 1869-1881
71. Standard conditions for Knoevenagel reaction: Benzyl alcohol (1 eq.), t-butyl-ketonitrile (1 eq.), piperidinium acetate (5 mol%), [Ru(xantphos)(PPh_3)(CO)H_2] (**2**) (0.5 mol%), refluxing toluene, 3 h.
72. Waugh, M. P., Mawby, R. J., Reid, A. J., Carter, R. J.; Reynolds, C. D.; *Inorg. Chim. Acta*; **1995**; *240*; (1-2); 263-271
73. This dechelation process could well account for the broad signals seen in the $^{31}P\{^{1}H\}$ NMR spectrum for [Ru(xantphos)(PPh_3)(CO)H_2] (**2**) at 298 K.
74. Iwai, T., Fujihara, T.; Tsuji, Y.; *Chem. Commun.*; **2008**; (46); 6215-6217
75. van der Sluys, L. S., Kubas, G. J.; Caulton, K. G.; *Organometallics*; **1991**; *10*; (4); 1033-1038

2. CHAPTER 2

2.1 N-heterocyclic carbene (NHC) ligands

N-heterocyclic carbenes (NHCs) are a particular class of nucleophilic singlet state carbenes where the carbenic carbon sits traditionally within a 5-membered heterocycle, flanked by two substituted nitrogen atoms in the 1 and 3 positions of the ring *(see Figure 1)*. Typically the substituents on nitrogen are alkyl or bulky aryl groups. The C-C bond between positions 4 and 5 constitutes the backbone of the carbene and can either be saturated or unsaturated. The notation for a NHC takes the form of $IR_2R'_2$ for an unsaturated carbene or $SIR_2R'_2$ for a saturated derivative. When R' = H it is omitted from the nomenclature, and if R is an aryl or cyclic alkyl group, the numeric suffix is also removed. For instance, the notation for ICy is derived from R' = H, with R = cyclohexyl.

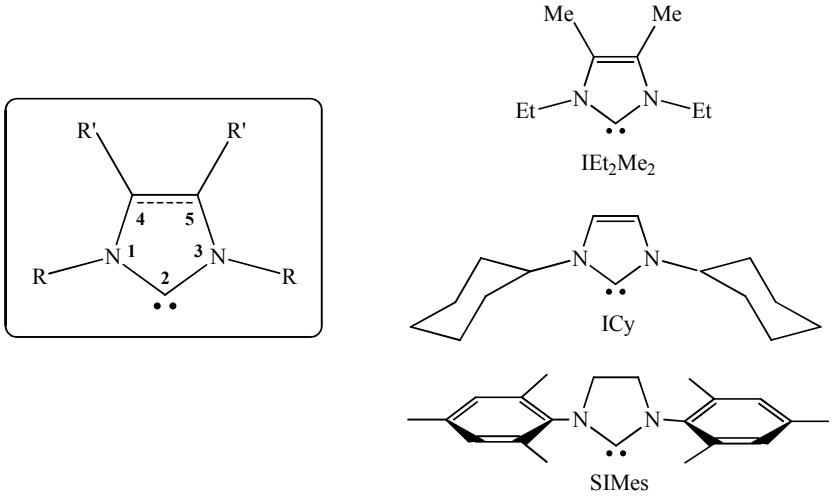

Figure 1: Structure and nomenclature of an N-heterocyclic carbene, along with some common saturated and unsaturated carbenes used in catalysis.

Their bonding to transition metal centres can be thought of as a Fischer-type interaction since the carbene has two π-donor N-substituents. However, a fundamental difference arises due to π-donation from the nitrogen lone pairs into the empty p_π orbital of the carbenic carbon *(see Figure 2)*, stabilising the carbene to such an extent that backbonding from the metal centre is significantly reduced and is generally considered to be minimal.[1] This is demonstrated by the difference in M-NHC bond lengths (>210 pm) in comparison with metal to Fischer-type carbene distances (<200 pm).[2] An NHC is therefore thought of as predominantly a σ-donor, the bonding represented by a

single bond to the metal centre rather than the double bond representation used for more traditional Fischer and Schrock type carbenes.

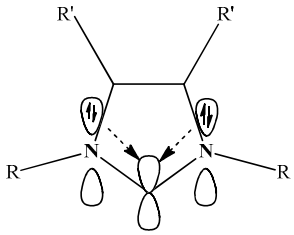

Figure 2: Diagram showing mesomeric induction from the nitrogen atoms, stabilising the NHC structure.

Initially, the inability of researchers to isolate the less sterically congested NHCs cast doubt on their use as effective ligands for catalysis. However, since then many catalytically active carbene complexes have been synthesised from imidazolium salts without ever isolating the free carbene.[3] Other researchers have successfully isolated a range of free NHC ligands for use in synthesis, and their commercial availability has increased dramatically.[4] NHC ligands have been applied extensively as spectator ligands to replace the long-established phosphines, and have often been referred to as 'phosphine mimics' in the literature. With the use of NHC ligands in catalysis rapidly increasing, these ligands have been found to differ in crucial ways from their phosphine counterparts, not least in their superior σ-donor abilities and their capacity to impart greater thermal stability on the resulting metal complexes.

Initial work by Nolan used the exothermic reaction between $[Cp^*RuCl]_4$ and L (various sterically demanding tertiary phosphines and a range of NHC ligands) to determine the enthalpy of reaction for the formation of [Cp*Ru(L)Cl]. These values could then be easily converted to bond dissociation enthalpies (BDE). The study confirmed that NHCs are better donors than phosphines for the examples examined, with the sterically demanding IAd the only exception.[5] IMes and ICy successfully displaced PCy_3 in 1:1 ligand exchange reactions that supported the findings based on the enthalpy of reaction.[6]

Early experimental reports assigned high pK_a values to the conjugate acids of NHCs – that of $I^iPr_2Me_2$ was measured at 24.0 in $[D_6]$-DMSO,[7] and a value of 22.7 recorded for the conjugate acid of I^tBu in *protio*-DMSO.[8] Theoretical studies by Yates have since provided calculated pK_a values for the conjugate acids of a series of NHCs and compared them with those of phosphines. When the average absolute pK_a values of the carbene were calculated in water, even the least basic carbene, IMe_2Cl_2, was still found to be approximately 10 pK_a units more basic than the most basic phosphine studied, $P(^tBu)_3$.[9] This leant further weight to the suggestion that NHCs have a higher capacity for σ-donation than their phosphine counterparts. More recently, work by O'Donoghue *et*

al. has provided pK_a values for the conjugate acids of nineteen NHCs in water. Once again, high values were reported (19.8-28.2) and the greatest effects on basicity were found on alteration of the ring size or N-substituent. The degree of backbone saturation had little effect on pK_a values.[10]

Other effective studies probing the differences in bonding interaction between phosphines and NHCs used the variation in carbonyl stretching frequencies in $[Ni(NHC)(CO)_3]$ and $[Rh(NHC)(CO)_2Cl]$ as markers for the strength of σ-donation.[11] All the NHC complexes prepared displayed lower carbonyl stretching frequencies than the phosphine analogues, again demonstrating their greater σ-donation. This work supported previous computational studies performed on nickel systems.[12]

The donating ability of an NHC, or the availability of its lone pair, is derived from a combination of steric and electronic effects. Less steric congestion around the carbenic carbon allows the ligand to approach the metal centre more closely, resulting in greater metal – lone pair overlap, and thereby stronger donating ability. Although studies into the steric and electronic effects of phosphines are well-established, analogous work for NHCs has only begun more recently. A better understanding of the stereo-electronic properties of these ligands should provide a more rational approach for their use in catalysis.

Early attempts were made to describe the steric characteristics of NHC ligands with various parameters, just as Tolman[11] had accomplished with phosphines. These likened an NHC to a 'fence' with both a length, expressed as the parameter A_L, and a height, A_H, and were derived from crystallographic data with the Ru-C(carbene) distance normalised at 2.105 Å.[5] Unsurprisingly, this model proved too simplistic, and a later effort instead expressed the steric bulk of the carbene in terms of % V_{Bur}.[13] This parameter described the volume occupied by a particular NHC ligand in a set sphere carved out over a 3 Å radius. This value was derived from DFT calculations positioning the carbenic carbon 2 Å from a ruthenium centre, and was also approximately the distance from the N atoms to the position of the normalised metal atom *(see Figure 3)*.

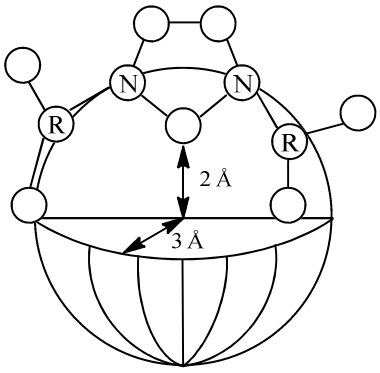

Figure 3: Steric parameter determination (% V_{Bur}) for NHC ligands, outlining sphere dimensions.

One of the main advantages of this model was that % V_{Bur} could also be applied to phosphine ligands, allowing a more direct comparison between NHC and PR_3 donors. The efficacy of this system was tested by correlating the experimentally-derived BDE values for the [Cp*Ru(L)Cl] complexes with the calculated % V_{Bur} values for each ligand L. A linear relationship was found, suggesting that the BDEs are essentially derived from the steric requirements of the NHC ligand, and that % V_{Bur} provided a reasonable parameter to describe the steric effects of various ligands.

More recent research has returned to the [Ni(NHC)$(CO)_3$] series of compounds as the basis for new DFT calculations. Gusev *et al.* have introduced a new parameter **r** (repulsiveness) to define the repulsive relationship between the carbene and the carbonyl ligands.[14] **r** itself is based upon the distance between the Ni centre and the α carbon of the carbene N-substituent. A distance of 3.493 Å was chosen as the reference (when **r** = 0.0) so that the descriptor **r** is then the deviation from this ideal. Good correlation was found between this new parameter and the more traditional % V_{bur}.

A recent review by Nolan *et al*. revisited the concept of % V_{bur}, but based calculations on linear Au(I) complexes of the form [(L)AuCl].[15] This aimed to minimise the steric effects of the surrounding moieties upon the ligand in question. In this review, the researchers were aided by the wealth of recently reported crystal structures of phosphine containing Au(I) compounds. Once again, good correlation was observed between the calculated % V_{bur} and the Tolman cone angle, θ, confirming a firm relationship between the two parameters. Initial analysis of monophosphine species was extended to bidentate phosphine analogues (by use of a [(AuCl)[R_2P-$(CH_2)_n$-PR_2](AuCl)] model) and NHC ligands, resulting in a comparison of % V_{bur} values derived from over 700 crystal structures.

Whilst the traditional view of NHC bonding considers the ligand purely as a σ-donor, more recent studies have shown that filled and empty π and π* orbitals on the imidazole ring can add to the bonding interaction between an NHC and a metal centre. Meyer *et al.* studied the tricationic portion of several electron-rich silver complexes incorporating a tridentate NHC, $TIME^{Me}$, using density functional theory.[16] Calculations concentrating on the metal to NHC bond revealed a significant overlap between the metal *d* orbitals and the carbene *p*-π hybrid orbitals. This indicated that stabilisation of the bond was at least part derived from π interactions. The electron-poor doubly C-H activated complex [Ir(I^tBu)'$_2$]PF_6 was studied by Cavallo *et al*. *(see Figure 4).*[17] Although the two vacant coordination sites are positioned in close proximity to the C-H bonds of the ^{t}Bu moieties, the crystal structure shows no evidence of agostic interactions to stabilise the 14-electron complex. Molecular orbital analysis revealed a strong electron density contribution from a filled NHC π orbital to the empty *d* orbitals on the metal centre, evidently preferred to σ donation from a C-H bond of either ^{t}Bu group.

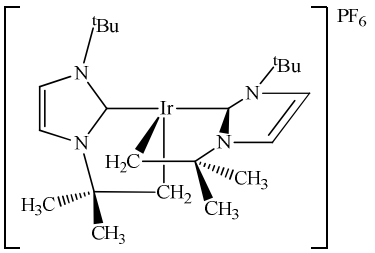

Figure 4: The electron-poor doubly C-H activated complex $[Ir(I^tBu)'_2]PF_6$.

Work on NHC complexes with both electron-rich and electron-poor metal centres has revealed that NHCs have the flexibility to either stabilise an electron-rich system as an acceptor via $d \rightarrow \pi^*$ back donation, or can contribute electron density into an electron-poor system via $\pi \rightarrow d$ donation. These π interactions may help to explain the added thermal stability of the metal-NHC bond over their phosphine-containing analogues in many catalytic systems.

Many well-established catalytic systems have benefited from the introduction of NHC ligands. In particular, the increased donor ability of NHC ligands enhanced the catalytic activity of the ruthenium-based Grubbs' alkene metathesis catalyst, $[Ru(=CHPh)(PCy_3)_2Cl_2]$, in one of the most well-known examples of modern catalyst design *(see Figure 5)*.[18]

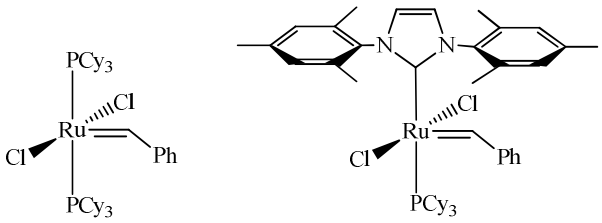

Figure 5: Grubbs' 1st generation and 2nd generation metathesis catalysts.

Initially, it was thought that the substitution of one phosphine for the strongly donating and sterically protected IMes ligand encouraged the dissociation of PCy_3 to give the 14-electron catalytic fragment, whilst also increasing the lifetime of this intermediate. In fact, later kinetic experiments with $[Ru(=CHPh)(SIMes)(C_5H_5N)_2Cl_2]$, containing substitutionally labile pyridine ligands, revealed that the carbene complex favoured alkene co-ordination over re-coordination of the phosphine to a greater extent than in $[Ru(=CHPh)(PCy_3)_2Cl_2]$.[19] This better explained the observed increase in catalytic activity upon incorporation of a carbene ligand. The concomitant increase detected in the thermal stability of $[Ru(=CHPh)(IMes)(PCy_3)Cl_2]$ also rendered it suitable for use at elevated temperatures.

Modifications to Crabtree's hydrogenation catalyst provided another example of the benefits of NHC incorporation on the thermal stability of a complex. Nolan *et al.* conducted catalytic hydrogenations of hindered alkenes with Crabtree's catalyst, $[Ir(cod)(py)(PCy_3)]PF_6$ and the NHC derivative $[Ir(cod)(py)(SIMes)]PF_6$ *(see Figure 6)*.[20] Reaction at room temperature under 60 psi of H_2 gave moderate yields of the corresponding alkanes with both catalysts. However, increasing the temperature to 323 K under the same H_2 pressure led to a marked increase in activity of the SIMes substituted complex, achieving 100% conversion in only 7 h. Crabtree's catalyst was deactivated at this temperature.

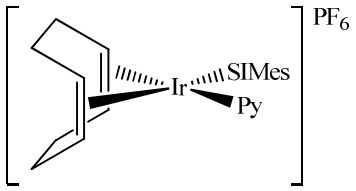

Figure 6: Structure of $[Ir(cod)(py)(SIMes)]PF_6$.

2.2 Non-Innocent Behaviour of NHCs – C-H Bond Activation

Originally regarded as inert spectator ligands, it is now evident that NHCs do not always play an innocent role. These ligands have been found to participate in a range of inter- and intra-molecular reactions and often demonstrate unexpected behaviour. This has included the observation of abnormal binding modes through the C-4/5 position,[21] recently including the first example on a ruthenium centre,[22] as well as C-N tautomerism of the carbene moiety.[23] Various migratory insertions[24] and decomposition pathways[25] involving coordinated NHC ligands have been noted, as well as substitutions of NHCs by trialkylphosphines.[26]

In particular, NHCs have been found to undergo facile intramolecular C-H bond activation.[27] This is thought to be due to a combination of two factors – the strongly σ donating NHC increasing the electron density on the metal centre, whilst the steric bulk of the carbene simultaneously forcing C-H bonds into closer proximity with the metal. Typically, C-H bond activation of the N-substituents of an NHC is observed on aryl substituted NHC complexes, as in the first example noted by Lappert in 1977.[28] Here the 16-electron complex $Ru(PPh_3)_3Cl_2$ was refluxed together with an electron rich carbene dimer in xylene to give an NHC complex with a metallated N-aryl arm. It was suggested that the excess dimer was able to act as a proton acceptor, allowing the C-H activation to occur.[29]

The carbene analogue of Chaudret's complex, [Ru(IMes)(PCy_3)(η^2-H_2)$_2$$H_2$], exhibits facile and reversible inter- and intra-molecular C-H bond activation at room temperature.[30] Both these processes were demonstrated by the rapid exchange of deuterium between [D_8]-toluene and the *ortho* methyl groups of the IMes ligand *(see Figure 7)*. Various aromatic compounds exhibited deuterium incorporation when added to a C_6D_6 solution of the complex, still at room temperature, indicating facile intermolecular C-H bond activation.

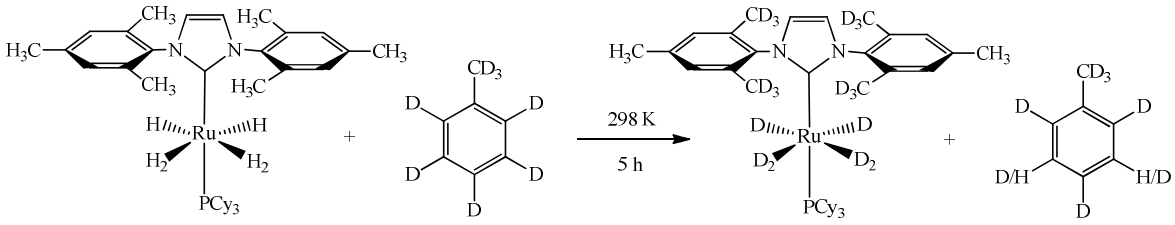

Figure 7: H/D exchange process between [Ru(IMes)(PCy_3)(η^2-H_2)$_2$$H_2$] and [$D_8$]-toluene.

Grubbs has recently reported an example of double C-H bond activation in the thermal decomposition products of a second generation alkene metathesis catalyst *(see Figure 8)*.[31] Here the benzylidene carbon atom inserted into the *ortho* C-H bond of one phenyl arm of the biph imidazol-2-ylidene ligand, displacing the PCy_3 ligand and forming an η^6 interaction to the phenyl moiety on the benzylidene group. Further insertion occurred into an *ortho* C-H bond on the other N-phenyl substituent, which created an almost perpendicular interaction between the two phenyl rings of the biph ligand. It is thought that the displaced PCy_3 ligand assists the C-H bond activation by accepting eliminated HCl to become [$HPCy_3$]Cl which was observed by NMR spectroscopy.

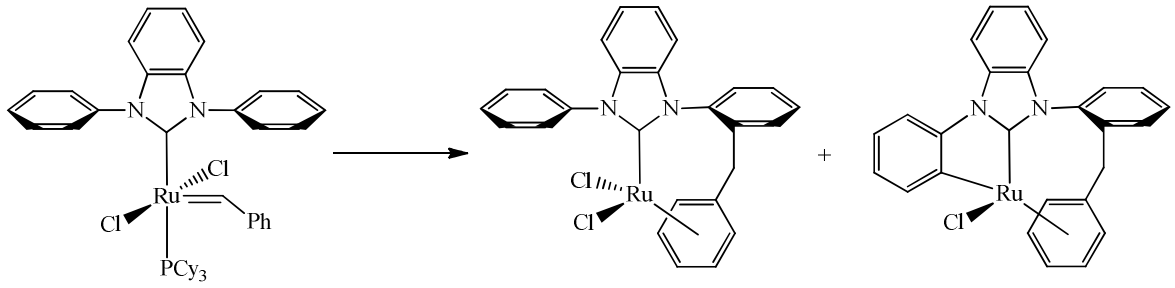

Figure 8: Thermal decomposition of a ruthenium alkene metathesis catalyst, resulting in double C-H activation of the NHC.

Work by Nolan described an example of C-H bond activation at rhodium upon complexation with a free carbene.[32] The reaction between $[Rh(COE)_2Cl]_2$ and IMes at room temperature saw the total displacement of the COE ligand along with splitting of the dimer, to form a bis-IMes product [Rh(IMes)(IMes)'HCl] with one C-H activated IMes methyl group *(see Figure 9)*. This process could be reversed by the room temperature addition of H_2 to form $[Rh(IMes)_2H_2Cl]$.

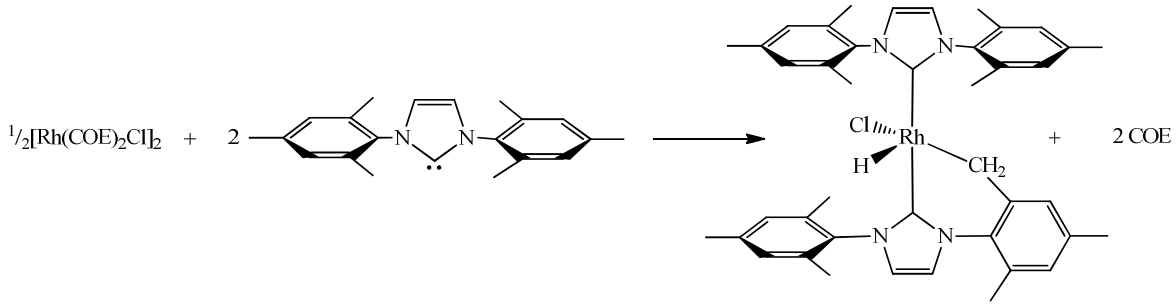

Figure 9: Reaction upon complexation between $[Rh(COE)_2Cl]_2$ and free IMes.

Work from the Whittlesey group has also proved that it is possible to activate C-H bonds in ruthenium IMes complexes.[33] $[Ru(PPh_3)_2(IMes)(CO)H_2]$ underwent C-H bond activation at room temperature to give $[Ru(PPh_3)_2(IMes)'(CO)H]$ after the addition of the hydrogen acceptor $H_2C{=}CHSiMe_3$. Only one isomer was observed and isolated; the C-H activated methyl arm of the IMes ligand sitting *trans* to the carbonyl. Morris *et al.* have also accessed another isomer of the same activated complex *via* a different route.[34]

With the aim of investigating the impact of chelating phosphines, the complexes $[Ru(dppp)(IMes)(CO)H_2]$ and the phosphine-arsine derivative $[Ru(arphos)(IMes)(CO)H_2]$ were also prepared by Whittlesey *et al.* and similarly treated with $H_2C{=}CHSiMe_3$ *(see Figure 10)*.[35] The reactions needed more forcing conditions, taking place at 373 K, but both complexes displayed C-H bond activation of one of the IMes *ortho* methyl groups along with concomitant production of $EtSiMe_3$. The ruthenium dppp complex gave only one isomer, again with the C-H activated arm *trans* to the carbonyl, whilst the arphos-containing complex, with potentially greater hemilability, gave three activated isomers. Both processes could be fully reversed with the addition of H_2.

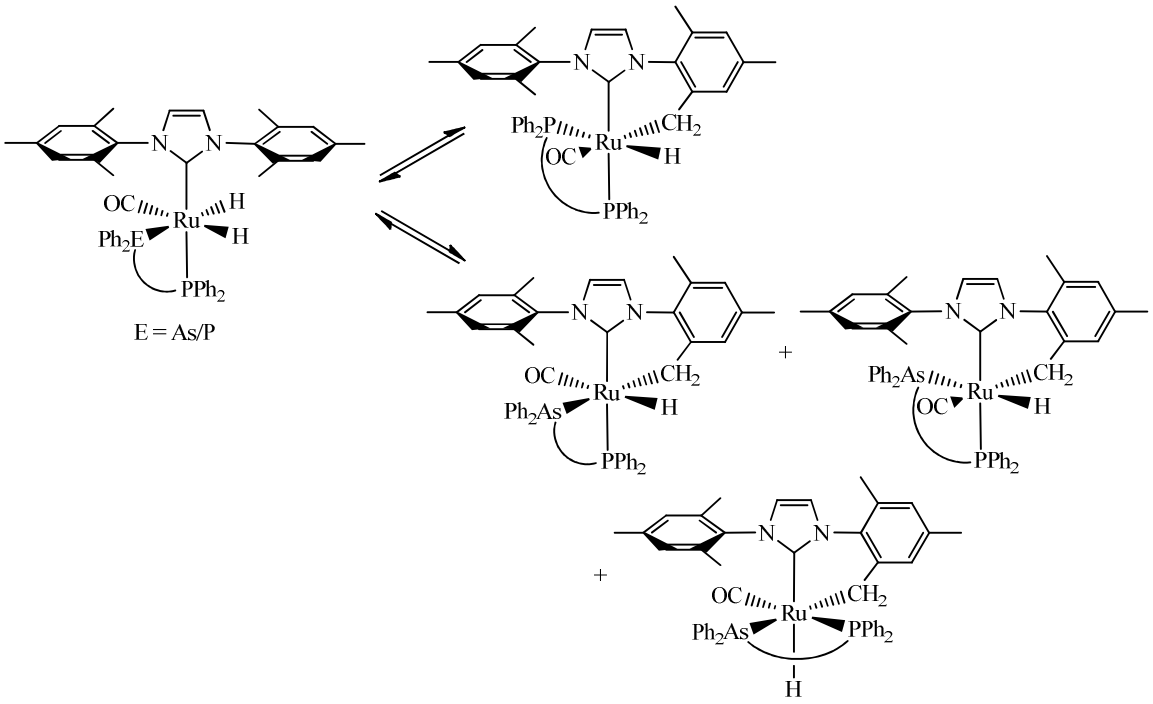

Figure 10: Reaction of [Ru(dppp)(IMes)(CO)H_2] and [Ru(arphos)(IMes)(CO)H_2] to give isomeric C-H bond activated products.

It is more difficult to induce C-H bond activation in N-alkyl substituted NHCs than in their N-aryl substituted derivatives. Although alkyl C-H bonds are weaker than aryl C-H bonds, making them easier to cleave, the M-C bonds formed in their activated products are also substantially weaker than their aryl counterparts.[36] An aryl system donates more favourable π bonding to the metal centre, whilst an aryl sp^2 carbon imparts greater s character to the bond. Both effects act to strengthen the M-C bond formed through C-H bond activation. A literature search reveals far fewer instances of C-H bond activation in N-alkyl substituted NHCs and these examples usually involve the bulkier analogues where the C-H bond is found in closer proximity to the metal centre.

Morris *et al.* tried to induce C-H bond activation in I^tBu using [Ru(PPh_3)$_3$HCl] as precursor but instead eliminated PPh_3 and I^tBuHCl to give a species proposed as "Ru(PPh_3)$_2$(I^tBu)."[34] This 14-electron species could not be isolated but its composition was deduced from NMR spectroscopy and the product, [Ru(PPh_3)$_2$(I^tBu)H_2], trapped on reaction with H_2. More recently, reaction of the same precursor with the less bulky alkyl carbenes IEt_2Me_2 and $I^iPr_2Me_2$ was reported to form a mixture of agostic and anagostic species as well as, in the case of $I^iPr_2Me_2$, the C-H activated compound, [Ru(PPh_3)$_2$($I^iPr_2Me_2$)'Cl]. Addition of 1 atm. C_2H_4 to the mixture of products found with $I^iPr_2Me_2$ led to sole formation of the C-H activated complex. Substitution of [Ru(PPh_3)$_3$HCl] for the more π-basic precursor [Ru(P^iPr_3)$_2$HCl]$_2$ resulted in a completely different set of reactions. Here, reaction with IEt_2Me_2 and $I^iPr_2Me_2$ led to initial formation of the anagostic compounds

$[Ru(P^iPr_3)_2(NHC)HCl]$. Reaction of these complexes with C_2H_4 gave an unusual double C-H activation of the carbene to give alkenyl-NHC complexes *(see Figure 11)*.[37] A subsequent one-pot reaction between $[Ru(Cl)_2(COD)]_x$, $I^iPr_2Me_2$, KO^tBu and either PCy_3 or PPh_3 led to the isolation of complexes of the form $[RuCl(I^iPr_2Me_2)''(PR_3)_2]$, again displaying double C-H activation of the N-alkyl substituent.[38]

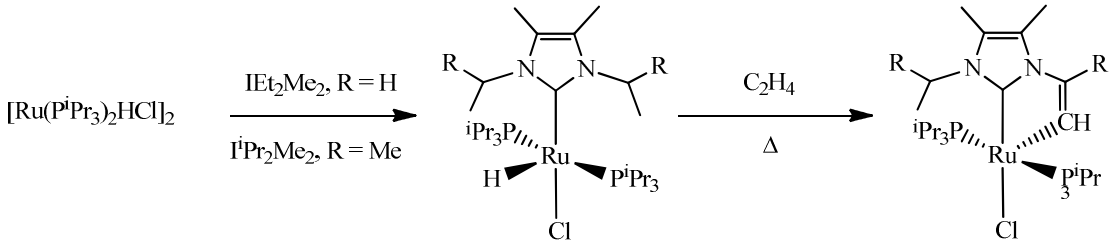

Figure 11: Products of the reaction between $[Ru(P^iPr_3)_2HCl]_2$ and IEt_2Me_2 and $I^iPr_2Me_2$ followed by reaction with 1 atm. C_2H_4.

Much work has been devoted to a more complete understanding of the factors governing C-H activation, in particular with unsymmetrical carbenes possessing both an alkyl and an aryl N-substituent. Whilst C-H bond activation of aryl hydrocarbons is favoured both thermodynamically and kinetically, the 5-membered metallacycle formed by C-H bond activation of an alkyl substituent is favoured over the 6-membered metallacycle formed on activation of an aryl substituent.

In work by Peris *et al.*,[39] unsymmetrical NHCs were reacted with $[Cp^*IrCl_2]_2$,[40] to see whether aryl or alkyl activation was favoured *(see Figure 12)*. Treatment of 1-benzyl-3-*tert*-butylimidazolium chloride with Ag_2O, followed by addition of $[Cp^*IrCl_2]_2$ resulted in the selective C-H bond activation of the alkyl arm. However, reaction of 1-benzyl-3-isopropylimidazolium chloride with $[Cp^*IrCl_2]_2$ in refluxing acetonitrile/KOH gave cyclometallation of the aryl arm. This difference in reactivity led the researchers to conclude that steric factors played the most important role in C-H bond activation – the *tert*-butyl group having a C-H bond in much closer proximity to the metal centre than in the isopropyl system.

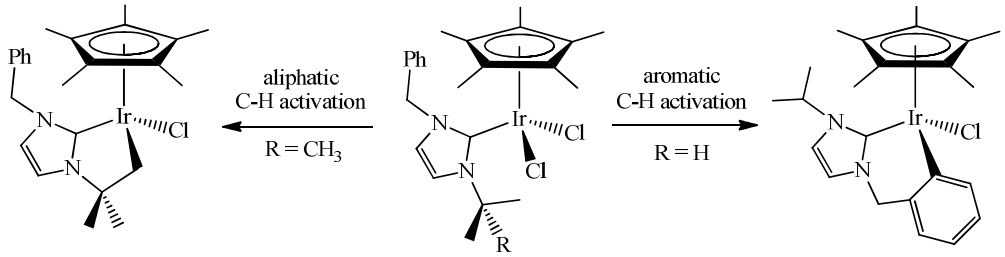

Figure 12: Alkyl and aryl C-H bond activation of unsymmetrical NHCs.[39]

Yamaguchi *et al.* also conducted a similar experiment, again synthesising a range of $[Cp^*Ir(NHC)Cl_2]$ complexes where the steric bulk of the NHC was gradually increased by lengthening the alkyl chain of the N-alkyl substituents, from IEt, to I^nPr, and finally through to I^nBu.[41] The reaction of $[Cp^*Ir(IEt)Cl_2]$ with 2 equivalents of i-PrONa in isopropyl alcohol resulted in the intramolecular C-H bond activation of one ethyl arm. In contrast, the reactions of the other derivatives gave $[Cp^*Ir(NHC)H_2]$ species as the main products, derived from β-hydride elimination of the intermediate alkoxo species $[Cp^*Ir(NHC)(O^iPr)]Cl$. Once again, the study demonstrated that the reactivity of these complexes is very sensitive towards steric variation of the N-alkyl substituent. An identical conclusion was drawn from a similar study reacting an aryl/alkyl substituted NHC with $[(p\text{-cymene})RuCl_2]_2$ rather than $[Cp^*IrCl_2]_2$.[42]

Nolan and co-workers have achieved the double C-H bond activation of I^tBu on both rhodium and iridium centres, isolating complexes of the form $[M(I^tBu)'_2Cl]$ via reaction with $[M(COE)_2Cl]_2$ *(see Figure 13)*.[43] Other products could also be isolated if the reaction was carried out in different solvents (Rh) or for varying lengths of time (Ir). This allowed a hydride species where only one I^tBu ligand had activated, $[M(I^tBu)(I^tBu)'HCl]$, to be isolated. Abstraction of the chloride anion in $[M(I^tBu)'_2Cl]$ with $AgPF_6$ enabled the isolation of the naked 14-electron complexes, $[M(I^tBu)'_2]PF_6$, which possessed an unusual all-carbon environment around the metal centre. As mentioned previously, these complexes lacked any agostic interactions, and later DFT calculations revealed the stabilisation of the empty *d*-orbitals on the metal centre by a filled NHC π orbital.

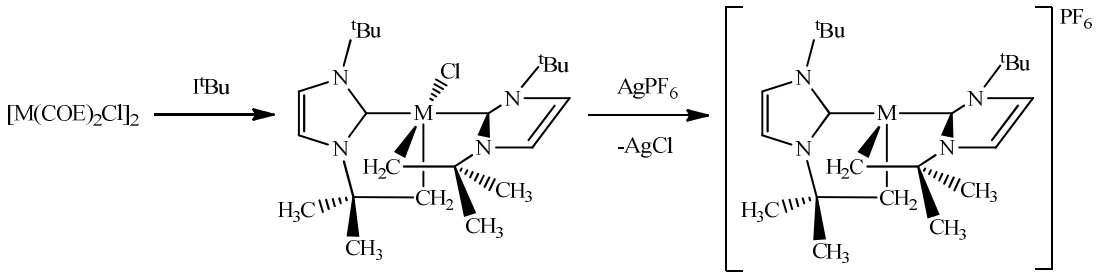

Figure 13: Complexes isolated on reaction of $[M(COE)_2Cl]_2$ (M = Rh, Ir) with I^tBu.

The Whittlesey group have also reported the C-H bond activation of N-alkyl substituted NHCs.[33] In particular, thermolysis of $[Ru(PPh_3)_2(IEt_2Me_2)(CO)H_2]$ in the presence of $H_2C{=}CHSiMe_3$ gave C-H bond activation to yield two isomers of $[Ru(PPh_3)_2(IEt_2Me_2)'(CO)H]$. The reaction was easily reversed by the introduction of a H_2 atmosphere. A more unusual reaction took place when the precursor $[Ru(PPh_3)_3(CO)H_2]$ was reacted with 4 equivalents of $I^iPr_2Me_2$. Here the C-H bond activated product $[Ru(PPh_3)_2(I^iPr_2Me_2)'(CO)H]$ was obtained directly without the need for a hydrogen acceptor in the reaction.[44]

2.3 Ruthenium NHC Complexes in C-C Bond Formation from Alcohols

Several groups have used ruthenium complexes incorporating NHC ligands as extremely effective 'borrowing hydrogen' catalysts. Peris *et al.* have utilised an unusual N-heterocyclic bis-carbene with a central triazole unit, and were able to form both dinuclear and tetranuclear ruthenium complexes on reaction with [Ru(*p*-cymene)Cl_2]$_2$ *(see Figure 14)*. Both types of complex then proved active for a β-alkylation reaction between primary and secondary alcohols, performing to a similar degree at only 1 mol% ruthenium loading.[45] More recently, the group have used another unusual N-heterocyclic carbene, pyrazolin-3-ylidene, and observed even greater activity in the same system with use of a mononuclear Ru(*p*-cymene)(NHC)-based complex.[46]

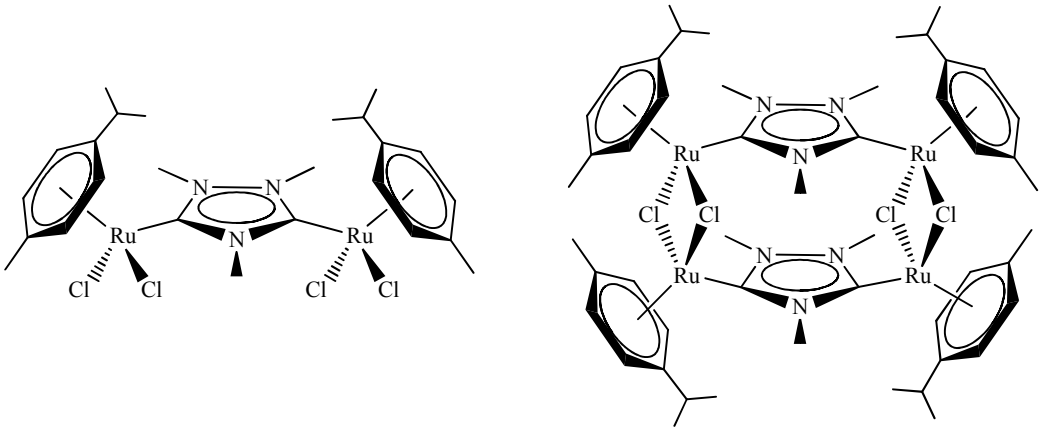

Figure 14: Dinuclear and tetranuclear ruthenium complexes formed on reaction of triazolediylidene (ditz) carbene with [Ru(*p*-cymene)Cl_2]$_2$.[45]

Another system developed by Crabtree *et al.* reacted a pyrimidine-NHC chelating ligand with [Ru(*p*-cymene)Cl_2]$_2$.[47] It was hoped that the pyrimidine group would introduce some lability to the system, resulting in higher catalytic activity. In practice, the ruthenium complex was effective for the β-alkylation of secondary alcohols and also for the N-alkylation of various amines with primary alcohols, although higher activities were observed when the NHC was employed alongside iridium rather than ruthenium.

Whilst the reaction between primary alcohols and amines generally results in the production of further substituted amines, Madsen and coworkers found that the addition of an NHC to their *in situ* catalytic system ([Ru(COD)Cl_2] in combination with P(Cyp)$_3$) resulted in the unusual formation of a range of amides from these two substrates.[48] The researchers argued that the strong coordination of the ruthenium centre to first the aldehyde and then the hemiaminal formed during the catalysis was able to prevent the formation of imines, resulting in the observed amide

products *(see Figure 15)*. The process has since been extended to a number of different Ru(II) precursors in combination with I^iPr_2. The different precursor combinations have allowed the researchers to synthesise a wide range of amides in good to excellent yields.[49]

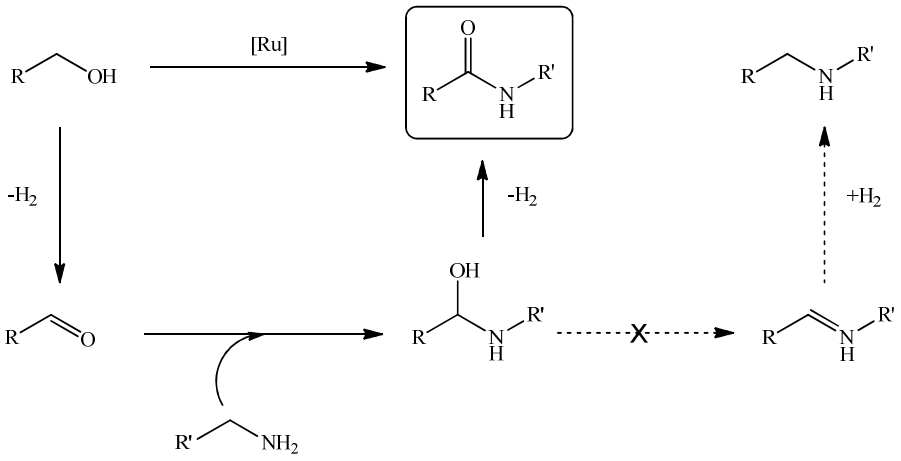

Figure 15: Proposed catalytic cycle for the formation of amides from alcohols and amines.[48]

Williams and Whittlesey have been able to exploit the facile C-H activation observed in their systems for transfer hydrogenation applications. Bubbling hydrogen through a solution of $[Ru(PPh_3)_2(I^iPr_2Me_2)'(CO)H]$, or reaction with isopropanol, afforded the corresponding dihydride complex $[Ru(PPh_3)_2(I^iPr_2Me_2)(CO)H_2]$ which could then be switched back to a mixture of two C-H activated isomers upon addition of $H_2C{=}CHSiMe_3$ *(see Figure 16)*. It proved possible to utilise this facile and reversible C-H activation in a 'borrowing hydrogen' methodology and the system formed a highly active catalyst for an indirect Wittig reaction.[50]

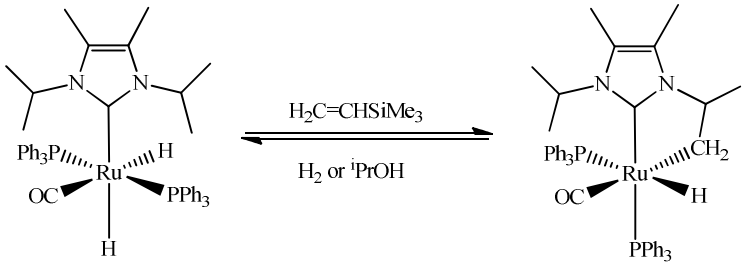

Figure 16: Switching back and forth between the dihydride and the C-H bond activated product.[50]

A number of ruthenium complexes have been used in combination with N-heterocyclic carbenes to affect a wide range of 'borrowing hydrogen' strategies. The reversible C-H bond activation of NHC ligands has been successfully utilised in a range of C-C bond forming reactions in previous work in the Whittlesey and Williams group collaboration. Similarly, the incorporation

of a xantphos diphosphine ligand has been very effective for the oxidation-Knoevenagel-reduction system, as described in Chapter 1. It was therefore of interest to assess the catalytic activity of a system where an NHC was coordinated in addition to the xantphos ligand. To this end, the PPh_3 ligand in [Ru(xantphos)(PPh_3)(CO)H_2] (**2**) was exchanged for various NHCs resulting in a series of [Ru(xantphos)(NHC)(CO)H_2] complexes.

2.4 Spontaneous C-H Activation of NHCs on Reaction with [Ru(xantphos)(PPh_3)(CO)H_2] (2)

Reaction of **2** with 3 equivalents of the N-alkyl substituted carbenes IEt_2Me_2 or $I^iPr_2Me_2$ in refluxing toluene for 3 h and 1.5 h respectively resulted in direct C-H bond activation of the carbene to give [Ru(xantphos)(NHC)'(CO)H] *(Figure 17)*. Unusually, the C-H bond activation was achieved spontaneously without the presence of a hydrogen acceptor in the reaction mixture.

The single hydride resonance at δ -7.63 in the ^1H NMR spectrum of [Ru(xantphos)(IEt_2Me_2)'(CO)H] (**8**) exhibited two ^{31}P couplings; one a *trans* coupling ($^2J_{HP}$ = 114.1 Hz), the other a *cis* coupling with $^2J_{HP}$ = 23.0 Hz. As expected, the xantphos ligand displayed two doublet resonances in the $^{31}P\{^1H\}$ NMR spectrum, the $^2J_{PP}$ value of 17.5 Hz clearly revealing a *cis* orientation of the diphosphine. The phosphorus signal at δ 29.1 was assigned as that *trans* to the hydride by a ^1H-$^{31}P\{^1H\}$ HMQC experiment. Both the carbonyl and carbenic carbon signals displayed a doublet of doublets multiplicity in the $^{13}C\{^1H\}$ NMR spectrum, with the latter exhibiting an obvious *trans* ^{31}P coupling of 85.7 Hz. This allowed the unambiguous assignment of a structure where the NHC sits *trans* to one arm of the xantphos ligand, with the carbonyl *cis* to both phosphorus atoms and therefore, by deduction, *trans* to the activated arm of the carbene.

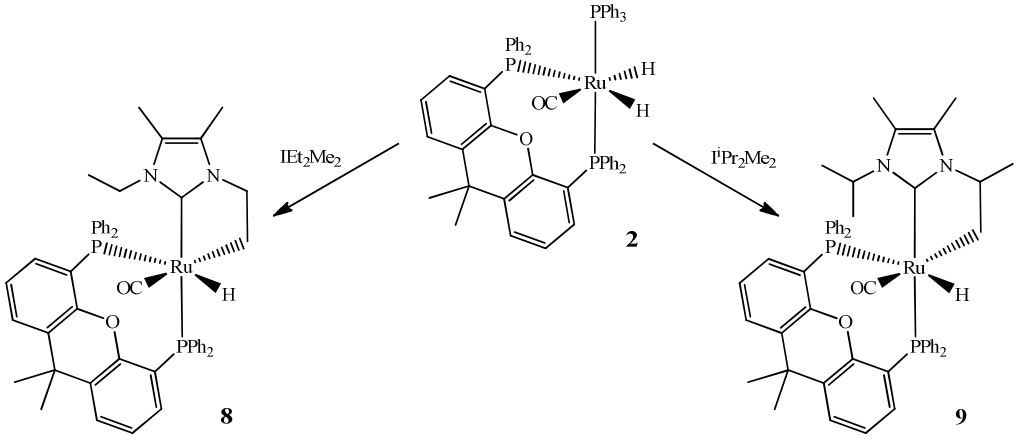

Figure 17: Synthesis of [Ru(xantphos)(NHC)'(CO)H] (IEt_2Me_2 = **8**, $I^iPr_2Me_2$ = **9**).

The N-^{i}Pr substituted analogue [Ru(xantphos)($I^iPr_2Me_2$)'(CO)H] (**9**) proved insoluble in most common NMR solvents (even [D_5]-pyridine) but showed partial solubility in toluene allowing

for limited NMR characterisation. The single hydride resonance indicative of C-H bond activation was detected at δ -7.96 in the ^{1}H NMR spectrum, with multiplicities echoing those of **8**. ^{31}P{^{1}H} NMR revealed two poorly resolved resonances at δ 28.4 and 46.7, and an extended (128 scans) ^{1}H-^{13}C{^{1}H} HMBC experiment was able to identify the carbonyl resonance at δ 208.1 and the carbenic carbon at δ 189.7 via correlation with the hydride resonance. The geometry of **9** was firmly established by an X-ray crystal structure *(Figure 18)*.

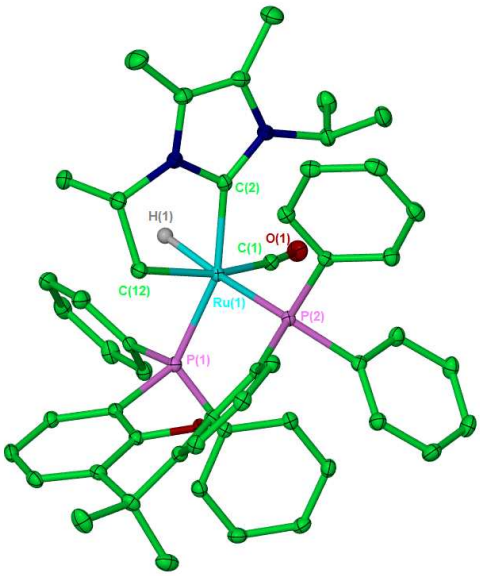

Figure 18: Molecular structure of [Ru(xantphos)(I^{i}Pr$_2$Me$_2$)'(CO)H] (**9**). All hydrogen atoms except Ru-H are omitted. Thermal ellipsoids are shown at the 30% probability level.

Table 1: Selected bond lengths [Å] and angles [˚] for [Ru(xantphos)(I^{i}Pr$_2$Me$_2$)'(CO)H] (**9**) and [Ru(PPh$_3$)$_2$(I^{i}Pr$_2$Me$_2$)'(CO)H][50]

	9	[Ru(PPh$_3$)$_2$(I^{i}Pr$_2$Me$_2$)'(CO)H]
Ru-C_{NHC}	2.056(2)	2.0594(16)
Ru-CH_2	2.196(2)	2.2100(16)
Ru-$P_{transNHC}$	2.3414(6)	2.3445(4)
Ru-P_{transH}	2.4558(6)	2.4357(4)
Ru-CO	1.866(3)	1.8626(17)
C_{NHC}-Ru-$P_{transNHC}$	160.43(7)	162.97(4)
P-Ru-P	103.32(2)	102.152(15)
C_{NHC}-Ru-CH_2	77.35(9)	76.72(6)

Comparison with the previously obtained crystal structure of [Ru(xantphos)(PPh_3)(CO)H_2] (**2**) reveals that the xantphos bite angle changes very little with the introduction and activation of a carbene, increasing only slightly from 102.76(2)˚ to 103.32(2)˚. The bond angles of **9** are actually much closer to those of a regular octahedron than in **2**, probably due to the smaller bulk of the carbene relative to the phosphine. The small size of the carbene and the activation of one isopropyl arm also allow it to sit much closer to the metal centre than the phosphine, the Ru-C_{NHC} distance measured at only 2.056(2) Å in comparison with the Ru-PPh_3 bond distance of 2.2973(6) Å found in **2**. The angle between the carbenic carbon and the activated arm is noticeably quite acute, and away from the octahedral ideal, at 77.35(9)˚.

The X-ray crystal structure of **9** can be compared directly with the *bis* triphenyl phosphine analogue [Ru(PPh_3)$_2$($I^iPr_2Me_2$)'(CO)H] previously prepared in the group,[50] since the two complexes adopt identical geometries. Despite the added steric bulk of the xantphos ligand, the bond lengths and angles found for the two complexes are remarkably similar *(see Table 1)*. The bite angles adopted by the xantphos diphosphine in both complexes are significantly smaller than that of the free ligand (111˚) suggesting that the angle on complexation is dictated more by the requirements of the complex than by xantphos itself.

The IR spectrum of [Ru(xantphos)($I^iPr_2Me_2$)'(CO)H] (**9**) revealed a carbonyl band at 1878 cm^{-1}, somewhat higher than that detected for the IEt_2Me_2 derivative (1863 cm^{-1}), indicating less back-bonding to the carbonyl from the metal centre. This suggests that the electron density at ruthenium is reduced when $I^iPr_2Me_2$ is substituted for IEt_2Me_2, although this could also result from a difference in the bond angles between the two structures.

The reaction of [Ru(xantphos)(PPh_3)(CO)H_2] (**2**) with the N-aryl carbene IMes again resulted in direct C-H bond activation of the NHC. In this case, the NMR data suggested the presence of two isomers of [Ru(xantphos)(IMes)'(CO)H] (**10**). ^{1}H NMR spectroscopy revealed the presence of two hydride signals at δ -8.72 and -9.51, in a 9:1 ratio. Both resonances displayed a doublet of doublets splitting pattern, with a *trans* coupling and a *cis* coupling to ^{31}P apparent in each - the major signal with $^2J_{HP}$ values of 114.7 and 27.6 Hz, the minor resonance with $^2J_{HP}$ values determined at 112.6 and 26.6 Hz. A ^{1}H-^{31}P{^{1}H} HMQC experiment correlated each hydride to two ^{31}P signals, with a $^2J_{PP}$ value of 18 Hz discernable in the major species. The carbonyl resonance for this product was detected as a triplet at δ 205.4 whilst the carbenic carbon appeared as doublet of doublets at δ 195.8, exhibiting an obvious *trans* ^{31}P coupling of 87 Hz. ^{13}C{^{1}H} NMR spectroscopy could not pick up signals for the minor isomer. The similarity of the data indicates that the two isomers are structurally close, and, we believe, differ only in the relative positions of the carbonyl and one terminus of the xantphos ligand *(see Figure 19)*, although we are unable to confirm this without ^{13}C{^{1}H} NMR data.

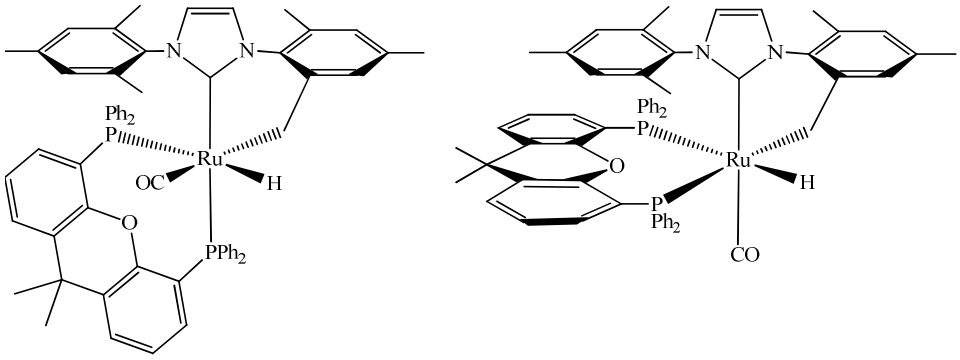

Figure 19: The two possible isomers of [Ru(xantphos)(IMes)'(CO)H] (**10**).

Attempts were made to synthesise additional analogues of [Ru(xantphos)(NHC)'(CO)H] with the N-alkyl carbene I^{t}Bu and the bulky N-aryl carbene IPr. The reaction between **2** and 6 equivalents of I^{t}Bu in refluxing toluene gave a large number of products, although a hydride apparently corresponding to a postulated C-H activated species was detectable at δ -8.02. The addition of trimethylvinyl silane failed to increase the proportion of this compound and attempts at recrystallization were unsuccessful.

The corresponding reaction between **2** and IPr also proved unsuccessful. No reaction occurred at 298 K, but after 1 h at 393 K, two new hydride resonances could be detected in the ^{1}H NMR spectrum at δ -6.44 and -8.68. A *trans* ^{31}P coupling of 86.4 Hz was discernable on the latter resonance. Both signals reduced to two doublets upon ^{31}P decoupling, suggesting formation of the dihydride complex [Ru(xantphos)(IPr)(CO)H_2]. Unfortunately the reaction never reached completion, achieving at best only 50% conversion to product even with a larger number of equivalents of carbene and longer reaction times. Evidently, the added steric bulk of IPr together with that of the xantphos ligand hinders the coordination of carbene suggesting a steric limit for these reactions, further demonstrated by the absence of any C-H activated product in the reaction mixture.

2.5 Interconversion of [Ru(xantphos)(NHC)'(CO)H] and [Ru(xantphos)(NHC)(CO)H_2]

As seen in previous studies, carbene C-H activation could be reversed by the addition of H_2.[33, 35, 50-51] The introduction of H_2 to a solution of [Ru(xantphos)(IEt$_2$Me$_2$)'(CO)H] (**8**) afforded the dihydride complex [Ru(xantphos)(IEt$_2$Me$_2$)(CO)H_2] (**11**) after 24 h at room temperature and could be accelerated to completion in only 3 h by heating at 343 K. The dihydride complex displayed two hydride resonances in the ^{1}H NMR spectrum at δ -5.54 and -7.62. The hydride at lower frequency appeared as a sharp and well-defined signal at room temperature, and could be

easily identified as that *trans* to phosphorus ($^2J_{HP}$ = 93.9 Hz). The higher frequency hydride resonance was extremely broad, indicating fluxionality in the structure, and remained poorly resolved, even upon cooling to 233 K. Two signals were observed for the methyl backbones of the carbene implying restricted rotation about the Ru-C_{NHC} bond. The $^{31}P\{^1H\}$ NMR spectrum at 298 K displayed two very broad resonances at δ 52.0 and 35.8, which resolved into the expected two doublets upon cooling ($^2J_{PP}$ = 16 Hz). A second minor species was also detected at low temperature which displayed two hydride signals at δ -5.98 and -7.54; these correlated to two ^{31}P signals at ca. δ 44 and 30 ($^2J_{PP}$ = 19 Hz). The low concentration of this species precluded further characterisation but it was tentatively assigned as an isomer of [Ru(xantphos)(IEt_2Me_2)(CO)H_2] (**11**).

Regeneration of **8** also proved facile; leaving a freeze-pump-thaw degassed solution of **11** under a vacuum reformed the C-H activated complex **8** after 24 h at room temperature, or within 3 h at 343 K. Successive use of H_2 and vacuum at 343 K allows the system to shuttle back and forth between **11** and **8** *(see Figure 20)*. Partial C-H bond activation could even be achieved under a H_2 atmosphere if temperatures over 343 K were employed, illustrating the ease of H_2 dissociation.

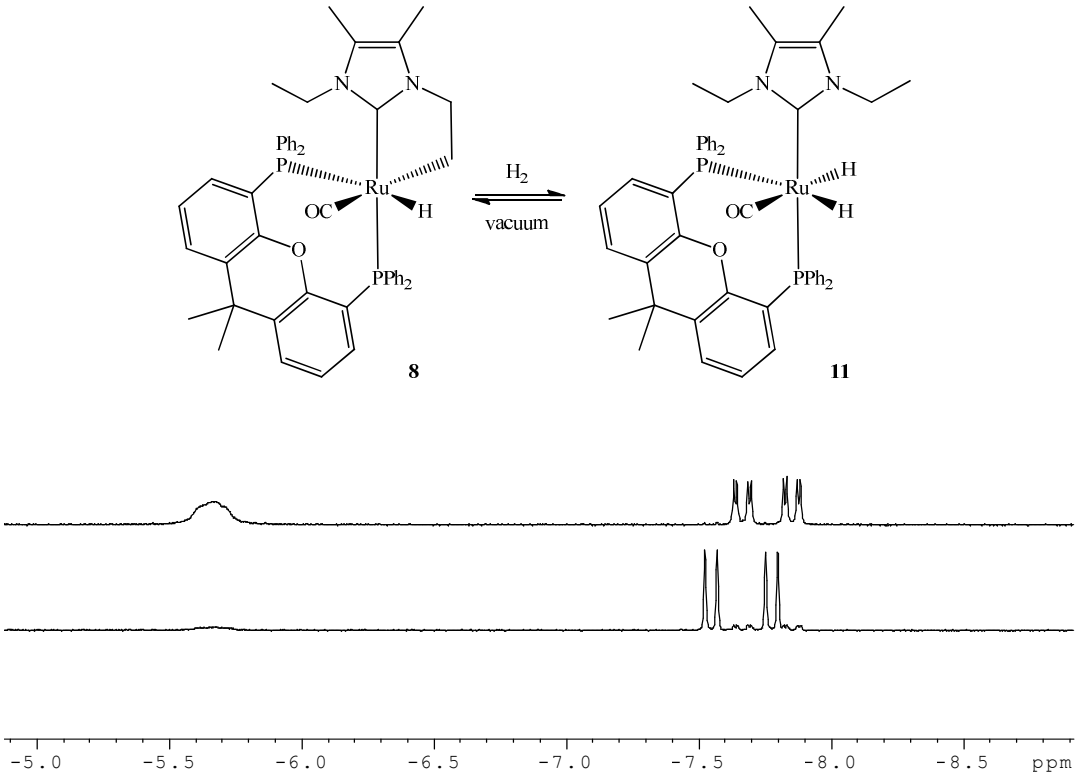

Figure 20: Selected ^1H NMR ([D_8]-toluene, 500 MHz, 298 K) *(hydride region)*: the dihydride complex [Ru(xantphos)(IEt_2Me_2)(CO)H_2] (**11**) *(upper spectrum)* and the C-H bond activated species [Ru(xantphos)(IEt_2Me_2')(CO)H] (**8**) *(lower spectrum)*.

The insolubility of [Ru(xantphos)($I^iPr_2Me_2$)'(CO)H] (**9**) and [Ru(xantphos)(IMes)'(CO)H] (**10**) precluded the addition of H_2 to the complexes, since any attempt to freeze-pump-thaw the solutions precipitated irreversibly [Ru(xantphos)(NHC)'(CO)H] before H_2 could be introduced. Similarly, attempts to add benzyl alcohol as a source of hydrogen to a solution of [Ru(xantphos)(NHC)'(CO)H] led to displacement of the carbine and decarbonylation of the alcohol to give [Ru(xantphos)$(CO)_2H_2$] (**4**) and [Ru(xantphos)$(CO)_3$] (**6**) as the ultimate products.

2.6 Treatment of [Ru(xantphos)$(PPh_3)(CO)H_2$] (2) with ICy

Reaction of (**2**) with the N-cyclohexyl carbene ICy gave quantitative formation of the ICy dihydride complex [Ru(xantphos)(ICy)$(CO)H_2$] (**12**) *(see Figure 21).* Two hydride resonances were detected in the ^{1}H NMR spectrum at δ –7.85 and -5.69, the lower frequency resonance exhibiting a *trans* coupling to phosphorus ($^2J_{HP}$ = 93.0 Hz). Once again, as in [Ru(xantphos)$(IEt_2Me_2)(CO)H_2$] (**11**), two signals were detected for the backbone resonances, indicating restricted rotation about the Ru-C_{NHC} bond, and two doublets ($^2J_{PP}$ = 15.0 Hz) in the $^{31}P\{^1H\}$ NMR confirmed the *cis* orientation of the xantphos ligand.

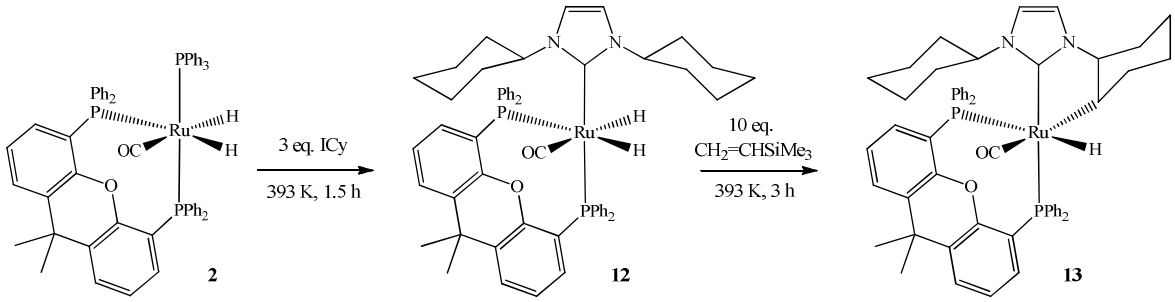

Figure 21: Reaction between [Ru(xantphos)$(PPh_3)(CO)H_2$] (**2**) and ICy, followed by C-H activation on addition of the hydrogen acceptor H_2C=CHSiMe_3.

The molecular structure of **12** was confirmed by X-ray crystallography *(see Figure 22)*, which revealed an identical geometry to **11**. Comparison with the monophosphine analogue [Ru$(PPh_3)_2$(ICy)$(CO)H_2$] revealed a shorter Ru-NHC distance in the xantphos analogue (2.140(4) Å vs. 2.106(3) Å) arising from the position of the carbene *trans* to hydride in the former and *trans* to one xantphos terminus in the latter. The Ru-C_{NHC} distance was comparable with that found in the bis-carbene complex [Ru$(PPh_3)(ICy)_2(CO)H_2$][52] (2.099(3) Å) where the carbene is once again found *trans* to phosphine. Examination of the crystal structure for the parent complex,

[Ru(xantphos)(PPh_3)(CO)H_2][53] (**2**) revealed little perturbation of the overall structure on introduction of the ICy ligand.

Bond activation of an ICy ligand is highly unusual, although Herrmann and coworkers have reported a cationic Ir(III) complex exhibiting an η^2-coordinated cyclohexenyl group arising from reaction of Cp*Ir(ICy)Me_2 with HOTf.[40a] It was therefore not surprising that, in contrast to **11**, only minimal C-H activation of the cyclohexyl arm was achieved on heating a solution of the complex under vacuum, even at the elevated temperature of 393 K. However, heating at this temperature in the presence of 10 equivalents of the hydrogen acceptor H_2C=CHSiMe_3 resulted in quantitative formation of the C-H activated compound [Ru(xantphos)(ICy)'(CO)H] (**13**) *(see Figure 21)*. The introduction of 1 atm. H_2 reformed the dihydride complex **11** in only 3 h at 298 K, further underlining the resistance of this ligand to C-H activation.

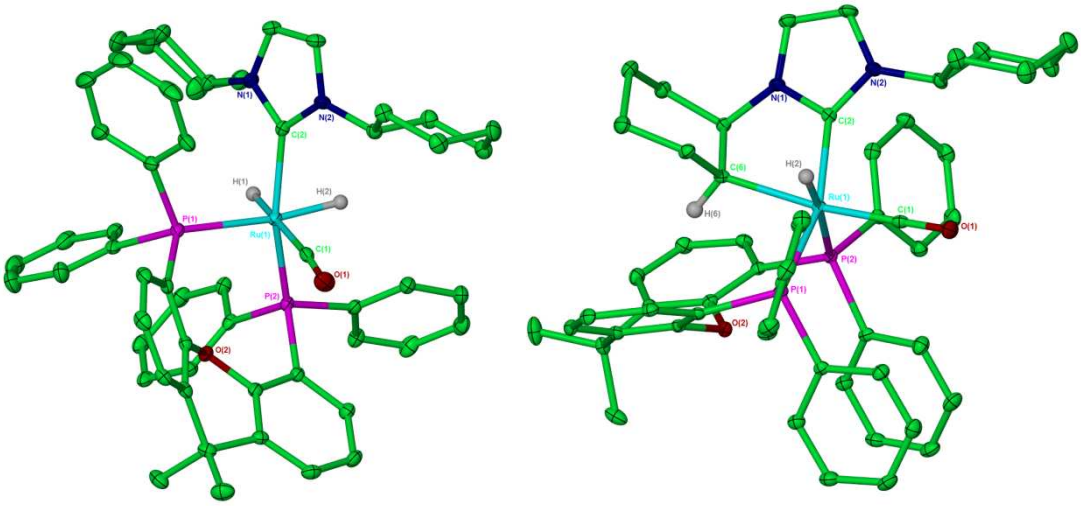

12 **13**

Figure 22: Molecular structures of [Ru(xantphos)(ICy)(CO)H_2] (**12**) and [Ru(xantphos)(ICy)'(CO)H] (**13**). All hydrogen atoms, except Ru-H and that at the activated position in **13**, are omitted. Ellipsoids are shown at the 30% probability level.

Table 2: Selected bond lengths (Å) and angles (˚) for [Ru(xantphos)(ICy)(CO)H_2] (**12**) and [Ru(xantphos)(ICy)'(CO)H] (**13**)

	12	**13**
Ru-C_{NHC}	2.106(3)	2.057(3)
Ru-$CH_{cyclohexyl}$	-	2.207(3)
Ru-$P_{transNHC}$	2.3140(9)	2.3477(9)
Ru-P_{transH}	2.3867(8)	2.4055(8)
Ru-CO	1.892(4)	1.864(3)
C_{NHC}-Ru-$P_{transNHC}$	157.94(9)	157.81(8)
P-Ru-P	102.68(3)	100.48(3)
C_{NHC}-Ru-$CH_{cyclohexyl}$	-	76.41(12)

A crystal structure of **13** *(see Figure 22)* revealed C-H activation at the CH_2 group α to the N-CH bond in one of the N-cyclohexyl substituents, thus creating a more strained C_{NHC}-N-$C_{cyclohexyl}$ angle of 115.8(2)˚ than that found for the unactivated group (124.2(3)˚). Activation of the N-cyclohexyl arm also resulted in a much shorter Ru-C_{NHC} bond distance than that found in **12** *(see Table 2)* with the Ru-CH distance (2.207(3) Å) comparable to the metallated Ru-CH_2 distance found for [Ru(xantphos)($I^iPr_2Me_2$)'(CO)H] (**9**) (2.196(2) Å). Activation of the cyclohexyl arm also resulted in a significant twist of this group in relation to its unactivated equivalent. A comparison of the mean plane of the NHC ring and those formed by each cyclohexyl group revealed a far more acute angle for the activated substituent over its unactivated counterpart - 45˚ vs. 77˚. The crystallographic observations were echoed in solution. ^{1}H-^{13}C{^{1}H} HMBC and HMQC NMR experiments were used to assign a multiplet in the proton spectra at δ -0.44 to the metallated CH proton, with the corresponding ^{13}C resonance detected as a triplet ($^2J_{CP}$ = 7.8 Hz) at δ 44.5.

Whilst η^1-coordination of the cyclohexyl ring is invoked mechanistically in the Herrmann system to explain the ultimate formation of [Cp*Ir{η^2-C_6H_9}ICy)H]OTf,[40a] [Ru(xantphos)(ICy)'(CO)H] (**13**) represents the first example of a fully characterised complex possessing an η^1-coordinated cyclohexyl ring of the ICy carbene.

2.7 Activity of NHC-Xantphos Complexes in a Catalytic Knoevenagel Reaction

The series of C-H activated [Ru(xantphos)(NHC)'(CO)H] complexes were tested for catalytic activity against the parent compound [Ru(xantphos)(PPh_3)(CO)H_2] (**2**) in the previously studied oxidation-Knoevenagel-reduction reaction between benzyl alcohol and t-butyl ketonitrile *(see Figure 23 & Experimental 5.3.5 for representative catalytic procedure)*.[53]

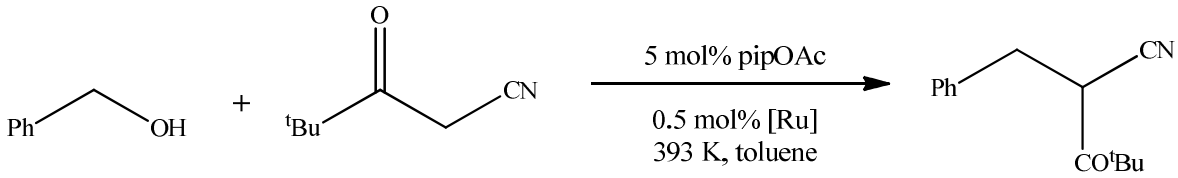

Figure 23: The oxidation-Knoevenagel-reduction reaction between benzyl alcohol and *tert*-butyl ketonitrile to give alkylated product.

None of the NHC complexes were initially as efficient as [Ru(xantphos)(PPh_3)(CO)H_2] (**2**) *(see Figure 24)*. However, the N-alkyl substituted complexes [Ru(xantphos)(IEt_2Me_2)'(CO)H] (**8**), [Ru(xantphos)($I^iPr_2Me_2$)'(CO)H] (**9**) and [Ru(xantphos)(ICy)'(CO)H] (**13**) gave comparable performances after 3.5 h *(see Table 3)*. The similar performance of **8** and **13** implied little relation between the ease of carbene C-H activation and catalytic performance. The mixture of isomers of the N-aryl substituted complex [Ru(xantphos)(IMes)'(CO)H] (**10**) performed relatively poorly, achieving only 52% conversion to product within 3.5 h, perhaps due to the added steric bulk of the IMes ligand.

The catalytic activity of [Ru(xantphos)(IEt_2Me_2)'(CO)H] (**8**) and [Ru(xantphos)(ICy)'(CO)H] (**13**) versus that of their respective dihydride analogues was also assessed in the Knoevenagel reaction *(see Table 3)*. No significant difference in performance was observed, thus demonstrating that no catalytic advantage could be gained by the use of either the C-H activated or dihydride precursors. A reaction with **8** was also run at 343 K since interconversion between this complex and its equivalent dihydride **11** was so facile at this temperature. Unfortunately, even after 5 h at 343 K, very little progress had been made towards alkylated product, with only 2% conversion measured after this time.

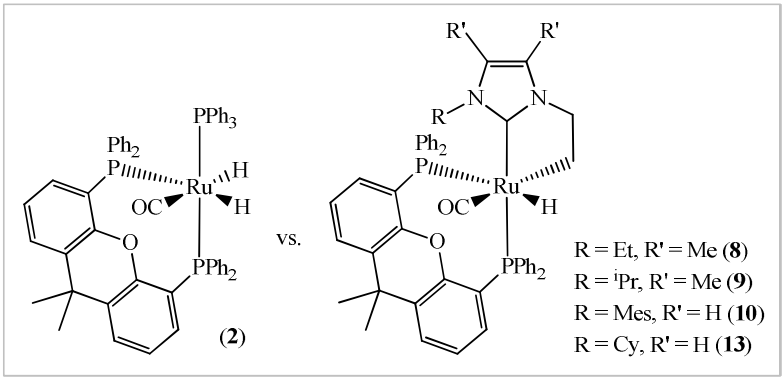

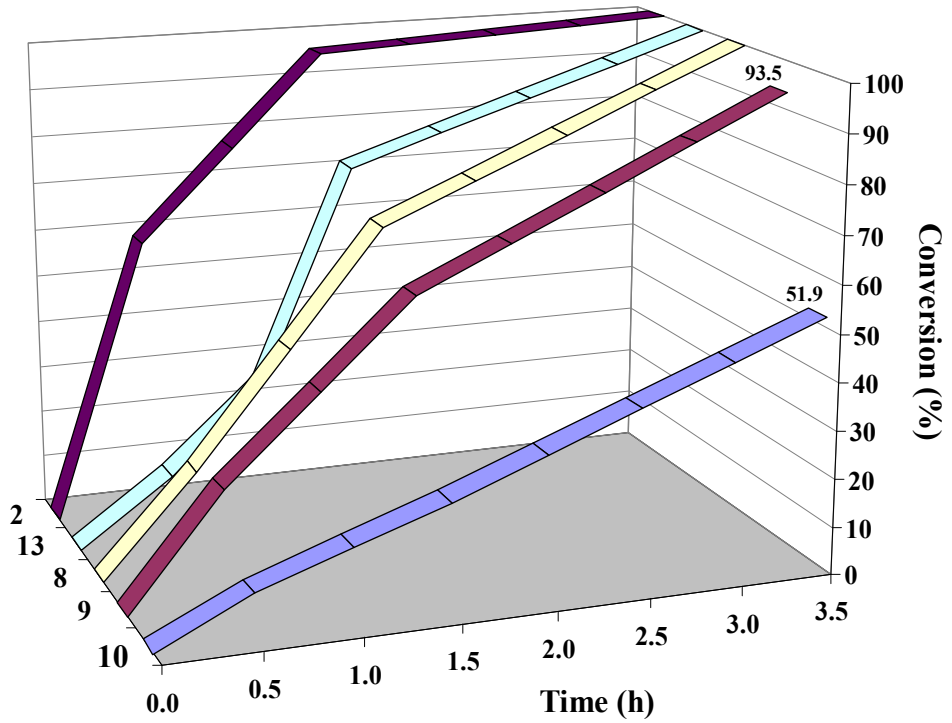

Figure 24: Comparison of catalyst precursors for the Knoevenagel reaction shown in *Figure 23*. Percentage conversions to the alkylated product 4,4-dimethyl-3-oxo-2-benzylpentanenitrile were determined by ^{1}H NMR spectroscopy.

Table 3: Comparison of various catalytic precursors for the oxidation-Knoevenagel-reduction system shown in *Figure 23*.

Catalyst precursor	Conversion (%) to alkylated product in time			
	0.5 h	1.5 h	3.5 h	24 h
2	59	96	100	-
2 + 20 eq. PPh_3	45	86	100	-
8	21	68	100	-
9	24	59	94	-
10	9	23	52	-
13	14	76	100	-
3	1	2	3	19
14	-	1	3	13
15	-	-	0.5	4

The success of this catalytic system relies on the formation of a vacant site to allow initial coordination of the alcohol substrate. The poor performance of the NHC analogues with respect to the all-phosphine parent complex [Ru(xantphos)(PPh_3)(CO)H_2] (**2**) could therefore be due to the relative ease of ligand dissociation from the metal centre. Ligand loss is likely to be more difficult when PPh_3 is substituted for NHC ligands. Indeed, the catalytic performance of **2** was inhibited by the addition of free PPh_3 to the reaction mixture.

The effect of NHC incorporation into systems known to be catalytically inactive was also investigated. [Ru(DPEphos)(PPh_3)(CO)H_2] (**14**) was probed as a possible precursor for NHC incorporation. This had previously been prepared *in situ*, and shown to demonstrate markedly lower catalytic activity than its xantphos analogue.[54] Synthesis of **14** was achieved by the reduction of [Ru(DPEphos)(PPh_3)HCl] (**24b**) with $NaBH_4$. The use of EtOH as solvent for this reaction rather than ^{i}PrOH resulted in concomitant decarbonylation of the alcohol to give **14** as the final product. As anticipated, the NMR data proved similar to **2**: the ^{1}H NMR displayed two hydride resonances at δ -8.33 and -6.44, the former with a large *trans* coupling to phosphorus. Three ^{31}P signals (δ 39, 49 and 60) with the expected multiplicities were observed in the ^{31}P{^{1}H} NMR spectrum. The molecular structure was further confirmed by an X-ray crystal structure *(see Figure 25)*.

Comparison of the metrics of **14** *(see Table 4)* with those of [Ru(xantphos)(PPh_3)(CO)H_2] (**2**) reveal the structures to be very similar, despite the increased flexibility of the DPEphos backbone,[55] resulting in ligand bite angles that are remarkably similar (103.317(18)° vs. 102.76(2)° respectively).

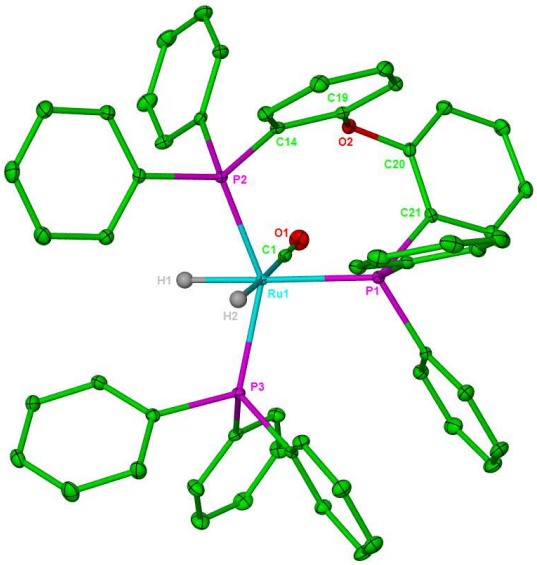

Figure 25: Molecular structure of [Ru(DPEphos)(PPh_3)(CO)H_2] (**14**). All hydrogen atoms except Ru-H are omitted. Thermal ellipsoids are shown at the 30% probability level.

Table 4: Selected bond lengths (Å) and angles (˚) for [Ru(DPEphos)(PPh_3)(CO)H_2] (**14**)

	14	**2**
Ru-P_{transH}	2.3952(5)	2.3950(6)
Ru-P_{transP}	2.2981(5)	2.3283(6)
Ru-PPh_3	2.3184(5)	2.2973(6)
Ru-CO	1.898(2)	1.897(3)
P_{transH}-Ru-P_{transP}	103.317(18)	102.76(2)
P_{transH}-Ru-PPh_3	102.944(18)	107.16(2)
P_{transP}-Ru-PPh_3	143.866(19)	145.06(2)

In spite of the structural parallels between the two complexes, **14** was far less reactive towards substitution of PPh_3; reaction of the complex with various NHC ligands (IEt_2Me_2, $I^iPr_2Me_2$ and ICy) was unsuccessful even under a variety of conditions. As expected [Ru(DPEphos)(PPh_3)(CO)H_2] (**14**) itself proved catalytically inactive in the Knoevenagel reaction, achieving only 19% conversion to alkylated product after 24 h at 393 K *(see Table 3).*

Instead, [Ru(dppp)(PPh_3)(CO)H_2] (**3**) and its ICy counterpart, [Ru(dppp)(ICy)(CO)H_2] (**15**) were prepared via literature methods[53-54, 56] and their performance in the Knoevenagel reaction

evaluated. Whilst both recorded extremely low yields after 24 h at 393 K, the introduction of a N-heterocyclic carbene once again actually impeded catalytic activity *(see Table 3)*.

2.8 Efforts to Prepare New Hydrodefluorination Catalysts

It was noted that the [Ru(xantphos)(NHC)(CO)H_2] complexes were structurally very similar to previously studied systems effective for the activation of C-F bonds. Prior work within the Whittlesey group had identified a series of [Ru(PPh_3)$_2$(NHC)(CO)H_2] complexes as highly effective hydrodefluorination (HDF) catalysts and found that replacing two monophosphine ligands for the chelating bisphosphine dppp formed a system capable of stoichiometric C-F bond activation. The next section describes work conducted into use of [Ru(xantphos)(NHC)(CO)H_2] complexes as precursors for hydrodefluorination (HDF).

Organofluorine compounds are present in a high percentage of pharmaceuticals and agrochemicals, and as such, the activation of C-F bonds is a commercially-relevant goal.[57] However, the high strength of the C-F interaction renders it one of the most inert carbon-heteroatom bonds, providing researchers with an interesting fundamental challenge. Whilst there are now a number of metal complexes that can induce stoichiometric C-F bond activation,[58] there are only a few examples of catalytic C-F bond functionalisation.[59] In particular, hydrodefluorination (HDF) is an important strategy, where a catalyst is able to replace one or more fluorine atoms in a fluoroaromatic substrate with hydrogen sourced from a reductant.

Milstein and Aizenberg described the first example of metal catalysed HDF in 1994 using the rhodium(I) complex, [Rh(C_6F_5)(PMe_3)$_3$], for the hydrodefluorination of C_6F_6 and C_6F_5H in combination with either R_3SiH or H_2 as reductants.[60] This reaction proved highly regioselective, forming exclusively 1,4-$C_6F_4H_2$ from C_6F_5H. Other HDF systems have since been developed, widening the number of metal centres able to catalyse C-F activation. In particular, Holland *et al.* have reported an iron(II) complex incorporating a β-diketiminate ligand, capable of catalysing the HDF of perfluoroaromatics and also perfluoroalkenes.[61] However, both the Milstein and the Holland systems suffer from the need for forcing conditions; the rhodium catalysis requiring approximately 6 atm. H_2 and 10 equivalents Et_3N (as a sink for the HF released), and the iron system needing high catalyst loadings of 20 mol%.

Subsequent work in the Whittlesey group revealed that [Ru(PPh_3)$_2$(NHC)(CO)H_2] complexes (NHC = IMes, SIMes, IPr and SIPr) formed effective catalysts for the hydrodefluorination of C_6F_6, C_6F_5H and also C_6F_5N *(see Figure 26)*.[62] They also proved highly regioselective, but in a contrasting fashion to the Milstein system, activated at the 2-position to

form 1,2-$C_6F_4H_2$ upon hydrodefluorination of C_6F_5H. In addition, HDF was able to take place at the relatively mild temperature of 343 K with a turnover frequency (TOF) of up to 0.86 h^{-1}.

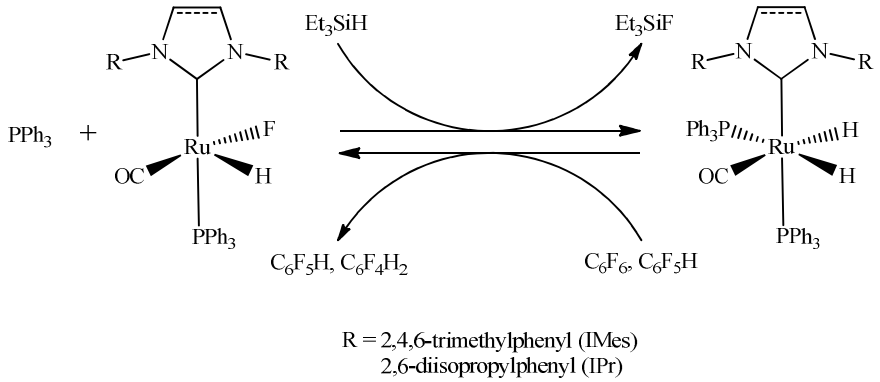

Figure 26: Hydrodefluorination (HDF) with $[Ru(PPh_3)_2(NHC)(CO)H_2]$ complexes.[62]

A series of $[Ru(dppp)(NHC)(CO)H_2]$ complexes were synthesised with the chelating diphosphine dppp, which were able to induce stoichiometric C-F activation, although the regioselectivity of the reaction was altered. In the case of substituted fluoroaromatics, such as $C_6F_5CF_3$, sole activation at the 4-position was observed, whilst partially fluorinated aromatics such as C_6F_5H gave rise to a mixture of C-F activation (at the 4-position) and intramolecular C-H activation.[56]

The structural similarity of the $[Ru(xantphos)(NHC)(CO)H_2]$ compounds to these previously studied systems and also their facility for C-H bond activation led us to assess the performance of these complexes in the activation of C-F bonds. Previous work by Reade *et al.* identified $[Ru(dppp)(PPh_3)(CO)HF]$ as the most suitable precursor to $[Ru(dppp)(NHC)(CO)HF]$.[56] Initial studies therefore concentrated on the synthesis of a new precursor, $[Ru(xantphos)(PPh_3)(CO)HF]$ (**17**), and subsequent reaction of this complex with a range of N-heterocyclic carbenes to give $[Ru(xantphos)(NHC)(CO)HF]$.

2.9 Synthesis of $[Ru(xantphos)(PPh_3)(CO)HF]$ (17) and Reaction with NHCs

Reaction of $[Ru(PPh_3)_3(CO)HF]$ (**16**) with 1.1 equivalents xantphos in refluxing benzene afforded $[Ru(xantphos)(PPh_3)(CO)HF]$ (**17**) as a white crystalline solid, although in poor yield (22%). The geometry of **17** was elucidated from an X-ray crystal structure and revealed a *trans* F-Ru-CO configuration, as observed in $[Ru(dppp)(PPh_3)(CO)HF]$[56] *(see Figure 27)*. Both these complexes possess a distorted octahedral geometry caused by the tilt of the mutually *trans* phosphine ligands towards the Ru-H bond. However, the tilt angle is far more acute in **17**

(154.36(4)˚) than in either of the two molecules that make up the unit cell of [Ru(dppp)(PPh_3)(CO)HF] (168˚ and 171˚), an effect attributable to the larger bite angle of the xantphos ligand (β_n = 111˚) in relation to dppp (β_n = 91˚).[55] A comparison of the Ru-P and Ru-CO bond distances *(see Table 5)* revealed only minor differences between the two complexes.

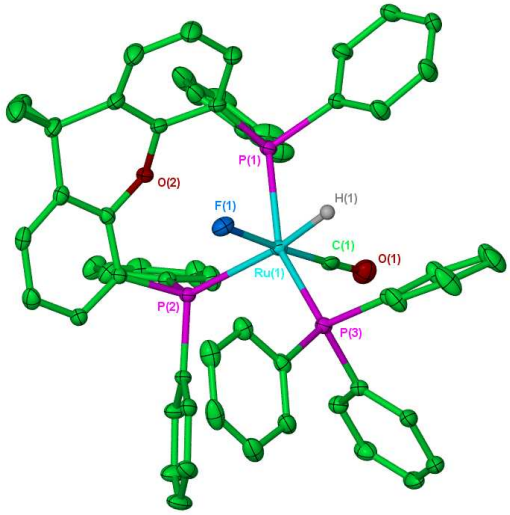

Figure 27: Molecular structure of [Ru(xantphos)(PPh_3)(CO)HF] (**17**). All hydrogen atoms except Ru-H are omitted. Thermal ellipsoids are shown at the 30% probability level.

Table 5: Selected bond lengths (Å) and angles (°) for [Ru(xantphos)(PPh_3)(CO)HF] (**17**) and [Ru(dppp)(PPh_3)(CO)HF][56]

	17	[Ru(dppp)(PPh_3)(CO)HF][a]
Ru-CO	1.813(5)	1.816(4) / 1.820(4)
Ru-F	2.054(2)	2.1005(18) / 2.0943(18)
Ru-PPh_3	2.3737(10)	2.3622(19) / 2.3752(9)
Ru-P_{transH}	2.4960(11)	2.4354(9) / 2.4396(9)
Ru-P_{transP}	2.3577(10)	2.3390(9) / 2.3418 (9)
PPh_3-Ru-P_{transH}	100.91(3)	98.92(3) / 97.39(3)
PPh_3-Ru-P_{transP}	154.36(4)	168.09(3) / 171.20(3)
P_{transP}-Ru-P_{transH}	104.43(3)	92.64(3) / 91.40(3)
CO-Ru-F	176.89(15)	174.71(12) / 173.39(12)

[a]*The two values refer to the two molecules found in the asymmetric unit.*

The room temperature ^{1}H NMR data for **17** was in agreement with the solid-state structure, displaying a sharp hydride signal at δ -5.57 with an easily identifiable *trans* coupling to phosphorus ($^{2}J_{HP}$ = 118 Hz) and two smaller *cis* couplings. The $^{31}P\{^{1}H\}$ NMR spectrum revealed only an extremely broad resonance at δ 40.0 and no signals could be observed in the ^{19}F NMR spectrum at 298 K, implying some fluxional behaviour. On cooling to 194 K, the hydride region resolved to two resonances at δ -4.92 and -5.22 (both with doublet of doublet of doublets multiplicities). It is possible that these two species might arise from different conformers of **17** or that they result from isomers formed by the xantphos ligand in either *cis* or *trans* coordination.[63]

Once again, a large *trans* coupling was visible on each hydride signal, indicating a *trans* H-Ru-P interaction present in both species. Each hydride was correlated to three ^{31}P resonances via ^{1}H-$^{31}P\{^{1}H\}$ HMQC spectroscopy (^{1}H: δ -4.92, $^{31}P\{^{1}H\}$: δ 47.0, 31.9 and 29.9; ^{1}H: δ -5.22, $^{31}P\{^{1}H\}$: δ 33.4, 26.3 and 5.4). A large *trans* $^{2}J_{PP}$ coupling could be identified in each set of signals ($^{2}J_{PP}$ = 310.5 Hz, 309.3 Hz). The NMR data would therefore appear to exclude the existence of isomers. At this temperature, two signals were visible in the ^{19}F NMR spectrum at δ -366 and -395, the chemical shifts consistent with the presence of coordinatively saturated ruthenium centres.[64] Unfortunately, even at this low temperature, the ^{19}F signals remained too broad to reveal any correlation to the hydrides by ^{1}H-$^{19}F\{^{1}H\}$ HMBC spectroscopy.

A ^{31}P-^{31}P EXSY revealed that the two species were in exchange and that traces of free PPh_3 also present in the sample showed no exchange with either form *(see Figure 28)*. Given the low temperature and lack of intermolecular exchange with free PPh_3, it appears likely that the species are indeed conformers. It is also worth noting the low frequency shift (δ = 5.4) in the $^{31}P\{^{1}H\}$ NMR spectrum of one conformer in comparison with the other signals. Indeed, ruthenium-xantphos complexes are known to exhibit fluxionality arising from different conformations of the phosphine ligands.[65]

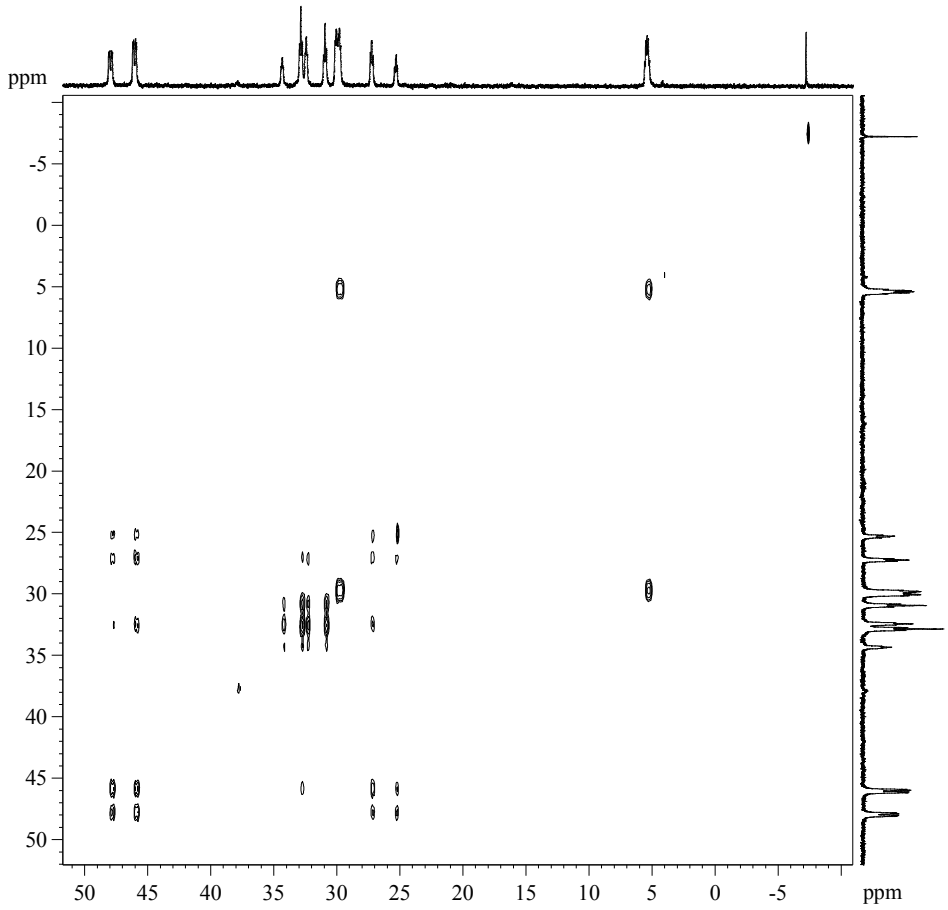

Figure 28: ^{31}P-^{31}P EXSY ([D_8]-toluene, 162 MHz, 194 K) of [Ru(xantphos)(PPh_3)(CO)HF] (**17**)

Unfortunately, formation of [Ru(xantphos)(NHC)(CO)HF] via reaction of **17** with the alkyl carbenes IEt_2Me_2 and ICy proved unsuccessful, requiring long reaction times and resulting in a wide array of hydride-containing species. Instead, the previously synthesised complexes [Ru(xantphos)(IEt_2Me_2](CO)H_2] (**11**) and [Ru(xantphos)(ICy)(CO)H_2] (**12**) were used as precursors, and reacted with $Et_3N{\cdot}3HF$ to afford the desired compounds.

2.10 Synthesis and Characterisation of [Ru(xantphos)(NHC)(CO)HF] (NHC = ICy, IEt_2Me_2)

Reaction of [Ru(xantphos)(ICy)(CO)H_2] (**12**) with 2.2 equivalents $Et_3N.3HF$ in benzene resulted in the instantaneous release of hydrogen to form [Ru(xantphos)(ICy)(CO)HF] (**18**). At room temperature the hydride region of the ^1H NMR spectrum displayed two broad signals at δ -6.1 and -7.5 in a 1:1 ratio. A broad $^{31}P\{^1H\}$ NMR spectrum was also recorded at the same temperature. Cooling to 217 K sharpened both spectra, to reveal two doublet of doublet hydrides, each displaying a large *trans* and a smaller *cis* coupling to phosphorus. ^1H-$^{31}P\{^1H\}$ HMQC spectroscopy

correlated each hydride signal to two doublet of doublet resonances in the $^{31}P\{^{1}H\}$ NMR spectrum. Each of these doublet of doublets displayed a *cis* coupling to fluorine and a smaller *cis* coupling to the corresponding phosphorus. The ^{19}F NMR spectrum of **18** at ambient temperature exhibited two broad singlets (δ -334 and -336). These sharpened slightly upon cooling to 217 K, but remained too broad to resolve further detail.

Broad $^{13}C\{^{1}H\}$ NMR spectra were observed across a range of temperatures (217 K, 298 K and 315 K), even with increasing sample strength. This precluded observation of the Ru-CO and Ru-C_{NHC} signals and prevented further elucidation of the two species' structures in solution. Whilst different conformers or cis/*trans* isomerism of the xantphos ligand could account for the two sets of signals seen for **18** in solution, it is also possible that isomers could arise purely from an alteration in the relative positions of the ligands *(see Figure 29)*.

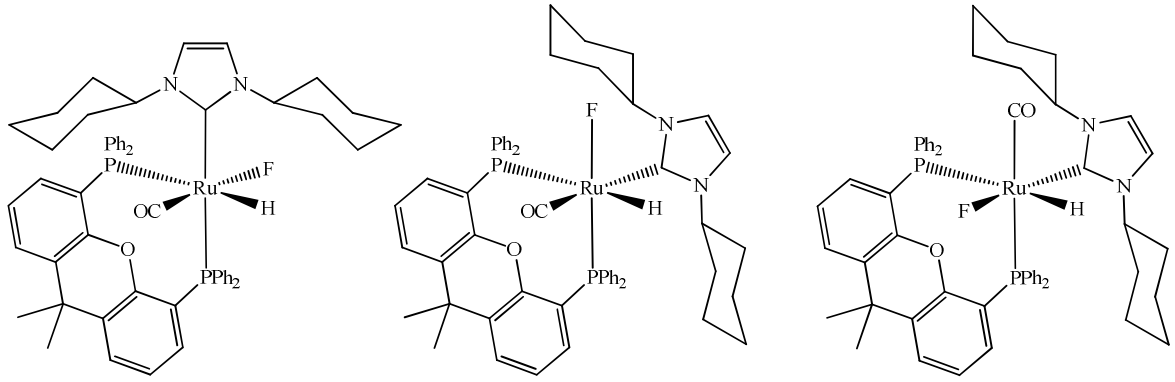

Figure 29: Possible isomers of [Ru(xantphos)(ICy)(CO)HF] (**18**).

Similar reaction of [Ru(xantphos)(IEt_2Me_2)(CO)H_2] (**11**) with $Et_3N{\cdot}3HF$ gave rise to [Ru(xantphos)(IEt_2Me_2)(CO)HF] (**19**). The NMR characterisation of **19** was very similar to that of [Ru(xantphos)(ICy)(CO)HF] (**18**), the complex once again existing as two species in solution. The ^{1}H, $^{31}P\{^{1}H\}$ and ^{19}F NMR spectra of **19** all exhibited broad signals at 298 K which could be resolved to a certain extent by cooling to 217 K. $^{13}C\{^{1}H\}$ NMR spectra were too broad to allow the exact nature of the two species to be differentiated. Attempts to recrystallise either **18** or **19** were unsuccessful despite variations of both concentration and solvent systems.

2.11 Synthesis and Characterisation of [Ru(dppf)(ICy)(CO)H_2] and [Ru(dppf)(ICy)(CO)HF]

Since the isolation of [Ru(xantphos)(NHC)(CO)HF] proved unsuccessful, xantphos was replaced by another chelating phosphine, the bidentate ferrocenyl-based ligand dppf. The precursor

dihydride complex [Ru(dppf)(ICy)(CO)H_2] (**21**) was prepared by reaction of the known literature compound [Ru(dppf)(PPh_3)(CO)H_2][66] (**20**) with 3 equivalents of ICy in refluxing toluene.

The ^{1}H NMR spectrum of **21** exhibited the two expected hydride resonances at δ -5.66 and -8.13, each with a doublet of doublets multiplicity. The higher frequency hydride signal was identified as that *trans* to one terminus of the dppf ligand ($^2J_{HP}$ = 88 Hz). Surprisingly the IR spectrum displayed three bands of equal intensity at 1923, 1907 and 1854 cm^{-1}. It would appear that two of these bands arise from Ru-H bonds which have stolen intensity from the Ru-CO stretch. This has also been observed in a related ruthenium compound prepared previously in the group, [Ru(IMes)$_2$(CO)$_2$(S(CH$_2$)$_2$CH$_3$)H].[67] Attempts to assign specific stretches in **21** to ν(CO) by use of the dideuteride complex [Ru(dppf)(ICy)(CO)D_2] were thwarted by the lack of H-D exchange between **21** and D_2. The molecular structure of **21** was confirmed through an X-ray crystal structure *(see Figure 30)*. As observed in previously isolated [Ru(P-P)(ICy)(CO)H_2] (P-P = xantphos (**12**), dppp (**15**)) complexes, **21** displayed a distorted octahedral geometry (CO-Ru-$P_{transCO}$ = 165.46(5)˚ c.f. 157.81(8)˚ (**12**) and 159.81(7)˚ (**15**)) *(see Table 6)*.

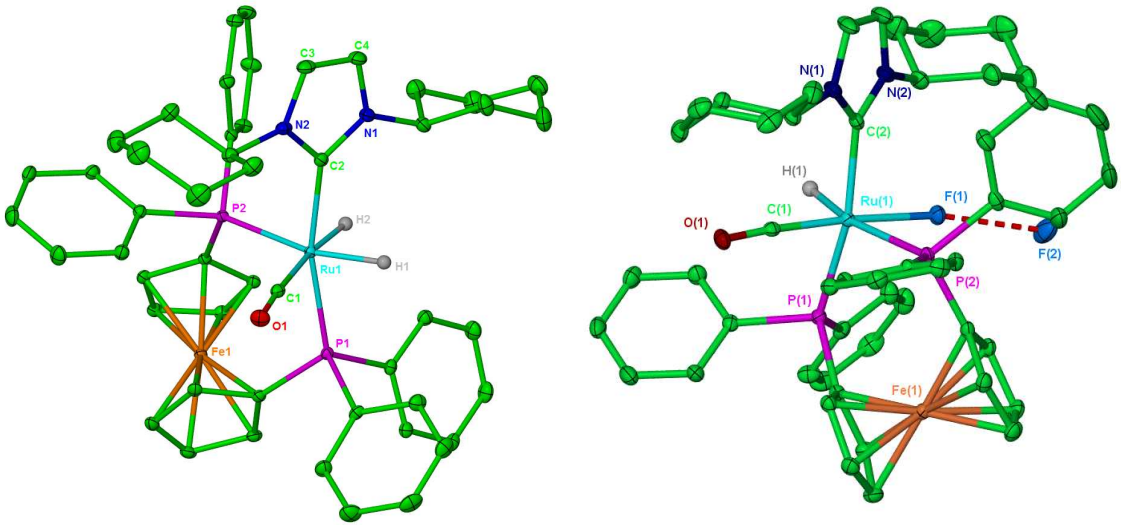

21 **22**

Figure 30: Molecular structures of [Ru(dppf)(ICy)(CO)H_2] (**21**) and [Ru(dppf)(ICy)(CO)HF] (**22**). Minor disordered fractional occupancy fluorine in HF moiety in **22** omitted for clarity, as are all hydrogen atoms except Ru-H. Thermal ellipsoids are shown at the 30% probability level.

Table 6: Selected bond lengths (Å) and angles (°) for [Ru(dppf)(ICy)(CO)H_2] (**21**) and [Ru(dppf)(ICy)(CO)HF] (**22**)

	21	**22**
Ru-CO	1.883(2)	1.803(3)
Ru-C_{NHC}	2.115(2)	2.129(3)
Ru-P_{transH}	2.3490(5)	2.4494(8)
Ru-P_{transC}	2.3262(5)	2.3679(8)
Ru-F	-	2.1275(16)
P_{transC}-Ru-P_{transH}	101.826(17)	101.79(3)
P_{transC}-Ru-C_{NHC}	165.46(5)	164.47(8)
P_{transH}-Ru-CO	107.71(6)	104.04(9)

Reaction of **21** with $Et_3N{\cdot}3HF$ successfully formed the desired hydride fluoride complex [Ru(dppf)(ICy)(CO)HF] (**22**). The molecular configuration of **22** was confirmed by an X-ray crystal structure *(see Figure 30)*, which revealed a *trans* F-Ru-CO configuration, as seen for **17**. The replacement of a hydride for a fluoride ligand appeared to have little effect on the geometry of the complex; a comparison of the bond angles reveals little perturbation between the two structures *(see Table 6)*. The bond distances are generally longer in **22** than in **21**, apart from the Ru-CO bond, while the Ru-F distance is close to that of other reported ruthenium fluorides.[68] A Ru-F(1)···F(2) interaction was also detected in the X-ray crystal structure. Whilst the hydrogen attached to F(2) could not be located using the X-ray data, the F···F distance of 2.413 Å suggested the presence of a F···H···F interaction in the solid state, although there was no evidence for this in solution.

The ^{1}H NMR spectrum of **22** at 298 K agreed with the solid state geometry, and displayed a doublet of doublets signal in the hydride region at δ -6.7 with *trans* and *cis* couplings to phosphorus. Any fluorine splitting was apparently lost within the line width of the signal. However, warming the sample to 320 K further resolved the hydride resonance to the expected doublet of doublet of doublets with a small *cis* coupling due to ^{19}F now observable ($^2J_{HP}$ = 128.5 Hz, $^2J_{HP}$ = 31.5, $^2J_{HF}$ = 8.4 Hz). ^{1}H-^{31}P{^{1}H} HMQC spectroscopy correlated the hydride signal to two doublet of doublet resonances in the ^{31}P{^{1}H} NMR spectrum at δ 31.7 and 18.7. The lower frequency signal displayed an unusually large *cis* J_{PF} splitting ($^2J_{PF}$ = 79.5 Hz) suggestive of a distorted P-Ru-F interaction,[56, 69] although this was not obviously apparent in the solid state (P_{transC}-Ru-F = 92.80(5)°, P_{transH}-Ru-F = 74.95(5)°).

On cooling to 217 K, two overlapping hydrides were observed in the ^{1}H NMR spectrum at δ -6.06 and -6.13, a difference in chemical shift of only 0.07 ppm. Two ^{31}P signals were correlated to each hydride resonance via ^{1}H-$^{31}P\{^{1}H\}$ spectroscopy, each set of signals consisting of one broad resonance and a doublet of doublets (δ 30.3 and 20.5, and δ 32.6 and 19.2 respectively). Whilst a broad signal at δ -347.4 was visible in the ^{19}F NMR spectrum at 320 K, two resonances at δ -322.1 and 351.9 were present on cooling to 217 K. It would seem unlikely that different conformers of the dppf ligand would be possible, and there are few instances of *trans* spanning dppf.[63b, 70] In the case of **22**, differences in the relative positions of Ru-ICy, Ru-F and Ru-CO are therefore likely to account for the two isomers that resolve at low temperature.

2.12 Attempted Hydrodefluorination of C_6F_6 by [Ru(P-P)(NHC)(CO)H_2]

For catalytic hydrodefluorination (HDF) to take place, both halves of the catalytic cycle must be viable. Thus, the hydride fluoride complexes, **18**, **19** and **22**, were reacted with 5 equivalents Et_3SiH at 343 K, to successfully generate the corresponding dihydride complexes **11**, **12** and **21**, as well as Et_3SiF. However, the converse reaction to regenerate the hydride fluoride precursors proved more problematic *(see Figure 31)*.

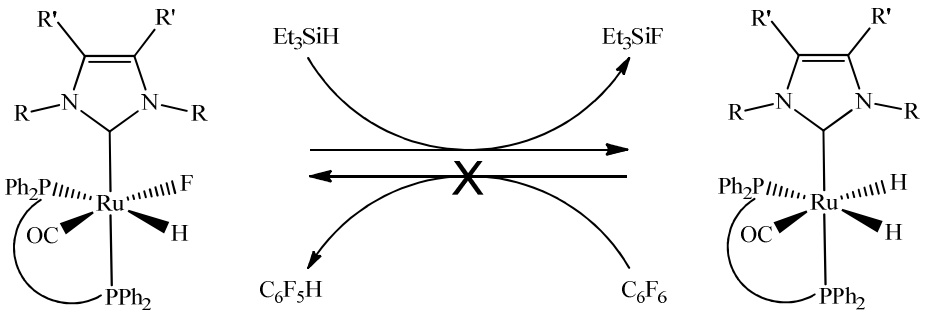

Figure 31: General catalytic cycle for the hydrodefluorination (HDF) of C_6F_6 with [Ru(P-P)(NHC)(CO)H_2] (P-P = xantphos, NHC = IEt_2Me_2 (**11**), ICy (**12**); P-P = dppf, NHC = ICy (**21**)) using Et_3SiH as reductant.

Intermolecular C-F activation of hexafluorobenzene using [Ru(xantphos)(NHC)(CO)H_2] (NHC = IEt_2Me_2 (**11**), ICy = (**12**)) was inhibited by the facile intramolecular C-H activation previously observed for these systems.[71,72] Reaction of these dihydride complexes with 10 equivalents C_6F_6 at 343 K resulted only in formation of the C-H activated species, [Ru(xantphos)(NHC)'(CO)H] (NHC = IEt_2Me_2 (**8**), ICy = (**13**)), with no observable C-F activation products. Increasing the reaction temperature to 393 K only exacerbated the problem. The

introduction of 1 atm. H_2 reduced the extent of carbene activation, but failed to bring about C-F bond activation even after 30 h at 343 K. Surprisingly, [Ru(dppf)(ICy)(CO)H_2] (**21**) proved completely inactive on reaction with hexafluorobenzene, with no evidence for either intramolecular C-H or intermolecular C-F activation.

The inactivity of these systems contrasts sharply with [Ru(PPh_3)$_2$(NHC)(CO)H_2][62] and [Ru(dppp)(NHC)(CO)H_2][56] since these compounds will readily undergo C-F bond activation in the presence of fluoroarenes. We would argue that the high affinity of the xantphos series for C-H bond activation ultimately precluded any C-F activation for [Ru(xantphos)(NHC)(CO)H_2] (NHC = IEt_2Me_2 (**11**), ICy = (**12**)), whilst explanations for the inactivity of [Ru(dppf)(ICy)(CO)H_2] (**21**) remain elusive. However, the choice of chelating phosphine clearly has a profound impact on the ability of [Ru(P-P)(NHC)(CO)H_2] to undergo hydrodefluorination (HDF) chemistry.

2.13 CHAPTER SUMMARY

A series of [Ru(xantphos)(NHC)'(CO)H] complexes have been synthesised incorporating a variety of aryl and alkyl substituted NHCs (IEt_2Me_2, $I^iPr_2Me_2$, IMes, ICy).

In many cases, these compounds exhibited spontaneous intramolecular C-H activation of the carbene N-substituents, and C-H cleavage could even be induced in the normally inert ICy ligand upon treatment with the hydrogen acceptor H_2C=CH$SiMe_3$.

The series of [Ru(xantphos)(NHC)'(CO)H] complexes (**8-10**, **13**) were tested for catalytic activity in the Knoevenagel reaction, but were found to be less active than the precursor compound, [Ru(xantphos)(PPh_3)(CO)H_2] (**2**).

NHC incorporation into two systems known to be catalytically inactive, [Ru(DPEphos)(PPh_3)(CO)H_2] (**14**) and [Ru(dppp)(PPh_3)(CO)H_2] (**3**), also resulted in a drop in catalytic activity.

[Ru(xantphos)(NHC)(CO)H_2] (NHC = IEt_2Me_2 (**11**), ICy = (**12**)) precursors were investigated as potential catalysts for the hydrodefluorination (HDF) of fluoroarenes, but proved to be ineffective since intramolecular C-H bond activation was preferred over any intermolecular C-F bond activation.

Replacement of the xantphos ligand for the ferrocenyl diphosphine dppf afforded [Ru(dppf)(ICy)(CO)H_2] (**21**) and [Ru(dppf)(ICy)(CO)HF] (**22**), which also failed to show any activity for HDF.

References

1. (a) Boehme, C.; Frenking, G. *J. Am. Chem. Soc.;* **1996;** *118;* 2039-2046; (b) Heinemann, C.; Muller, T.; Apeloig, Y.; Schwarz, H. *J. Am. Chem. Soc.;* **1996;** *118;* 2023-2038.
2. Herrmann, W. A. *Angew. Chem. Int. Ed.;* **2002;** *41;* 1290-1309.
3. Peris, E.; Crabtree, R. H. *C. R. Chim.;* **2003;** *6;* 33-37.
4. For example, the carbenes IPr, IMes, I^{t}Bu, I^{i}Pr and IAd are all available as the imidazolium BF_4 or chloride salts from Sigma-Aldrich.
5. Huang, J. K.; Schanz, H. J.; Stevens, E. D.; Nolan, S. P. *Organometallics;* **1999;** *18;* 2370-2375.
6. Herrmann, W. A.; Weskamp, T.; Böhm, V. P. W. *Adv. Organomet. Chem.;* **2001;** *48;* 1-69.
7. Alder, R. W.; Allen, P. R.; Williams, S. J. *J. Chem. Soc., Chem. Commun.;* **1995;** 1267-1268.
8. Kim, Y. J.; Streitwieser, A. *J. Am. Chem. Soc.;* **2002;** *124;* 5757-5761.
9. Magill, A. M.; Cavell, K. J.; Yates, B. F. *J. Am. Chem. Soc.;* **2004;** *126;* 8717-8724.
10. Higgins, E. M.; Sherwood, J. A.; Lindsay, A. G.; Armstrong, J.; Massey, R. S.; Alder, R. W.; O'Donoghue, A. C. *Chem. Commun.;* **2011;** *47;* 1559-1561.
11. (a) Dorta, R.; Stevens, E. D.; Hoff, C. D.; Nolan, S. P. *J. Am. Chem. Soc.;* **2003;** *125;* 10490-10491; (b) Kocher, C.; Herrmann, W. A. *J. Organomet. Chem.;* **1997;** *532;* 261-265.
12. Perrin, L.; Clot, E.; Eisenstein, O.; Loch, J.; Crabtree, R. H. *Inorg. Chem.;* **2001;** *40;* 5806-5811.
13. Hillier, A. C.; Sommer, W. J.; Yong, B. S.; Petersen, J. L.; Cavallo, L.; Nolan, S. P. *Organometallics;* **2003;** *22;* 4322-4326.
14. Gusev, D. G. *Organometallics;* **2009;** *28;* 6458-6461.
15. Clavier, H.; Nolan, S. P. *Chem. Commun.;* **2010;** *46;* 841-861.
16. Hu, X. L.; Tang, Y. J.; Gantzel, P.; Meyer, K. *Organometallics;* **2003;** *22;* 612-614.
17. Cavallo, L.; Correa, A.; Costabile, C.; Jacobsen, H. *J. Organomet. Chem.;* **2005;** *690;* 5407-5413.
18. (a) Huang, J. K.; Schanz, H. J.; Stevens, E. D.; Nolan, S. P. *Organometallics;* **1999;** *18;* 5375-5380; (b) Scholl, M.; Ding, S.; Lee, C. W.; Grubbs, R. H. *Org. Lett.;* **1999;** *1;* 953-956.
19. Sanford, M. S.; Love, J. A.; Grubbs, R. H. *Organometallics;* **2001;** *20;* 5314-5318.
20. Lee, H. M.; Jiang, T.; Stevens, E. D.; Nolan, S. P. *Organometallics;* **2001;** *20;* 1255-1258.
21. Arnold, P. L.; Pearson, S. *Coord. Chem. Rev.;* **2007;** *251;* 596-609.
22. Ellul, C. E.; Mahon, M. F.; Saker, O.; Whittlesey, M. K. *Angew. Chem. Int. Ed.;* **2007;** *46;* 6343-6345.
23. Burling, S.; Mahon, M. F.; Powell, R. E.; Whittlesey, M. K.; Williams, J. M. J. *J. Am. Chem. Soc.;* **2006;** *128;* 13702-13703.
24. (a) Danopoulos, A. A.; Tsoureas, N.; Green, J. C.; Hursthouse, M. B. *Chem. Commun.;* **2003;** 756-757; (b) Becker, E.; Stingl, V.; Dazinger, G.; Puchberger, M.; Mereiter, K.; Kirchner, K. *J. Am. Chem. Soc.;* **2006;** *128;* 6572-6573.
25. Davies, C. J. E.; Page, M. J.; Ellul, C. E.; Mahon, M. F.; Whittlesey, M. K. *Chem. Commun.;* **2010;** *46;* 5151-5153.
26. (a) Titcomb, L. R.; Caddick, S.; Cloke, F. G. N.; Wilson, D. J.; McKerrecher, D. *Chem. Commun.;* **2001;** 1388-1389; (b) Simms, R. W.; Drewitt, M. J.; Baird, M. C. *Organometallics;* **2002;** *21;* 2958-2963.
27. Crudden, C. M.; Allen, D. P. *Coord. Chem. Rev.;* **2004;** *248;* 2247-2273.
28. Hitchcock, P. B.; Lappert, M. F.; Pye, P. L. *J. Chem. Soc., Chem. Commun.;* **1977;** 196-198.
29. Hitchcock, P. B.; Lappert, M. F.; Terreros, P. *J. Organomet. Chem.;* **1982;** *239;* C26-C30.

30. Giunta, D.; Holscher, M.; Lehmann, C. W.; Mynott, R.; Wirtz, C.; Leitner, W. *Adv. Synth. Catal.;* **2003;** *345;* 1139-1145.
31. Hong, S. H.; Chlenov, A.; Day, M. W.; Grubbs, R. H. *Angew. Chem. Int. Ed.;* **2007;** *46;* 5148-5151.
32. Huang, J. K.; Stevens, E. D.; Nolan, S. P. *Organometallics;* **2000;** *19;* 1194-1197.
33. Jazzar, R. F. R.; Macgregor, S. A.; Mahon, M. F.; Richards, S. P.; Whittlesey, M. K. *J. Am. Chem. Soc.;* **2002;** *124;* 4944-4945.
34. Abdur-Rashid, K.; Fedorkiw, T.; Lough, A. J.; Morris, R. H. *Organometallics;* **2004;** *23;* 86-94.
35. Chilvers, M. J.; Jazzar, R. F. R.; Mahon, M. F.; Whittlesey, M. K. *Adv. Synth. Catal.;* **2003;** *345;* 1111-1114.
36. Crabtree, R. H. *J. Chem. Soc., Dalton Trans.;* **2001;** 2437-2450.
37. Burling, S.; Mas-Marzá, E.; Valpuesta, J. E. V.; Mahon, M. F.; Whittlesey, M. K. *Organometallics;* **2009;** *28;* 6676-6686.
38. Wolf, R.; Plois, M. *Eur. J. Inorg. Chem.;* **2010;** 4419-4422.
39. Corberan, R.; Sanau, M.; Peris, E. *Organometallics;* **2006;** *25;* 4002-4008.
40. (a) Prinz, M.; Grosche, M.; Herdtweck, E.; Herrmann, W. A. *Organometallics;* **2000;** *19;* 1692-1694; (b) Corberan, R.; Sanau, M.; Peris, E. *J. Am. Chem. Soc.;* **2006;** *128;* 3974-3979.
41. Tanabe, Y.; Hanasaka, F.; Fujita, K.; Yamaguchi, R. *Organometallics;* **2007;** *26;* 4618-4626.
42. Zhang, C. Y.; Zhao, Y.; Li, B.; Song, H. B.; Xu, S. S.; Wang, B. Q. *Dalton Trans.;* **2009;** 5182-5189.
43. (a) Dorta, R.; Stevens, E. D.; Nolan, S. P. *J. Am. Chem. Soc.;* **2004;** *126;* 5054-5055; (b) Scott, N. M.; Dorta, R.; Stevens, E. D.; Correa, A.; Cavallo, L.; Nolan, S. P. *J. Am. Chem. Soc.;* **2005;** *127;* 3516-3526.
44. Häller, L. J. L.; Page, M. J.; Macgregor, S. A.; Mahon, M. F.; Whittlesey, M. K. *J. Am. Chem. Soc.;* **2009;** *131;* 4604-4605.
45. Viciano, M.; Sanau, M.; Peris, E. *Organometallics;* **2007;** *26;* 6050-6054.
46. Prades, A.; Viciano, M.; Sanau, M.; Peris, E. *Organometallics;* **2008;** *27;* 4254-4259.
47. Gnanamgari, D.; Sauer, E. L. O.; Schley, N. D.; Butler, C.; Incarvito, C. D.; Crabtree, R. H. *Organometallics;* **2009;** *28;* 321-325.
48. Nordstrøm, L. U.; Vogt, H.; Madsen, R. *J. Am. Chem. Soc.;* **2008;** *130;* 17672-17673.
49. Dam, J. H.; Osztrovszky, G.; Nordstrom, L. U.; Madsen, R. *Chem. Eur. J.;* **2010;** *16;* 6820-6827.
50. Burling, S.; Paine, B. M.; Nama, D.; Brown, V. S.; Mahon, M. F.; Prior, T. J.; Pregosin, P. S.; Whittlesey, M. K.; Williams, J. M. J. *J. Am. Chem. Soc.;* **2007;** *129;* 1987-1995.
51. Burling, S.; Mahon, M. F.; Paine, B. M.; Whittlesey, M. K.; Williams, J. M. J. *Organometallics;* **2004;** *23;* 4537-4539.
52. Burling, S.; Kociok-Köhn, G.; Mahon, M. F.; Whittlesey, M. K.; Williams, J. M. J. *Organometallics;* **2005;** *24;* 5868-5878.
53. Ledger, A. E. W.; Slatford, P. A.; Lowe, J. P.; Mahon, M. F.; Whittlesey, M. K.; Williams, J. M. J. *Dalton Trans.;* **2009;** 716-722.
54. Slatford, P. A.; Whittlesey, M. K.; Williams, J. M. J. *Tetrahedron Lett.;* **2006;** *47;* 6787-6789.
55. Dierkes, P.; van Leeuwen, P. W. N. M. *J. Chem. Soc., Dalton Trans.;* **1999;** 1519-1529.
56. Reade, S. P.; Acton, A. L.; Mahon, M. F.; Martin, T. A.; Whittlesey, M. K. *Eur. J. Inorg. Chem.;* **2009;** 1774-1785.
57. Grushin, V. V. *Acc. Chem. Res.;* **2010;** *43;* 160-171.
58. (a) Kiplinger, J. L.; Richmond, T. G.; Osterberg, C. E. *Chem. Rev.;* **1994;** *94;* 373-431; (b) Torrens, H. *Coord. Chem. Rev.;* **2005;** *249;* 1957-1985; (c) Amii, H.; Uneyama, K. *Chem. Rev.;* **2009;** *109;* 2119-2183.

59. (a) Braun, T.; Izundu, J.; Steffen, A.; Neumann, B.; Stammler, H. G. *Dalton Trans.;* **2006;** 5118-5123; (b) Braun, T.; Perutz, R. N.; Sladek, M. I. *Chem. Commun.;* **2001;** 2254-2255; (c) Braun, T.; Salomon, M. A.; Altenhoner, K.; Teltewskoi, M.; Hinze, S. *Angew. Chem. Int. Ed.;* **2009;** *48;* 1818-1822; (d) Braun, T.; Wehmeier, F.; Altenhoner, K. *Angew. Chem. Int. Ed.;* **2007;** *46;* 5321-5324; (e) Böhm, V. P. W.; Gstottmayr, C. W. K.; Weskamp, T.; Herrmann, W. A. *Angew. Chem. Int. Ed.;* **2001;** *40;* 3387-3389; (f) Schaub, T.; Backes, M.; Radius, U. *J. Am. Chem. Soc.;* **2006;** *128;* 15964-15965; (g) Arisawa, M.; Suzuki, T.; Ishikawa, T.; Yamaguchi, M. *J. Am. Chem. Soc.;* **2008;** *130;* 12214-12215.
60. Aizenberg, M.; Milstein, D. *Science;* **1994;** *265;* 359-361.
61. Vela, J.; Smith, J. M.; Yu, Y.; Ketterer, N. A.; Flaschenriem, C. J.; Lachicotte, R. J.; Holland, P. L. *J. Am. Chem. Soc.;* **2005;** *127;* 7857-7870.
62. Reade, S. P.; Mahon, M. F.; Whittlesey, M. K. *J. Am. Chem. Soc.;* **2009;** *131;* 1847-1861.
63. (a) Nieczypor, P.; van Leeuwen, P. W. N. M.; Mol, J. C.; Lutz, M.; Spek, A. L. *J. Organomet. Chem.;* **2001;** *625;* 58-66; (b) Zuideveld, M. A.; Swennenhuis, B. H. G.; Boele, M. D. K.; Guari, Y.; van Strijdonck, G. P. F.; Reek, J. N. H.; Kamer, P. C. J.; Goubitz, K.; Fraanje, J.; Lutz, M.; Spek, A. L.; van Leeuwen, P. W. N. M. *J. Chem. Soc., Dalton Trans.;* **2002;** 2308-2317; (c) Yin, J. J.; Buchwald, S. L. *J. Am. Chem. Soc.;* **2002;** *124;* 6043-6048; (d) Fujita, K.; Yamashita, M.; Puschmann, F.; Alvarez-Falcon, M. M.; Incarvito, C. D.; Hartwig, J. F. *J. Am. Chem. Soc.;* **2006;** *128;* 9044-9045; (e) Grushin, V. V.; Marshall, W. J. *J. Am. Chem. Soc.;* **2006;** *128;* 12644-12645.
64. Huang, D. J.; Koren, P. R.; Folting, K.; Davidson, E. R.; Caulton, K. G. *J. Am. Chem. Soc.;* **2000;** *122;* 8916-8931.
65. (a) Kranenburg, M.; Kamer, P. C. J.; van Leeuwen, P. W. N. M.; Chaudret, B. *Chem. Commun.;* **1997;** 373-374; (b) Lenero, K. A.; Kranenburg, M.; Guari, Y.; Kamer, P. C. J.; van Leeuwen, P. W. N. M.; Sabo-Etienne, S.; Chaudret, B. *Inorg. Chem.;* **2003;** *42;* 2859-2866.
66. Kawano, H.; Tanaka, R.; Fujikawa, T.; Hiraki, K.; Onishi, M. *Chem. Lett.;* **1999;** 401-402.
67. Jazzar, R. F. R.; Bhatia, P. H.; Mahon, M. F.; Whittlesey, M. K. *Organometallics;* **2003;** *22;* 670-683.
68. Reade, S. P.; Nama, D.; Mahon, M. F.; Pregosin, P. S.; Whittlesey, M. K. *Organometallics;* **2007;** *26;* 3484-3491.
69. Barthazy, P.; Stoop, R. M.; Worle, M.; Togni, A.; Mezzetti, A. *Organometallics;* **2000;** *19;* 2844-2852.
70. (a) Kawano, H.; Nishimura, Y.; Onishi, M. *Dalton Trans.;* **2003;** 1808-1812; (b) Reddy, N. D.; Fanwick, P. E.; Walton, R. A. *Inorg. Chem.;* **2001;** *40;* 1732-1733.
71. Ledger, A. E. W.; Mahon, M. F.; Whittlesey, M. K.; Williams, J. M. J. *Dalton Trans.;* **2009;** 6941-6947.
72. Indeed, reaction of [Ru(xantphos)(PPh_3)(CO)H_2] with the ring expanded carbenes 6-Mes and 7-Mes at 343 K resulted in formation of the C-H insertion products previously isolated by the Whittlesey group: *see Ref 25*.

3. CHAPTER 3

3.1 PXP Pincer Ligands

The ability to control the reactivity of a metal centre by a structured but easily variable ligand system is one of the main aims of organometallic chemistry *(see also Chapters 1 & 2)*. Recent research has often focused on the use of polydentate ligands to achieve these aims since they offer a number of advantages over their monodentate and bidentate counterparts.[1]

Chelating ligands provide a unique combination of stabilization and reactivity, imparting strong metal-ligand interactions in some cases and exhibiting some degree of lability in others. A combination of steric and electronic effects can stabilize reactive intermediates or provide a barrier to unwanted side reactions and decomposition processes. Chelation can also create highly protected environments for the coordination of substrates, or enforce particular geometries around a metal centre.[2]

In particular, tridentate P-based pincer ligands containing two phosphorus atoms connected by a central linker group have become more and more popular.[3] This central linker group can consist of a metallated aryl ring to form an anionic PCP ligand, or an N or O atom, giving rise to neutral PNP or POP ligands respectively *(see Figure 1)*. Although PXP pincer ligands can enforce a variety of conformations, the most often encountered is a meridonal coordination mode, creating a *trans* P-M-P interaction. In general, the central linker group of a PCP pincer ligand remains coordinated to a metal centre throughout a reaction, whilst the neutral PNP and POP analogues can temporarily dissociate either the central atom or a phosphine substituent to introduce some hemilabile behaviour to the system.

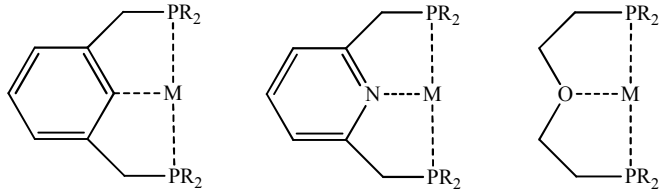

Figure 1: Various PXP ligands derived from variation of the central linker atom.

The following is not intended as a comprehensive review of transition metal complexes incorporating PXP pincer ligands. Instead, it hopes to provide a flavour of the current research in this area, with a particular focus on the use of PXP ligands in catalysis and as effective support

structures for the coordination of small molecules, and is also generally restricted to ruthenium-based systems.

3.2 PXP Pincer Ligands in Catalysis

The ability of PXP pincer ligands to enforce particular geometries is a useful attribute for catalytic applications. For instance, in some cases the PXP ligand is able to promote catalytic activity by ensuring that a reactive metal-hydride is orientated *cis* to the incoming substrate. van Koten *et al*. have developed ruthenium-PCP complexes for the transfer hydrogenation of ketones to their corresponding alcohols, using isopropanol.[4] KOH is added stoichiometrically to increase the concentration of the alkoxide ion present in the reaction. When [Ru(PCP)(PPh_3)X] (X = Cl or OSO_2CF_3) was reacted with isopropanol and KOH in the absence of any ketone, an alkoxy-hydride species was observed *via* NMR spectroscopy, with the hydride located *trans* to the metallated aryl ring of the PCP ligand *(see Figure 2)*. β-hydride elimination from this intermediate could then take place to afford acetone and a reactive metal-hydride species likely to be the catalytically active fragment. Isolation of the alkoxy hydride also confirmed that the structural unit enforced by the pincer ligand was retained during the catalysis. The system was able to hydrogenate a wide range of ketones in refluxing isopropanol to give good yields with excellent turnover frequencies that out-performed the analogous monophosphine systems, [Ru(PPh_3)$_3$$Cl_2$] and [Ru($PPh_3$)$_3$HCl].[5]

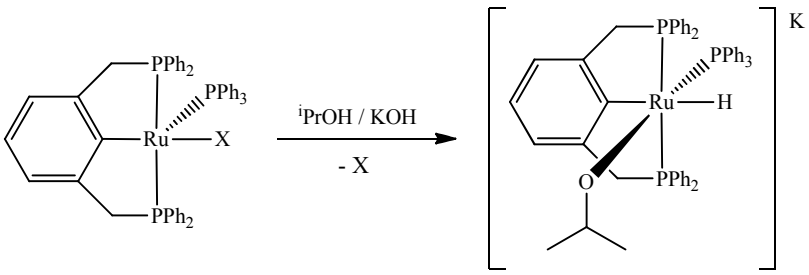

Figure 2: van Koten's [Ru(PCP)(PPh_3)X] complex (X = Cl or OSO_2CF_3) for the hydrogenation of ketones and formation of an anionic alkoxy-hydride intermediate.

The particular electronic and steric properties of pincer ligands are known to assist the stabilisation of reactive intermediates within a catalytic cycle. Occasionally this has resulted in the formation of complexes with limited activity. Reactions of these complexes can be halted at earlier stages than anticipated, revealing valuable mechanistic information about the exact configuration of the intermediates involved. Indeed, treatment of van Koten's [Ru(PCP)(PPh_3)Cl] complex with terminal alkynes resulted in the isolation of an unusual bridging carbene species rather than the

expected vinylidene compound *(see Figure 3)*.[6] This complex is derived from a C-C bond forming reaction between the aryl moiety of the PCP ligand and a vinylidene species. Evidently the combined orbital effects of the carbene and the chelating phosphine donors are able to support the bridging conformation of the observed product over dissociation of the ruthenium centre, resulting in the isolation of an arrested intermediate.

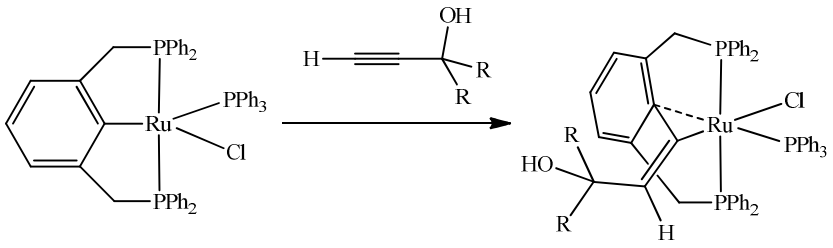

Figure 3: Reaction coordinate of [Ru(PCP)(PPh_3)Cl] and terminal alkynes resulting in an unusual bridging carbene complex.

Complexes incorporating pincer ligands have been widely used as mechanistic probes for C-H bond activation processes since examining their cyclometallation on introduction to a metal centre can yield useful information.[7] It has been argued that intermediate steps in the cyclometallation of these ligands might involve an agostic metal-ligand interaction followed by the aromatic substitution of the aryl proton by the metal centre. A cationic ruthenium (II) complex, [Ru(PCP)(PCHP)]OTf, has been isolated and appears to illustrate such an intermediate – the complex possesses one cyclometallated PCP ligand and one PCP ligand in a bidentate P-P conformation with an agostic interaction present between the aryl C-H bond and the ruthenium centre *(see Figure 4)*.[8] NMR spectroscopy revealed that the two forms of the PCP ligand were in exchange with the agostic proton switching from the neutral ligand to the cyclometallated carbon.[9] The metallated carbon of a PCP ligand has previously been considered a fixed interaction, but interestingly this study points to a flexible coordination mode of even the anionic pincer ligands.

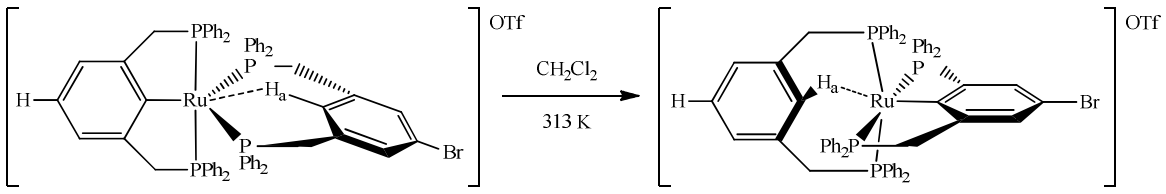

Figure 4: Exchange observed between the two forms of the PCP ligands in [Ru(PCP)(PCHP)]OTf.

Whilst the lability of an anionic PCP ligand is infrequently observed, the hemilability of neutral PNP ligands has been widely exploited for catalysis, with flexible coordination modes invoked in the catalytic cycle.

Milstein *et al.* have developed a number of ruthenium catalysts with hemilabile PNP pincer ligands. A [Ru(PNP)(CO)HCl] complex has been used to catalyse the direct synthesis of imines from primary alcohols and amines.[10] The reversible coordination of one phosphine arm was invoked to complete the catalytic cycle *(see Figure 5)*. The initial step involves coordination of the alcohol to form intermediate **i**. This is then followed by β-hydride elimination to afford the coordinated aldehyde species **ii**, with the process involving temporary dechelation of one phosphine terminus. Rapid closure of the phosphine arm results in the dissociation of the aldehyde (intermediate **iii**) which then goes on to react with the amine to form the hemiaminal **iv**. The elimination of water from this intermediate results in the substituted imine product.

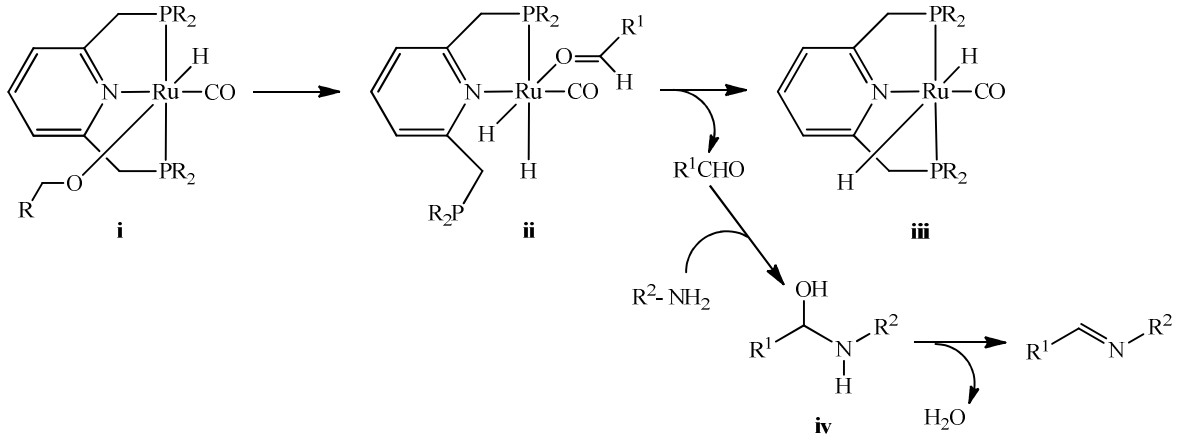

Figure 5: Possible mechanism for imine formation (R = ^{i}Pr, ^{t}Bu).[10]

An acridine-based pincer complex, [Ru(A-^{i}Pr-PNP)(CO)HCl] *(see Figure 6)*, has been used by the group to prepare primary amines, rather than secondary imines, directly from ammonia and primary alcohol substrates.[11] Once again, the catalytic cycle proposed involves reversible dechelation of one phosphine terminus to allow formation of an aldehyde from the initial coordination of the alcohol. However, in this case, the dissociated aldehyde reacts with ammonia (rather than a primary amine) to form a singly substituted imine. Unlike the previous example, this imine is less bulky and can therefore recoordinate to the ruthenium centre (*via* another reversible dechelation of the phosphine arm) where it is hydrogenated to give the corresponding primary amine.

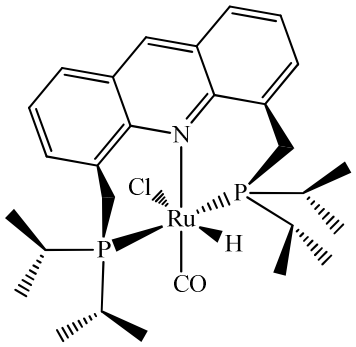

Figure 6: The acridine-based pincer complex, [Ru(A-^{i}Pr-PNP)(CO)HCl].[11]

Interestingly, the pyridine-based PNP ligand utilised by the Milstein group *(see Figure 5)* is able to facilitate catalysis by an additional process. This involves the reversible aromatisation of one arm of the pincer, allowing the PNP ligand to switch between neutral (**v**) and anionic (**vi**) coordination of the N moiety on treatment with hydrogen *(see Figure 7)*.[12] The dearomatised species **vi** is also able to activate N-H bonds. Reaction of **vi** with an amine or ammonia results in N-H bond activation *via* hydrogen transfer to the unsaturated arm, reforming the neutral PNP ligand. Evidence for this process was provided by treatment of the complex with ND_3 as ^{1}H NMR spectroscopy revealed the disappearance of one of the arm CH_2 signals due to deuterium incorporation.[13] This unusual metal-ligand cooperation has been observed in a number of catalytic systems developed by the Milstein group. In particular, it has created an effective system for the hydrogenation of esters to alcohols[12a] and is implicated in an unprecedented reaction forming amides from simple amine and alcohol substrates.[14]

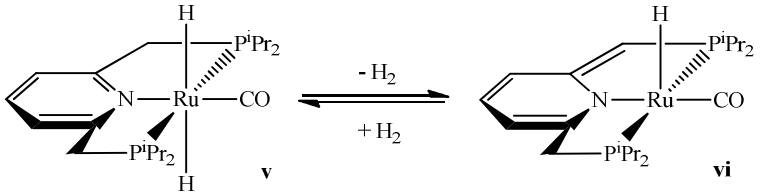

Figure 7: The unusual aromatisation/dearomatisation process to give species **v** and **vi** promoted by H_2.[12a]

POP ligands are much less prevalent in the literature than PCP or PNP ligands. The vast majority of studies on POP ligands, and in particular ligands such as xantphos or DPEphos, employ them as bidentate, rather than tridentate, ligands.[15] Despite this, a number of reports implicate a tridentate binding mode of POP ligands in catalysis. $[Rh(POP)(nbd)]^{+}$ (nbd = norbornadiene, POP = DPEphos) systems were developed by Weller *et al.* as catalysts for the intermolecular hydroacylation of alkenes and alkynes. In this study, the central O atom of a DPEphos ligand was

able to act in a hemilabile fashion, conferring added stability on the rhodium centre when coordinated but allowing access to the vacant site for incoming substrates by temporarily dissociating *(see Figure 8)*.[16]

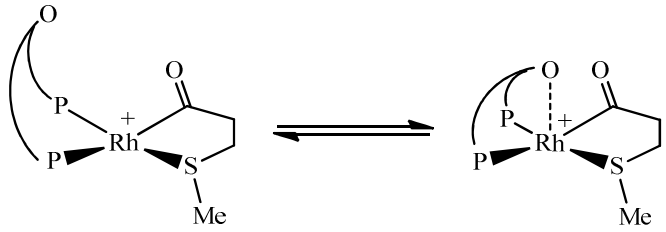

Figure 8: The equilibrium between bidentate and tridentate coordination of $[Rh(POP)(nbd)]^+$ (nbd = norbornadiene, POP = DPEphos).

Work by Mashima and coworkers described the addition of various bidentate phosphines to an *in situ* $[Pt(COD)Cl_2]$ catalysed amination of allylic alcohols to investigate the effect on reactivity, and identified xantphos and DPEphos as particularly effective ligands. Experimentation with other electron-rich bidentate phosphines established that the high catalytic activity was strongly related to the presence of a central O substituent, suggesting that tridentate coordination of the ligands played a role in the catalytic cycle.[17]

The use of PXP pincer ligands in catalysis is still relatively new, but, as discussed, has already had a large impact. Although reversible substrate coordination is a necessary requirement for any catalytic process to occur, the complex reaction chemistry involved in these systems is not yet fully understood. To this end, more fundamental studies have to take place to probe the varying effects of ancillary ligands on these systems by investigating the coordination and activation of small molecules such as H_2, O_2 and N_2.

3.3 PXP Pincer Ligands and Small Molecule Coordination

The field of small molecule coordination and activation is dominated by examples of Group 8 $[M(P\text{-}P)_2(X)L]^+$ complexes (M = Fe, Ru, Os) that incorporate bidentate phosphines, where L = η^2-H_2, O_2 or N_2 and X = H or Cl. Ruthenium compounds of this type were among the first dihydrogen hydride complexes to be isolated[18] and subsequent work has also demonstrated their ability to bind O_2 and N_2 ligands *(see Figure 9)*.[19]

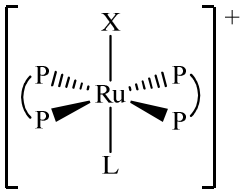

Figure 9: Basic representation of $[Ru(P\text{-}P)_2(X)L]^+$ complexes, where L = η^2-H_2, O_2 or N_2 and X = H or Cl.

The vast majority of the $[Ru(P\text{-}P)_2(X)L]^+$ literature examples display *trans* L-Ru-X geometries *(see Figure 9)*. Studies undertaken on dihydrogen hydrides of this form have found that this configuration corresponds to the energy minimum for the structure and that the dihydrogen moiety favours coordination *trans* to the ligand possessing the highest *trans* influence.[20] A theoretical study was carried out by Maseras and coworkers to evaluate both electronic and steric effects on the dihydrogen hydride systems through a combination of molecular orbital and molecular mechanics calculations respectively. They concluded that the energy minimum of the system was dependent on the bite angles of the particular diphosphine ligands involved. Thus smaller bite angles gave rise to *trans* H-Ru-H_2 interactions whilst larger bite angles led to a distorted *cis* configuration.[21] Indeed, synthesis of $[Ru(P\text{-}P)_2(\eta^2\text{-}H_2)H]^+$ analogues incorporating wide bite angle diphosphines such as homoxantphos, sixantphos and thixantphos resulted in a *cis* configuration of the dihydrogen ligand and the terminal hydride *(see Figure 10)*.[22]

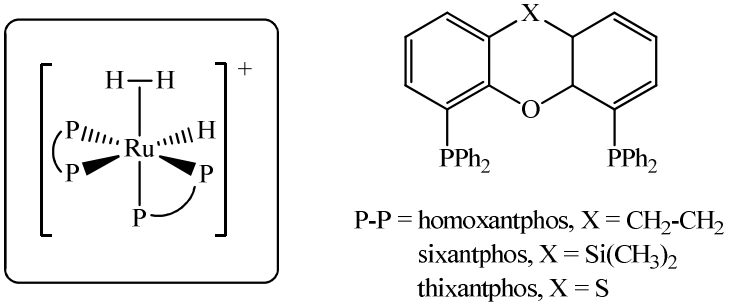

Figure 10: *Cis* conformation of $[Ru(P\text{-}P)_2(\eta^2\text{-}H_2)H]^+$.[22]

In contrast to ruthenium systems incorporating bidentate phosphines, very few examples of small molecule coordination onto ruthenium-PXP centres are known. In particular, the author is unaware of any examples of dioxygen coordination onto ruthenium-PXP complexes, although there are examples of rhodium-O_2 complexes with both PCP and PNP ligands[23] and a recent study also synthesised the first example of a late transition metal *bis*-dioxygen complex from an iridium-PCP framework.[24]

A small number of ruthenium dihydrogen complexes have been prepared with a PCP or PNP skeleton. Jia and coworkers have characterised the dihydrogen complexes $[Ru(PNP)(L)(\eta^2\text{-}H_2)Cl]^+$ (L = PPh_3 or CO),[25] whilst Amoroso *et al.* have synthesised a $[Ru(PCP)(PPh_3)(\eta^2\text{-}H_2)H]^+$ complex *(see **vii** and **viii**, Figure 11)*.[26] These can be considered as analogous compounds to the well studied dihydrogen complexes, $[Ru(P\text{-}P)_2(\eta^2\text{-}H_2)Cl]^+$ and $[Ru(P\text{-}P)(\eta^2\text{-}H_2)H]^+$ prepared by Morris *et al.*[18, 27] since both series of compounds exhibit coordination of the dihydrogen moiety *trans* to the chloride, or hydride, ligand.

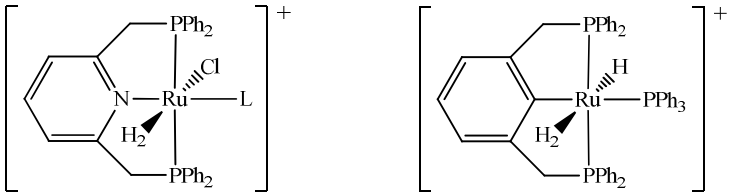

vii **viii**

Figure 11: The dihydrogen complexes $[Ru(PNP)(L)(\eta^2\text{-}H_2)Cl]^+$ (L = PPh_3 or CO) (**vii**) and $[Ru(PCP)(PPh_3)(\eta^2\text{-}H_2)H]^+$ (**viii**).

Ruthenium dihydrogen complexes have also been synthesised with anionic PNP ligands. A *trans* H-Ru-η^2-H_2 arrangement was found in a complex isolated by Fasulo and coworkers which incorporated the anionic PNP ligand, $[N(2\text{-}PPh_2\text{-}4\text{-}Me\text{-}C_6H_3)_2]$ *(see **ix**, Figure 12)*.[28] Watson *et al*. have prepared a number of dihydrogen hydride compounds with a silicon-based PNP ligand that was first developed by Fryzuk.[29] The dihydrogen hydride complexes $[Ru(HPNP\text{-}Cy)H_3Cl]$ and $[Ru(PNP\text{-}Cy)H_3]$ were isolated, featuring both protonated (neutral) and deprotonated (anionic) forms of the ligand respectively *(see **x** and **xi**, Figure 12)*.[30] Both complexes displayed only one hydride resonance of integral 3 in the ^{1}H NMR spectrum even at low temperature. However, T_1(min) values were measured at 59 and 45 ms for **x** and **xi** respectively, values in agreement with an averaged T_1 arising from *cis* dihydrogen and hydride ligands rather than a trihydride system.

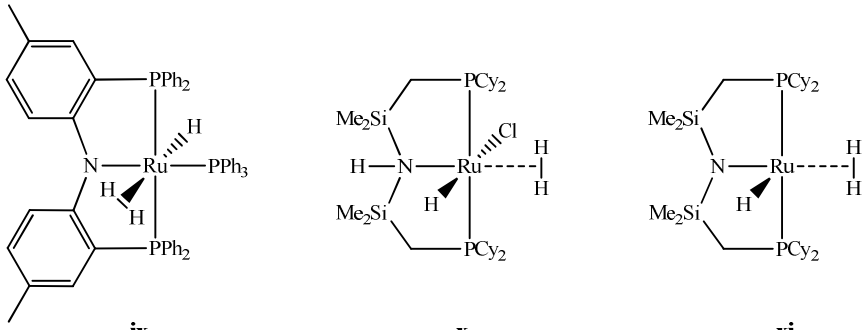

ix **x** **xi**

Figure 12: Ruthenium dihydrogen hydride complexes featuring anionic PNP ligands.

Milstein and coworkers have attempted to rectify the lack of research in this area and have synthesised neutral ruthenium dihydrogen compounds with both PCP and PNP ligands.[31] They were able to synthesise the unusual *bis*-dihydrogen hydride compound [Ru(PCP)(η^2-H_2)$_2$H] on reaction of [Ru(COD)(Me-allyl)$_2$] with the PCP ligand under 7 bar H_2 *(see Figure 13)*. The two dihydrogen ligands were located *trans* to one another with the hydride found *trans* to the metallated aryl ring of the PCP ligand. Although only one broad resonance of integral 5 was identified in the hydride region of the ^{1}H NMR spectrum at room temperature, studies at low temperature were able to resolve three signals; two broad η^2-H_2 resonances at δ -5.05 and -7.01 and one sharp hydride signal at δ -11.83 (t, $^2J_{HP}$ = 17.7 Hz).

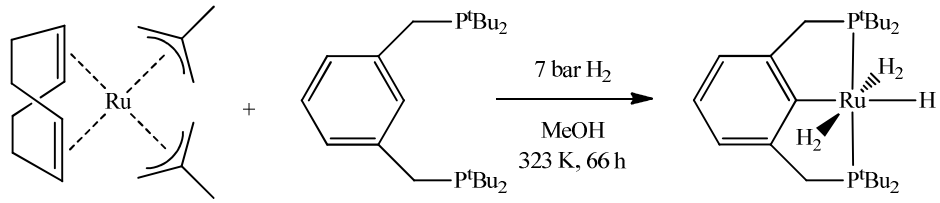

Figure 13: Reaction to form the unusual *bis* dihydrogen complex [Ru(PCP)(η^2-H_2)$_2$H].[31]

An analogous reaction with the PNP ligand instead produced the dihydrogen dihydride complex [Ru(PNP)(η^2-H_2)H_2] *(see Figure 14)*. In this case, the ^{1}H NMR spectrum at 298 K revealed a single sharp signal at δ –7.3 (t, 4H, $^2J_{HP}$ = 13.2 Hz). Cooling the sample to 193 K broadened this signal significantly. T_1(min) for this resonance was calculated at 77 ms, θ_{min} = 228 K, confirming that the signal arose from a dihydrogen ligand. This data allowed an upper limit of 1.11 Å to be calculated for the H-H distance.

A stream of N_2 bubbled through a sample of the dihydrogen complex resulted in the formation of a dinitrogen complex *(see Figure 14)*. This transformation was rather slow (66% conversion after 1.5 h) with traces of the dihydrogen precursor remaining even after 24 h. The reaction proved completely reversible, with the dihydrogen complex regenerated under 1 atm. of H_2.

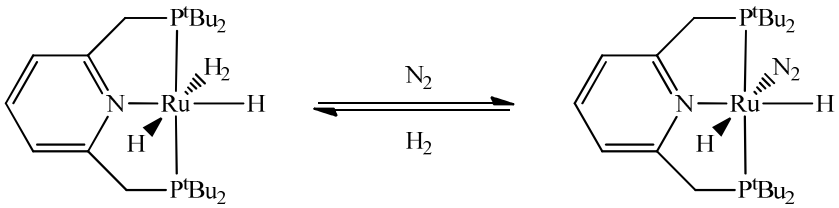

Figure 14: Reversible formation of dinitrogen complex and dihydrogen complex under N_2 and H_2 atm. respectively.[31]

Gusev *et al*. have isolated a number of ruthenium dinitrogen complexes with both aryl and alkyl PCP ligands featuring coordination of the dinitrogen ligand *trans* to the metallated carbon, such as $[Ru(CH(C_2H_4\text{-}P^tBu_2)_2)(N_2)H]$ and the silyl complex $[Ru(1,3\text{-}(CH_2P^tBu_2)_2\text{-}C_6H_4)(PhSi(H)Cl)HCl]$ *(see **xii** and **xiii**, Figure 15)*.[32]

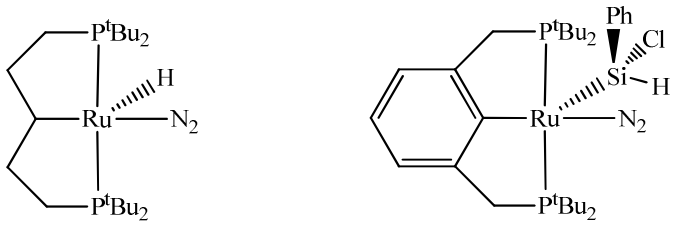

xii **xiii**

Figure 15: Ruthenium dinitrogen complexes featuring both alkyl and aryl PCP ligands.

Further ruthenium (II) dinitrogen complexes have been prepared by Gusev[33] and Milstein,[34] incorporating PCP and PNP ligands respectively. In these species, the dinitrogen ligand is bound end-on and *trans* to either the metallated carbon of the aryl ring in the former or the N-substituent in the latter case. Both systems were found to be in equilibrium between a monomeric and a dimeric form where the dinitrogen ligand was coordinated to one or both ruthenium centres. The Gusev system exists as three species in solution *(see Scheme 1, Figure 16)*, **xv** and **xvi** arising when a solution of **xiv** was left under nitrogen. Although **xvi** was the most prevalent form in solution, it was also the most soluble so that a mixture of **xiv** and **xv** was recrystallised from the reaction mixture when left under N_2. The equilibrium position in the Milstein system *(see Scheme 2, Figure 16)* was dependent on the amount of compound in solution and the N_2 pressure.

Scheme 1

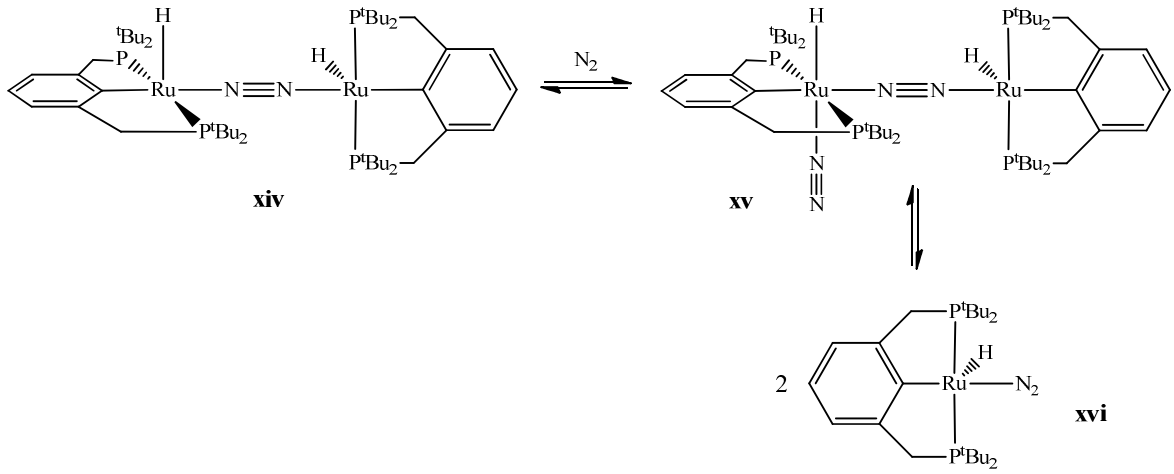

Scheme 2

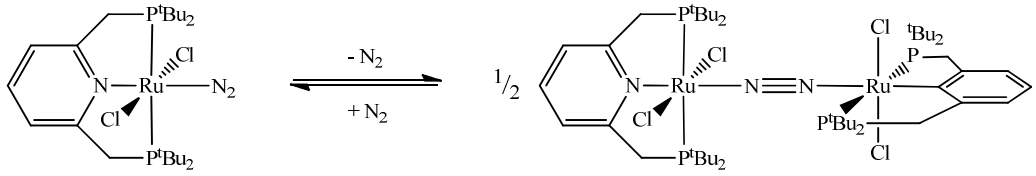

Figure 16: Reaction in solution of the Gusev[33] and Milstein[34] systems *(Scheme 1 and 2 respectively)*.

In general, POP pincer ligands are far less prevalent in the literature than their PCP or PNP counterparts. Gusev *et al*. were the first to synthesise ruthenium POP complexes, and examined their coordination chemistry with small molecules.[35] To offer the most direct comparison with the PCP and PNP systems, the researchers used the simplest POP ligand structure possible. This consisted of an ethyl ether backbone linking together two phosphine groups with either ^{t}Bu or ^{i}Pr substituents. Initial reaction of these POP ligands with $[Ru(p\text{-cymene})Cl_2]_2$ gave $[Ru(POP\text{-}^{t}Bu)Cl_2]$ (**xvii**), stabilised by a γ-agostic C-H···Ru interaction from one ^{t}Bu group, and a dimeric complex, $[Ru_2(POP\text{-}^{i}Pr)_2(\mu\text{-}Cl)_3]Cl$ (**xviii**) *(see Figure 17)*. A number of monomeric dihydrogen and dinitrogen complexes (**xix-xxii**) were synthesised from these two precursors by introduction of a H_2 or N_2 atmosphere.

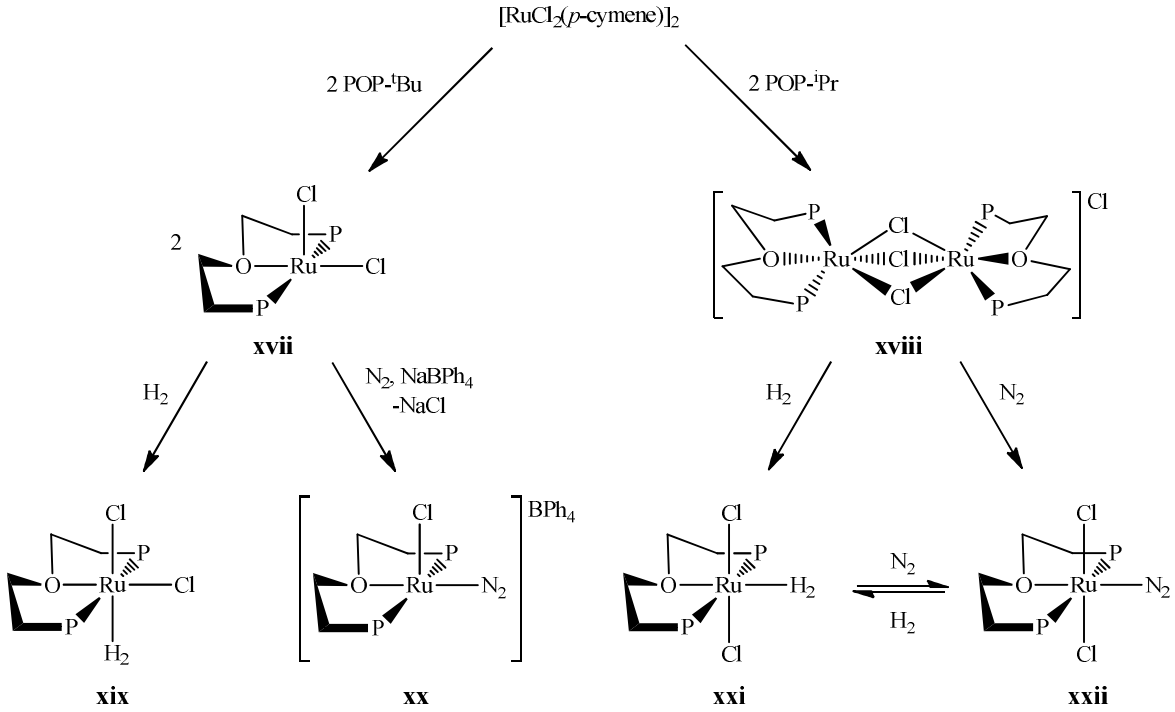

Figure 17: Reactions of ruthenium POP complexes with H_2 and N_2.[35]

In particular, the researchers noted the contrasting reactivity between the Ru-POP-^{t}Bu system and the analogous Milstein Ru-PNP-^{t}Bu complexes *(see Scheme 2, Figure 16)*.[34] They drew attention to the instability of [Ru(POP-^{t}Bu)(N_2)Cl_2] and [Ru_2(POP-^{t}Bu)$_2$(μ-N_2)Cl_4] complexes in relation to their stable PNP-^{t}Bu counterparts. These observations were contrasted with their isolation of the agostically stabilised [Ru(POP-^{t}Bu)Cl_2] (**xvii**) and [Ru(POP-^{t}Bu)(N_2)Cl]$^+$ (**xx**), since PNP analogues of these complexes were not observed by Milstein *et al*.

Gusev and coworkers explained these differences in reactivity by examining the backbone orientation of the POP-^{t}Bu and PNP-^{t}Bu ligands *(see Figure 18)*. The two five membered rings formed by coordination of the POP ligand are coplanar, placing the ^{t}Bu groups in an *eclipsed* conformation with two of these substituents flanking the vacant coordination site. In contrast, the pyridine ring of the PNP ligand is tilted, forcing one CH_2 group above the plane and one below and the ^{t}Bu groups into a *gauche* conformation. This effectively makes the POP-^{t}Bu ligand more bulky than its PNP counterpart resulting in a number of consequences. Whilst agostic interactions are more favourable, a chloride ligand has to be substituted to allow the dinitrogen ligand to coordinate in **xx**, and the dihydrogen ligand in **xix** has to coordinate below the ligand plane (an effect not seen in its ^{i}Pr analogue **xxi** or in the Milstein system). In contrast, the smaller effective bulk of the PNP-^{t}Bu ligand favours the formation of dimers and the coordination of small molecules within the ligand plane.

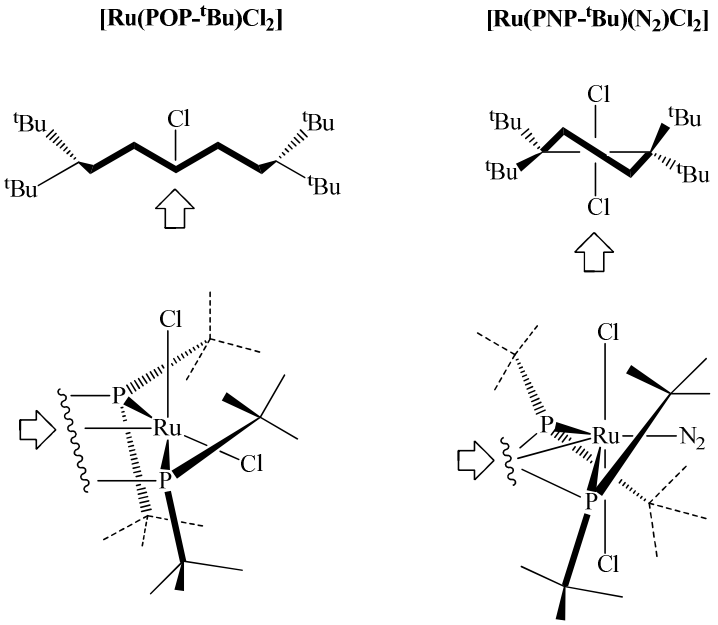

Figure 18: View along the O-Ru axis and side view of [Ru(POP-^{t}Bu)Cl_2][35] (**xvii**) and view along the N-Ru axis and side view of Milstein's [Ru(PNP-^{t}Bu)$(N_2)Cl_2$] complex *(see also Scheme 2, Figure 16).*[34]

Whilst the tridentate coordination of POP ligands are implicated in a number of catalytic processes,[16-17] the greater majority of studies demonstrate their bidentate ('O-out') coordination.[15] Although the reversible coordination of substrates is implied in the progress of any catalytic reaction, there is a distinct lack of information available regarding small molecule coordination to M-POP structures, particularly where M = Ru. More fundamental studies on the tridentate coordination of POP ligands and their use as frameworks for small molecule coordination need to take place to understand the complex reaction chemistry at work in these systems.

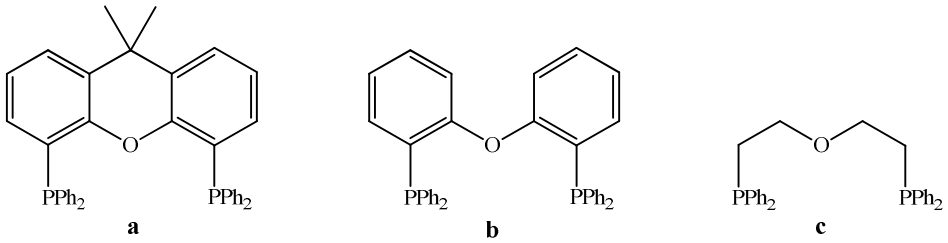

Figure 19: The POP ligands xantphos, **a**, DPEphos, **b**, and $(Ph_2PCH_2CH_2)_2O$, **c**.

Previous work focused on the coordinatively saturated systems [Ru(xantphos)(L)$(CO)H_2$] and [Ru(xantphos)(L)(CO)HF] (L = PPh_3 or NHC), where the xantphos ligand adopted a bidentate ('O-out') conformation *(see Chapters 1 & 2)*. We wished to further investigate the coordination

chemistry of xantphos and the related POP ligands, DPEphos and $(Ph_2PCH_2CH_2)_2O$ ***(a, b and c** respectively, see Figure 19)*. To this end, the tridentate coordination of these ligands was induced by reaction with the coordinatively unsaturated precursor $[Ru(PPh_3)_3HCl]$ (**23**) to give a series of $[Ru(POP)(PPh_3)HCl]$ complexes (**24a-c**). The coordination chemistry of these compounds was subsequently investigated, and also contrasted with that of $[Ru(dppf)(PPh_3)HCl]$ (**31**) in order to highlight the effects of oxygen coordination in these systems.

3.4 Synthesis and Characterisation of $[Ru(POP)(PPh_3)HCl]$ Precursors

Reaction of $[Ru(PPh_3)_3HCl]$ (**23**) with 1-3 equivalents of the chelating phosphines in refluxing THF resulted in the formation of the coordinatively saturated complexes $[Ru(POP)(PPh_3)HCl]$ (POP = xantphos, **24a**; DPEphos, **24b**; $(Ph_2PCH_2CH_2)_2O$, **24c**) *(see Figure 20)*. Each complex displayed a single hydride resonance in the ^1H NMR spectrum at 298 K, with a doublet of triplets multiplicity (**24a**: δ -16.22, **24b**: δ -16.34, **24c**: δ -17.54), and *cis* $^2J_{HP}$ couplings to both the chelating ligands and the PPh_3 moiety. $^{31}P\{^1H\}$ NMR spectra at 298 K of **24a** and **24c** exhibited the expected doublet (**24a**: δ 46.7; **24c**: δ 42.3) and triplet resonances (**24a**: δ 75.2; **24c**: δ 71.0) corresponding to the coordinated POP and PPh_3 ligands respectively, with small *cis* $^2J_{PP}$ values indicative of *mer* configuration of the POP ligand. In contrast to both the coordinated xantphos and $(Ph_2CH_2CH_2)_2O$ ligands, DPEphos can assume a conformation in which the four P-phenyl groups adopt pseudo-equatorial and pseudo-axial positions. The non-equivalence of the phosphorus atoms was reflected in a broad ^{31}P resonance for the DPEphos ligand at 298 K which resolved upon cooling to two doublet of doublets, each possessing a large *trans* splitting of 285 Hz.

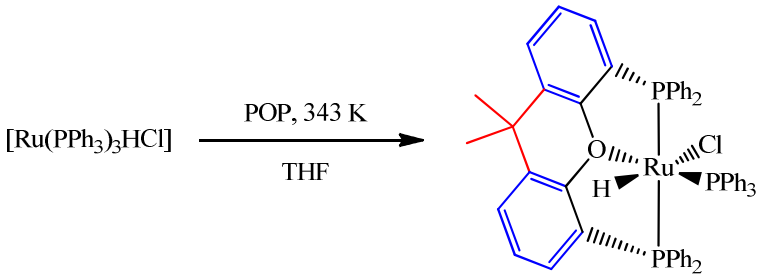

Figure 20: Reaction to form $[Ru(POP)(PPh_3)HCl]$ (POP = xantphos, **24a**, DPEphos, **24b**, and $(Ph_2PCH_2CH_2)_2O$, **24c**).

The NMR data of **24a-c** were consistent with a *trans* H-Ru-Cl interaction across an equatorial plane containing the chelating POP ligand and the PPh_3 group. This geometry was confirmed by the X-ray crystal structures of **24a-c** *(see Figure 21)*. In all three cases, the POP

ligands formed a tridentate pincer, coordinating through the oxygen atom and the two phosphorus termini in a *mer* conformation. Tridentate coordination of the POP ligand presumably allows the complexes to reach an 18-electron configuration. The two PPh_2 termini of the POP ligand are found *trans* to one another, and the wide P-Ru-P angles (156-158°) result in a lengthening of the Ru-$P_{chelate}$ bonds (2.29-2.34 Å) in relation to their Ru-PPh_3 counterparts (all ca. 2.22 Å) *(see Table 1)*. Ru-O bond distances were measured in the range 2.25-2.28 Å *(see Table 1)*. A significantly longer Ru-O contact (2.33 Å) was found in [Ru(xantphos)(=CHPh)Cl_2],[36] presumably due to the high *trans* influence of the carbene,[37] whilst shorter contacts (2.12-2.17 Å) were found in ruthenium POP complexes in which POP = ($^{i}Pr_2CH_2CH_2)_2O$ and ($^{t}Bu_2CH_2CH_2)_2O$, where the more flexible ligand backbones allowed for closer contact with the ruthenium centre.[35] Complexes **24a** and **24b** exhibit significant π-stacking between the phenyl rings of the chelating phosphine and those of the PPh_3 moiety. The shortest distance between the mean planes of the rings based on C29 and C41 in **24a** was measured at 3.28 Å, with those of C25 and C37 in **24b** recorded at 3.24 Å. Typical accepted distances for π-stacking are in the range 3.3-3.8 Å.[38]

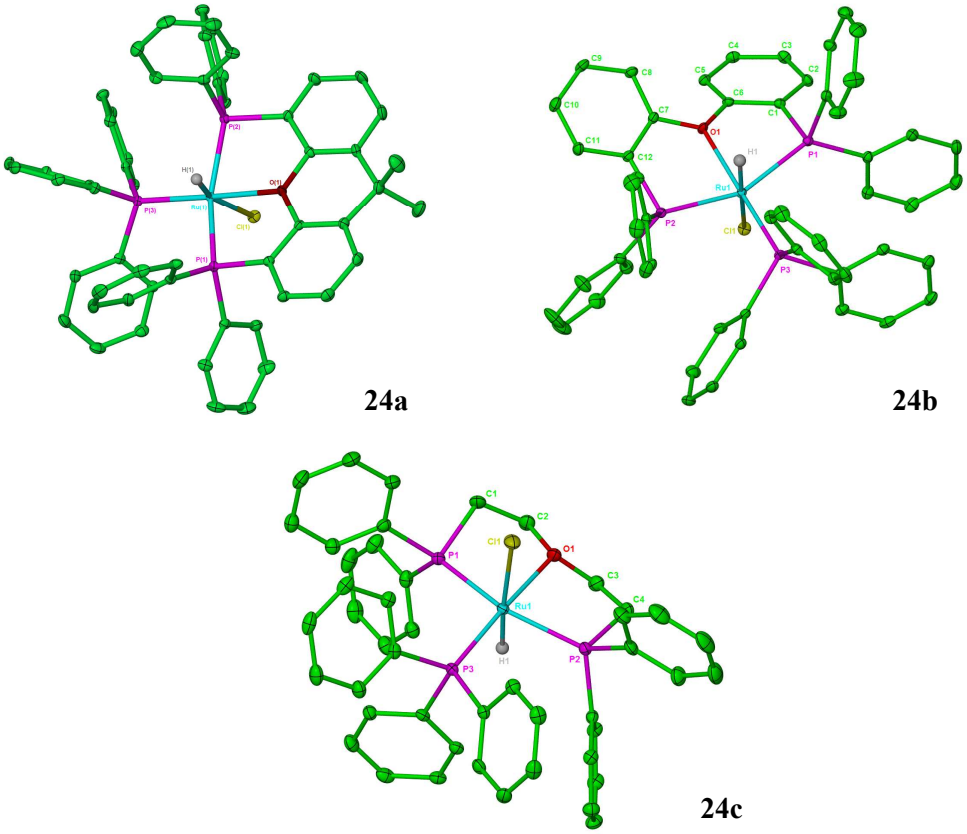

Figure 21: Molecular structures of [Ru(xantphos)(PPh_3)HCl] (**24a**), [Ru(DPEphos)(PPh_3)HCl] (**24b**) and [Ru(($Ph_2PCH_2CH_2)_2O$)(PPh_3)HCl] (**24c**). Thermal ellipsoids are shown at 30% level. Solvent moieties and all hydrogen atoms, except Ru-H, are omitted for clarity.

Table 1: Selected bond lengths [Å] and angles [˚] for [Ru(xantphos)(PPh_3)HCl] (**24a**), [Ru(DPEphos)(PPh_3)HCl] (**24b**) and [Ru(($Ph_2CH_2CH_2)_2O$)(PPh_3)HCl] (**24c**)

	24a	**24b**	**24c**
Ru-P1	2.3037(8)	2.3319(7)	2.3085(9)
Ru-P2	2.3060(8)	2.2918(7)	2.3364(8)
Ru-PPh_3	2.2277(8)	2.2271(7)	2.2292(8)
Ru-O	2.2509(19)	2.2480(17)	2.278(2)
Ru-Cl	2.5200(8)	2.5120(7)	2.5192(9)
P1-Ru-P2	156.39(3)	156.52(3)	158.31(3)
P1-Ru-PPh_3	98.66(3)	101.76(2)	98.91(3)
P2-Ru-PPh_3	100.18(3)	98.52(3)	99.48(3)
O-Ru-PPh_3	176.46(6)	177.05(6)	171.08(6)
Cl-Ru-PPh_3	100.16(3)	96.82(2)	101.63(3)

Substitution of the PPh_3 moiety was attempted by reaction of **24a** with the N-heterocyclic carbenes IEt_2Me_2 and I^{t}Bu. However, no reaction was observed with 3 equivalents IEt_2Me_2 after 3 h in refluxing THF, while the analogous reaction with I^{t}Bu resulted in the formation of a number of low intensity hydride species alongside a large amount of unreacted starting material. This resistance to substitution pointed towards a highly stable O-Ru-PPh_3 interaction.

Treatment of **24a** with $NaBH_4$ in refluxing EtOH resulted in the decarbonylation of the solvent to form [Ru(xantphos)(PPh_3)(CO)H_2] (**2**) *(see Section 1.6, Chapters 1 & Section 2.7, Chapter 2)*, the xantphos ligand reverting to a bidentate coordination mode.[39] Repeating the reaction in ^{i}PrOH gave rise to a second order multiplet at δ -6.14 in the ^{1}H NMR spectrum *(see **a**, Figure 22)* and doublet and triplet resonances at δ 46.6 and δ 86.7 in the $^{31}P\{^1H\}$ NMR spectrum. A $^2J_{PP}$ coupling of 14.3 Hz indicated *cis* disposition of the xantphos ligand with respect to the PPh_3 group. In addition, selective ^{31}P decoupling of the doublet resonance at δ 46.6 gave rise to a doublet at δ -6.14 in the ^{1}H NMR spectrum ($^2J_{HP}$ = 25.4 Hz) arising from *cis* orientation of the hydride with respect to PPh_3 *(see **c**, Figure 22)*. This data suggested possible formation of a *trans* dihydride complex retaining tridentate coordination of the xantphos ligand *(see **xxiii**, Figure 23)*. However, on selective ^{31}P decoupling of the triplet resonance at δ 86.7 the hydride signal resolved into a second-order multiplet with *trans* coupling to ^{31}P still evident *(see **b**, Figure 22)*. This instead pointed towards a structure with two *trans* H-Ru-PPh_2 interactions (and bidentate coordination of the xantphos ligand), arising from chemically identical *cis* dihydrides *(see **xxiv**, Figure 23)*.

Unfortunately this species gradually degraded in solution over two weeks at 298 K and could not be isolated, despite attempts at recrystallisation from various solvent systems.

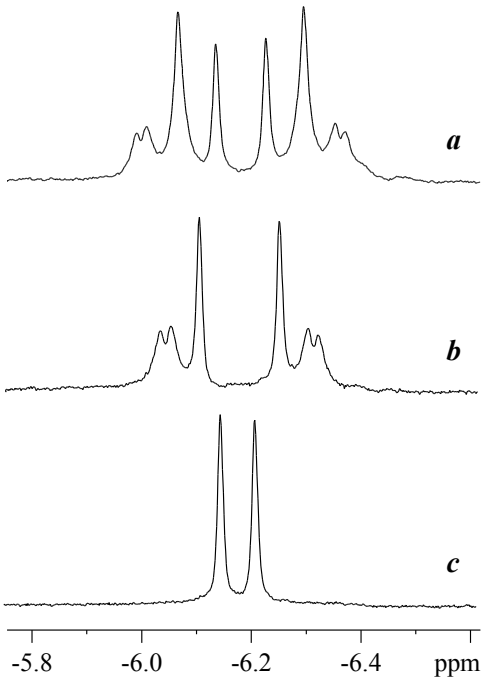

Figure 22: Hydride region of the ^{1}H NMR spectrum (C_6D_6, 400 MHz, 298 K) following reaction of [Ru(xantphos)(PPh_3)HCl] (**24a**) and $NaBH_4$ in ^{i}PrOH. The initial second order multiplet is shown in spectrum ***a***, with the resulting signals on selective ^{31}P decoupling at δ 86.7 in spectrum ***b***, and selective ^{31}P decoupling at δ 46.6 in spectrum ***c***.

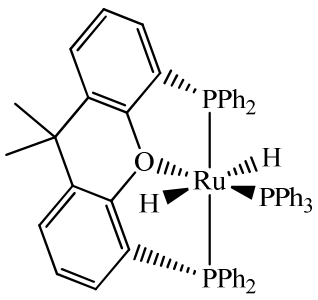

xxiii

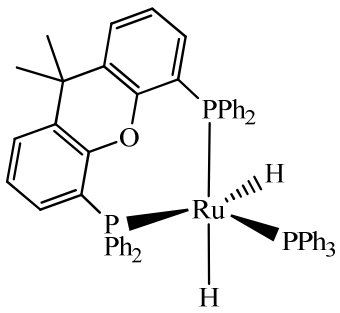

xxiv

Figure 23: The two possible structures of the [Ru(xantphos)(PPh_3)H_2] dihydride product formed on reaction of [Ru(xantphos)(PPh_3)HCl] (**24a**) and $NaBH_4$ in ^{i}PrOH.

The reaction of **24a** with MeLi in THF afforded a doublet of doublet of doublets hydride signal at δ -8.36 in the ^{1}H NMR spectrum with one larger *trans* and two *cis* splittings to phosphorus ($^{2}J_{HP}$ = 96.4, 24.3 and 17.6 Hz). A new broad singlet emerged at δ -0.95 in a 3:1 ratio with the

hydride resonance. Although this NMR data was suggestive of a methyl hydride complex, it swiftly decomposed over 12 h in solution at ambient temperature and again could not be isolated.

3.5 Chloride Abstraction from [Ru(POP)(PPh_3)HCl] (24a-c)

Reaction of [Ru(POP)(PPh_3)HCl], **24a-c**, with 1.1 equivalents $NaBAr_4^F$ (BAr_4^F = B(3,5-$C_6H_3(CF_3)_2)_4$) in dichloromethane resulted in abstraction of the chloride ligands to form the cationic species **25a-c** *(see Figure 24)*. Their ^1H NMR spectra at 298 K exhibited hydride signals at considerably lower frequencies (**25a**: δ -19.67; **25b**: δ -18.67 and **25c**: δ -21.05) than those observed for the neutral precursors with doublet of triplets splitting patterns and *cis* $^2J_{HP}$ couplings. The $^{31}P\{^1H\}$ NMR spectra at 298 K revealed the expected doublet and triplet signals with *cis* $^2J_{PP}$ values, suggesting identical conformations of the hydride and phosphine ligands to those found in the starting materials.

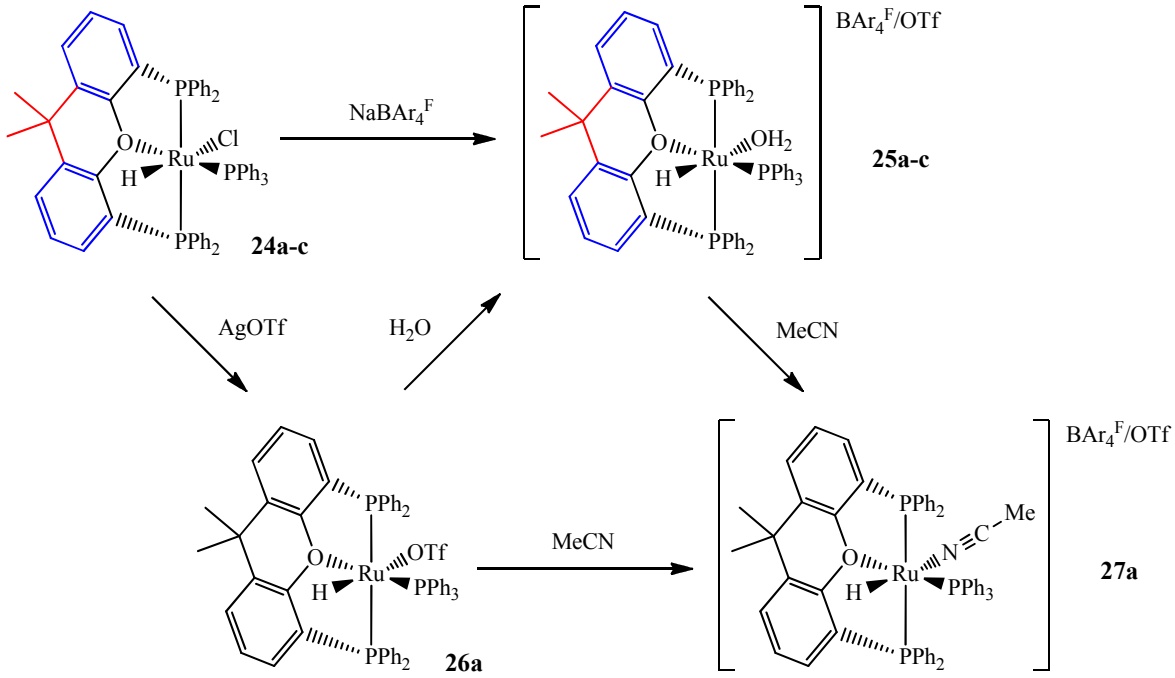

Figure 24: Reaction of [Ru(POP)(PPh_3)HCl] with $NaBAr_4^F$ and AgOTf to form [Ru(POP)(PPh_3)(OH_2)H]BAr_4^F/OTf

Initially it was unclear whether the hydride in species **25a-c** was located *trans* to a vacant site or to a weakly bound solvent moiety.[40] The serendipitous isolation of a crystal of **25a** revealed a loosely coordinated water molecule *trans* to the hydride in the X-ray crystal structure *(see Figure 25)*, with an unusually long Ru-OH_2 bond length of 2.32(4) Å *(see Table 2)*. A number of cationic

ruthenium (II) structures featuring aqua ligands are present in the literature, with Ru-OH_2 bonds in the range 2.14-2.17 Å.[41] However, a species also featuring a *trans* H-Ru-OH_2 interaction, $[Ru(dppe)_2(OH_2)H]^+$, exhibited a Ru-OH_2 bond distance of 2.280(6) Å, suggesting that the length of the Ru-OH_2 bond is heavily influenced by the high *trans* influence of the hydride.[42]

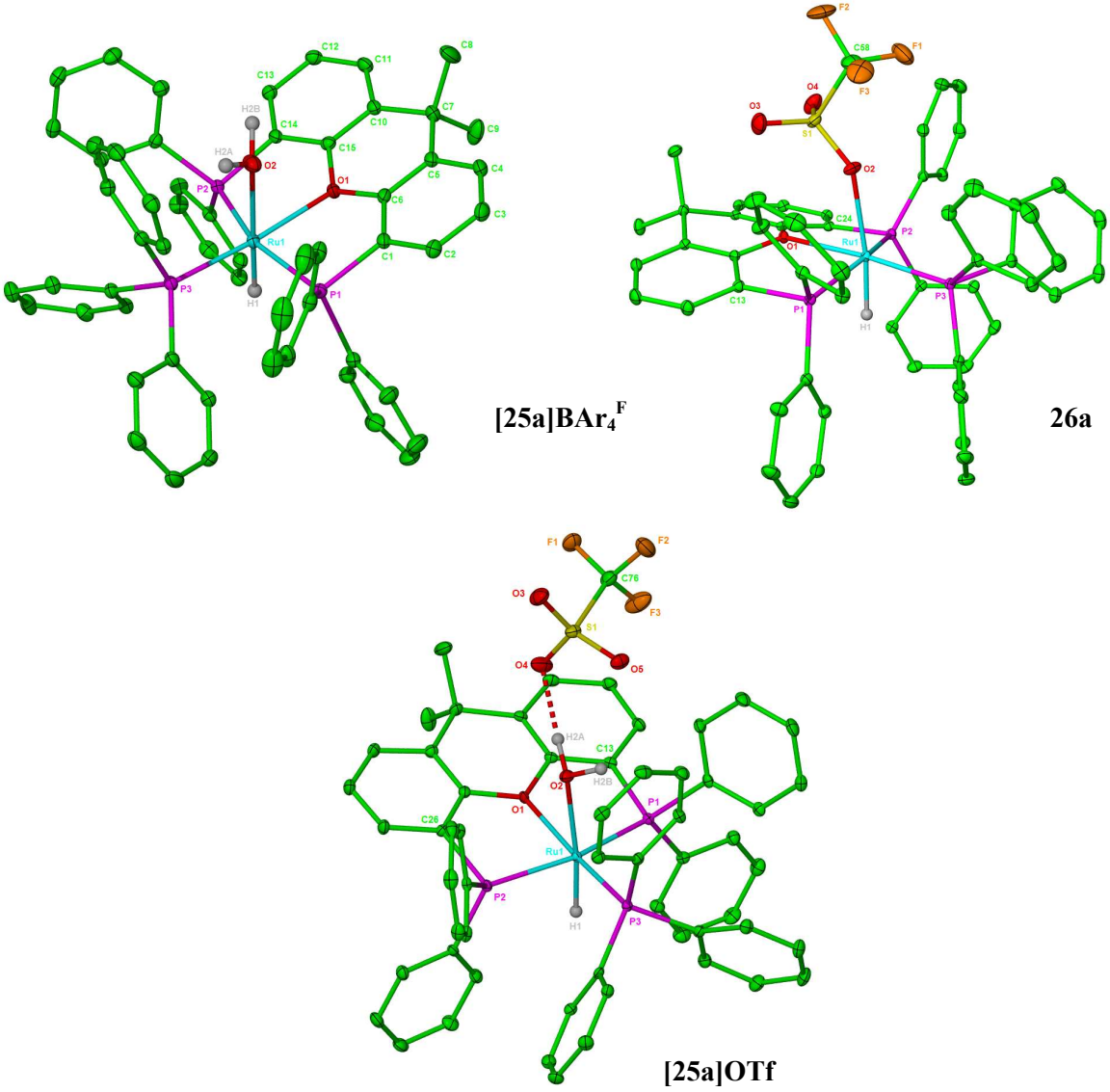

Figure 25: Molecular structures of the cations in $[Ru(xantphos)(PPh_3)(OH_2)H]BAr_4^F$, **[25a]$BAr_4^F$**, and the complexes $[Ru(xantphos)(PPh_3)(OH_2)H]OTf$, **[25a]OTf**, and $[Ru(xantphos)(PPh_3)(OTf)H]$, **26a**. Thermal ellipsoids are shown at the 30% probability level. All hydrogen atoms, except Ru-H and Ru-OH_2, are omitted.

Table 2: Selected bond lengths [Å] and angles [°] in [Ru(xantphos)(PPh_3)(OH_2)H]BAr_4^F (**[25a]BAr_4^F**), [Ru(xantphos)(PPh_3)(OH_2)H]OTf (**[25a]OTf**) and [Ru(xantphos)(PPh_3)(OTf)H] (**26a**)

	[25a]BAr_4^F	**[25a]OTf**	**26a**
Ru-P1	2.306(13)	2.3029(8)	2.3062(6)
Ru-P2	2.298(13)	2.3039(7)	2.3118(5)
Ru-PPh_3	2.228(13)	2.2237(8)	2.2424(6)
Ru-O	2.25(3)	2.243(2)	2.2563(15)
Ru-OH_2	2.32(4)	2.297(2)	-
Ru-OTf	-	-	2.3139(17)
P1-Ru-P2	160.1(5)	160.27(3)	156.72(2)
P1-Ru-PPh_3	99.4(5)	100.59(3)	96.72(2)
P2-Ru-PPh_3	99.5(5)	98.24(3)	98.92(2)
O-Ru-PPh_3	173.1(10)	171.54(6)	175.34(4)

Despite evidence for the coordination of H_2O in the solid state, further confirmation was sought for coordination in solution. To this end, **24a** was reacted with $NaBAr_4^F$ in degassed, but undried, dichloromethane. The ^1H NMR spectrum of the reaction revealed a broad hydride resonance at the same frequency as that observed for **25a** (δ -19.67), the broad signal suggesting exchange. A signal corresponding to the coordinated H_2O moiety could not be identified.

A different route to the aqua complex **25a** was also attempted *(see Figure 24)*. The triflate complex [Ru(xantphos)(PPh_3)(OTf)H], **26a**, was synthesised by reaction of **24a** with AgOTf (OTf = OSO_2CF_3) in dichloromethane *(see Figure 25 and Table 2)*. The complex exhibited a broad hydride signal at δ -22.27 in the ^1H NMR spectrum, which sharpened to the expected doublet of triplets multiplicity upon heating to 315 K. Addition of 2 equivalents H_2O to a sample of **26a** resulted in a broadening of the hydride signal, and a shift to higher frequency (δ -21.81). This effect was magnified on the addition of 10 equivalents H_2O to the sample, with the hydride resonance broadened still further and shifted to δ -19.98. The triflate salt of **25a** was crystallised from this reaction, with OH_2 coordination *trans* to the hydride once again observed *(see Figure 25)*. A shorter Ru-OH_2 interaction was found (Ru-OH_2 = 2.297(2) Å) *(see Table 2)*, and there was close association of the triflate anion with one of the hydrogen atoms on the H_2O ligand (O-H···OSO_2CF_3 = 1.80 Å).

More coordinating solvents were able to displace the triflate ligand. Thus reaction of [Ru(xantphos)(PPh_3)(OTf)H], **26a**, with 5 equivalents MeCN resulted in formation of the

acetonitrile complex [Ru(xantphos)(PPh_3)(MeCN)H]OTf, **27a** and a shift of the hydride resonance to higher frequency in the ^{1}H NMR spectrum (δ -13.42) *(see Figure 24)*. Similarly, the analogous reaction of **25a** with MeCN saw a comparable shift of the hydride signal to δ -13.39 with identical multiplicities as observed for the triflate analogue. Acetonitrile coordination was confirmed by a singlet at δ 1.36 in the ^{1}H NMR spectrum of **27a** corresponding to the methyl protons, and signals at δ 2.9 and 121.8 in the ^{13}C{^{1}H} NMR spectrum. The expected ν(CN) stretch was observed at 2241 cm^{-1} in the IR spectrum.

3.6 Reaction of [Ru(POP)(PPh_3)(OH_2)H]BAr_4^F (25a-c) with O_2

Immediate and irreversible formation of the cationic complexes [Ru(POP)(PPh_3)(η^2-O_2)H]BAr_4^F, **28a-c**, occurred when dichloromethane solutions of **25a-c** were exposed to air *(see Figure 26)*. High frequency hydride signals were observed for **28a-c** between δ -1.5 and -2.9 in the ^{1}H NMR spectra, each displaying a doublet of triplets multiplicity. The magnitude of $^2J_{HP}$ (26-32 Hz) suggested coordination of the oxygen moiety *trans* to the hydride, retaining the geometry observed for the aqua complexes, **25a-c**. The hydride chemical shifts **28a-c** fall within the range of values recorded for other cationic ruthenium systems with *trans* H-Ru-O_2 interactions. Thus the hydride signal for [Ru(dippe)$_2$(η^2-O_2)H]$^+$ (dippe = ^{i}Pr$_2$PCH$_2$CH$_2$P^{i}Pr$_2$) occurs at δ -5.8,[19a, 43] whilst the N-heterocyclic carbene analogue recently synthesised by the Whittlesey group, [Ru(I^{i}Pr$_2$Me$_2$)$_4$(η^2-O_2)H]$^+$, reveals an unusual positive chemical shift for the hydride resonance at δ 5.8.[44] In general, the doublet and triplet signals observed in the ^{31}P{^{1}H} NMR spectra for **25a-c** shifted to lower frequencies on formation of **28a-c** (**28a**: δ 48.2, 44.4; **28b**: δ 41.4, 36.2; **28c**: 48.2, 45.8).

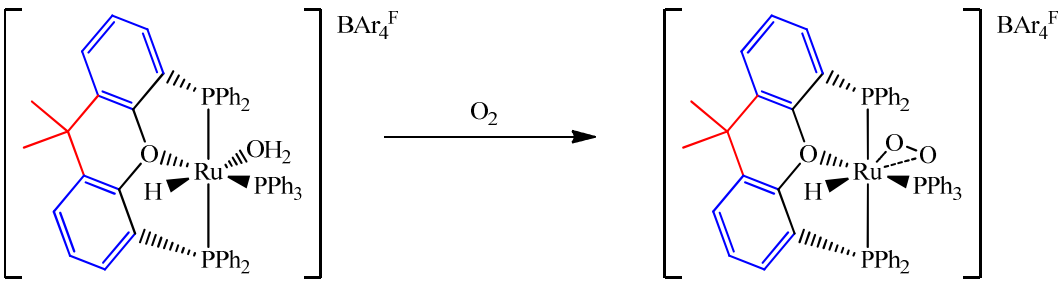

25a-c **28a-c**

Figure 26: Reaction of [Ru(POP)(PPh_3)(OH_2)H]BAr_4^F, **25a-c**, with O_2 (air) to form the cationic complexes [Ru(POP)(PPh_3)(η^2-O_2)H]BAr_4^F, **28a-c**.

The yellow solutions of **28a-c** acquire a green tint over time, suggesting that the complexes are susceptible to further oxidation to Ru(III). For [Ru(xantphos)(PPh_3)(η^2-O_2)H]BAr_4^F, **28a**, and [Ru(DPEphos)(PPh_3)(η^2-O_2)H]BAr_4^F (**28b**) this process was slow enough to allow the isolation of the complexes. **28a** gradually decomposed over a week at ambient temperature to form a dark green solution, whilst the degradation of **28b** occurred within 3 days under identical conditions. [Ru(($Ph_2CH_2CH_2)_2O$)(PPh_3)(η^2-O_2)H]BAr_4^F, **28c**, could not be isolated since decomposition was rapid, and no trace of the complex remained in solution after 12 h at 298 K. Oxidation to Ru(III) was accelerated if the complexes were formed by reaction with O_2 rather than on exposure to air.

The molecular structures of **28a** and **28b** were confirmed by X-ray crystallography *(see Figure 27)*. The P-Ru-P angle observed for the precursor complexes [Ru(POP)(PPh_3)HCl], **24a-b**, (ca. 156˚ for all three structures) narrows significantly to 125.58(7)˚ in **28a** and 119.48(4)˚ in **28b** *(see Table 3)*. This is accompanied by more acute 'hinging' of the xantphos ligand about the O-$C(CH_3)_2$ axis, forming a more acute angle between the mean planes of the aromatic xanthene rings of 149.3˚ in **28a**. A greater twist is also observed across the $(Ph_2CH_2CH_2)_2O$ backbone of the DPEphos ligand, shown by an increase in the angle between the mean planes of the aromatic DPEphos rings along this axis (43.5˚ in **24b** rising to 78.8˚ in **28b**). The O-O distances in **28a** and **28b** were 1.453(7) Å and 1.436(5) Å respectively. Although these distances are considerably longer than either those of [Ru(dippe)$_2$(η^2-O_2)H]$^+$ (1.360(10) Å)[19a, 43] or [Ru($I^iPr_2Me_2$)$_4$(η^2-O_2)H]$^+$ (1.354(5) Å),[44] they still fall within the range for coordinated peroxide.[45] IR spectroscopy was unable to add further information about the character of the O-O bond since the isotopomers of both $^{16}O_2$ and $^{18}O_2$ were hidden by other absorption bands, precluding identification of ν(O-O).

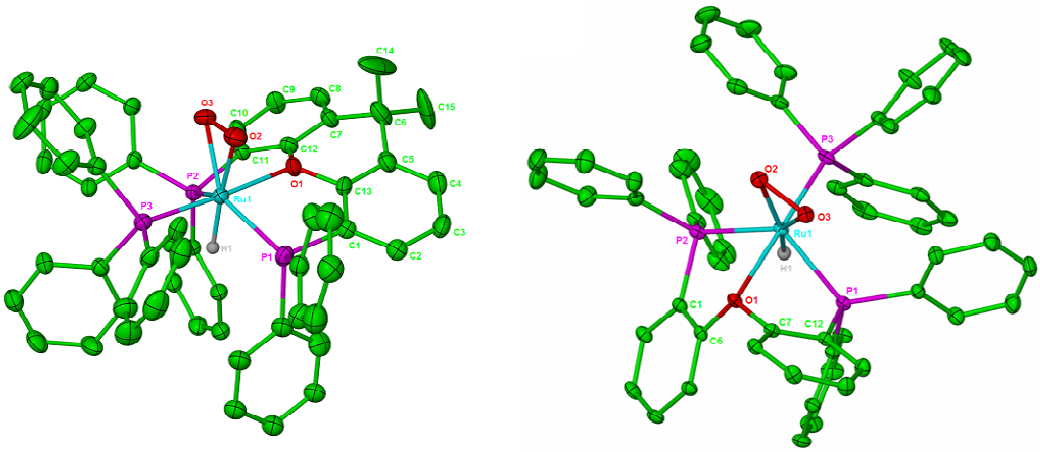

28a **28b**

Figure 27: Molecular structures of the cations in [Ru(xantphos)(PPh_3)(η^2-O_2)H]BAr_4^F, **28a**, and [Ru(DPEphos)(PPh_3)(η^2-O_2)H]BAr_4^F, **28b**. Thermal ellipsoids are shown at the 30% probability level. All hydrogen atoms, except Ru-H, are omitted.

Table 3: Selected bond lengths [Å] and angles [°] for [Ru(xantphos)(PPh$_3$)(η^2-O$_2$)H]BAr$_4^F$ (**28a**) and [Ru(DPEphos)(PPh$_3$)(η^2-O$_2$)H]BAr$_4^F$ (**28b**)

	28a	**28b**
Ru-P1	2.339(2)	2.3477(13)
Ru-P2	2.3493(19)	2.3294(13)
Ru-PPh$_3$	2.2883(19)	2.2867(13)
Ru-O1	2.257(4)	2.298(3)
O2-O3	1.453(7)	1.436(5)
Ru-O2	2.006(5)	2.2024(3)
Ru-O3	2.026(5)	2.005(3)
P1-Ru-P2	125.58(7)	119.48(4)
P1-Ru-PPh$_3$	102.49(7)	103.89(5)
P2-Ru-PPh$_3$	101.78(7)	102.20(5)
O1-Ru-PPh$_3$	176.79(13)	179.32(9)

3.7 Reaction of [Ru(POP)(PPh$_3$)(OH$_2$)H]BAr$_4^F$ (25a-c) with H$_2$ and D$_2$

The thermally unstable dihydrogen hydride complexes [Ru(POP)(PPh$_3$)(η^2-H$_2$)H]BAr$_4^F$, **29a-c**, were formed on the introduction of 1 atm. H$_2$ to pre-formed solutions of the aqua precursors **25a-c** *(see Figure 28)*.

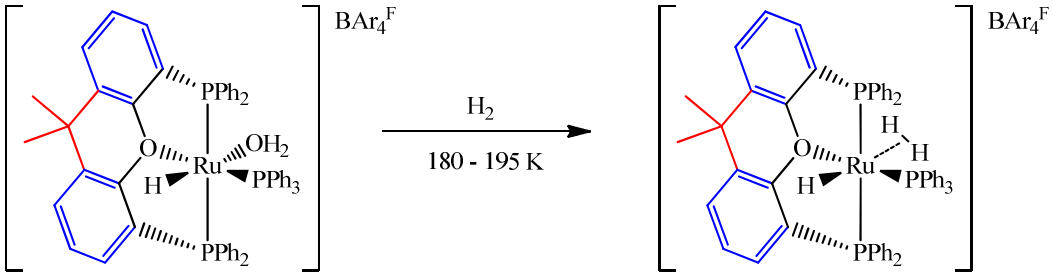

25a-c **29a-c**

Figure 28: Reactions of [Ru(POP)(PPh$_3$)(OH$_2$)H]BAr$_4^F$, **25a-c**, with H$_2$ to form the thermally unstable dihydrogen complexes [Ru(POP)(PPh$_3$)(η^2-H$_2$)H]BAr$_4^F$, **29a-c**.

The hydride region of the ^{1}H NMR spectra at low temperature (**29a**: 180 K, **29b-c**: 195 K) revealed in each case a broad singlet between δ -0.2 and -1.9 in a 2:1 ratio to a hydride signal at

lower frequency (δ -7.9 – δ -9.2). Comparison with analogous ruthenium species in the literature suggested that the broad high frequency resonances arose from η^2-H_2 ligands.[19b, 46] Once again, the multiplicities and magnitude of $^2J_{HP}$ apparent in the hydride signals pointed towards a *trans* H-Ru-η^2-H_2 interaction, and the expected doublet and triplet signals were seen for **29a** and **29c** in the $^{31}P\{^1H\}$ NMR at low temperature (**29a**: δ 51.9, 67.6; **29c**: δ 56.2, 66.9). As observed with the hydride chloride precursor, **24b**, two doublet of doublet signals were recorded for the DPEphos ligand in **29b**, each possessing a *trans* $^2J_{PP}$ splitting of 226 Hz.

Complexes **29a-c** were only stable under 1 atm. H_2, and were in equilibrium with the aqua precursors, **25a-c**. For the xantphos derivative, **29a**, a 3.8:1 ratio of **29a**:**25a** was found at 180 K, this value then falling to 2.1:1 at 239 K. Competition between H_2 and H_2O for coordination sites is well known with a number of studies attempting to assess the binding strength of H_2O against H_2.[47] A recent study conducted on *trans*-$[Ru(P\text{-}P)_2(\eta^2\text{-}H_2)H]^+$ complexes used DFT calculations to assess ligand substitution reactions.[42] It was concluded that the Ru-H_2 and Ru-OH_2 complexes were energetically very similar, and that the lability of the η^2-H_2 ligand could be greatly affected by only small changes to the skeletons of the bidentate phosphines. Thus, the coordinated η^2-H_2 ligand became inert to substitution by H_2O when more electron rich phosphines were present. Traces of the dioxygen complexes, **28a-c**, were also observed in most reactions suggesting the preferential binding of O_2 over both H_2O and H_2 in these systems.

The spin-lattice relaxation times of the η^2-H_2 and Ru-H ligands in complexes **29a-c** were also measured *(see Table 4 & Appendix 2)*. T_1(min) values of 7.7-9.6 ms at 400 MHz were determined for the η^2-H_2 moiety in complexes **29a-c**, and as expected, contrasted with much longer T_1 values for the hydride at the same temperatures. The T_1(min) value of 9.0 ms measured for the dihydrogen ligand in **29a** (240 K, 400 MHz) corresponds to an H-H separation of 0.98 or 0.78 Å depending on whether there is a slow-spinning or a fast-spinning regime.[48]

Table 4: T_1(min) data for $[Ru(POP)(PPh_3)(\eta^2\text{-}H_2)H]BAr_4^F$ (**29a-c**)

	T_1 (400 MHz)	
	η^2-H_2 / ms	Ru-H / ms
29a	9.0 (240 K)	381 (239 K)
29b	9.6 (236 K)	324 (239 K)
29c	7.7 (224 K)	273 (228 K)

Addition of 1 atm. D_2 rather than H_2 resulted in isotopic scrambling and relatively complicated low temperature ^1H NMR spectra due to signal overlap of the isotopomeric mixture.

Phosphorus decoupling of the ^{1}H NMR spectrum of the DPEphos analogue **29b** at 180 K revealed four new hydride signals immediately after the addition of D_2 *(see **a**, Figure 29)*. These new hydride resonances occurred within ±0.1 ppm of δ -7.9, with the relative intensities of the peaks changing over time. After 24 h at 298 K, the lowest frequency signal had increased in intensity relative to the highest frequency signal *(see **b**, Figure 29)*. This trend could be reversed with freeze-pump-thaw degassing and the reintroduction of 1 atm. D_2, whereupon the lowest frequency signal was again found to be the smallest in intensity *(see **c**, Figure 29)*. Another 24 h at 298 K once more revealed the growth of the lowest frequency signal *(see **d**, Figure 29)*. This variation of signal intensity with time led to the assignment of the highest frequency signal as $[Ru(DPEphos)(PPh_3)(\eta^2\text{-}D_2)H]BAr_4^F$. It was noted that the lowest frequency signal overlapped exactly with the Ru-H signal present in the $^{1}H\{^{31}P\}$ NMR spectrum of the *dihydrogen* hydride species, and this resonance was therefore assigned as $[Ru(DPEphos)(PPh_3)(\eta^2\text{-}H_2)H]BAr_4^F$. Previous work by Heinekey *et al*. has also studied isotope shifts with partially deuterated compounds, and observed that the more highly deuterated species occurred at higher chemical shifts than their *protio* counterparts.[49]

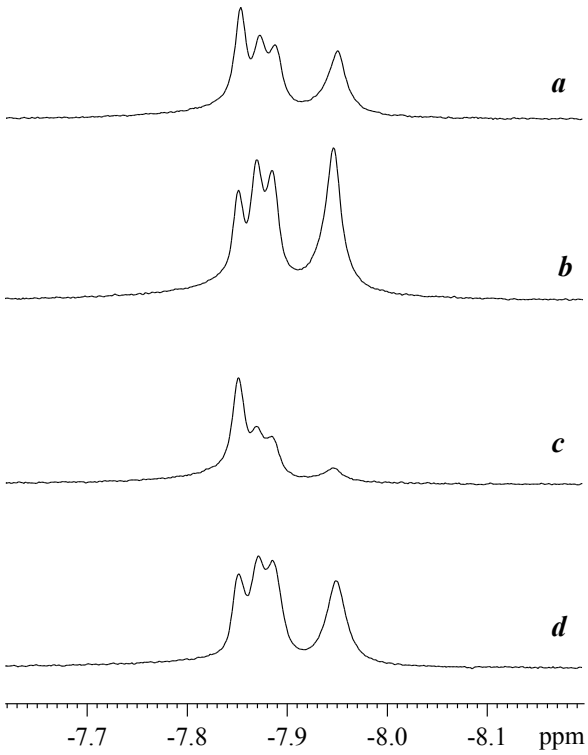

Figure 29: Hydride region of the $^{1}H\{^{31}P\}$ NMR spectrum (CD_2Cl_2, 400 MHz, 180 K) (***a***) immediately after addition of 1 atm. D_2 to $[Ru(DPEphos)(PPh_3)(OH_2)H]BAr_4^F$ (**25b**), (***b***) after a further 24 h at room temperature, (***c***) after then being freeze-pump-thaw degassed and 1 atm. D_2 reintroduced, and (***d***) a further 24 h later.

Since the formation of the dihydrogen hydride species implied H-D exchange, a ^{2}H NMR spectrum was run. This revealed deuterium incorporation into the aromatic region, supporting H-D exchange via orthometallation of the aryl rings on the phosphine ligands.[50] It is likely that the remaining two hydride signals arise from HD incorporation to give two isomers of [Ru(DPEphos)(PPh_3)(η^2-HD)H]BAr_4^F. These could either form as a result of the non-planarity of the DPEphos ligand, with η^2-HD sitting on either side of the POP plane *(see Figure 30)*, or from specific orientations of the η^2-HD moiety along a particular ligand vector.[51]

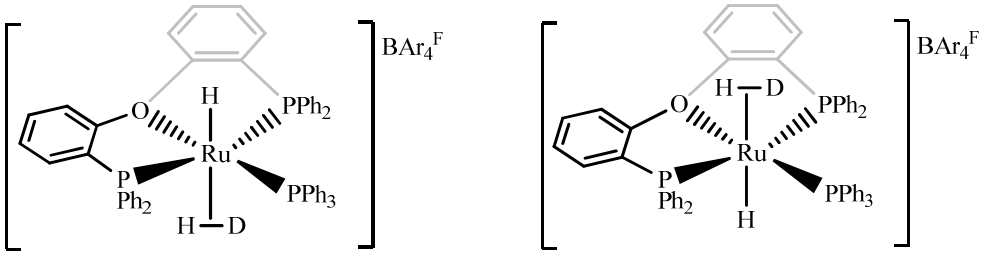

Figure 30: Two possible forms of the [Ru(DPEphos)(PPh_3)(η^2-HD)H]BAr_4^F isotopomer.

The isotopomeric mixture formed under 1 atm. D_2 also resulted in a very broad and unresolved dihydrogen region of the ^{1}H NMR spectrum of [Ru(DPEphos)(PPh_3)(η^2-H_2)H]BAr_4^F, **29b**, even with ^{31}P decoupling. This made elucidation of $^{1}J_{HD}$ difficult, and an inversion recovery T_1 experiment was attempted *(see Figure 31)*. This NMR experiment involved the initial application of a 180˚ pulse to completely invert the magnetisation into the –z plane. Over a time, τ, this applied magnetisation slowly decays back from the –z axis, through the origin, or null point, into the +z axis. Application of a 90˚ pulse then flips this magnetisation into the xy plane where it can be detected. If τ is chosen such that the magnetisation from a particular species reaches the null point, the magnetisation of this species will be undetectable in the ^{1}H NMR spectrum on application of the 90˚ pulse. The experiment aimed to differentiate between the different isotopomers by judicious application of τ, since each isotopomer possesses a different relaxation time and therefore a different null point. Those species associated with hydrogen were expected to null out more quickly than their deuterated counterparts.[52] Unfortunately, the dihydrogen region of the spectrum remained broad, and the null points of the isotopomers were too close together to accurately resolve $^{1}J_{HD}$.

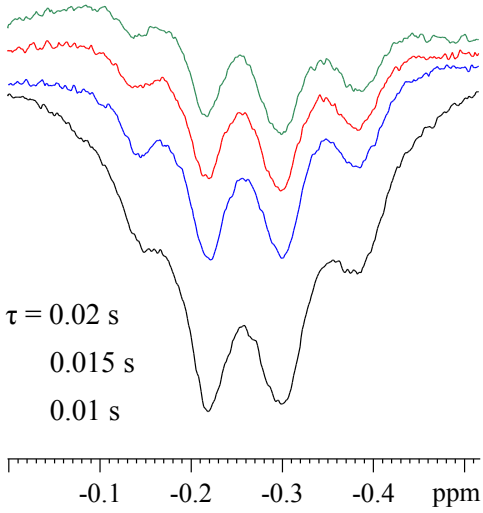

Figure 31: Inversion recovery T_1 NMR experiment, where τ = 0.02, 0.015 and 0.01 s, plotted against a standard $^1H\{^{31}P\}$ NMR spectrum (inverted 180˚) *(lower trace)*.

Instead, a delay was chosen (τ = 0.01 s) at which the dihydrogen isotopomer had reached its null point. Simulation was then used to model the signal centred at δ -0.25 in the ^1H NMR spectrum as a resonance arising from the combination of four η^2-HD isotopomers with overlapping 1:1:1 triplets *(see Figure 32)*.[53] These would arise from the η^2-HD ligand on either side of the non-planar DPEphos bisphosphine *(see Figure 30)*, and then *trans* to either Ru-H or Ru-D. The simulated $^1J_{HD}$ values of 29.7 Hz to 31.7 Hz *(see Table 5)* translated to an H-H distance of 0.89-0.92 Å, relatively close to the value of 0.98 Å for a slow spinning dihydrogen ligand derived from the measurement of T_1(min). However, this would prove contrary to the general trend for dihydrogen ligands in a *trans* H-Ru-η^2-H_2 environment, since these are generally in the fast-spinning regime.[48]

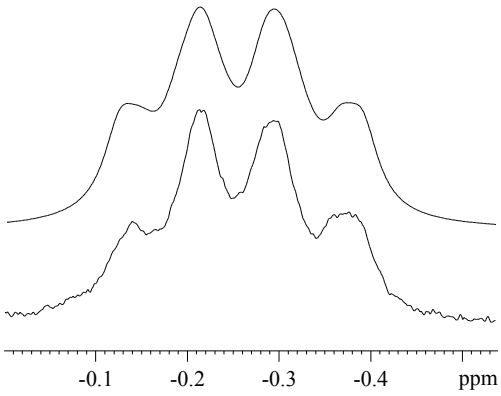

Figure 32: Experimental *(lower trace)* ^1H NMR spectrum (CD_2Cl_2, 400 MHz, 180 K), τ = 0.01 s, of $[Ru(DPEphos)(PPh_3)(OH_2)H]BAr_4^F$ (**25b**) under 1 atm D_2 along with the simulated spectrum *(upper trace)*.

Table 5: NMR data for WIN-Daisy Simulation for D_2 incorporation into $[Ru(DPEPhos)(PPh_3)(OH_2)H]BAr_4^F$ (**25a**)

δ (^{1}H) / ppm	$^1J_{HD}$ / Hz	$\Delta\nu_{1/2}$ / Hz
-0.2118	29.7209	15.3316
-0.2357	31.0454	19.2084
-0.2760	32.0426	16.9602
-0.2993	31.1602	15.0958

3.8 Reaction of $[Ru(POP)(PPh_3)(OH_2)H]BAr_4^F$ (25a-c) with N_2

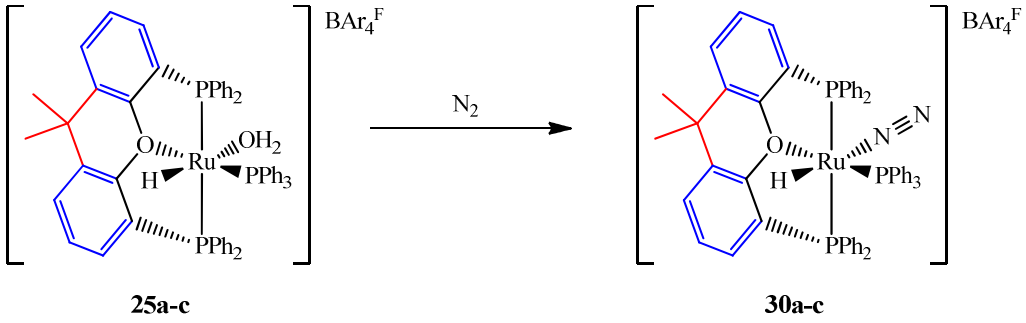

25a-c **30a-c**

Figure 33: Reaction of $[Ru(POP)(PPh_3)(OH_2)H]BAr_4F$ (**25a-c**) with 1 atm. N_2 to form $[Ru(POP)(PPh_3)(N_2)H]BAr_4F$ (**30a-c**).

The introduction of 1 atm. N_2 to CH_2Cl_2 solutions of **25a-c** resulted in the formation of the thermally unstable *trans* dinitrogen hydride complexes $[Ru(POP)(PPh_3)(N_2)H]BAr_4^F$, **30a-c** *(see Figure 33)*. These compounds were only stable under 1 atm. N_2 and were characterised at low temperature (**30a-b**: 180 K; **30c**: 195 K) by a combination of 1 and 2D ^{1}H and ^{15}N NMR spectroscopy. ^{1}H NMR spectra of **30a-c** revealed hydride resonances at higher frequency than in the aqua precursors, **25a-c** (**30a**: δ -11.72; **30b**: δ -11.04; **30c**: δ -12.06). Once again, the hydrides exhibited a doublet of triplets multiplicity and $^2J_{HP}$ values (16.5 – 26.7 Hz) which indicated *cis* disposition of the phosphines. $^1H\{^{31}P\}$ NMR experiments performed on $^{15}N_2$ labelled samples of **30a-c** reduced the hydride signals to the corresponding doublets with relatively large *trans* $^2J_{HN}$ splittings of 16.9 to 18.1 Hz.

$^{15}N\{^1H\}$ NMR spectra of each complex revealed two resonances, with the lower frequency signal assigned to the α-N on the basis of literature comparison[54] (**30a**: -88.7, -57.6; **30b**: -82.6, -51.8; **30c**: -86.2, -59.1). The frequencies recorded were in line with other ruthenium complexes

featuring end-on bound N_2 ligands.[55] ^1H-^{15}N HMQC experiments on **30a-c** correlated both the α- and β-N resonances to the hydride signal *(see Figure 34)*. ^{15}N NMR saturation transfer experiments were performed on **30a-b**, and revealed exchange between the coordinated N_2 and the free N_2 present in solution.[56]

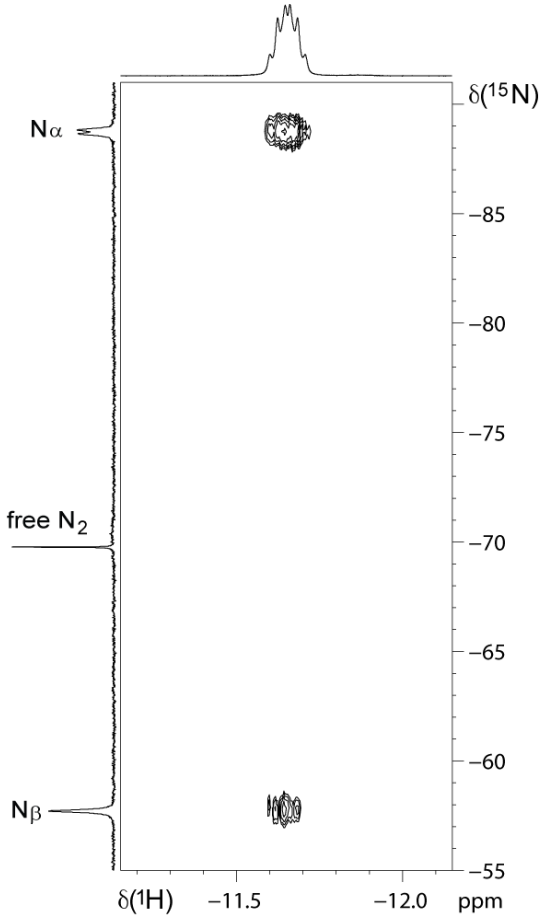

Figure 34: The ^1H-^{15}N HMQC NMR spectrum (700 MHz, CD_2Cl_2, 193 K) of $[Ru(xantphos)(PPh_3)(^{15}N_2)H]BAr_4^F$ (**30a**), showing the cross peaks arising from the 2-bond correlation to α-N and the 3-bond correlation to β-N.

As with the dihydrogen hydride complexes **29a-c**, the dinitrogen complexes remained in equilibrium with the aqua precursors, **25a-c**, with higher concentrations of the dinitrogen species observed at lower temperatures. The xantphos analogue, **30a**, was present in a 6.7:1 ratio with **25a** at 190 K, but in a 1.2:1 ratio at 210 K. On warming to 266 K, only a broad hydride signal corresponding to **25a** was apparent in the hydride region of the ^1H NMR spectrum.

Reaction to form the dioxygen compounds **28a-c** was achieved by exposure to air. On cooling samples of **28a-c**, no trace of the dinitrogen complexes **30a-c** could be detected by NMR, implying preferential binding of O_2 over N_2. This observation is consistent with other literature

studies,[57] and also recent computational research which compared the competitive coordination of O_2 and N_2 to $[Ru(NHC)_4H]^+$ and $[Ru(dippe)_2H]^+$.[58]

3.9 η^6-PPh_3 Coordination Upon Halide Abstraction from $[Ru(dppf)(PPh_3)HCl]$ (31)

The $[Ru(POP)(PPh_3)H]^+$ fragment evidently creates a system capable of small molecule coordination. In an attempt to examine the importance of the tridentate pincer configuration, the POP ligands were substituted for the fixed bidentate phosphine ligand, dppf, and a new hydride chloride precursor, $[Ru(dppf)(PPh_3)HCl]$ (**31**) synthesised. The reactivity of **31** was then investigated to highlight the role played by coordination of the O moiety.

$[Ru(PPh_3)_3HCl]$ (**23**) was reacted with 1.2 equivalents dppf in refluxing THF to afford $[Ru(dppf)(PPh_3)HCl]$ (**31**) as an orange solid in moderate yield.[59] The ^1H NMR spectrum of **31** displayed a single hydride resonance with doublet of triplets multiplicity with small values of $^2J_{HP}$ (20-30 Hz) indicating a *cis* disposition with respect to the phosphine ligands. The $^{31}P\{^1H\}$ NMR spectrum at 298 K revealed fluxional behaviour, with a triplet at δ 41.4 and a broad resonance at δ 64.9. The broad signal resolved on cooling to two doublet of doublets, each possessing a large *trans* splitting of 294 Hz. Although dppf has been known to adopt a *trans* conformation,[60] the data is consistent with a trigonal bipyramidal configuration of the complex with *cis* conformation of the dppf ligand, in which one arm of the chelating ligand and the PPh_3 group occupy the apical positions. This arrangement is displayed by the tricyclohexylphosphine analogue, $[Ru(dppf)(PCy_3)HCl]$, which also exhibits fluxional behaviour in solution.[61]

The molecular structure of **31** was established by X-ray crystallography *(see Figure 35)*, which confirmed the *trans* orientation of the PPh_3 group and one arm of the dppf ligand in the apical positions of a distorted trigonal bipyramidal structure. The Ru-P distance to the equatorial phosphine (2.1850(7) Å) was found to be significantly shorter than those to the apical phosphines ($Ru\text{-}P_{ap}$ = 2.3086(7) Å and $Ru\text{-}PPh_3$ = 2.3587(7) Å) *(see Table 6)*. The dppf ligand enforced a bite angle of 99.96(3)˚ on the complex, in comparison to the P-Ru-P angle of ~156˚ exhibited in the $[Ru(POP)(PPh_3)HCl]$ structures (**24a-c**).

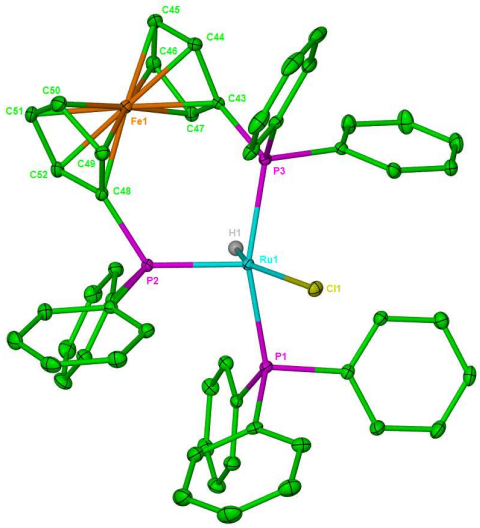

Figure 35: Molecular structure of [Ru(dppf)(PPh_3)HCl] (**31**). Thermal ellipsoids are shown at 30% probability level. Solvent and all hydrogen atoms, except for Ru-H, are omitted for clarity.

Table 6: Selected bond lengths [Å] and angles [˚] for [Ru(dppf)(PPh_3)HCl] (**31**)

Ru-PPh_3	2.3587(7)
Ru-P_{eq}	2.1850(7)
Ru-P_{ap}	2.3086(7)
Ru-Cl	2.4400(7)
P_{eq}-Ru-PPh_3	98.84(3)
P_{ap}-Ru-PPh_3	159.45(3)
P_{eq}-Ru-P_{ap}	99.96(3)
P_{eq}-Ru-Cl	126.18(3)

Reaction of [Ru(dppf)(PPh_3)HCl] (**31**) with $NaBAr_4^F$ produced a very different reaction product than those observed for the analogous reaction with [Ru(POP)(PPh_3)HCl] (**24a-c**). In this instance, abstraction of the chloride ligand resulted in coordination of the PPh_3 group through one of the aryl rings rather than the phosphorus atom, to give [Ru(dppf){(η^6-C_6H_5)-PPh_2}H]BAr_4^F (**32**) *(see Figure 36)*. Presumably, this unusual transformation arises from the need of the initially formed [Ru(dppf)(PPh_3)H]$^+$ cation to gain more electron density, and allows the ruthenium centre to retain an 18 electron configuration.[62]

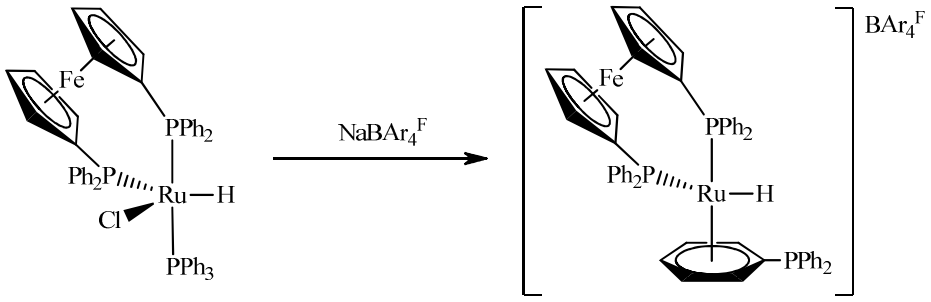

31 **32**

Figure 36: Reaction of [Ru(dppf)(PPh$_3$)HCl] (**31**) with NaBAr$_4^F$ to form [Ru(dppf){(η^6-C$_6$H$_5$)-PPh$_2$}H]BAr$_4^F$ (**32**).

The molecular structure of **32** was elucidated by X-ray crystallography *(see Figure 37)*, and showed the η^6 arene, dppf and hydride groups arranged in a distorted piano stool configuration. The η^6 arene is tilted away from the ruthenium centre, with the Ru···C distance from the P-bound carbon atom considerably longer than the analogous distances from the other carbon atoms (2.392(3) Å vs. ~ 2.23 Å respectively) *(see Table 7)*.

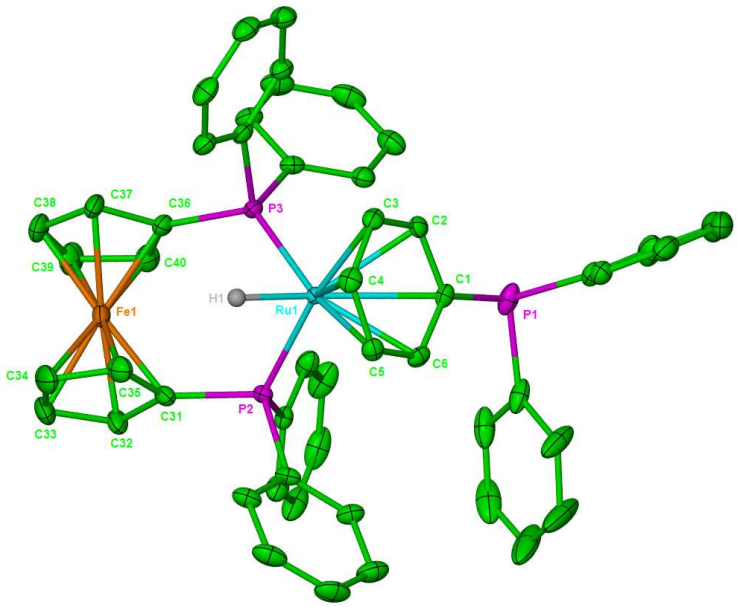

Figure 37: Structure of the cation in [Ru(dppf){(η^6-C$_6$H$_5$)-PPh$_2$}H]BAr$_4^F$ (**32**). Thermal ellipsoids are shown at 30% probability level. All hydrogen atoms, except Ru-H, are omitted for clarity.

Table 7: Selected bond lengths [Å] and angles [°] for [Ru(dppf){(η^6-C_6H_5)-PPh_2}H]BAr_4^F (**32**)

Ru-P2	2.3001(8)
Ru-P3	2.3131(8)
Ru-C1	2.392(3)
Ru-C2	2.295(3)
Ru-C3	2.223(3)
Ru-C4	2.183(3)
Ru-C5	2.195(3)
Ru-C6	2.282(3)
C1-PPh_2	1.838(3)
P2-Ru-P3	96.03(3)

The dppf ligand and the uncoordinated PPh_2 moiety were identified in the $^{31}P\{^1H\}$ NMR spectrum of **32** as two singlets at δ 50.2 and δ -8.1 respectively, assigned by comparison with the literature.[63] The ^1H NMR at 298 K displayed a single hydride resonance at δ -9.32 possessing a triplet of doublets multiplicity, arising from coupling to the dppf ligand ($^2J_{HP}$ = 39 Hz), and also, unusually, the uncoordinated PPh_2 terminus of the η^6 arene (J_{HP} = 7 Hz). The η^6 arene gave rise to four low frequency signals in the $^{13}C\{^1H\}$ NMR spectrum between δ 95 and δ 110.

3.10 Solution Reactivity of [Ru(dppf){(η^6-C_6H_5)-PPh_2}H]BAr_4^F (32)

Treatment of **32** with 1 atm. H_2 and N_2 produced no reaction, presumably due to the lack of any vacant coordination site. Reaction of **32** with 1 atm. CO at 298 K also resulted in little reaction, although after heating at 343 K for 15 h, a new hydride was present in the ^1H NMR spectrum at δ -8.56 with a doublet of doublet of doublets splitting pattern. The magnitude of $^2J_{HP}$ ($^2J_{HP}$ = 62.2, 24.3 and 19.3 Hz) together with the appearance of three doublet of doublets in the $^{31}P\{^1H\}$ NMR spectrum indicated the reformation of a Ru-PPh_3 group. A single ν(CO) band was present in the IR spectrum of this new species, implying a possible *trans* dicarbonyl geometry *(see Figure 38)*. Formation of [Ru(dppf)(PPh_3)$(CO)_2$H]BAr_4^F (**33**) was confirmed by the reaction of **32** with 1 atm. ^{13}CO, which resulted in the appearance of a triplet hydride signal at δ -8.56 ($^2J_{HC}$ = 5.6 Hz) upon ^{31}P decoupling of the proton spectrum. The complex was isolated as a yellow solid, and the molecular assignment confirmed by mass spectrometry.

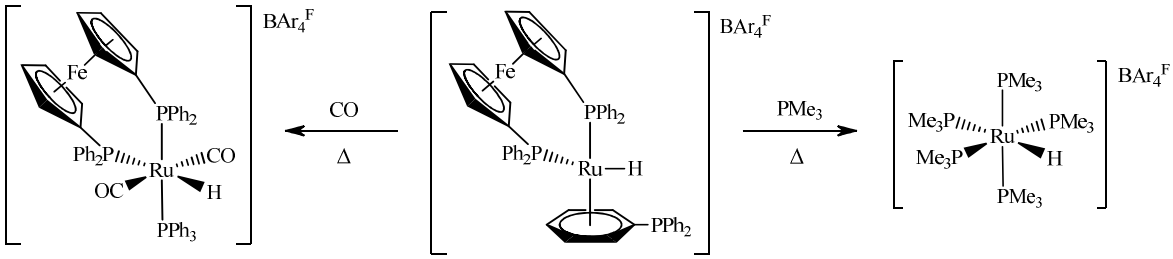

33 **32** **34**

Figure 38: Reaction of [Ru(dppf){(η^6-C_6H_5)-PPh_2}H]BAr_4^F (**32**) with CO and PMe_3 to form [Ru(dppf)(PPh_3)$(CO)_2$H]BAr_4^F (**33**) and [Ru$(PMe_3)_5$H]BAr_4^F (**34**) respectively.

Reaction of **32** with 5 equivalents PMe_3 in THF at ambient temperature also yielded little reaction. However, on refluxing for 1 h, two new hydride signals were observed in the ^{1}H NMR spectrum at δ -9.25 and -11.35, both exhibiting a high degree of coupling. After 3 h, the lower frequency hydride was the sole remaining product of the reaction, and after a literature search, was identified as the cationic penta-trimethylphosphine complex [Ru$(PMe_3)_5$H]BAr_4^F (**34**) *(see Figure 38)*.[64] This compound has been spectroscopically characterised a number of times, but neither the X-ray crystal structure nor elemental analysis has been reported. The molecular configuration of **34** was confirmed by X-ray crystallography *(see Figure 39)*, which revealed a distorted octahedral geometry with the hydride occupying a position *trans* to PMe_3 (H-Ru-P5 = 172.0(3)˚) *(see Table 8)*. The equatorial plane bisecting the H-Ru-PMe_3 interaction in **34** was disturbed only by P2, which lay 0.99 Å beneath the plane formed by P1, P3-4 and the ruthenium centre.[65]

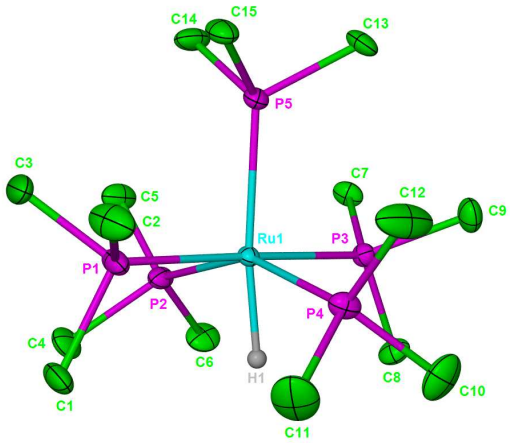

Figure 39: Structure of the cation in [Ru$(PMe_3)_5$H]BAr_4^F (**34**). Thermal ellipsoids are shown at 30% probability level. All hydrogen atoms, except Ru-H, are omitted for clarity.

Table 8: Selected bond lengths [Å] and angles [°] for $[Ru(PMe_3)_5H]BAr_4^F$ (**34**)

Ru-P1	2.3619(12)
Ru-P2	2.3774(12)
Ru-P3	2.3653(11)
Ru-P4	2.3385(13)
Ru-P5	2.3962(11)
P1-Ru-P3	177.58(4)
P2-Ru-P4	154.02(4)
P1-Ru-P5	91.02(4)
P2-Ru-P5	104.35(4)
P5-Ru-H	172.0(3)

3.11 CHAPTER SUMMARY

Reaction between $[Ru(PPh_3)_3HCl]$ (**23**) and the POP pincer ligands xantphos, **a**, DPEphos, **b**, and $(Ph_2CH_2CH_2)_2O$, **c**, results in formation of $[Ru(POP)(PPh_3)HCl]$ precursors (**24a-c**), all of which demonstrate tridentate coordination of the POP ligand.

Chloride abstraction with $NaBAr_4^F$ affords the cationic aqua complexes $[Ru(POP)(PPh_3)(OH_2)H]BAr_4^F$ (**25a-c**), and subsequent introduction of either 1 atm. O_2, H_2 and N_2 results in coordination of the gaseous ligands *trans* to the hydride. In contrast to the dioxygen compounds, the dihydrogen and dinitrogen complexes are thermally unstable, and exist in equilibrium with the aqua precursors. However, systems capable of both O_2 and H_2 coordination are relatively unusual.[66]

The role of the POP pincer ligand was highlighted by the contrasting reactivity exhibited by $[Ru(dppf)(PPh_3)HCl]$ (**31**), which forms an unusual η^6-aryl phosphine cationic complex $[Ru(dppf)\{(\eta^6\text{-}C_6H_5)\text{-}PPh_2\}H]BAr_4^F$ (**32**) on reaction with $NaBAr_4^F$.

Further reaction of **32** with CO regenerates the P-bound PPh_3 ligand in the *trans* dicarbonyl compound $[Ru(dppf)(PPh_3)(CO)_2H]BAr_4^F$ (**33**), whilst reaction with PMe_3 eliminates both dppf and PPh_3 to give the cationic penta-trimethylphosphine complex $[Ru(PMe_3)_5H]BAr_4^F$ (**34**).

References

1. Hu, X. L.; Meyer, K. *J. Organomet. Chem.* **2005**, *690,* 5474-5484.
2. van der Boom, M. E.; Milstein, D. *Chem. Rev.* **2003**, *103,* 1759-1792.
3. (a) Albrecht, M.; van Koten, G. *Angew. Chem. Int. Ed.* **2001**, *40,* 3750-3781; (b) Singleton, J. T. *Tetrahedron* **2003**, *59,* 1837-1857; (c) Benito-Garagorri, D.; Kirchner, K. *Acc. Chem. Res.* **2008**, *41,* 201-213.
4. Dani, P.; Karlen, T.; Gossage, R. A.; Gladiali, S.; van Koten, G. *Angew. Chem. Int. Ed.* **2000**, *39,* 743-745.
5. Naota, T.; Takaya, H.; Murahashi, S. I. *Chem. Rev.* **1998**, *98,* 2599-2660.
6. Lee, H. M.; Yao, J. Z.; Jia, G. C. *Organometallics* **1997**, *16,* 3927-3933.
7. (a) Ryabov, A. D. *Chem. Rev.* **1990**, *90,* 403-424; (b) Canty, A. J.; van Koten, G. *Acc. Chem. Res.* **1995**, *28,* 406-413.
8. Dani, P.; Karlen, T.; Gossage, R. A.; Smeets, W. J. J.; Spek, A. L.; van Koten, G. *J. Am. Chem. Soc.* **1997**, *119,* 11317-11318.
9. Dani, P.; Toorneman, M. A. M.; van Klink, G. P. M.; van Koten, G. *Organometallics* **2000**, *19,* 5287-5296.
10. Gnanaprakasam, B.; Zhang, J.; Milstein, D. *Angew. Chem. Int. Ed.* **2010**, *49,* 1468-1471.
11. Gunanathan, C.; Milstein, D. *Angew. Chem. Int. Ed.* **2008**, *47,* 8661-8664.
12. (a) Zhang, J.; Leitus, G.; Ben-David, Y.; Milstein, D. *Angew. Chem. Int. Ed.* **2006**, *45,* 1113-1115; (b) Ben-Ari, E.; Leitus, G.; Shimon, L. J. W.; Milstein, D. *J. Am. Chem. Soc.* **2006**, *128,* 15390-15391.
13. Khaskin, E.; Iron, M. A.; Shimon, L. J. W.; Zhang, J.; Milstein, D. *J. Am. Chem. Soc.* **2010**, *132,* 8542-8543.
14. Gunanathan, C.; Ben-David, Y.; Milstein, D. *Science* **2007**, *317,* 790-792.
15. (a) Asensio, G.; Cuenca, A. B.; Esteruelas, M. A.; Medio-Simon, M.; Olivan, M.; Valencia, M. *Inorg. Chem.* **2010**, *49,* 8665-8667; (b) Moxham, G. L.; Randell-Sly, H.; Brayshaw, S. K.; Weller, A. S.; Willis, M. C. *Chem. Eur. J.* **2008**, *14,* 8383-8397; (c) Bolzati, C.; Boschi, A.; Uccelli, L.; Tisato, F.; Refosco, F.; Cagnolini, A.; Duatti, A.; Prakash, S.; Bandoli, G.; Vittadini, A. *J. Am. Chem. Soc.* **2002**, *124,* 11468-11479; (d) Kataoka, Y.; Tsuji, Y.; Matsumoto, O.; Ohashi, M.; Yamagata, T.; Tani, K. *J. Chem. Soc., Chem. Commun.* **1995**, 2099-2100; (e) Steffey, B. D.; Miedaner, A.; Maciejewskifarmer, M. L.; Bernatis, P. R.; Herring, A. M.; Allured, V. S.; Carperos, V.; Dubois, D. L. *Organometallics* **1994**, *13,* 4844-4855; (f) Alcock, N. W.; Brown, J. M.; Jeffery, J. C. *J. Chem. Soc., Dalton Trans.* **1976**, 583-588.
16. Moxham, G. L.; Randell-Sly, H. E.; Brayshaw, S. K.; Woodward, R. L.; Weller, A. S.; Willis, M. C. *Angew. Chem. Int. Ed.* **2006**, *45,* 7618-7622.
17. Ohshima, T.; Miyamoto, Y.; Ipposhi, J.; Nakahara, Y.; Utsunomiya, M.; Mashima, K. *J. Am. Chem. Soc.* **2009**, *131,* 14317-14328.
18. (a) Morris, R. H.; Sawyer, J. F.; Shiralian, M.; Zubkowski, J. D. *J. Am. Chem. Soc.* **1985**, *107,* 5581-5582; (b) Heinekey, D. M.; Oldham, W. J. *Chem. Rev.* **1993**, *93,* 913-926.
19. (a) Jimenez-Tenorio, M.; Puerta, M. C.; Valerga, P. *J. Am. Chem. Soc.* **1993**, *115,* 9794-9795; (b) Schlaf, M.; Lough, A. J.; Morris, R. H. *Organometallics* **1997**, *16,* 1253-1259; (c) Martelletti, A.; Gramlich, V.; Zurcher, F.; Mezzetti, A. *New J. Chem.* **1999**, *23,* 199-206.
20. Maseras, F.; Lledos, A.; Clot, E.; Eisenstein, O. *Chem. Rev.* **2000**, *100,* 601-636.
21. Maseras, F.; Koga, N.; Morokuma, K. *Organometallics* **1994**, *13,* 4008-4016.
22. Lenero, K. A.; Kranenburg, M.; Guari, Y.; Kamer, P. C. J.; van Leeuwen, P. W. N. M.; Sabo-Etienne, S.; Chaudret, B. *Inorg. Chem.* **2003**, *42,* 2859-2866.
23. (a) Vigalok, A.; Shimon, L. J. W.; Milstein, D. *Chem. Commun.* **1996**, 1673-1674; (b) Frech, C. M.; Shimon, L. J. W.; Milstein, D. *Helv. Chim. Acta* **2006**, *89,* 1730-1739; (c)

Verat, A. Y.; Fan, H. J.; Pink, M.; Chen, Y. S.; Caulton, K. G. *Chem. Eur. J.* **2008**, *14,* 7680-7686.
24. Williams, D. B.; Kaminsky, W.; Mayer, J. M.; Goldberg, K. I. *Chem. Commun.* **2008**, 4195-4197.
25. Jia, G. C.; Lee, H. M.; Williams, I. D.; Lau, C. P.; Chen, Y. Z. *Organometallics* **1997**, *16,* 3941-3949.
26. Amoroso, D.; Jabri, A.; Yap, G. P. A.; Gusev, D. G.; dos Santos, E. N.; Fogg, D. E. *Organometallics* **2004**, *23,* 4047-4054.
27. (a) Maltby, P. A.; Schlaf, M.; Steinbeck, M.; Lough, A. J.; Morris, R. H.; Klooster, W. T.; Koetzle, T. F.; Srivastava, R. C. *J. Am. Chem. Soc.* **1996**, *118,* 5396-5407; (b) Chin, B.; Lough, A. J.; Morris, R. H.; Schweitzer, C. T.; Dagostino, C. *Inorg. Chem.* **1994**, *33,* 6278-6288.
28. Fasulo, M. E.; Tilley, T. D. *Inorg. Chim. Acta* **2010**, *364,* 246-250.
29. Fryzuk, M. D.; Montgomery, C. D.; Rettig, S. J. *Organometallics* **1991**, *10,* 467-473.
30. Watson, L. A.; Coalter, J. N.; Ozerov, O.; Pink, M.; Huffman, J. C.; Caulton, K. G. *New J. Chem.* **2003**, *27,* 263-273.
31. Prechtl, M. H. G.; Ben-David, Y.; Giunta, D.; Busch, S.; Taniguchi, Y.; Wisniewski, W.; Gorls, H.; Mynott, R. J.; Theyssen, N.; Milstein, D.; Leitner, W. *Chem. Eur. J.* **2007**, *13,* 1539-1546.
32. (a) Gusev, D. G.; Lough, A. J. *Organometallics* **2002**, *21,* 5091-5099; (b) Gusev, D. G.; Fontaine, F. G.; Lough, A. J.; Zargarian, D. *Angew. Chem. Int. Ed.* **2003**, *42,* 216-219.
33. Gusev, D. G.; Dolgushin, F. M.; Antipin, M. Y. *Organometallics* **2000**, *19,* 3429-3434.
34. Zhang, J.; Gandelman, M.; Shimon, L. J. W.; Rozenberg, H.; Milstein, D. *Organometallics* **2004**, *23,* 4026-4033.
35. Major, Q.; Lough, A. J.; Gusev, D. G. *Organometallics* **2005**, *24,* 2492-2501.
36. Nieczypor, P.; van Leeuwen, P. W. N. M.; Mol, J. C.; Lutz, M.; Spek, A. L. *J. Organomet. Chem.* **2001**, *625,* 58-66.
37. Cetinkaya.B; Dixneuf, P.; Lappert, M. F. *J. Chem. Soc., Dalton Trans.* **1974**, 1827-1833.
38. Janiak, C. *J. Chem. Soc., Dalton Trans.* **2000**, 3885-3896.
39. This observation was used to synthesise [Ru(DPEphos)(PPh_3)$(CO)H_2$] (**14**) by reaction of [Ru(DPEphos)(PPh_3)HCl] (**24b**) with $NaBH_4$ in refluxing ethanol *(see Chapter 2)*.
40. (a) Esteruelas, M. A.; Werner, H. *J. Organomet. Chem.* **1986**, *303,* 221-231; (b) Salem, H.; Shimon, L. J. W.; Diskin-Posner, Y.; Leitus, G.; Ben-David, Y.; Milstein, D. *Organometallics* **2009**, *28,* 4791-4806.
41. (a) Boniface, S. M.; Clark, G. R.; Collins, T. J.; Roper, W. R. *J. Organomet. Chem.* **1981**, *206,* 109-117; (b) Goicoechea, J. M.; Mahon, M. F.; Whittlesey, M. K.; Kumar, P. G. A.; Pregosin, P. S. *Dalton Trans.* **2005**, 588-597; (c) Zhang, J.; Gandelman, M.; Shimon, L. J. W.; Milstein, D. *Dalton Trans.* **2007**, 107-113.
42. Szymczak, N. K.; Braden, D. A.; Crossland, J. L.; Turov, Y.; Zakharov, L. N.; Tyler, D. R. *Inorg. Chem.* **2009**, *48,* 2976-2984.
43. Jimenez-Tenorio, M.; Puerta, M. C.; Valerga, P. *Inorg. Chem.* **1994**, *33,* 3515-3520.
44. Häller, L. J. L.; Mas-Marza, E.; Moreno, A.; Lowe, J. P.; Macgregor, S. A.; Mahon, M. F.; Pregosin, P. S.; Whittlesey, M. K. *J. Am. Chem. Soc.* **2009**, *131,* 9618-9619.
45. (a) Vaska, L. *Acc. Chem. Res.* **1976**, *9,* 175-183; (b) Mezzetti, A.; Zangrando, E.; Delzotto, A.; Rigo, P. *J. Chem. Soc., Chem. Commun.* **1994**, 1597-1598; (c) Yu, X. Y.; Patrick, B. O.; James, B. R. *Organometallics* **2006**, *25,* 4870-4877; (d) Cramer, C. J.; Tolman, W. B.; Theopold, K. H.; Rheingold, A. L. *Proc. Natl. Acad. Sci. U. S. A.* **2003**, *100,* 3635-3640.
46. (a) Bautista, M. T.; Cappellani, E. P.; Drouin, S. D.; Morris, R. H.; Schweitzer, C. T.; Sella, A.; Zubkowski, J. *J. Am. Chem. Soc.* **1991**, *113,* 4876-4887; (b) Jia, G. C.; Drouin, S. D.; Jessop, P. G.; Lough, A. J.; Morris, R. H. *Organometallics* **1993**, *12,* 906-916; (c) Field, L. D.; Hambley, T. W.; Yau, B. C. K. *Inorg. Chem.* **1994**, *33,* 2009-2017; (d) Ogasawara, M.; Saburi, M. *J. Organomet. Chem.* **1994**, *482,* 7-14.

47. (a) Kubas, G. J.; Burns, C. J.; Khalsa, G. R. K.; Vandersluys, L. S.; Kiss, G.; Hoff, C. D. *Organometallics* **1992**, *11,* 3390-3404; (b) Kovacs, G.; Nadasdi, L.; Laurenczy, G.; Joo, F. *Green Chem.* **2003**, *5,* 213-217; (c) Jazzar, R. F. R.; Bhatia, P. H.; Mahon, M. F.; Whittlesey, M. K. *Organometallics* **2003**, *22,* 670-683; (d) Grundler, P. V.; Yazyev, O. V.; Aebischer, N.; Helm, L.; Laurenczy, G.; Merbach, A. E. *Inorg. Chim. Acta* **2006**, *359,* 1795-1806.
48. (a) Morris, R. H. *Coord. Chem. Rev.* **2008**, *252,* 2381-2394; (b) Morris, R. H. *Coord. Chem. Rev.* **2009**, *253,* 1219-1219.
49. Oldham, W. J.; Hinkle, A. S.; Heinekey, D. M. *J. Am. Chem. Soc.* **1997**, *119,* 11028-11036.
50. This is assumed to arise from metallation of the PPh_3 group rather than the POP ligand, but this remains unconfirmed.
51. For instance, either the H or D atom could be positioned directly above the Ru-O bond along the O-Ru-PPh_3 vector.
52. This experiment was carried out as the result of helpful discussions with Prof. Robert Morris.
53. Simulated using the Bruker Daisy software program: DAISY version 2.0.0, Bruker BioSpin GmbH, Rheinstetten, Germany, 2007.
54. (a) Chatt, J.; Fakley, M. E.; Richards, R. L.; Mason, J.; Stenhouse, I. A. *J. Chem. Res-S* **1979**, 44-45; (b) Dilworth, J. R.; Donovanmtunzi, S.; Kan, C. T.; Richards, R. L.; Mason, J. *Inorg. Chim. Acta* **1981**, *53,* L161-L162.
55. Donovan-Mtunzi, S.; Richards, R. L.; Mason, J. *J. Chem. Soc., Dalton Trans.* **1984**, 469-474.
56. Performed by Dr A. Moreno and Prof. P. S. Pregosin at ETHZ, Zurich, Switzerland.
57. Jia, G. C.; Ng, W. S.; Chu, H. S.; Wong, W. T.; Yu, N. T.; Williams, I. D. *Organometallics* **1999**, *18,* 3597-3602.
58. Burling, S.; Häller, L. J. L.; Mas-Marzá, E.; Moreno, A.; Macgregor, S. A.; Mahon, M. F.; Pregosin, P. S.; Whittlesey, M. K. *Chem. Eur. J.* **2009**, *15,* 10912-10923.
59. An alternative synthetic route to [Ru(dppf)(PPh_3)HCl] (**31**) has also been described in a patent: Rautenstrauch, V., Challand, R., Churland, R., Morris, R. H., Abdur-Rashid, K., Brazi, E., Mimoun, H.; World Patent WO 2002022526 A2 20020321; 2002
60. Kawano, H.; Nishimura, Y.; Onishi, M. *Dalton Trans.* **2003**, 1808-1812.
61. Jung, S.; Brandt, C. D.; Wolf, J.; Werner, H. *Dalton Trans.* **2004**, 375-383.
62. Geldbach, T. J.; Drago, D.; Pregosin, P. S. *Chem. Commun.* **2000**, 1629-1630.
63. Pregosin, P. S. *Coord. Chem. Rev.* **2008**, *252,* 2156-2170.
64. (a) Werner, H.; Werner, R. *J. Organomet. Chem.* **1981**, *209,* C60-C64; (b) Nkosi, B. S.; Coville, N. J.; Albers, M. O.; Gordon, C.; Viney, M. M.; Singleton, E. *J. Organomet. Chem.* **1990**, *386,* 111-119; (c) Burn, M. J.; Bergman, R. G. *J. Organomet. Chem.* **1994**, *472,* 43-54; (d) Holland, A. W.; Bergman, R. G. *J. Am. Chem. Soc.* **2002**, *124,* 9010-9011; (e) Caballero, A.; Carrion, M. C.; Espino, G.; Jalon, F. A.; Manzano, B. R. *Polyhedron* **2004**, *23,* 361-371; (f) Kayaki, Y.; Ikeda, H.; Tsurumaki, J. I.; Shimizu, I.; Yamamoto, A. *Bull. Chem. Soc. Jpn.* **2008**, *81,* 1053-1061; (g) Getty, A. D.; Tai, C. C.; Linehan, J. C.; Jessop, P. G.; Olmstead, M. M.; Rheingold, A. L. *Organometallics* **2009**, *28,* 5466-5477.
65. (a) Mathew, N.; Jagirdar, B. R. *Organometallics* **2000**, *19,* 4506-4517; (b) Mathew, N.; Jagirdar, B. R.; Ranganathan, A. *Inorg. Chem.* **2003**, *42,* 187-197.
66. Kubas, G. J. *Metal Dihydrogen and σ-Bond Complexes* **2001**, *Kluwer/Plenum: New York*.

4. CHAPTER 4

4.1 Dehydrogenative Coupling of Amine and Phosphine Boranes

The coordination and subsequent activation of B-H bonds has attracted considerable research interest since this process is implicated in a number of environmentally important catalytic processes.[1] In particular, much research has focussed on the release of H_2 via the catalytic dehydrogenative coupling (dehydrocoupling) of phosphine- and amine-boranes ($H_3B{\cdot}LR_{3-n}H_n$, where L = N or P, and n = 1-3) *(see Figure 1)* as this reaction could be utilised for hydrogen storage.[2] Ammonia-borane in particular has sparked interest as a hydrogen storage material since it possesses a high H_2 content (19.6 wt%) which could be readily accessed.[3] The use of amine-boranes as an environmentally benign hydrogen source for organic transformations has also been investigated.[4] In addition, the products resulting from the dehydrocoupling of amine- and phosphine-boranes could have potential as unusual polymeric materials.[5]

$$x\ H_3B{\cdot}LR_{3-n}H_n \xrightarrow[-xH_2]{[M]} [H_2B{\cdot}LR_{3-n}H_{n-1}]_x$$

Figure 1: Basic scheme for the catalytic dehydrocoupling of amine- and phosphine-boranes, where L = N or P, and n = 1-3.

The thermal dehydrocoupling of amine- and phosphine-boranes has been known since the 1950s. Researchers were able to isolate and characterise a range of coupled products, such as cyclic aminoborane $[R_2B\text{-}NR'_2]_x$ (x = 2 or 3) and borazine $[RB\text{-}NR']_3$ derivatives,[6] as well as phosphinoboranes $[R_2B\text{-}PR'_2]_3$,[7] and also some low molecular weight phosphine-borane polymers. However, high temperatures of 373-473 K were needed.[8] Catalytic dehydrocoupling could allow access to these species under milder conditions with greater product control. The first detailed example of metal catalysed dehydrocoupling was reported by the Manners group in 1999, when $[Rh(COD)(\mu\text{-}Cl)]_2$ was used at 0.3 mol% loading to dehydrocouple $H_3B{\cdot}PPh_2H$, giving rise to a phosphine-borane dimer *(see Figure 2, Scheme 1)*.[9] The scope of this catalyst was then extended to amine-borane systems with typical loadings between 0.5-5 mol%, producing a range of cyclic dimers from secondary amine-boranes and borazines from primary amine-boranes *(see Figure 2, Scheme 2)*.[10]

Scheme 1

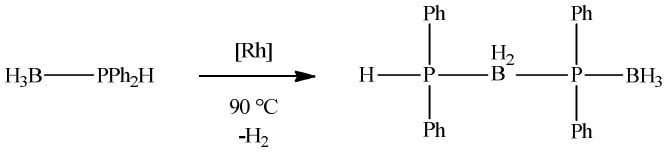

Scheme 2

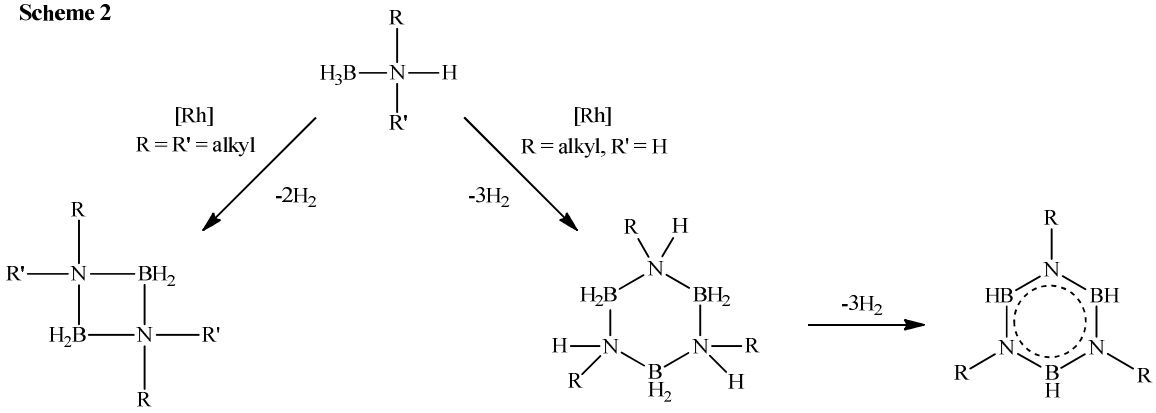

Figure 2: The $[Rh(COD)(\mu\text{-}Cl)]_2$ catalysed dehydrogenation of the phosphine-borane, $H_3B{\cdot}PPh_2H$ *(Scheme 1)*[9] and amine-boranes, $H_3B{\cdot}NRR'H$ *(Scheme 2)*.[10]

From these beginnings, the field of catalytic dehydrocoupling has rapidly expanded. A large proportion of work is centred on the development of catalysts for the dehydrocoupling of amine-boranes, due to the immense interest surrounding their use as hydrogen storage materials. It is now recognised that catalyst structure and the nature of the metal centre has a great impact on the performance of these systems. Fagnou and co-workers noted that whilst ammonia-borane is isoelectronic with ethane, the polarity of the bond confers greatest similarities with methanol. They rationalised that catalysts effective for the transfer hydrogenation of alcohols could function for the dehydrogenation of amine-boranes. A range of ruthenium catalysts were therefore screened in the dehydrocoupling of ammonia borane.[11] A series of $[Ru(R_2PCH_2CH_2NH_2)_2Cl_2]$ complexes (R = ^{t}Bu, ^{i}Pr, Ph) *(see Figure 3)*, based on previous work by Morris *et al*., proved to be the most effective catalysts.[12] These complexes required activation by KO^{t}Bu, and were able to remove 1 equivalent H_2 from $H_3B{\cdot}NH_3$ in just 5 minutes at 298 K at ruthenium loadings as low as 0.03 mol%.

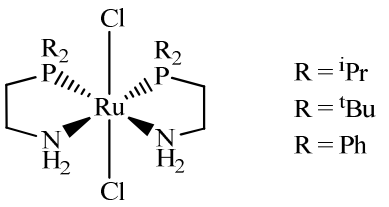

Figure 3: $[Ru(R_2PCH_2CH_2NH_2)_2Cl_2]$ (R = ^{i}Pr, ^{t}Bu, Ph) catalysts utilised by Fagnou *et al*.[11]

Once again, as with transfer hydrogenation catalysts, the incorporation of pincer ligands into catalyst structures has yielded effective systems. Schneider *et al*. developed the most effective catalyst system for the dehydrocoupling of ammonia borane to date, comprising a ruthenium(II) PNP complex.[13] The PNP ligand involved was an aliphatic analogue of Milstein's pyridine-based pincer[14] *(see Section 3.2, Chapter 3)*, and displayed the same equilibrium between saturation and unsaturation of one ligand arm that assisted the reaction pathway *(see Figure 4)*. The complex was able to generate greater than one equivalent H_2 within 10 minutes at room temperature using 0.1 mol% ruthenium loading. However, even catalyst loadings as low as 0.01 mol% could effect the transformation.

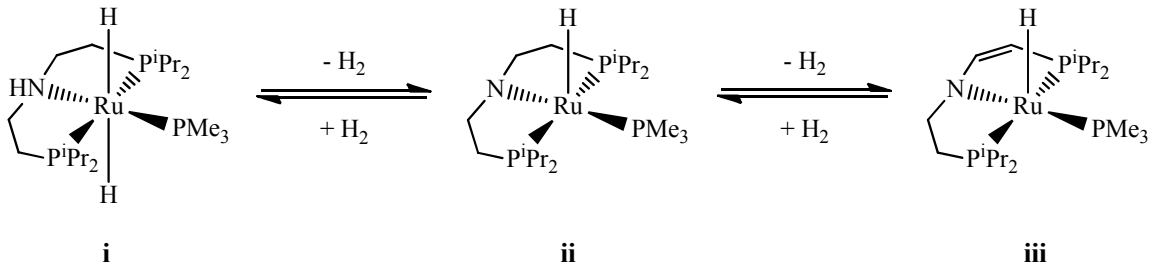

i **ii** **iii**

Figure 4: The dehydrogenation/hydrogenation equilibria present between the amino (**i**), amido (**ii**) and enamino (**iii**) forms of the Schneider catalyst.[5, 13]

Unlike the Fagnou system, prior activation of Schneider's catalyst was not needed, allowing more detailed mechanistic and kinetic studies to be carried out.[15] A heterogeneous mechanism was ruled out after the addition of mercury failed to poison the catalyst. The researchers concluded that each dehydrogenation and B-N coupling step to form aminoborane took place at the metal centre, whilst the cyclodimerisation of aminoborane was thermodynamically driven and occurred without participation of the catalyst.

Brookhart's iridium pincer complex, [Ir(POCOP)H_2], (POCOP = 1,3-(OP^{t}Bu$_2$C$_6$H$_3$))[16] *(see Figure 5)* was also found to be an effective catalyst for the dehydrogenation of ammonia borane by Goldberg and Heinekey *et al*.[17] The insolubility of the reaction product in this case precluded full characterisation, but was proposed to be cyclopentaborazane, $[H_2B\text{-}NH_2]_5$, concurrent with the release of only one equivalent H_2. The steric bulk at the iridium centre was assumed to halt the reaction at this stage. Interestingly, use of this catalyst introduced some selectivity to the reaction, with the ability to dehydrocouple primary amine-boranes only and not the secondary analogues, a feature which again appeared to arise from steric crowding at the metal centre.

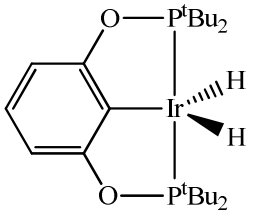

Figure 5: Brookhart's [Ir(POCOP)H_2] (POCOP = 1,3-(OP^{t}Bu$_2$C$_6$H$_3$)) complex.[16]

4.2 Coordination of Amine- and Phosphine- Boranes to Metal Centres

The mechanisms at work for the catalytic dehydrocoupling of amine- and phosphine-boranes are complicated and, in the majority of cases, not fully understood. Once again, improvements in catalysis can only be achieved with more fundamental research into the coordination and subsequent activation of the substrates involved. Broadly speaking, the dehydrogenation of amine- and phosphine-boranes must proceed through a mechanism involving the consecutive activation of B-H and N-H bonds. However, before this chemistry can occur, the substrate must approach the metal centre to form amine-borane (or phosphine-borane) σ-complexes. Much work has therefore concentrated on isolating σ-complexes of these species and establishing their role in the catalytic cycle.

Complexes formed from the η^1 coordination of tertiary amine- and phosphine-borane adducts are well known although they are unable to undergo dehydrogenation. Referred to as Shimoi complexes, they have been isolated across a range of metal centres from chromium and tungsten in Group 6 to manganese and ruthenium in Groups 7-8 *(see Figure 6)*.[18] The bonding in these systems is best described as a 3-centre-2-electron bond across a significantly bent M-H-B bridge. The interaction arises mainly from donation of the BH σ orbital into the d_σ orbital, with little concomitant back-donation from the metal centre as the BH σ* orbital is too high in energy.

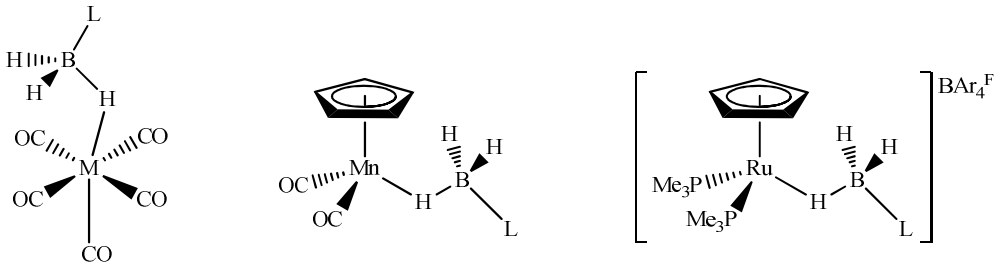

Figure 6: A range of isolated Shimoi-type complexes.[18-19]

Weller *et al*. isolated a cationic dinuclear rhodium complex which exhibited several unusual activation modes of $H_3B{\cdot}NMe_3$.[20] In this compound, one amine-borane unit was able to act as a bridging ligand, with an η^1-B-H interaction to each rhodium centre. Two other amine-borane units had activated still further, each undergoing oxidative addition of a B-H bond to leave the boron atoms directly coordinated to the same rhodium centre. Each of these boryl groups then stabilised the second rhodium centre with another η^1-B-H interaction *(see Figure 7)*.

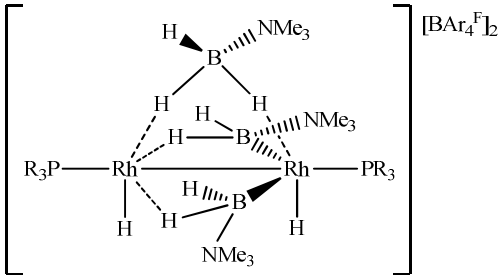

Figure 7: Formation of a cationic dinuclear rhodium species exhibiting bridging η^1-B-H interactions and oxidative addition of B-H bonds (R = ^{i}Pr, Cy).[20]

η^2 coordination of amine- and phosphine-boranes is much more unusual, and there are few literature examples. In contrast to η^1 coordination, an η^2 bonding mode can arise if the metal centre is able to donate electron density into a vacant p orbital of boron. This back-donation accounts for the 'side-on' orientation of the B-H bond.

Weller and coworkers isolated η^2 amine-borane complexes of rhodium by reaction of $H_3B{\cdot}NMe_2H$ with $[Rh(P^iBu_3)_2]BAr_4^F$ (**iv**).[21] Initially a rhodium(I) species, $[Rh(P^iBu_3)_2(\eta^2\text{-}H_3B{\cdot}NHMe_2)]BAr_4^F$ (**v**) was observed, but this proved highly unstable, and quickly decomposed to give the rhodium(III) complex, $[Rh(P^iBu_3)_2(\eta^2\text{-}H_3B{\cdot}NMe_2H)H_2]BAr_4^F$ (**vi**) which could be isolated. It was postulated that **vi** was formed by the dehydrogenation of **v** to give the dihydride complex $[Rh(P^iBu_3)_2H_2]BAr_4^F$ (**vii**) which then reacted with another equivalent of $H_3B{\cdot}NMe_2H$, and indeed a separate reaction of **vii** with $H_3B{\cdot}NMe_2H$ was shown to reform **vi**. Interestingly, **iv**, **vi** and **vii** were all effective catalysts for the dehydrocoupling of $H_3B{\cdot}NMe_2H$, leading to their postulation as intermediates in the catalytic cycle of amine-borane dehydrogenation *(see Figure 8)*.

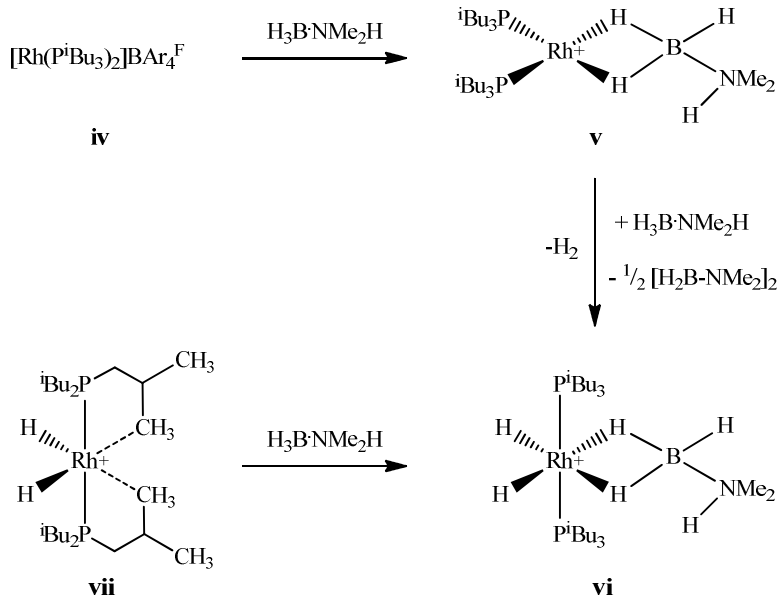

Figure 8: Postulated intermedates in the Rh catalysed dehydrocoupling of $H_3B{\cdot}NMe_2H$.[21]

The reaction of a different rhodium precursor, namely $[Rh(\eta^6\text{-}C_6H_5F)\{P(C_5H_9)_2(\eta^2\text{-}C_5H_7)\}]BAr_4^F$, with the amine-boranes $H_3B{\cdot}NMeH_2$, $H_3B{\cdot}NMe_2H$ and $H_3B{\cdot}NMe_3$ allowed Weller *et al*. to isolate complexes exhibiting both η^1 and η^2 coordination of the BH bonds *(see Figure 9)*.[22] NMR spectroscopy revealed fluxional behaviour at ambient temperature, likely due to exchange between the η^1 and η^2 bonding modes of the two $H_3B{\cdot}NRR'H$ moieties. These complexes represented the first examples of *bis*(σ-amine-borane) coordination.

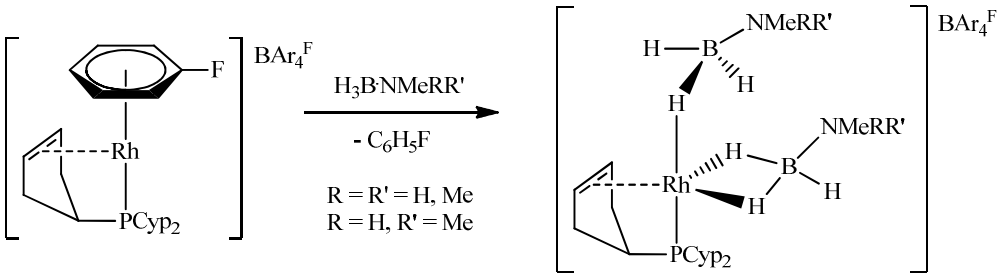

Figure 9: η^1 and η^2 B-H activation at a cationic rhodium centre.[22]

η^2 coordination has also been observed for phosphine-boranes. In one example, a bidentate phosphine-monoborane adduct, $H_3B{\cdot}dppm$, was used as a chelating ligand.[23] Reaction of this ligand with $[Cp^*Ru(NCMe)_2]PF_6$, generated $[Cp^*Ru(\eta^2\text{-}BH_3\text{-}dppm)]PF_6$. The borane bonding mode could be altered by the addition of CO or PMe_3 to give $[Cp^*Ru(L)(\eta^1\text{-}BH_3\text{-}dppm)]PF_6$ (L = CO, PMe_3) *(see Scheme 1, Figure 10)*. In a similar manner, reaction of another chelating bidentate phosphine

borane adduct with $[Rh(COD)(\mu\text{-}Cl)]_2$ gave rise to η^2 coordination of the borane moiety *(see Scheme 2, Figure 10)*.[24]

Scheme 1

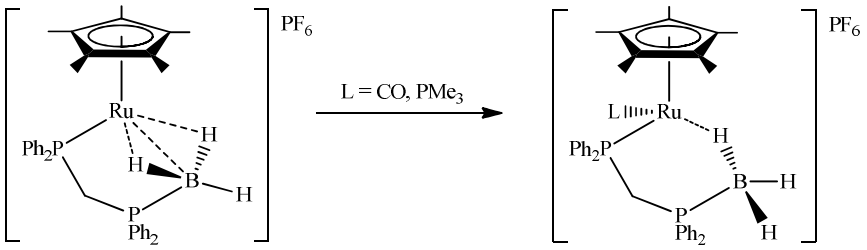

Scheme 2

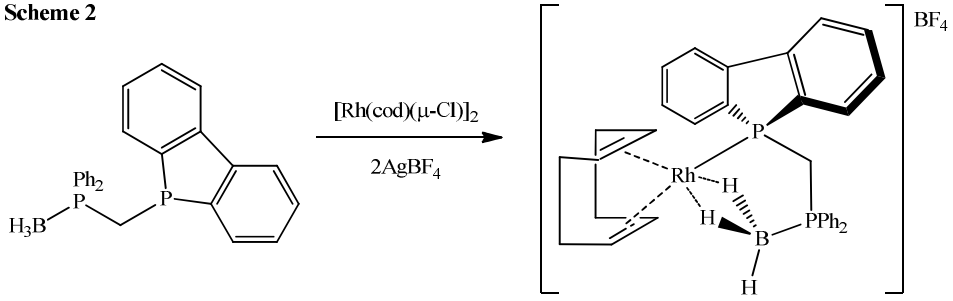

Figure 10: η^2 coordination of chelating phosphine borane ligands on ruthenium and rhodium centres *(Scheme 1 & 2 respectively)*.[23-24]

Whilst the formation of amine-borane (or phosphine-borane) σ-complexes is accepted as the initial step in the homogeneous reaction pathway *(see Figure 11)*, the manner in which these coordinated substrates undergo dehydrogenation has been highly debated.

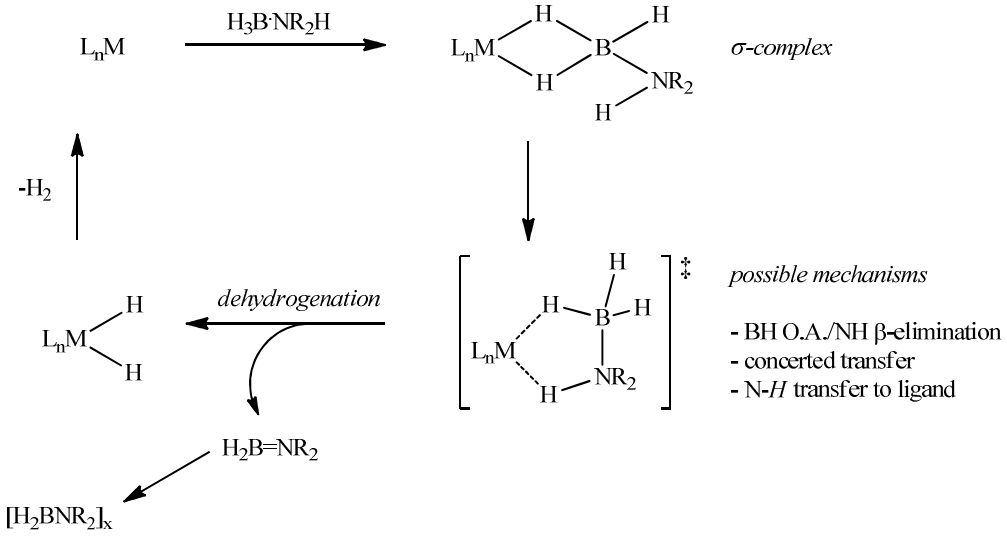

Figure 11: Reaction pathway for homogeneous amine-borane dehydrogenation.[21]

Computational studies have hinted at a number of possibilities depending on the metal centre. Work on Cp_2Ti-derivatives supports the stepwise intermolecular transfer of the NH and then the BH proton to the titanium centre,[25] whilst the Ir-pincer complexes are thought to dehydrogenate *via* a concerted pathway.[26] Baker *et al*. developed a highly effective Ni-NHC system for the dehydrogenation of amine-boranes and suggested that this step could involve oxidative addition of the B-H bond, with subsequent NH β-elimination.[27] However, DFT calculations on the same system revealed possible auxiliary ligand involvement, with transfer of an NH proton to the carbenic carbon followed by C-H and then B-H activation to dehydrogenate the amine-borane *(see Figure 12)*.[28]

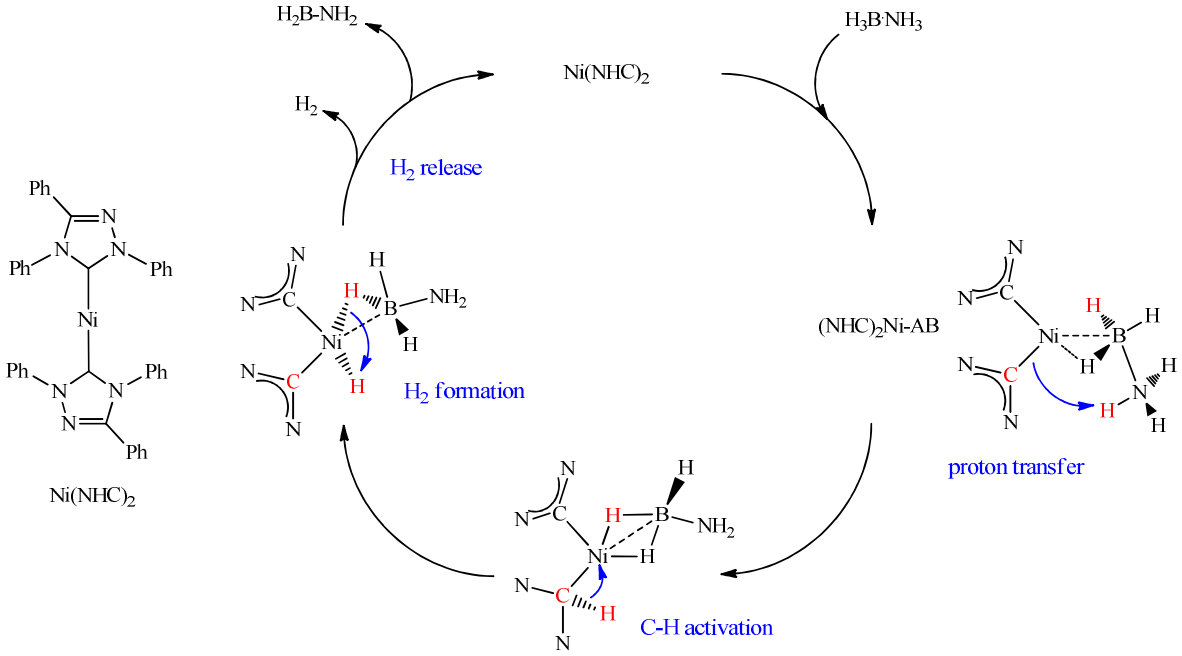

Figure 12: Dehydrogenation of amine-borane with $Ni(NHC)_2$ *via* auxiliary ligand involvement.[28]

Some unusual compounds have been isolated from catalytic dehydrocoupling studies, and implicated as intermediates within the catalytic cycle. Schneider *et al*. isolated an unusual complex possessing a four-membered ruthenium metallacycle formed on coordination of the aminoborane to their ruthenium(II) PNP catalyst[13] *(see Figure 4 & 13)*. This compound was implicated in the catalytic cycle since it too was able to quantitatively dehydrogenate ammonia-borane at 2 mol% catalyst loading.[15]

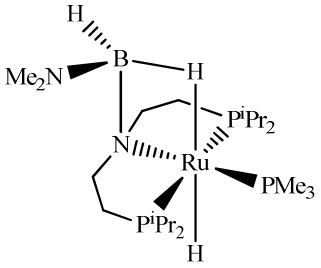

Figure 13: The unusual four-membered Ru-N-B-H metallacycle formed on reaction of the amido form of the Schneider catalyst with dimethylamine borane.[15]

Work conducted on dehydrocoupling using Brookhart's iridium pincer complex, [Ir(POCOP)H_2], (POCOP = μ^3-1,3-(OP^{t}Bu$_2$C$_6$H$_3$))[16] *(see Figure 5)* revealed conversion of the catalyst into another species as the reaction progressed.[17] This species was identified as either a bidentate borohydride complex or a BH_3 adduct of the initial iridium dihydride complex *(see Figure 14)*, which could be regenerated by the introduction of H_2. The complex was confirmed as the latter species by determination of a crystal structure which confirmed the presence of a σ-B-H bond.[29]

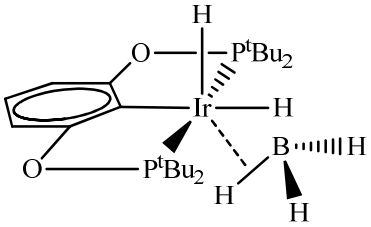

Figure 14: The resting state species, the BH_3 adduct of Brookhart's iridium pincer complex, [Ir(POCOP)H_2].[29]

Several studies have also probed the fate of the aminoborane unit, $H_2B{=}NR_{2-n}H_n$ which results upon the loss of one equivalent of H_2 from amine-boranes. It is generally accepted that the dissociation of these final dehydrogenation products from the metal centre, followed by their subsequent combination, results in the formation of polymeric structures, $[H_2BNR_{2-n}H_n]_x$, as the thermodynamic products of the reaction. However, these structures vary widely, particularly in the dehydrogenation products of ammonia-borane, where a number of different cyclic oligomers[10b, 17] and also linear polymers have been isolated.[30] It is thought that the strength of the metal interaction with $H_2B{=}NR_{2-n}H_n$ and the ease of dissociation from the metal centre might lead to the selectivity observed in many dehydrocoupling reactions.[31]

The coordination modes of the $H_2B{=}NR_{2-n}H_n$ unit have therefore been examined by a number of groups. Weller *et al*. observed a [Rh(η^2:η^2-H_2B-NMe$_2$)(P^{i}Bu$_3$)$_2H_2$]BAr$_4^F$ species which

appeared to be the end product of the reaction between $H_3B{\cdot}NMe_2H$ and $[Rh(P^iBu_3)_2]BAr_4^F$ *(see Figure 8)*, but the complex was only characterised spectroscopically.[21] More recently, Alcaraz and Sabo-Etienne reported the synthesis and isolation of several $[Ru(\eta^2{:}\eta^2\text{-}H_2B\text{-}NR^1R^2)(PCy_3)_2H_2]$ complexes, described as 'true' *bis*(σ-B-H) aminoborane complexes due to the 3-coordinate nature of the boron atom *(see Figure 15)*.[32] A recent paper in collaboration with the Weller group detailed ruthenium, rhodium and iridium complexes of this form with $\eta^2{:}\eta^2$ coordinated $H_2B\text{-}N^iPr_2$ *(see Figure 15)*.[33] The N-heterocyclic carbene analogues of these complexes were also developed by Aldridge and coworkers, coordinating $H_2B\text{-}N^iPr_2$ onto both rhodium and iridium centres in the same fashion to form $[M(\eta^2{:}\eta^2\text{-}H_2B\text{-}N^iPr_2)(IMes)_2H_2]BAr_4^F$ *(see Figure 15)*.[34]

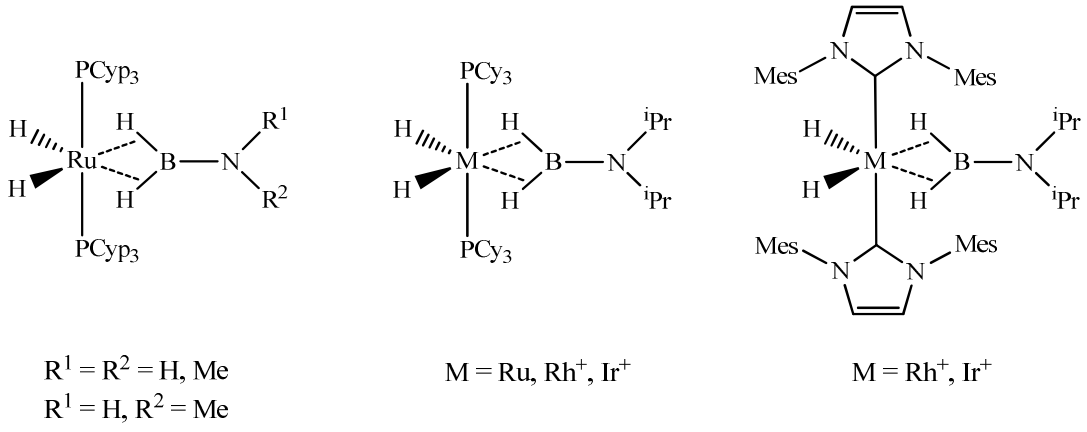

Figure 15: *Bis*(σ-B-H) aminoborane complexes.[32-34]

Previous work within the Whittlesey group had shown that the cationic fragment '$[Ru(xantphos)(PPh_3)H]^+$' was able to coordinate a range of small molecules such as OH_2, O_2, H_2 and N_2 *(see Chapter 3)*. The recent work on coordination of amine- and phosphine-boranes to organometallic complexes identified these substrates as interesting small molecules to consider. In particular, the η^2 coordination of H_2 to '$[Ru(xantphos)(PPh_3)H]^+$' observed at low temperatures was seen as an encouraging result for the possible σ-coordination of a B-H bond. The reactivity of various amine-boranes ($H_3B{\cdot}N^tBuH_2$, $H_3B{\cdot}NMe_2H$, $H_3B{\cdot}HN\{CH_2CH_2\}_2O$ and $H_3B{\cdot}NH_3$) and the phosphine-borane, $H_3B{\cdot}PPh_2H$, towards the cationic species $[Ru(xantphos)(PPh_3)(OH_2)H]^+$ (**25a**) was therefore examined and also contrasted with the reactivity displayed towards the 16-electron complexes [Ru(dppf)(L)HCl] (L = PPh_3 (**31**), NHC). All isolated species were also investigated as catalysts for the dehydrocoupling of $H_3B{\cdot}NMe_2H$.

4.3 Reactivity of [Ru(xantphos)(PPh$_3$)(OH$_2$)H]BAr$_4^F$ (25a) with Amine-Boranes

Reaction of pre-formed CD_2Cl_2 solutions of [Ru(xantphos)(PPh$_3$)(OH$_2$)H]BAr$_4^F$ (**25a**) with 2 equivalents of the amine-boranes $H_3B{\cdot}N^tBuH_2$, $H_3B{\cdot}NMe_2H$, $H_3B{\cdot}HN\{CH_2CH_2\}_2O$ and $H_3B{\cdot}NH_3$ resulted in the formation of the η^1-B-H bound amine-borane complexes [Ru(xantphos)(PPh$_3$)($H_3B{\cdot}N^tBuH_2$)H]BAr$_4^F$ (**35**), [Ru(xantphos)(PPh$_3$)($H_3B{\cdot}NMe_2H$)H]BAr$_4^F$ (**36**), [Ru(xantphos)(PPh$_3$)($H_3B{\cdot}HN\{CH_2CH_2\}_2O$)H]BAr$_4^F$ (**37**) and the parent ammonia-borane complex [Ru(xantphos)(PPh$_3$)($H_3B{\cdot}NH_3$)H]BAr$_4^F$ (**38**) *(see Figure 16)*.

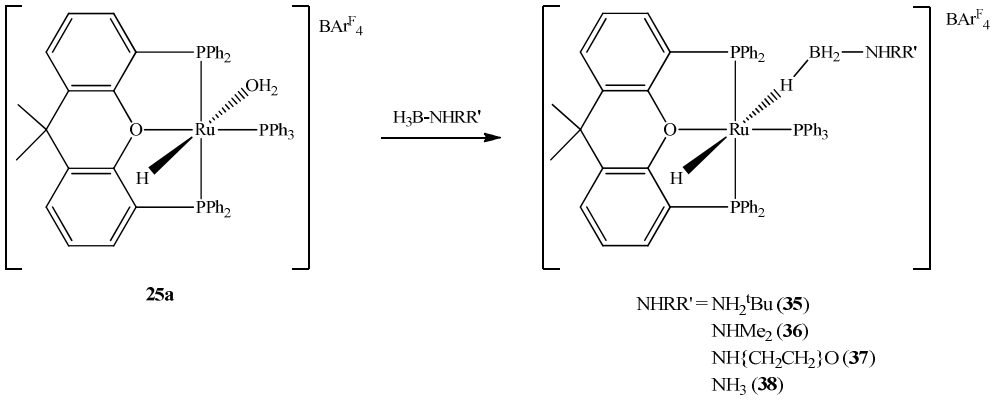

Figure 16: Synthesis of the amine-borane complexes **35-38**.

The room temperature ^{1}H NMR spectrum of each complex displayed a single hydride resonance between δ -14.5 and δ -15.4 with a doublet of triplets multiplicity, and *cis* $^2J_{HP}$ couplings to both the chelating ligands and the PPh$_3$ moiety. In each case, the hydride signal was found in a 1:3 ratio with a broad resonance between δ -0.7 and -1.6. Comparison with the literature suggested that this arose from a metal coordinated B-H bond in rapid exchange with the two terminal B-H protons of a BH$_3$ group.[18a] The $^{31}P\{^1H\}$ NMR spectra at 298 K of **35-38** exhibited the expected doublet and higher frequency triplet resonances corresponding to the coordinated POP and PPh$_3$ ligands respectively. Small *cis* $^2J_{PP}$ values were indicative of a *mer* configuration of the POP ligand.

The *tert*-butyl-amine complex **35** remained stable in solution in the presence of free amine-borane which allowed its isolation with the BAr$_4^F$ counter-ion. However, **37** decomposed in solution to form the product of amine-borane decomposition, the dihydrogen hydride complex, [Ru(xantphos)(PPh$_3$)(η^2-H$_2$)H]BAr$_4^F$ (**29a**), resulting in a 1:6.2 ratio of the two species respectively after 6 days at 298 K. The ^{11}B NMR spectrum revealed only a triplet at δ 4.4 corresponding to the dimer $[H_2B{\text{-}}NMe_2]_2$.[15] Whilst **36** and **38** remained stable in solution, large scale reactions repeatedly resulted in orange oils upon attempts at recrystallisation, despite experimentation with a variety of solvent systems. The substitution of the BAr$_4^F$ counter-ion for BPh$_4$ allowed the isolation of the parent ammonia-borane complex **38**, but badly affected the solution stability of **36** which

now decomposed more easily to form [Ru(xantphos)(PPh_3)(η^2-H_2)H]BPh_4 (**29a**), resulting in a 1:6.7 mixture of the two compounds after 3 days at 298 K.

The X-ray crystal structures of **35** and **38** confirmed the η^1-B-H Shimoi-type coordination of the amine-borane ligands *trans* to hydride, with **38** representing the first structurally characterised example of a coordinated ammonia-borane complex *(see Figure 17)*.

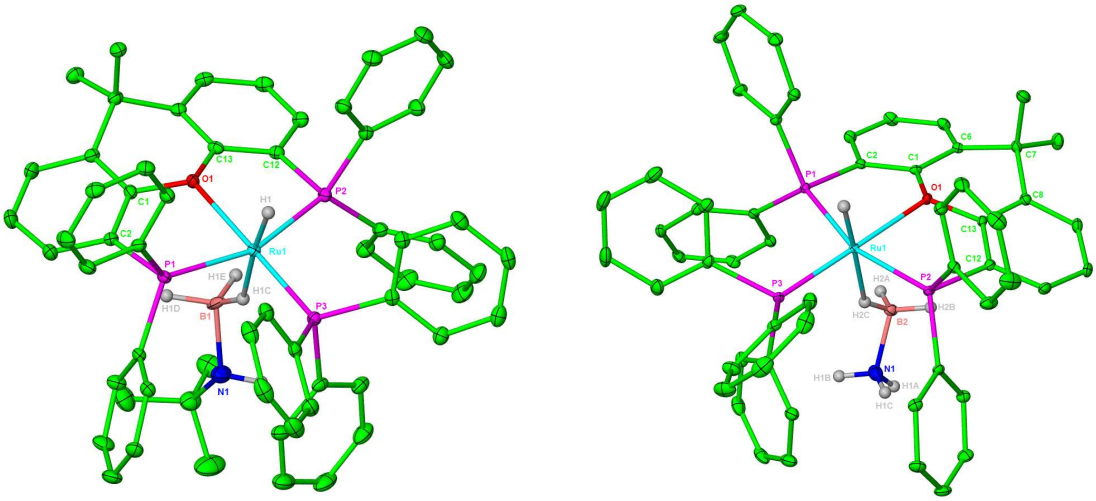

35 **38**

Figure 17: Structures of the cations in complexes **35** and **38**. Carbon-bound hydrogen atoms and solvent are omitted for clarity. Ellipsoids are shown at the 30% probability level.

Table 1: Selected bond lengths [Å] and angles [˚] for [Ru(xantphos)(PPh_3)($H_3B{\cdot}N^tBuH_2$]H]BAr_4^F (**35**) and [Ru(xantphos)(PPh_3)($H_3B{\cdot}NH_3$)H]BPh_4 (**38**)

	35	**38**
Ru-HB	1.89(2)	2.107(14)
B-N	1.656(5)	1.591(13)
Ru-P1	2.3041(8)	2.3068(5)
Ru-P2	2.3114(8)	2.3141(5)
Ru-PPh_3	2.2369(8)	2.2332(5)
Ru-O	2.276(2)	2.2768(11)
P1-Ru-P2	160.42(3)	161.330(17)

The Ru···B distances revealed in the X-ray crystal structures of **35** and **38** of 2.85 and 2.94 Å respectively are significantly longer than in the ruthenium η^1-H-BH_2 complexes

$[Cp'Ru(PMe_3)_2(\eta^1\text{-H-}BH_2\cdot L]^+$ (Cp' = Cp or Cp*, L = PMe_3; Cp' = Cp, L = NMe_3) which exhibit Ru···B distances between 2.57 and 2.66 Å.[18c, 35] This increase in Ru···B distance is likely to be a consequence of the more sterically demanding phosphine ligands surrounding the ruthenium centres in **35** and **38**. Examination of the structures also revealed a bent orientation of the xantphos ligand to cradle the borane substituent in each structure *(see Figure 18 for a representation of this in **35**)*, an effect illustrated by the C1-O1-C13 angles in each complex (117.3˚ and 117.0˚ in **35** and **38** respectively). Both structures display almost mirror symmetry about the plane bisecting the xantphos ligand, the ruthenium centre and the PPh_3 moiety. This orientation of the xantphos ligand results in B···O distances of approximately 3.15 Å in both cations, significantly less than the sum of the van der Waal's radii for both elements (3.48 Å). In line with other isolated Shimoi-type complexes, the Ru-H-B interaction is not linear (142.4˚ and 141.0˚ in **35** and **38** respectively), although the bonding can still be considered as end-on in each case.[18c, 35]

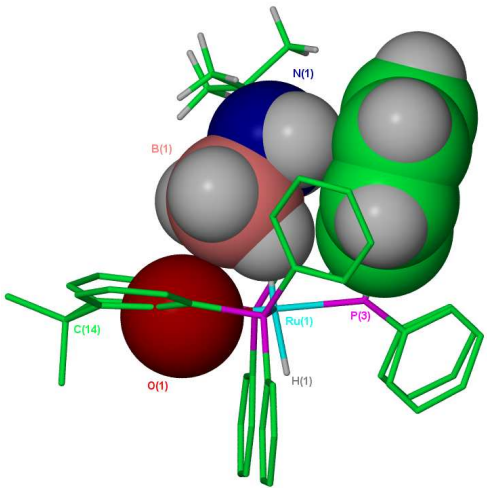

Figure 18: Side-on view of the cation present in **35** demonstrating the steric congestion about the ruthenium centre. Atoms O1, B1, N1, C47-52 and their associated hydrogen atoms have been represented as van der Waal's spheres.

Further NMR spectroscopy was performed on the isolated complexes **35** and **38**. At 298 K, a CD_2Cl_2 solution of crystalline **35** displayed the expected broad resonance of integral 3 at δ -1.63. On cooling to 180 K, the rapid exchange between the protons of the BH_3 moiety was frozen out, revealing two separate resonances at δ 0.24 and -7.59 in a 2:1 ratio, corresponding to the terminal B-H protons and the ruthenium-bound B-H proton respectively. The $^{11}B\{^1H\}$ NMR spectra of redissolved crystalline **35** and **38** revealed very broad resonances for the coordinated amine-boranes at δ -21.5 and -20.5 respectively.[36] The sample of **35** decomposed slowly at ambient temperature, forming a mixture of **35**, the aqua complex **25a** and the dihydrogen hydride complex **29a** in a 1:1.4:1.4 ratio after 48 h. The solution behaviour of crystalline **38** over time at ambient

temperature was more complex. After 72 h, a CD_2Cl_2 solution of **38** partially decomposed to form the dihydrogen hydride complex **29a** and a new product, **39**. This new species displayed a hydride resonance at δ -13.92 in the ^1H NMR spectrum, and doublet and triplet resonances in the $^{31}P\{^1H\}$ NMR spectrum at δ 54.2 and 80.0 respectively. Once again, the multiplicities and magnitude of $^2J_{HP}$ and $^2J_{PP}$ apparent in the signals pointed towards a *trans* H-Ru-L structure. The identity of L was subsequently confirmed as NH_3 following an independent reaction of a CD_2Cl_2 solution of $[Ru(xantphos)(PPh_3)(OH_2)H]BPh_4$ (**25a**) with 1 atm. NH_3 to form $[Ru(xantphos)(PPh_3)(NH_3)H]$-$BPh_4$ (**39**). A resonance at δ 0.2 of integral 3 in the ^1H NMR spectrum was assigned to the NH_3 group. The formation of **39** in the degradation of **38** arises as the result of a reaction between the coordinated $H_3B{\cdot}NH_3$ and any 'adventitious' H_2O present in solution.[37] This was shown by the addition of H_2O to a CD_2Cl_2 solution of a 2.1:1 mixture of **38** and **39** respectively. Treatment with 5.5 equivalents H_2O resulted in an immediate increase in the amount of NH_3 complex to give a solution comprising of **38** and **39** in a 1:10.8 ratio.

4.4 Reactivity of $[Ru(xantphos)(PPh_3)(OH_2)H]BAr_4^F$ (25a) towards $H_3B{\cdot}PPh_2H$

In contrast to the sole formation of complexes **35-38**, treatment of a pre-formed CD_2Cl_2 solution of **25a** with 2 equivalents $H_3B{\cdot}PPh_2H$ resulted in the initial formation of three products; the mixed PPh_3/PPh_2H phosphine product $[Ru(xantphos)(PPh_3)(PPh_2H)H]BAr_4^F$ (**40**), the secondary *bis*-phosphine complex $[Ru(xantphos)(PPh_2H)_2H]BAr_4^F$ (**41**) and the η^1-H-B phosphine-borane species, $[Ru(xantphos)(PPh_3)(H_3B{\cdot}PPh_2H)H]BAr_4^F$ (**42**) *(see Figure 19)*. After 1 h at 298 K, the ^1H NMR spectrum exhibited a 1.1:1.0:1.0 ratio of **40**:**41**:**42**. After 4 h, the mixed PPh_3/PPh_2H complex **40** had fully converted into the secondary *bis*-phosphine species **41**. Treatment of $[Ru(xantphos)(PPh_3)(OH_2)H]BAr_4^F$ (**25a**) with only one equivalent of $H_3B{\cdot}PPh_2H$ slowed this transformation (completion within 24 h instead of 4 h) but failed to arrest its progress altogether.

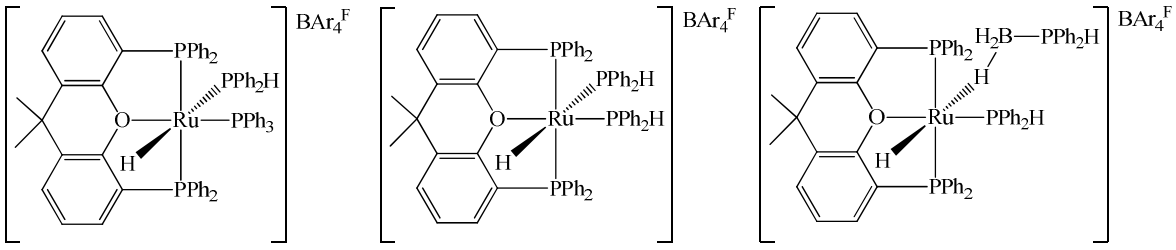

Figure 19: Products of the reaction between **25a** and $H_3B{\cdot}PPh_2H$.

The facile transformation of **40** prevented the isolation and full characterisation of this complex, which was only characterised spectroscopically. This revealed a doublet of quartets hydride resonance at δ -7.51 in the ^{1}H NMR spectrum with a large *trans* $^{2}J_{HP}$ splitting of 82 Hz. Three highly coupled signals in the $^{31}P\{^{1}H\}$ NMR spectrum at δ 65.7, 45.3 and 10.0 corresponded to the three separate phosphine environments present in the complex. $^{31}P\{^{1}H\}$ NMR spectra run periodically throughout the reaction also revealed the formation of $H_3B{\cdot}PPh_3$ (δ 22.3) as a sink for the PPh_3 released on conversion of **40** to **41**. Further assignment of **40** was provided by an independent reaction between a CD_2Cl_2 solution of the aqua precursor **25a** and 2 equivalents PPh_2H. After 15 min at ambient temperature, the ^{1}H NMR spectrum of this reaction revealed a 7.9:1 ratio of **40**:**41**, with complete conversion to **41** observed within 3 h at 298 K.

The borane bound complex **42** proved more stable than **40** in solution, decomposing over 5 days at room temperature to form **41**. As with complexes **35-38**, **42** displayed diagnostic ^{1}H NMR signals at δ -13.91 and -1.89 in a 1:3 ratio, for the hydride and BH_3 group. Three separate ^{31}P environments were observed at δ 55.5, 53.7 and -5.6. The lowest frequency resonance was assigned to the bound secondary phosphine-borane on the basis of a proton coupled ^{31}P NMR spectrum, which split this signal with a large and characteristic $^{1}J_{PH}$ coupling of 405 Hz.

The secondary *bis*-phosphine complex **41** was isolated with a BPh_4 anion as an air-stable yellow crystalline solid in 43% yield. The ^{1}H NMR spectrum revealed a highly coupled hydride resonance at δ -6.47 with a large *trans* $^{2}J_{HP}$ splitting of 81 Hz. The secondary phosphine protons were assigned to two signals at δ 5.07 and 5.92, each split with characteristically large $^{1}J_{HP}$ couplings of 338 and 361 Hz respectively. Once again, a proton coupled ^{31}P NMR spectrum led to the assignment of signals at δ 57.8 and 15.4 as those arising from the PPh_2H moieties, and a triplet at δ 52.4 was attributed to the xantphos ligand.

The molecular structure of **41** was confirmed by X-ray crystallography *(see Figure 20)*, which revealed a distorted octahedral geometry about the ruthenium centre. In agreement with the NMR data, two PPh_2H ligands were present in the structure, one *trans* to hydride and the other trans to oxygen. The differing *trans* influence of these ligands accounts for the difference in Ru-P bond lengths to the two PPh_2H groups (2.3761(7) Å and 2.2373(7) Å respectively) *(see Table 2)*.

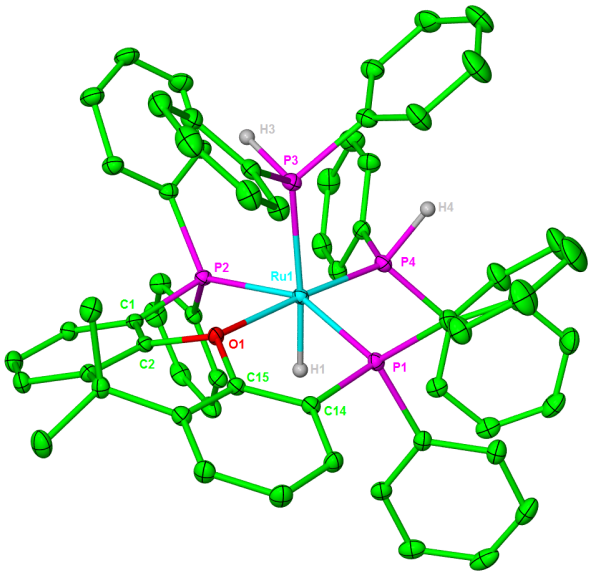

Figure 20: Structure of the cation in $[Ru(xantphos)(PPh_2H)_2H]BPh_4$ (**41**). Carbon-bound hydrogen atoms and solvent omitted for clarity. Ellipsoids are shown at the 30% probability level.

Table 2: Selected bond lengths [Å] and angles [˚] for $[Ru(xantphos)(PPh_2H]_2H]BAr_4^F$ (**41**)

Ru-P1	2.3174(7)
Ru-P2	2.3186(6)
Ru-P3	2.3761(7)
Ru-P4	2.2373(7)
Ru-O	2.2593(17)
P1-Ru-P2	155.45(2)
P3-Ru-P4	93.87(2)
O-Ru-P4	177.12(5)

The η^1-H-B coordination of phosphine-boranes is well known.[18a,18c,23,35,38] However, the author is unaware of any other examples of P-B cleavage to form phosphine compounds on coordination of phosphine-boranes to metal centres, although the displacement of intact phosphine-boranes from metal centres has been achieved by the introduction of Lewis bases such as CO or MeCN.[18c]

It was hoped that examination of the ^{11}B NMR spectra throughout the reaction might shed some light on the mechanism of P-B cleavage, but unfortunately no characterisable 'BH_3' species

such as B_2H_6 were observed, although these might be highly volatile. A water-mediated mechanism, similar to that which resulted in formation of the ammonia complex **39** was also considered, but no change was observed on the addition of 5 equivalents H_2O to a CD_2Cl_2 solution of $H_3B{\cdot}PPh_2H$.

Instead, the formation of a number of more thermodynamically stable species might well have a bearing on the observed P-B cleavage. In particular, the tertiary phosphine-borane, $H_3B{\cdot}PPh_3$, formed on displacement of PPh_3 from the ruthenium centre, is known to be more thermodynamically stable than its less substituted counterparts.[39] The stability of the final reaction product, $[Ru(xantphos)(PPh_2H)_2H]BPh_4$ (**41**), was also examined. Treatment of a CD_2Cl_2 solution of **41** with 3 equivalents PPh_3 resulted in no exchange of the secondary phosphine for the tertiary analogue even after 24 h at ambient temperature. However, it is also worth commenting that recent work by Manners *et al*. observed only the substitution of CO on the addition of PMe_3 to $[CpRu(CO)_2(PPh_2\text{-}BH_3)]$.[40]

4.5 Ruthenium Bis-Phosphine Complexes for Catalytic Amine-Borane Dehydrogenation

A number of isolated M-σ(B-H) species have been implicated as catalytic intermediates for the dehydrocoupling of amine-boranes.[15, 21] It was therefore disappointing that reaction of 5 mol% $[Ru(xantphos)(PPh_3)(H_3B{\cdot}N^tBuH_2]H]BAr_4^F$ (**35**) with 0.125 mmol $H_3B{\cdot}NMe_2H$[41] resulted in only 5% conversion to the dimer $[H_2B\text{-}NMe_2]_2$ by ^{11}B NMR spectroscopy after 72 h at 298 K *(see Entry 1, Table 4)*. Examination of the ^1H NMR spectrum during the reaction revealed the partial formation of $[Ru(xantphos)(PPh_3)(H_3B{\cdot}NMe_2H)H]BAr_4^F$ (**36**); after 72 h, the mixture was composed of **35** and **36** in a 1:3.4 ratio. The aqua precursor $[Ru(xantphos)(PPh_3)(OH_2)H]BAr_4^F$ (**25a**) demonstrated greater catalytic activity, affording a 48% conversion to the coupled product after 72 h under the same conditions *(see Entry 2, Table 4)*. Interestingly, in this case, the ^1H NMR spectrum after 72 h at 298 K revealed **36** as the sole remaining ruthenium species. Other xantphos-containing species, such as $[Ru(xantphos)(PPh_3)HCl]$ (**24a**) and the secondary *bis*-phosphine complex, $[Ru(xantphos)(PPh_2H)_2H]BPh_4$ (**41**), performed poorly at the same catalyst loading, with both systems reaching less than 10% conversion to dimer within 72 h at ambient temperature *(see Entries 3 & 4, Table 4)*. In these cases, the ^1H NMR spectra recorded at the end of the reaction revealed only the presence of the ruthenium precursors.

Expansion of the catalytic testing to include ruthenium dppf complexes resulted in much higher conversions to $[H_2B\text{-}NH_2]_2$. Catalytic dehydrocoupling with 0.5 mol% $[Ru(dppf)(PPh_3)HCl]$ (**31**) resulted in 82% conversion to product after 72 h at 298 K, whilst $[Ru(dppf)(\{\eta^6\text{-}C_6H_5\}\text{-}PPh_2)H]BAr_4^F$ (**32**) gave 100% conversion to dimer under the same conditions *(see Entries 5 & 6,*

Table 4). Interestingly, the ^{1}H NMR spectra of these reactions exhibited an array of new hydride containing species, and free PPh_3 was apparent in the $^{31}P\{^{1}H\}$ NMR spectra in both cases. Although the latter complex possesses an 18-electron configuration, it is known to be substitutionally labile *(see Chapter 3)*, reacting with both CO and PMe_3 to form $[Ru(dppf)(PPh_3)(CO)_2H]BAr_4^F$ (**33**) and $[Ru(PMe_3)_5H]BAr_4^F$ (**34**).[42]

4.6 Ru(dppf)(NHC) Complex Development for Catalytic Amine-Borane Dehydrogenation

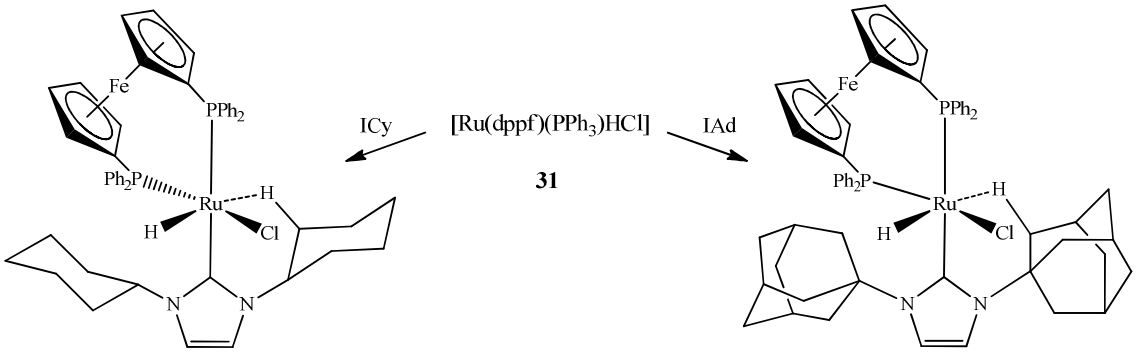

Figure 21: Reaction of $[Ru(dppf)(PPh_3)HCl]$ (**31**) with the bulky NHCs ICy and IAd to form [Ru(dppf)(ICy)HCl] (**43**) and [Ru(dppf)(IAd)HCl] (**44**).

Attempts were made to modify the structure of $[Ru(dppf)(PPh_3)HCl]$ (**31**) to form more catalytically active complexes as this was deemed an easier approach than the modification of $[Ru(dppf)(\{\eta^6\text{-}C_6H_5\}\text{-}PPh_2)H]BAr_4^F$ (**32**). To this end, **31** was reacted with a number of N-alkyl and N-aryl substituted N-heterocyclic carbene (NHC) ligands. Treatment of THF solutions of **31** with 2 equivalents IMes, $I^iPr_2Me_2$ and IMe_4 at 343 K showed the formation of multiple hydride-containing species on examination of the ^{1}H NMR spectra. Large amounts of free dppf and PPh_3 were also apparent in the $^{31}P\{^{1}H\}$ NMR spectra of both reactions.[43] However, reaction of **31** with the bulky N-alkyl substituted NHCs ICy and IAd under the same conditions resulted in the clean formation of [Ru(dppf)(ICy)HCl] (**43**) and [Ru(dppf)(IAd)HCl] (**44**) *(see Figure 21)*. These complexes were isolated as orange crystalline solids in moderate yields, and proved highly air sensitive. The molecular structures of **43** and **44** were established by X-ray crystallography *(see Figure 22)* in combination with NMR spectroscopy.

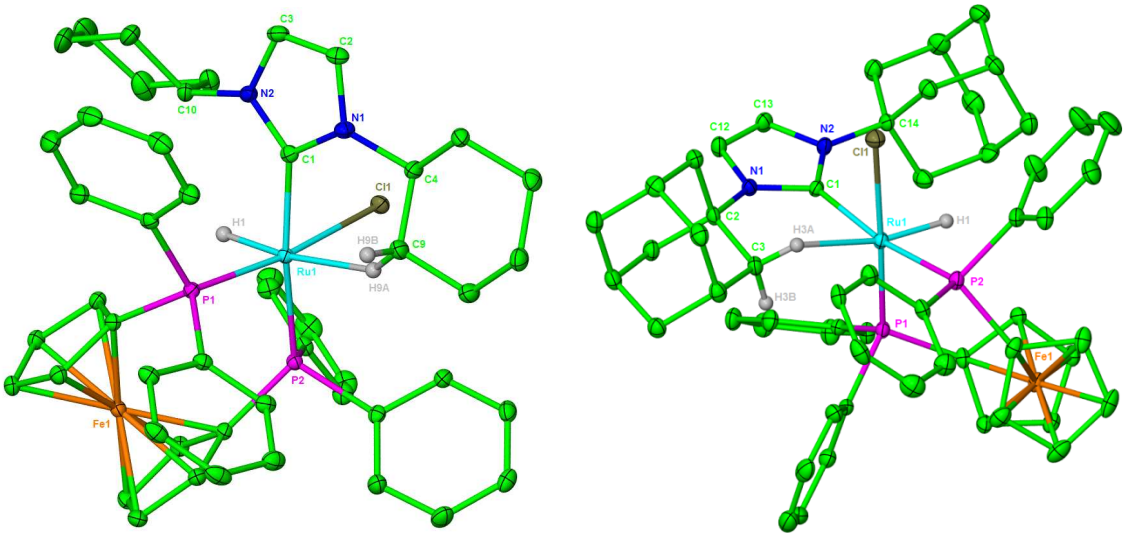

43 **44**

Figure 22: Molecular structures of [Ru(dppf)(ICy)HCl] (**43**) and [Ru(dppf)(IAd)HCl] (**44**). Carbon-bound hydrogen atoms (and minor disordered cyclohexyl component of **43**) omitted for clarity. Ellipsoids are shown at the 30% probability level.

Table 3: Selected bond lengths [Å] and angles [˚] for [Ru(dppf)(ICy)HCl] (**43**) and [Ru(dppf)(IAd)HCl] (**44**)

	43	**44**
Ru-C_{NHC}	2.0501(19)	2.096(5)
Ru-$P_{transCl}$	2.2230(5)	2.2268(14)
Ru-$P_{transNHC}$	2.3375(5)	2.3416(15)
Ru-Cl	2.4666(5)	2.5013(14)
Ru···$C_{agostic}$	2.973	2.760
C_{NHC}-Ru-$P_{transCl}$	93.68(5)	94.16(15)
C_{NHC}-Ru-$P_{transNHC}$	169.19(5)	169.81(15)

Each structure displayed a distorted octahedral geometry *(see Table 3)* with an agostic interaction apparent in the vacant site *trans* to the hydride. This arose from a β-C-H proton of one cyclohexyl carbene substituent in [Ru(dppf)(ICy)HCl] (**43**), and from a β-CH_2 group on the IAd ligand in [Ru(dppf)(IAd)HCl] (**44**).

Some disorder in one cyclohexyl arm of **43** resulted in the inclusion at calculated positions of those hydrogen atoms on C9 which were involved in the agostic contact. More reliable

information on the agostic interaction was therefore obtained by examination of the Ru···$C_{agostic}$ distance, measured at 2.973 Å *(see Table 3)*, which suggested a weak agostic contact.[44] This cyclohexyl moiety also exhibited a significant rotation relative to the NHC which assisted the formation of an agostic interaction. In particular, the angle between a mean plane drawn through the carbon atoms of the cyclohexyl ring containing C9/C9a and another drawn through the N1, N2 and C1-3 atoms of the NHC moiety was measured at 61.6˚. This was a large distortion in comparison with the analogous measurement for the unaffected cyclohexyl counterpart (10˚). The observation of an agostic contact was mirrored in solution, with a correlation in the ^{1}H-^{1}H COSY detected between one of the α-cyclohexyl resonances and a low frequency resonance at δ 0.7.[45] The second non-agostic proton of the β-CH_2 group was assigned to a signal at δ 3.5, with the corresponding $C_{agostic}$ signal identified at δ 31.8 using ^{1}H-^{13}C HMQC spectroscopy.

The Ru···$C_{agostic}$ distance in [Ru(dppf)(IAd)HCl] (**44**) was measured at 2.760 Å, a significantly shorter contact than that present in **43**.[46] The ^{1}H NMR spectrum of redissolved crystals of **44** revealed two hydride signals δ -20.6 (t, $^{2}J_{HP}$ = 31 Hz) and δ -21.6 (dd, $^{2}J_{HP}$ = 34 Hz, $^{2}J_{HP}$ = 28 Hz) in a 1:2 ratio respectively. Although this data indicated the presence of two isomers, the ^{13}C{^{1}H} NMR spectrum failed to provide any further information as to the difference in structure of these two species since the carbene resonance for each exhibited a doublet of doublets multiplicity with one large *trans* splitting ($^{2}J_{CP}$ = 108 Hz and 99 Hz respectively) and one smaller *cis* splitting ($^{2}J_{CP}$ = 10 Hz and 14 Hz respectively). A ^{1}H-^{13}C HMBC experiment was used to correlate the hydride signal for the major isomer (δ -21.6) to a resonance at δ 37.7 corresponding to the agostic carbon. This in turn exhibited a correlation via ^{1}H-^{13}C HMQC to a proton resonance at δ 1.0, which was assigned as the agostic proton. The lower concentration and broader NMR signals for the minor species precluded the clear identification of any agostic signals.

The newly synthesised complexes [Ru(dppf)(ICy)HCl] (**43**) and [Ru(dppf)(IAd)HCl] (**44**) were both evaluated for catalytic dehydrocoupling activity, and demonstrated very different reactivity *(see Table 4)*. [Ru(dppf)(ICy)HCl] (**43**) (5 mol%) essentially completed the dehydrogenation of 0.125 mmol $H_3B{\cdot}NMe_2H$ to form $[H_2B\text{-}NMe_2]_2$ after only 15 min at room temperature, which translated to a turnover frequency (TOF) of 76 h^{-1}. Indeed, the rapid evolution of H_2 was observed immediately on addition of CD_2Cl_2 to the mixture of substrate and catalyst. In contrast, **44** was notably less active than the precursor [Ru(dppf)(PPh_3)HCl] (**31**), achieving only 26% conversion to $[H_2B\text{-}NMe_2]_2$ after 72 h at 298 K.

The periodic examination of the ^{1}H NMR spectra of both reactions during the dehydrogenation process revealed no change to the ruthenium complex **44** even after 72 h at 298 K, whereas only trace amounts of **43** remained after 15 min at room temperature. In this case, multiple new hydride containing species were observed. Interestingly, the addition of a second charge of

0.125 mmol $H_3B{\cdot}NMe_2H$ to this reaction mixture resulted in a further 53% conversion to $[H_2B\text{-}NMe_2]_2$ over another 15 min, indicating the retention of some catalytic activity.

Table 4: Comparison of the catalytic activity of ruthenium catalysts (5 mol%) for the room temperature dehydrogenation of $H_3B{\cdot}NMe_2H$

Entry	Catalyst precursor[a]	Yield (%)[b]		TOF (h^{-1})
		0.25 h	72 h	
1	**35**	2	5	0.01
2	**25a**	0	48	0.1
3	**24a**	0	10[c]	0.03
4	**41**	2	9	0.03
5	**31**	0	82	0.2
6	**32**	0	100	0.3
8	**43**	95	100	76
7	**44**	1	26	0.07

[a]Reactions were performed using 0.125 mmol $Me_2NH{\cdot}BH_3$ in CD_2Cl_2 (0.5 mL) with 5 mol% [Ru] at 298 K, and were monitored via ^{11}B spectroscopy. [b]Based on integration of the ^{11}B NMR spectrum of the reaction mixture. [c]Reaction time of 168 h.

In addition to $H_3B{\cdot}NMe_2H$, both $H_3B{\cdot}NH_3$ and $H_3B{\cdot}NH\{CH_2CH_2\}_2O$ were dehydrogenated by **43** (5 mol%). Dehydrogenation of ammonia-borane resulted in the formation of an insoluble white precipitate, likely to be $[H_2B\text{-}NH_2]_2$.[11,47] After 2 h at ambient temperature, the ^{11}B NMR spectrum of the morpholine-borane reaction exhibited only a triplet signal at δ 2.2 ($^1J_{BH}$ = 114 Hz). Comparison with the literature led to the assignment of this product as $H_2B\text{-}N\{CH_2CH_2\}O$.[48] The dehydrogenation of $H_3B{\cdot}N^tBuH_2$ was also attempted. After 72 h at 298 K, examination of the ^{11}B NMR spectrum revealed the disappearance of *tert*-butylamine-borane but the formation of multiple higher frequency ^{11}B resonances, none of which could be definitively assigned.

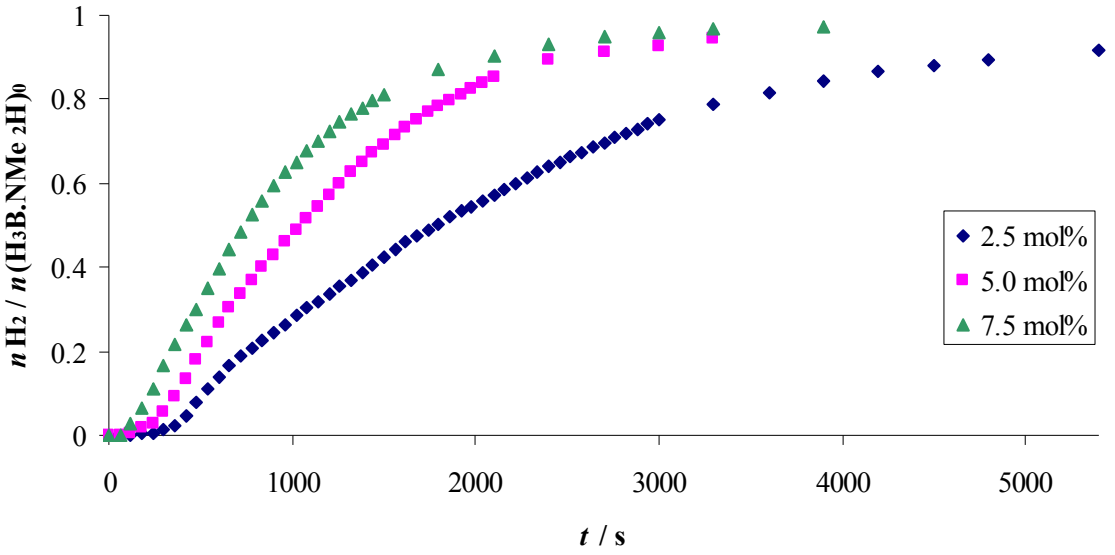

Figure 23: The production of H_2 with time for the dehydrogenation of $H_3B{\cdot}NMe_2H$ (0.6 mmol) catalysed by various loadings of [Ru(dppf)(ICy)HCl] (**43**) in toluene at 298 K.

Due to the high activity of **43**, the catalytic performance was assessed on a large scale (0.6 mmol $H_3B{\cdot}NMe_2H$) using the volumetric monitoring of H_2 evolution with time *(see Figure 23, Experimental 5.6.11 & Appendix 4)*.[49] This method allowed the effect of catalyst loading on H_2 evolution to be evaluated. As expected, an increase in the catalyst loading from 2.5 mol% to 7.5 mol% resulted in an increase in the rate of H_2 evolution, although only one equivalent of H_2 was produced in each case. An induction period for H_2 formation was also apparent at each catalyst loading (ca. 120 s at 2.5 mol%, and ca. 60 s at 5 and 7.5 mol%) and the volumetric curves possessed a sinusoidal appearance. This behaviour is often observed in heterogeneous systems where the initial pre-catalyst has to be reduced to metal nanoclusters or colloids before any dehydrogenation occurs.[4a,10b,17,50] However, no evidence was found for the formation of a heterogeneous system from **43**; the solution retained a yellow homogeneous appearance throughout each reaction, with no darkening or precipitation observed. Moreover, the rate of H_2 evolution remained largely unchanged upon the addition of 100 equivalents of Hg to the catalyst system *(see Figure 24, Experimental 5.6.11 & Appendix 4)*.[51] It is therefore likely that the observed induction period arises from the formation of a vacant site from [Ru(dppf)(ICy)HCl] (**43**) to give homogeneous ruthenium fragments. It is currently unclear whether the vacant site is generated *via* dissociation of the agostic contact or the loss of another ancillary ligand.[52]

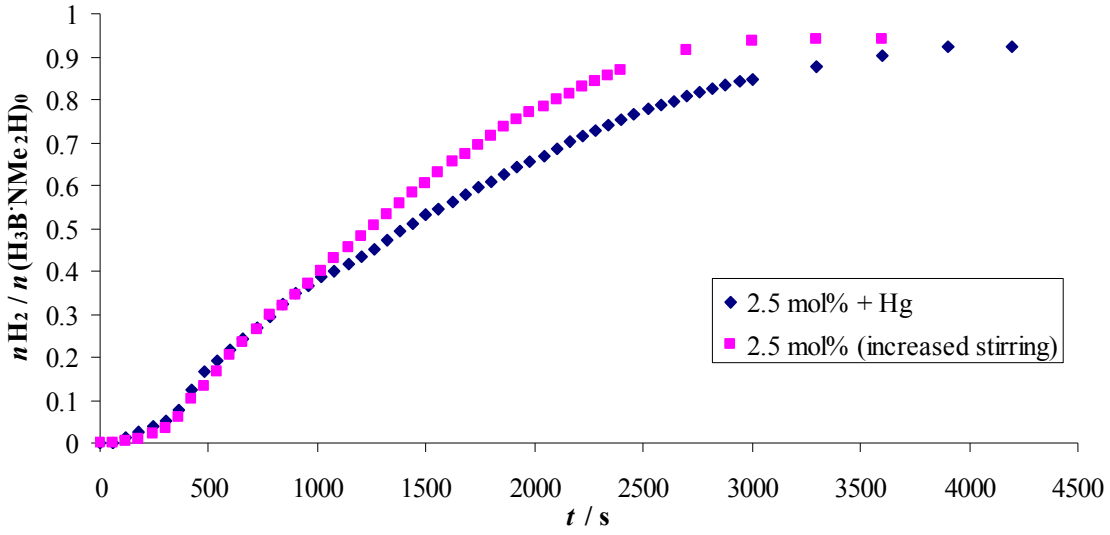

Figure 24: The production of H_2 with time for the dehydrogenation of $H_3B{\cdot}NMe_2H$ (0.6 mmol) catalysed by [Ru(dppf)(ICy)HCl] (**43**) at 2.5 mol% loading in toluene at 298 K, with and without the addition of mercury (100 equivalents).[53]

There are very few examples of NHC-based catalysts for the dehydrocoupling of amine-boranes in the literature,[54] although, as mentioned previously, Baker *et al*. have developed a highly effective Ni-NHC system *(see Figure 12)* for the dehydrogenation of amine-boranes.[27] DFT calculations on this system suggested significant involvement of the carbenic carbon in promoting the catalytic cycle.[28] At present, the mechanism at work in this ruthenium system is unclear. It would be interesting to conduct further studies to elucidate the mechanism, particularly with respect to the role of the NHC ligand, and also to develop new phosphine/NHC catalyst combinations for the dehydrocoupling of amine-boranes.

4.7 CHAPTER SUMMARY

The reactivity of [Ru(xantphos)(PPh_3)(OH_2)H]BAr_4^F (**25a**) towards a range of amine-boranes has been investigated, and the η^1-H-B Shimoi-type complexes [Ru(xantphos)(PPh_3)($H_3B{\cdot}N^tBuH_2$)H]BAr_4^F (**35**) and [Ru(xantphos)(PPh_3)($H_3B{\cdot}NH_3$)H]BPh_4 (**38**) have been isolated and structurally characterised.

In contrast, treatment of [Ru(xantphos)(PPh_3)(OH_2)H]BAr_4^F (**25a**) with the secondary phoshine-borane, $H_3B{\cdot}PPh_2H$, resulted in P-B cleavage to yield the secondary *bis*-phosphine complex [Ru(xantphos)($PPh_2H)_2$H]BAr_4^F (**41**) as the final product of the reaction.

The ruthenium complexes incorporating the xantphos ligand all prove inactive for the catalytic dehydrogenation of $H_3B{\cdot}NMe_2H$. However, the ruthenium complexes [Ru(dppf)(PPh_3)HCl] (**31**) and [Ru(dppf)({η^6-C_6H_5}-PPh_2)H]BAr_4^F (**32**) both catalyse the dehydrogenation of $H_3B{\cdot}NMe_2H$ to form the dimeric species $[H_2B\text{-}NMe_2]_2$.

Modification of [Ru(dppf)(PPh_3)HCl] (**31**) by substitution of the PPh_3 ligand for the N-heterocyclic carbene (NHC) ligands ICy and IAd resulted in the formation of [Ru(dppf)(ICy)HCl] (**43**), which proved highly active for the dehydrogenation of $H_3B{\cdot}NMe_2H$ (TOF = 75 h^{-1}), and also [Ru(dppf)(IAd)HCl] (**44**) which proved to be catalytically inactive.

References

1. Mkhalid, I. A. I.; Barnard, J. H.; Marder, T. B.; Murphy, J. M.; Hartwig, J. F. *Chem. Rev.* **2010**, *110,* 890-931.
2. Hamilton, C. W.; Baker, R. T.; Staubitz, A.; Manners, I. *Chem. Soc. Rev.* **2009**, *38,* 279-293.
3. (a) Stephens, F. H.; Pons, V.; Baker, R. T. *Dalton Trans.* **2007**, 2613-2626; (b) Marder, T. B. *Angew. Chem. Int. Ed.* **2007**, *46,* 8116-8118.
4. (a) Jaska, C. A.; Manners, I. *J. Am. Chem. Soc.* **2004**, *126,* 2698-2699; (b) Jiang, Y.; Berke, H. *Chem. Commun.* **2007**, 3571-3573; (c) Jana, A.; Schulzke, C.; Roesky, H. W. *J. Am. Chem. Soc.* **2009**, *131,* 4600-4601.
5. Staubitz, A.; Robertson, A. P. M.; Sloan, M. E.; Manners, I. *Chem. Rev.* **2010**, *110,* 4023-4078.
6. Niedenzu, K.; Dawson, J. W. *Boron-Nitrogen Compounds* **1965**, Academic Press Inc., New York.
7. (a) Burg, A. B.; Wagner, R. I. *J. Am. Chem. Soc.* **1953**, *75,* 3872-3877; (b) Gee, W.; Holden, J. B.; Shaw, R. A.; Smith, B. C. *J. Chem. Soc.* **1965**, 3171-3174.
8. Wagner, R. I.; Caserio, F. F. *J. Inorg. Nucl. Chem.* **1959**, *11,* 259-259.
9. Dorn, H.; Singh, R. A.; Massey, J. A.; Lough, A. J.; Manners, I. *Angew. Chem. Int. Ed.* **1999**, *38,* 3321-3323.
10. (a) Jaska, C. A.; Temple, K.; Lough, A. J.; Manners, I. *Chem. Commun.* **2001**, 962-963; (b) Jaska, C. A.; Temple, K.; Lough, A. J.; Manners, I. *J. Am. Chem. Soc.* **2003**, *125,* 9424-9434.
11. Blaquiere, N.; Diallo-Garcia, S.; Gorelsky, S. I.; Black, D. A.; Fagnou, K. *J. Am. Chem. Soc.* **2008**, *130,* 14034-14035.
12. Morris, R.; Habtemariam, A.; Guo, Z. J.; Parsons, S.; Sadler, P. J. *Inorg. Chim. Acta* **2002**, *339,* 551-559.
13. Kass, M.; Friedrich, A.; Drees, M.; Schneider, S. *Angew. Chem. Int. Ed.* **2009**, *48,* 905-907.
14. (a) Zhang, J.; Leitus, G.; Ben-David, Y.; Milstein, D. *Angew. Chem. Int. Ed.* **2006**, *45,* 1113-1115; (b) Ben-Ari, E.; Leitus, G.; Shimon, L. J. W.; Milstein, D. *J. Am. Chem. Soc.* **2006**, *128,* 15390-15391; (c) Gnanaprakasam, B.; Zhang, J.; Milstein, D. *Angew. Chem. Int. Ed.* **2010**, *49,* 1468-1471.
15. Friedrich, A.; Drees, M.; Schneider, S. *Chem. Eur. J.* **2009**, *15,* 10339-10342.
16. Gottker-Schnetmann, I.; White, P.; Brookhart, M. *J. Am. Chem. Soc.* **2004**, *126,* 1804-1811.
17. Denney, M. C.; Pons, V.; Hebden, T. J.; Heinekey, D. M.; Goldberg, K. I. *J. Am. Chem. Soc.* **2006**, *128,* 12048-12049.
18. (a) Shimoi, M.; Nagai, S.; Ichikawa, M.; Kawano, Y.; Katoh, K.; Uruichi, M.; Ogino, H. *J. Am. Chem. Soc.* **1999**, *121,* 11704-11712; (b) Kakizawa, T.; Kawano, Y.; Shimoi, M. *Organometallics* **2001**, *20,* 3211-3213; (c) Kawano, Y.; Hashiva, M.; Shimoi, M. *Organometallics* **2006**, *25,* 4420-4426.
19. Alcaraz, G.; Sabo-Etienne, S. *Angew. Chem. Int. Ed.* **2010**, *49,* 7170-7179.
20. Chaplin, A. B.; Weller, A. S. *Angew. Chem. Int. Ed.* **2010**, *49,* 581-584.
21. Douglas, T. M.; Chaplin, A. B.; Weller, A. S. *J. Am. Chem. Soc.* **2008**, *130,* 14432-14433.
22. Dallanegra, R.; Chaplin, A. B.; Weller, A. S. *Angew. Chem. Int. Ed.* **2009**, *48,* 6875-6878.
23. Merle, N.; Koicok-Köhn, G.; Mahon, M. F.; Frost, C. G.; Ruggerio, G. D.; Weller, A. S.; Willis, M. C. *Dalton Trans.* **2004**, 3883-3892.
24. Nguyen, D. H.; Laureano, H.; Juge, S.; Kalck, P.; Daran, J. C.; Coppel, Y.; Urrutigoity, M.; Gouygou, M. *Organometallics* **2009**, *28,* 6288-6292.
25. Luo, Y.; Ohno, K. *Organometallics* **2007**, *26,* 3597-3600.
26. Paul, A.; Musgrave, C. B. *Angew. Chem. Int. Ed.* **2007**, *46,* 8153-8156.
27. Keaton, R. J.; Blacquiere, J. M.; Baker, R. T. *J. Am. Chem. Soc.* **2007**, *129,* 1844-1845.

28. Yang, X. Z.; Hall, M. B. *J. Am. Chem. Soc.* **2008**, *130,* 1798-1799.
29. Hebden, T. J.; Denney, M. C.; Pons, V.; Piccoli, P. M. B.; Koetzle, T. F.; Schultz, A. J.; Kaminsky, W.; Goldberg, K. I.; Heinekey, D. M. *J. Am. Chem. Soc.* **2008**, *130,* 10812-10820.
30. Staubitz, A.; Soto, A. P.; Manners, I. *Angew. Chem. Int. Ed.* **2008**, *47,* 6212-6215.
31. (a) Pons, V.; Baker, R. T. *Angew. Chem. Int. Ed.* **2008**, *47,* 9600-9602; (b) Pons, V.; Baker, R. T.; Szymczak, N. K.; Heldebrant, D. J.; Linehan, J. C.; Matus, M. H.; Grant, D. J.; Dixon, D. A. *Chem. Commun.* **2008**, 6597-6599.
32. Alcaraz, G.; Vendier, L.; Clot, E.; Sabo-Etienne, S. *Angew. Chem. Int. Ed.* **2010**, *49,* 918-920.
33. Alcaraz, G.; Chaplin, A. B.; Stevens, C. J.; Clot, E.; Vendier, L.; Weller, A. S.; Sabo-Etienne, S. *Organometallics* **2010**, *29,* 5591-5595.
34. Tang, C. Y.; Thompson, A. L.; Aldridge, S. *Angew. Chem. Int. Ed.* **2010**, *49,* 921-925.
35. (a) Yasue, T.; Kawano, Y.; Shimoi, M. *Angew. Chem. Int. Ed.* **2003**, *42,* 1727-1730; (b) Nagaraja, C. M.; Parameswaran, P.; Jemmis, E. D.; Jagirdar, B. R. *J. Am. Chem. Soc.* **2007**, *129,* 5587-5596; (c) Kawano, Y.; Yamaguchi, K.; Miyake, S. Y.; Kakizawa, T.; Shimoi, M. *Chem. Eur. J.* **2007**, *13,* 6920-6931.
36. No resonances were observed in the ^{11}B NMR spectra of *in-situ* prepared **36** and **37**. This is thought to be a consequence of rapid exchange between the free and bound amine-boranes in these samples.
37. It seems likely that 'adventitious' water could arise from both the chlorinated solvents and the $NaBAr_4^F/BPh_4$ salts.
38. (a) Ingleson, M.; Patmore, N. J.; Ruggiero, G. D.; Frost, C. G.; Mahon, M. F.; Willis, M. C.; Weller, A. S. *Organometallics* **2001**, *20,* 4434-4436; (b) Volkov, O.; Macias, R.; Rath, N. P.; Barton, L. *Inorg. Chem.* **2002**, *41,* 5837-5843.
39. (a) Frisch, M. A.; Heal, H. G.; Mackle, H.; Madden, I. O. *J. Chem. Soc.* **1965**, 899-907; (b) Gaumont, A. C.; Carboni, B. *Sci. Synth.* **2004**, *6,* 485-512.
40. Lee, K.; Clark, T. J.; Lough, A. J.; Manners, I. *Dalton Trans.* **2008**, 2732-2740.
41. Despite the huge interest surrounding the use of ammonia-borane, the substrate itself is only sparingly soluble in many common solvents, with its coupled products often completely insoluble. Most catalytic testing therefore uses the highly soluble dimethylamine-borane which is also commercially available.
42. Ledger, A. E. W.; Moreno, A.; Ellul, C. E.; Mahon, M. F.; Pregosin, P. S.; Whittlesey, M. K.; Williams, J. M. J. *Inorg. Chem.* **2010**, *49,* 7244-7256.
43. The serendipitous isolation of a crystal from the reaction with IMe_4 resulted in an X-ray crystal structure of the unusual four-carbene hydride chloride species, $[Ru(IMe_4)_4HCl]$ *(for the X-ray crystal structure and metrics, see Appendix 3)*.
44. (a) Baratta, W.; Herdtweck, E.; Rigo, P. *Angew. Chem. Int. Ed.* **1999**, *38,* 1629-1631; (b) Huang, D. J.; Streib, W. E.; Bollinger, J. C.; Caulton, K. G.; Winter, R. F.; Scheiring, T. *J. Am. Chem. Soc.* **1999**, *121,* 8087-8097; (c) Abdur-Rashid, K.; Fedorkiw, T.; Lough, A. J.; Morris, R. H. *Organometallics* **2004**, *23,* 86-94.
45. (a) Burling, S.; Kociok-Köhn, G.; Mahon, M. F.; Whittlesey, M. K.; Williams, J. M. J. *Organometallics* **2005**, *24,* 5868-5878; (b) Burling, S.; Mas-Marzá, E.; Valpuesta, J. E. V.; Mahon, M. F.; Whittlesey, M. K. *Organometallics* **2009**, *28,* 6676-6686.
46. Dinger, M. B.; Nieczypor, P.; Mol, J. C. *Organometallics* **2003**, *22,* 5291-5296.
47. Jiang, Y. F.; Blacque, O.; Fox, T.; Frech, C. M.; Berke, H. *Organometallics* **2009**, *28,* 5493-5504.
48. Pasumansky, L.; Haddenham, D.; Clary, J. W.; Fisher, G. B.; Goralski, C. T.; Singaram, B. *J. Org. Chem.* **2008**, *73,* 1898-1905.
49. Although CD_2Cl_2 was used as the solvent for the NMR scale studies of amine-borane dehydrogenation, the high vapour pressure of CH_2Cl_2 made accurate volumetric measurements very difficult on a large scale. Dichloromethane was therefore replaced by toluene for these large scale dehydrogenation experiments.

50. Jaska, C. A.; Manners, I. *J. Am. Chem. Soc.* **2004**, *126,* 9776-9785.
51. Boulho, C.; Djukic, J. P. *Dalton Trans.* **2010**, *39,* 8893-8905.
52. Staubitz, A.; Sloan, M. E.; Robertson, A. P. M.; Friedrich, A.; Schneider, S.; Gates, P. J.; Gunne, J. S. A. D.; Manners, I. *J. Am. Chem. Soc.* **2010**, *132,* 13332-13345.
53. The 2.5 mol% experiment with 100 equivalents Hg was run at a higher stirring speed to ensure adequate contact of the catalyst with Hg. The corresponding standard 2.5 mol% experiment was therefore also run at this stirring speed which accounts for the difference between this 2.5 mol% trace and that presented in Figure 23.
54. Tang, C. Y.; Thompson, A. L.; Aldridge, S. *J. Am. Chem. Soc.* **2010**, *132,* 10578-10591.

5. EXPERIMENTAL

5.1 SYNTHESIS

All manipulations were carried out using standard Schlenk and high-vacuum techniques, or under argon in a moisture-free MBraun LABmaster glovebox. Glassware was oven dried at 413 K overnight and subsequently flame dried under vacuum. Solvents were purified either using an MBraun SPS solvent system (CH_2Cl_2, Et_2O, hexane, toluene), Innovative Technologies PS-400-7 solvent system (methanol, THF) or under a nitrogen atmosphere from sodium benzophenone ketyl (C_6H_6) or Mg/I_2 (ethanol). Deuterated solvents (Aldrich) were vacuum transferred from potassium (C_6D_6, [D_8]-toluene, [D_8]-THF) or calcium hydride (CD_2Cl_2, $CDCl_3$). The following were acquired from commercial sources and used as received: CO, D_2, H_2, N_2 and O_2 (BOC, 99.9%); $Ph^{13}CH_2OH$ (Cambridge Isotope Laboratories, 99%); $^{15}N_2$ (Aldrich, 98%); xantphos (Acros Organics, 98%), DPEphos (Aldrich, 98%) and dppf (Alfa Aesar, 97%). $RuCl_3.3H_2O$ was kindly donated from Johnson-Matthey.

5.2 ANALYSIS METHODS

NMR spectra were recorded on Bruker Avance 300, 400 and 500 MHz NMR spectrometers, at 298 K unless otherwise stated, and referenced as follows: benzene (^{1}H, δ 7.15; ^{13}C{^{1}H}, δ 128.0), toluene (^{1}H, δ 2.09, ^{13}C{^{1}H}, δ 21.3), dichloromethane (^{1}H, δ 5.31, ^{13}C{^{1}H}, δ 54.0), THF (^{1}H, δ 1.73, ^{13}C{^{1}H}, δ 25.4). ^{31}P{^{1}H} NMR, ^{19}F NMR, and ^{11}B{^{1}H} NMR chemical shifts were referenced externally to 85% H_3PO_4 (δ 0.0), $CFCl_3$ (δ 0.0), and $BF_3{\cdot}OEt_2$ (δ 0.0) respectively. ^{1}H COSY, ^{1}H-X{^{1}H} (X = ^{13}C, ^{31}P) HMQC and HMBC experiments were performed using standard Bruker pulse sequences. ^{1}H and ^{13}C resonances arising from the xantphos and DPEphos ligands are not reported, although all signals have been accounted for and integrate correctly. IR spectra were recorded on a Nicolet Nexus FTIR spectrometer in solution, or as nujol mulls or KBr discs. Mass spectrometry was performed in the Department of Chemistry, University of Bath on a micrOTOF electrospray time-of-flight (ESI-TOF) mass spectrometer (Bruker Daltonik GmbH), coupled to an Agilent 1200 LC system (Agilent Technologies). Elemental analyses were performed by Elemental Microanalysis Ltd, Okehampton, Devon, and the Elemental Analysis Service, London Metropolitan University, London. X-ray crystal structures were recorded at 150 K on a Nonius Kappa CCD diffractometer or at 100 K on an Oxford Diffraction Gemini diffractometer, with structural solutions and refinement performed using SHELXS-97[1] and represented as POVray structures.

5.3 CHAPTER 1

$[Ru(PPh_3)_3(CO)H_2]$[2] (**1**), $[Ru(dppp)(PPh_3)(CO)H_2]$[3] (**3**) and $[Ru(PPh_3)_2(CO)_3]$[4] were prepared according to literature procedures.

5.3.1 Synthesis of $[Ru(xantphos)(PPh_3)(CO)H_2]$ (2)

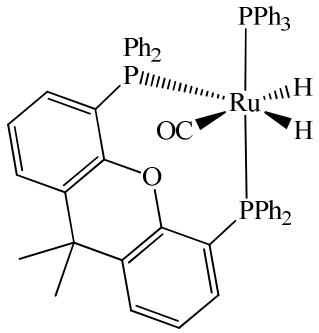

To a solution of **1** (0.25 g, 0.27 mmol) in toluene (10 mL) was added xantphos (0.19 g, 0.33 mmol) and the mixture refluxed for 3 h. Removal of the solvent gave a red oily residue, which was washed with ethanol (2 x 10 mL) and hexane (1 x 10 mL). The resulting solid was recrystallised from C_6H_6/hexane to give **2** as an orange solid (0.121 g, 46% yield). Selected ^1H NMR ([D_8]-toluene, 500 MHz, 298 K): δ -6.67 (dddd, $^2J_{HP}$ = 35.0 Hz, $^2J_{HP}$ = 28.0 Hz, $^2J_{HP}$ = 15.5 Hz, $^2J_{HH}$ = 6.6 Hz, 1H, Ru*H*), -8.72 (dddd, $^2J_{HP}$ = 77.0 Hz, $^2J_{HP}$ = 33.9 Hz, $^2J_{HP}$ = 27.3 Hz, $^2J_{HH}$ = 6.6 Hz, 1H, Ru*H*); $^{31}P\{^1H\}$ NMR ([D_8]-toluene, 202 MHz, 203 K): δ 30.5 (br m, P_{transH}), 45.2 (dd, $^2J_{PP}$ = 237.2, $^2J_{PP}$ = 15.3 Hz, P_{transP}), 58.5 (dd, $^2J_{PP}$ = 237.2 Hz, $^2J_{PP}$ = 15.5 Hz, P_{transP}). Selected $^{13}C\{^1H\}$ NMR ([D_8]-toluene, 125 MHz, 298 K): δ 205.7 (m, *C*O); IR (KBr, cm^{-1}): ν(CO) = 1946 (s); Elemental analysis calcd (%) for $C_{58}H_{49}O_2P_3Ru$ (971.96): C 71.66, H 5.08; found: C 71.14, H 5.29; ESI-TOF MS: $[M + H - H_2]^+$ *m*/*z* = 971.1917 (theoretical 971.1921).

5.3.2 Synthesis of [Ru(xantphos)(CO)$_2$H$_2$] (4)

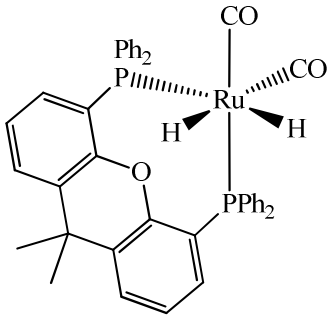

A THF (10 mL) solution of [Ru(xantphos)(CO)$_3$] (**6**) (0.05 g, 0.065 mmol) was photolysed (300 W Xe arc) at *ca*. 273 K under a steady flow of H_2 for 0.5 h. In this time, the orange solution turned a pale straw colour. The solvent was removed under vacuum to leave a pale yellow residue, which was washed with ethanol (10 mL) and hexane (2 x 10 mL). The resulting solid was recrystallised from THF/ethanol to give **4** as small, pale yellow crystals (0.037 g, 76% yield). Selected ^{1}H NMR ([D$_8$]-Toluene, 500 MHz, 298 K): δ = -6.13 (ddd, $^2J_{HP}$ = 26.8 Hz, $^2J_{HP}$ = 17.6 Hz, $^2J_{HH}$ = 6.5 Hz, 1H, Ru*H*), -7.65 (ddd, $^2J_{HP}$ = 83.1 Hz, $^2J_{HP}$ = 30.5 Hz, $^2J_{HH}$ = 6.5 Hz, 1H, Ru*H*); ^{31}P{^{1}H} NMR ([D$_8$]-Toluene, 202 MHz, 298 K): δ = 24.6 (d, $^2J_{PP}$ = 21.5 Hz), 35.1 (d, $^2J_{PP}$ = 21.5 Hz); Selected ^{13}C{^{1}H} NMR ([D$_8$]-Toluene, 125 MHz, 298 K): δ = 203.3 (dd, $^2J_{CP}$ = 81.9 Hz, $^2J_{CP}$ = 7.1 Hz; *C*O), 201.5 (dd, $^2J_{CP}$ = 11.2 Hz, $^2J_{CP}$ = 8.5 Hz; *C*O); IR (nujol, cm^{-1}): ν(CO) = 2007 (s), 1960 (s); Elemental analysis calcd (%) for $C_{41}H_{34}O_3P_2Ru$ (737.71): C 66.75, H 4.65; found: C 66.66, H 4.63.

5.3.3 Synthesis of [Ru(xantphos)(PPh$_3$)(CO)$_2$] (5)

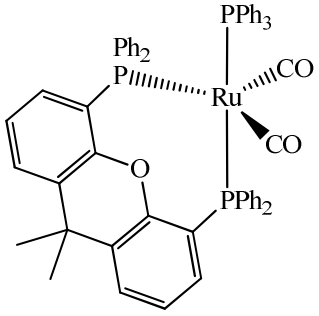

[Ru(PPh$_3$)$_2$(CO)$_3$] (0.075 g, 0.105 mmol) and xantphos (0.073 g, 0.126 mmol) were refluxed together at 393 K in toluene (10 mL) for 3 h to result in an orange solution. The solvent was removed under vacuum to leave an orange residue, which was washed with hexane (3 x 10

mL). The resulting solid was recrystallised from THF/pentane to afford a microcrystalline solid (0.027 g, 26% yield). $^{31}P\{^{1}H\}$ ([D_8]-Toluene, 162 MHz, 298 K): δ = 34.4 (d, $^{2}J_{PP}$ = 84.3 Hz), 54.8 (t, $^{2}J_{PP}$ = 84.3 Hz); IR (nujol, cm^{-1}): ν(CO) = 2003 (s), 1909 (s); ESI-TOF MS: $[M + H - CO]^{+}$ *m/z* = 971.1990 (theoretical 971.1990).

5.3.4 Synthesis of [Ru(xantphos)$(CO)_3$] (6)

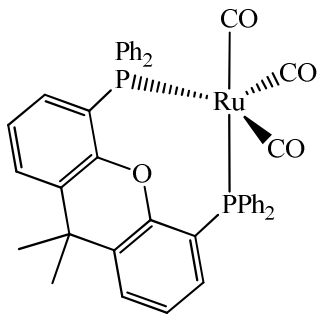

[$Ru_3(CO)_{12}$] (0.1 g, 0.16 mmol) and xantphos (0.27 g, 0.47 mmol) were dissolved in toluene (20 mL) and the solution transferred to a 100 mL stainless steel autoclave. The sample was placed under 25 atm. CO and heated at 373 K for 72 h. The solution was then cooled to room temperature, the pressure released and the yellow solution transferred to a Schlenk tube. Removal of the solvent afforded an orange oil, which was crystallized from C_6H_6/hexane to give **6** as crystalline yellow blocks (0.25 g, 70% yield). $^{31}P\{^{1}H\}$ NMR ([D_8]-Toluene, 162 MHz, 298 K): δ = 27.9 (s); Selected $^{13}C\{^{1}H\}$ NMR ([D_8]-Toluene, 100 MHz, 298 K): δ = 215.4 (t, $^{2}J_{CP}$ = 3.6 Hz, *C*O); IR (nujol, cm^{-1}): ν(CO) = 2007 (s), 1921 (s), 1920 (s); Elemental analysis calcd (%) for $C_{42}H_{32}O_4P_2Ru$ (763.70): C 66.05, H 4.22; found: C 66.11, H 4.28.

5.3.5 Representative catalytic procedure: 4,4-dimethyl-3-oxo-2-benzylpentanenitrile

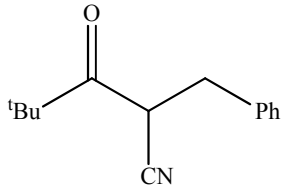

To a solution of benzyl alcohol (310 μL, 3 mmol) and 4,4-dimethyl-3-oxopentanenitrile (0.376 g, 3 mmol) in toluene (3.0 mL) in a carousel reaction tube, was added [$Ru(PPh_3)_3(CO)H_2$] (**1**) (0.014 g, 0.015 mmol), xantphos (0.009 g, 0.015 mmol) and piperidinium acetate (0.022 g, 0.15

mmol). The reaction mixture was heated to 383 K in a pre-heated carousel reaction station and stirred for 3 h. After cooling, the solvent was removed under vacuum and the crude product was purified by column chromatography on silica using 19:1 petroleum ether (bp. 313-333 K)-ether as the eluent, giving the title compound as a colourless oil (0.509 g, 79% yield). ^{1}H NMR ($CDCl_3$, 300 MHZ, 298 K): δ 0.99 (s, 9H, C(C*H*$_3$)$_3$), 3.03 (dd, $^{2}J_{HH}$ = 13.6 Hz, $^{3}J_{HH}$ = 7.6 Hz, 1H, C*H*H), 3.11 (dd, $^{2}J_{HH}$ = 13.6 Hz, $^{3}J_{HH}$ = 7.6 Hz, 1H, CH*H*), 3.96 (app. t, $^{3}J_{HH}$ = 7.6 Hz, 1H, C*H*), 7.09-7.25 (m, 5H, Ar-*H*); ^{13}C{^{1}H} NMR ($CDCl_3$, 75.5 MHz, 298 K): δ 205.2 (CO), 136.4 (Ar), 129.3 (Ar), 129.1 (Ar), 127.8 (Ar), 117.3 (*C*N), 45.7 (*C*(CH$_3$)$_3$), 38.9 (*C*H), 36.2 (*C*H$_2$), 25.8 (C(*C*H$_3$)$_3$); IR (nujol, cm^{-1}): ν(CN) = 2242 (s), ν(CO) = 1716 (s); Elemental analysis calcd (%) for $C_{14}H_{17}NO$ (215.30): C 78.10, H 7.41, N 6.06; found: C 78.01, H 7.95, N 6.48; ESI-TOF MS: [M + NH$_4$]$^{+}$ *m/z* = 233.1649 (theoretical 233.1648).[5]

5.4 CHAPTER 2

Literature routes were used to prepare [Ru(dppp)(ICy)(CO)H$_2$][6] (**15**), [Ru(PPh$_3$)$_3$(CO)HF][7] (**16**), [Ru(dppf)(PPh$_3$)(CO)H$_2$][8] (**20**), IEt$_2$Me$_2$,[9] I^{i}Pr$_2$Me$_2$,[9] IMes,[10] and ICy.[11]

5.4.1 Synthesis of [Ru(xantphos)(IEt$_2$Me$_2$)'(CO)H] (8)

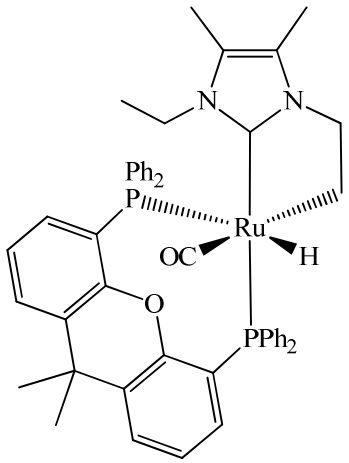

[Ru(xantphos)(PPh$_3$)(CO)H$_2$] (**2**) (0.097 g, 0.1 mmol) and IEt$_2$Me$_2$ (0.047 g, 0.31 mmol) were charged to an ampoule fitted with a J. Young's PTFE tap, dissolved in dry toluene (10 mL), and then heated at reflux for 3 h. Removal of the solvent gave an orange oily residue, which was washed with hexane (3 x 10 mL). The resulting solid was recrystallised from C_6H_6/hexane to give a cream solid (0.064 g, 75% yield). Selected ^{1}H NMR ([D$_8$]-toluene, 500 MHz, 298 K): δ = -7.63

(dd, $^2J_{HP}$ = 114.1 Hz, $^2J_{HP}$ = 23.0 Hz, 1H, Ru*H*), 0.17 (m, 1H, RuC*H*H), 0.73 (m, 1H, RuCH*H*), 1.11 (t, $^3J_{HH}$ = 7.1 Hz, 3H, NCH_2CH_3), 1.59 (s, 6H, $NCCH_3$), 2.53 (m, 1H, $RuCHHCH_3$), 3.42-3.56 (m, 2H, $RuCH_2CH_2$), 3.77 (m, 1H, $RuCHHCH_3$); $^{31}P\{^1H\}$ NMR ([D_8]-toluene, 202 MHz, 298 K): δ = 29.1 (d, $^2J_{PP}$ = 17.5 Hz, P_{transH}), 47.6 (d, $^2J_{PP}$ = 17.5 Hz, P_{transC}); Selected $^{13}C\{^1H\}$ NMR ([D_8]-toluene, 125 MHz, 298 K): δ = 207.9 (dd, $^2J_{CP}$ = 10.5 Hz, $^2J_{CP}$ = 5.9 Hz, *C*O), 189.7 (dd, $^2J_{CP}$ = 85.7 Hz, $^2J_{CP}$ = 9.0 Hz, N*C*N), 123.1 (m, $NCCH_3$), 53.9 (s, NCH_2CH_2), 43.1 (s, NCH_2CH_3), 17.1 (s, NCH_2CH_3), 13.2 (s, $RuCH_2$), 9.8 (s, $NCCH_3$); IR (nujol, cm^{-1}): ν(CO) = 1863 (s); Elemental analysis calcd (%) for $C_{49}H_{48}N_2O_2P_2Ru$ (859.95): C 68.44, H 5.63, N 3.26; found: C 68.54, H 5.72, N 3.37.

5.4.2 Synthesis of [Ru(xantphos)($I^iPr_2Me_2$)'(CO)H] (9)

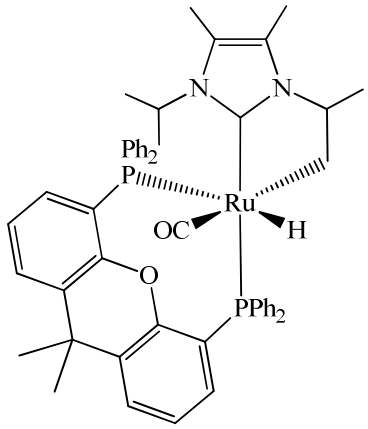

[Ru(xantphos)(PPh_3)($CO)H_2$] (**2**) (0.097 g, 0.1 mmol) and $I^iPr_2Me_2$ (0.054 g, 0.31 mmol) were charged to an ampoule fitted with a J. Young's PTFE tap, dissolved in dry toluene (10 mL), and then heated at reflux for 1.5 h. The product appeared as a white precipitate. The remaining solution was removed, and the white solid was washed with hexane (3 x 10 mL). Cooling a solution of hot toluene afforded light purple crystals (0.055 g, 64% yield). The insolubility of this complex in common solvents prevented complete NMR characterisation. Selected ^1H NMR ([D_8]-toluene, 500MHz, 298 K): δ = -7.96 (dd, $^2J_{HP}$ = 115.1 Hz, $^2J_{HP}$ = 23.8 Hz, 1H, Ru*H*); $^{31}P\{^1H\}$ NMR ([D_8]-toluene, 202 MHz, 298 K): δ = 28.4 (m, P_{transH}), 46.7 (m, P_{transC}); Selected $^{13}C\{^1H\}$ NMR ([D_8]-toluene, 125 MHz, 298 K): δ = 208.1 (m, *C*O), 189.7 (m, N*C*N); IR (nujol, cm^{-1}): ν(CO) = 1878 (s); Elemental analysis calcd (%) for $C_{51}H_{52}N_2O_2P_2Ru$ (887.99): C 68.98, H 5.90, N 3.15; found: C 68.58, H 6.11, N 3.46.

5.4.3 Synthesis of [Ru(xantphos)(IMes)'(CO)H] (10)

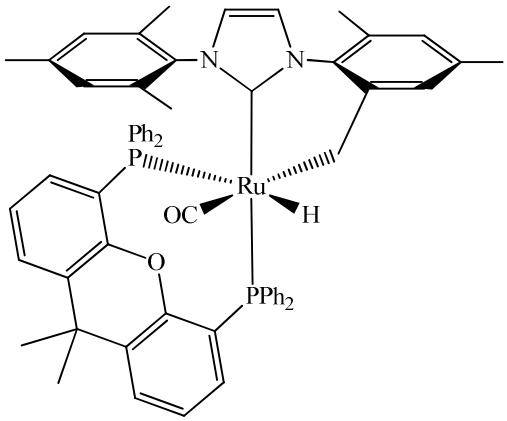

[Ru(xantphos)(PPh_3)$(CO)H_2$] (**2**) (0.097 g, 0.1 mmol) and IMes (0.091 g, 0.31 mmol) were charged to an ampoule fitted with a J. Young's PTFE tap, dissolved in dry toluene (10 mL), and then heated at reflux for 3 h. The product appeared as a white precipitate. The unreacted solution was then removed to another ampoule and refluxed for another 3 h to form further product. The white solid was washed with hexane (3 x 10 mL) and then dissolved in refluxing THF. White microcrystals formed on cooling (0.062 g, 62% yield). Selected NMR data for **isomer a**: ^{1}H NMR ($CDCl_3$, 500 MHz, 298 K): δ = -8.72 (dd, $^{2}J_{HP}$ = 114.7 Hz, $^{2}J_{HP}$ = 27.6 Hz, 1H, Ru*H*), -0.05 (dd, $^{1}J_{HH}$ = 17.5 Hz, $^{2}J_{HH}$ = 11.0 Hz, RuC*H*H), 1.67 (s, 3H, Ar-CH_3), 1.88 (s, 3H, Ar-CH_3), 2.22 (s, 3H, Ar-CH_3), 2.26 (s, 3H, Ar-CH_3), 2.29 (m, 1H, RuCH*H*), 2.32 (s, 3H, Ar-CH_3), 4.95 (s, 1H, NC*H*), 6.06 (s, 1H, NC*H*); ^{31}P{^{1}H} NMR ($CDCl_3$, 202 MHz, 298 K): δ = 16.4 (d, $^{2}J_{PP}$ = 18.2 Hz, P_{transH}), 42.8 (d, $^{2}J_{PP}$ = 18.2 Hz, P_{transC}); ^{13}C{^{1}H} NMR ($CDCl_3$, 125 MHz, 298 K): δ = 205.4 (t, $^{2}J_{CP}$ = 8.0 Hz, *C*O), 195.8 (dd, $^{2}J_{CP}$ = 87.3 Hz, $^{2}J_{CP}$ = 7.6 Hz, N*C*N), 125.6 (s, N*C*H), 123.9 (s, N*C*H), 21.6 (s, Ar-*C*H_3), 21.4 (s, Ar-*C*H_3), 20.4 (s, Ar-*C*H_3), 19.2 (s, Ar-*C*H_3), 18.8 (s, Ar-*C*H_3), 10.9 (s, Ru*C*H_2); Selected NMR data for **isomer b**: ^{1}H NMR ($CDCl_3$, 500 MHz, 298 K): δ = -9.51 (dd, $^{2}J_{HP}$ = 112.6 Hz, $^{2}J_{HP}$ = 26.6 Hz, 1H, Ru*H*); ^{31}P{^{1}H} NMR ($CDCl_3$, 202 MHz, 298 K): δ = 15.9 (d, $^{2}J_{PP}$ = 20.1 Hz), 40.8 (d, $^{2}J_{PP}$ = 20.1 Hz); IR (nujol, cm^{-1}): ν(CO) = 1888 (s); Elemental analysis calcd (%) for $C_{61}H_{56}N_2O_2P_2Ru.C_4H_8O$ (1084.23): C 72.00 H 5.95 N 2.58; found: C 71.68 H 5.84 N 2.53.

5.4.4 Synthesis of [Ru(xantphos)(IEt_2Me_2)(CO)H_2] (11)

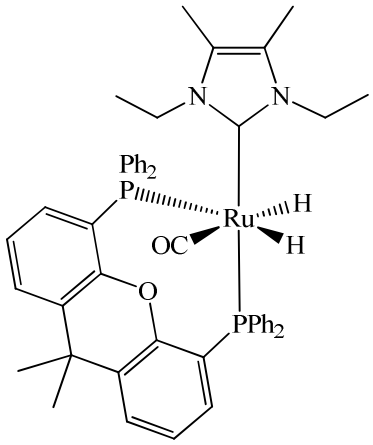

]Ru(xantphos)(PPh_3)(CO)H_2] (**2**) (0.097 g, 0.1 mmol) and IEt_2Me_2 (0.047 g, 0.31 mmol) were charged to an ampoule fitted with a J. Young's PTFE tap, dissolved in dry toluene (10 mL), and then heated at reflux for 3 h. The solution was then cooled, an atmosphere of H_2 added, and re-heated at 343 K for 2.5 h. Removal of the solvent gave an orange, oily residue which was washed with hexane (3 x 10 mL). The resulting solid was dissolved in C_6H_6, left under H_2 overnight, and then layered with hexane, still under an H_2 atmosphere, to give **11** as a white solid (0.045g, 52% yield). Selected ^{1}H NMR (C_6D_6, 500 MHz, 298 K): δ = -7.62 (ddd, $^2J_{HP}$ = 93.9 Hz, $^2J_{HP}$ = 26.0 Hz, $^2J_{HH}$ = 5.3 Hz, 1H, Ru*H*), -5.54 (broad, 1H, Ru*H*), 1.07 (broad, 3H, NCH_2CH_3), 1.27 (t, $^3J_{HH}$ = 6.8 Hz, 3H, NCH_2CH_3), 1.40 (s, 3H, NCH_3), 1.55 (s, 3H, NCH_3), 4.14 (broad, 2H, NCH_2CH_3), 4.55 (broad, 2H, NCH_2CH_3); $^{31}P\{^1H\}$ NMR ([D_8]-toluene, 162 MHz, 233 K): δ = 35.0 (d, $^2J_{PP}$ = 16.3 Hz, P_{transH}), 51.1 (d, $^2J_{pp}$ = 16.3 Hz, P_{transC}); Selected $^{13}C\{^1H\}$ NMR (C_6D_6, 125 MHz, 298 K): δ = 207.5 (t, $^2J_{CP}$ = 12.9 Hz, *C*O), 187.9 (dd, $^2J_{CP}$ = 80.4 Hz, $^2J_{CP}$ = 8.4 Hz, N*C*N), 124.2 (s, $NCCH_3$), 123.7 (s, $NCCH_3$), 45.0 (s, NCH_2CH_3), 44.3 (s, NCH_2CH_3), 16.4 (s, NCH_2CH_3), 15.4 (s, NCH_2CH_3), 10.2 (broad, $NCCH_3$), 9.9 (broad, $NCCH_3$); IR (nujol, cm^{-1}): ν(CO) = 1901 (s); Elemental analysis calcd (%) for $C_{49}H_{50}N_2O_2P_2Ru.0.5C_6H_6$ (901.01): C 69.32, H 5.93, N 3.11; found: C 69.15, H 6.14, N 3.18.

5.4.5 Synthesis of [Ru(xantphos)(ICy)(CO)H_2] (12)

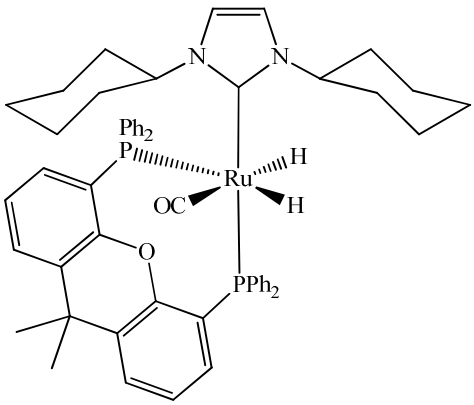

[Ru(xantphos)(PPh_3)(CO)H_2] (**2**) (0.075 g, 0.08 mmol) and ICy (0.050 g, 0.23 mmol) were refluxed together in dry toluene for 1.5 h. After removal of the solvent, the product was washed in hexane (2 x 10 mL) and recrystallised from C_6H_6/hexane to give small, clear crystals of **12** suitable for X-ray analysis (0.039 g, 54% yield). Selected ^{1}H NMR ([D_8]-toluene, 500 MHz, 298 K): δ = -7.85 (ddd, $^2J_{HP}$ = 93.0 Hz, $^2J_{HP}$ = 26.9 Hz, $^2J_{HH}$ = 6.9 Hz, 1H, Ru*H*), -5.69 (ddd, $^2J_{HP}$ = 35.1 Hz, $^2J_{HP}$ = 14.3 Hz, $^2J_{HH}$ = 6.9 Hz, 1H, Ru*H*), 0.44 - 1.33 (m, 12H, Cy-CH_2), 1.42 – 1.54 (m, 4H, Cy-CH_2), 1.63 – 1.78 (m, 2H, Cy-CH_2), 2.28 (m, 1H, Cy-C*H*H), 2.66 (m, 1H, Cy-CH*H*), 4.84 (m, 1H, NC*H*(CH_2)$_2$), 5.72 (m, 1H, NC*H*(CH_2)$_2$), 6.35 (s, 1H, NC*H*), 6.60 (s, 1H, NC*H*); ^{31}P{^{1}H} NMR ([D_8]-toluene, 162 MHz, 253 K): δ = 34.4 (d, $^2J_{PP}$ = 15.0 Hz, P_{transH}), 51.3 (d, $^2J_{pp}$ = 15.0 Hz, P_{transC}); Selected ^{13}C{^{1}H} NMR (C_6D_6, 125 MHz, 298 K): δ = 206.9 (t, $^2J_{CP}$ = 9.4 Hz, *C*O), 190.7 (dd, $^2J_{CP}$ = 80.2 Hz, $^2J_{CP}$ = 8.1 Hz, N*C*N), 117.0 (s, N*C*H), 60.3 (s, N*C*H(CH_2)$_2$), 60.1 (s, N*C*H(CH_2)$_2$), 37.2 (s, Cy-*C*H_2), 35.7 (s, Cy-*C*H_2), 34.9 (s, Cy-*C*H_2), 34.8 (s, Cy-*C*H_2), 32.9 (s, Cy-*C*H_2), 27.7 (s, Cy-*C*H_2), 27.2 (s, Cy-*C*H_2), 27.1 (s, Cy-*C*H_2), 27.0 (s, Cy-*C*H_2), 26.7 (s, Cy-*C*H_2); IR (nujol, cm^{-1}): ν(CO) = 1913 (s); Elemental analysis calcd (%) for $C_{55}H_{58}N_2O_2P_2Ru$ (942.10): C 70.12, H 6.21, N 2.97; found: C 70.47, H 6.21, N 3.18.

5.4.6 Synthesis of [Ru(xantphos)(ICy)'(CO)H] (13)

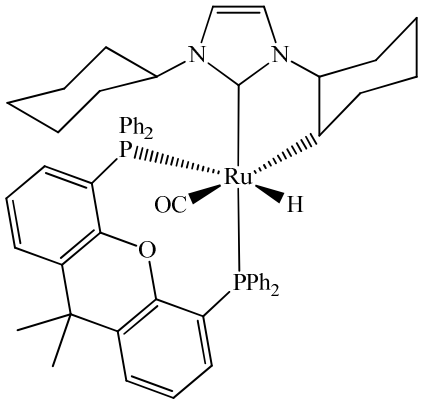

Trimethylvinylsilane, $H_2C{=}CHSiMe_3$, (109 μL, 0.79 mmol) was added to a solution of [Ru(xantphos)(ICy)(CO)H_2] (**12**) (0.075 g, 0.08 mmol) in dry toluene (10 mL), and the reaction mixture refluxed together for 2 h. After removal of the solvent, the product was redissolved in C_6H_6 and layered with hexane to recrystallise. Small needle-like crystals resulted, and were submitted for X-ray crystal analysis (0.037 g, 51% yield). Selected ^{1}H NMR (C_6D_6, 500 MHz, 298 K): δ = -7.65 (dd, $^2J_{HP}$ = 103.0 Hz, $^2J_{HP}$ = 21.2 Hz, 1H, Ru*H*), -0.44 (m, 1H, RuC*H*), 0.84 – 0.92 (m, 2H, Cy-C*H*$_2$), 1.03 – 1.41 (m, 8H, Cy-C*H*$_2$), 1.51 – 1.65 (m, 6H, Cy-C*H*$_2$), 1.68 – 1.87 (m, 2H, Cy-C*H*$_2$), 3.43 (m, 1H, NC*H*(CH)(CH$_2$)), 4.95 (m, 1H, NC*H*(CH$_2$)$_2$), 6.66 (s, 2H, NC*H*); ^{31}P{^{1}H} NMR (C_6D_6, 162 MHz, 298 K): δ = 24.9 (d, $^2J_{PP}$ = 15.0 Hz, P_{transH}), 49.6 (d, $^2J_{PP}$ = 15.0 Hz, P_{transC}); Selected ^{13}C{^{1}H} NMR (C_6D_6, 125 MHz, 298 K): δ = 207.2 (dd, $^2J_{CP}$ = 9.6 Hz, $^2J_{CP}$ = 7.4 Hz, *C*O), 193.5 (dd, $^2J_{CP}$ = 82.3 Hz, $^2J_{CP}$ = 8.3 Hz, N*C*N), 116.5 (s, N*C*H), 64.2 (s, N*C*H(CH)(CH$_2$)), 58.4 (s, N*C*H(CH$_2$)$_2$), 44.5 (t, $^2J_{CP}$ = 7.8 Hz, Ru*C*H), 39.9 (s, Cy-*C*H$_2$), 33.8 (s, Cy-*C*H$_2$), 33.7 (s, Cy-*C*H$_2$), 31.7 (s, Cy-*C*H$_2$), 30.3 (s, Cy-*C*H$_2$), 30.0 (s, Cy-*C*H$_2$), 25.7 (s, Cy-*C*H$_2$), 25.4 (s, Cy-*C*H$_2$), 22.4 (s, Cy-*C*H$_2$); IR (nujol, cm^{-1}): ν(CO) = 1872 (s); Elemental analysis calcd (%) for $C_{55}H_{56}N_2O_2P_2Ru$ (940.08): C 70.27, H 6.00, N 2.98; found: C 70.13, H 6.22, N 2.72.

5.4.7 Synthesis of [Ru(DPEphos)(PPh_3)(CO)H_2] (14)

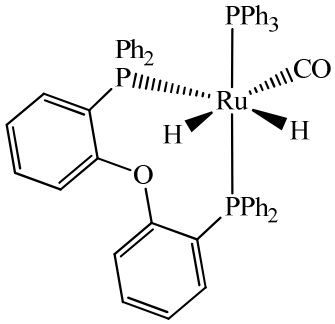

[Ru(DPEphos)(PPh_3)HCl] (**24b**) (0.150 g, 0.16 mmol) and $NaBH_4$ (0.018 g, 0.48 mmol) were dissolved in dry ethanol and heated for 6 h at 343 K. The reaction mixture was reduced to dryness *in vacuo*, and the product extracted in C_6H_6. After removal of the solvent, the product was dissolved in CH_2Cl_2 and layered with hexane to afford colourless crystals of **14** suitable for X-ray crystal analysis (0.072 g, 49% yield). Selected ^{1}H NMR ([D_8]-toluene, 500 MHz, 298 K): δ = -8.33 (dtd, $^2J_{HP}$ = 77.5 Hz, $^2J_{HP}$ = 30.9 Hz, $^2J_{HH}$ = 6.0 Hz, 1H, Ru*H*), - 6.44 (tdd, $^2J_{HP}$ = 24.8 Hz, $^2J_{HP}$ = 24.1 Hz, $^2J_{HH}$ = 6.0 Hz, 1H, Ru*H*); ^{31}P{^{1}H} NMR ([D_8]-toluene, 202 MHz, 333 K): δ = 59.8 (dd, $^2J_{PP}$ = 239.8 Hz, $^2J_{PP}$ = 15.5 Hz, P_{transP}), 49.4 (dd, $^2J_{PP}$ = 239.8 Hz, $^2J_{PP}$ = 18.5 Hz, P_{transP}), 38.7 (dd, $^2J_{PP}$ = 18.5 Hz, $^2J_{PP}$ = 15.5 Hz, P_{transH}); Selected ^{13}C{^{1}H} NMR ([D_8]-toluene, 125 MHz, 298 K): δ = 205.9 (m, *C*O); IR (nujol, cm^{-1}): ν(CO) = 1938 (s); ESI-TOF MS: $[M + H - H_2]^+$ *m/z* = 931.1607 (theoretical 931.1607).

5.4.8 Synthesis of [Ru(xantphos)(PPh_3)(CO)HF] (17)

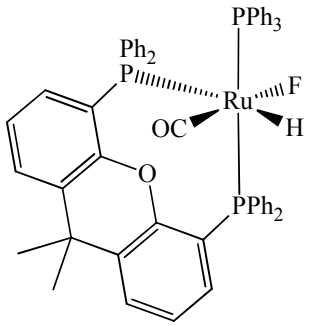

[Ru(PPh_3)$_3$(CO)HF] (**16**) (0.325 g, 0.35 mmol) and xantphos (0.256 g, 0.44 mmol) were dissolved in C_6H_6 (10 mL) and refluxed at 343 K for 16 h to give a brown solution. The solvent was removed under vacuum and the resulting white solid washed with hexane (2 x 30 mL) to leave the product as a white solid. The complex was recrystallised from THF/hexane. (0.074 g, 22%

yield). Selected NMR data: ^{1}H NMR ([D$_8$]-toluene, 400 MHz, 298 K): δ -5.57 (dtd, $^{2}J_{HP}$ = 117.9 Hz, $^{2}J_{HP}$ = 27.4 Hz, $^{2}J_{HF}$ = 2.9 Hz, 1H, Ru*H*); ^{31}P{^{1}H} NMR ([D$_8$]-toluene, 162 MHz, 298 K): δ 33.9 (br s); ^{13}C{^{1}H} NMR ([D$_8$]-toluene, 100 MHz, 298 K): δ 205.5 (m, *C*O); ^{19}F NMR ([D$_8$]-toluene, 376 MHz, 388 K): δ - 382.2 (br s); ^{19}F NMR ([D$_8$]-toluene, 376 MHz, 194 K) (both isomers): δ -365.9 (s), -395.1 (s); Selected low temperature NMR data for **isomer a**: ^{1}H NMR ([D$_8$]-toluene, 400 MHz, 194 K): δ -5.22 (ddd, $^{2}J_{HP}$ = 95.5 Hz, $^{2}J_{HP}$ = 28.4 Hz, $^{2}J_{HP}$ = 21.7 Hz, 1H, Ru*H*); ^{31}P{^{1}H} NMR ([D$_8$]-toluene, 162 MHz, 194 K): δ 33.4 (dt, $^{2}J_{PP}$ = 309.3 Hz, $^{2}J_{PP}$ = 13.6 Hz, $^{2}J_{PF}$ = 13.6 Hz), 26.3 (ddd, $^{2}J_{PP}$ = 309.3 Hz, $^{2}J_{PP}$ = 19.2 Hz, $^{2}J_{PF}$ = 14.8 Hz), 5.4 (dt, $^{2}J_{PF}$ = 29.7 Hz, $^{2}J_{PP}$ = 14.8 Hz, $^{2}J_{PP}$ = 13.6 Hz); Selected low temperature NMR data for **isomer b**: ^{1}H NMR ([D$_8$]-toluene, 400 MHz, 194 K): δ -4.92 (ddd, $^{2}J_{HP}$ = 91.7 Hz, $^{2}J_{HP}$ = 27.4 Hz, $^{2}J_{HP}$ = 21.7 Hz, 1H, Ru*H*); ^{31}P{^{1}H} NMR ([D$_8$]-toluene, 162 MHz, 194 K): δ 47.0 (ddd, $^{2}J_{PP}$ = 310.5 Hz, $^{2}J_{PF}$ = 33.3 Hz, $^{2}J_{PP}$ = 11.6 Hz), 31.9 (dt, $^{2}J_{PP}$ = 310.5 Hz, $^{2}J_{PP}$ = 18.2 Hz, $^{2}J_{PF}$ = 18.2 Hz), 29.9 (ddd, $^{2}J_{PF}$ = 41.5 Hz, $^{2}J_{PP}$ = 18.2 Hz, $^{2}J_{PP}$ = 11.6 Hz); IR (nujol, cm^{-1}): ν(CO) = 1899 (s); Elemental analysis calcd (%) for $C_{58}H_{48}FP_3O_2Ru.C_4H_8O$ (1062.12): C 70.10, H 5.33; found: C 69.80, H 5.28.

5.4.9 Synthesis of [Ru(xantphos)(ICy)(CO)HF] (18)

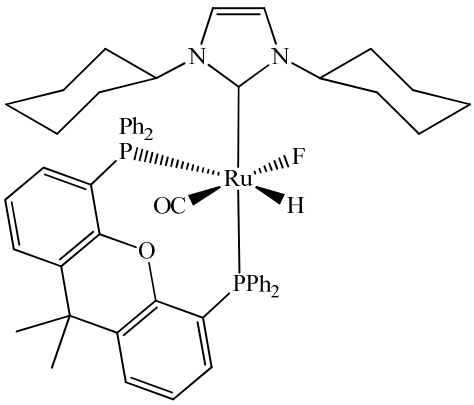

A C_6D_6 solution of [Ru(xantphos)(ICy)(CO)H$_2$] (**12**) (0.009 g, 0.01 mmol) was prepared in an NMR tube fitted with a resealable J. Young's PTFE valve and Et$_3$N·3HF (3.6 μL, 0.022 mmol) added via syringe. Excess CsF (0.050 g, 0.33 mmol) was added, and the tube left to stand for 2 h at room temperature. Attempts to synthesise **18** on a preparative scale for elemental analysis proved unsuccessful as the product continually oiled out on attempted recrystallisation. Selected NMR data for **isomer a**: ^{1} H NMR ([D$_8$]-toluene, 400 MHz, 217 K): δ -5.50 (dd, $^{2}J_{HP}$ = 136.7 Hz, $^{2}J_{HP}$ = 22.0 Hz, 1H, Ru*H*); ^{31}P{^{1}H} NMR ([D$_8$]-toluene, 162 MHz, 217 K): δ 29.7 (dd, $^{2}J_{PF}$ = 28.6 Hz, $^{2}J_{PP}$ = 13.1 Hz), 4.8 (dd, $^{2}J_{PF}$ = 30.5 Hz, $^{2}J_{PP}$ = 13.1 Hz); ^{19}F NMR ([D$_8$]-toluene, 376 MHz, 217 K): δ -366.0 (br s); Selected NMR data for **isomer b**: ^{1}H NMR ([D$_8$]-toluene, 400 MHz, 217 K): δ -

7.38 (dd, $^{2}J_{HP}$ = 137.3 Hz, $^{2}J_{HP}$ = 25.9 Hz, 1H, Ru*H*); $^{31}P\{^{1}H\}$ NMR ([D_8]-toluene, 162 MHz, 217 K): δ 37.7 (dd, $^{2}J_{PF}$ = 29.5 Hz, $^{2}J_{PP}$ = 17.0 Hz), 16.1 (dd, $^{2}J_{PF}$ = 71.1 Hz, $^{2}J_{PP}$ = 17.0 Hz); ^{19}F NMR ([D_8]-toluene, 376 MHz, 217 K): δ -336.4 (br s); IR (nujol, cm^{-1}): ν(CO/RuH) = 1908 (s), 1897 (s) and 1875 (s); ESI-TOF MS: $[M-H]^{+}$ *m/z* = 959.2867 (theoretical 959.2854).

5.4.10 Synthesis of [Ru(xantphos)(IEt_2Me_2)(CO)HF] (19)

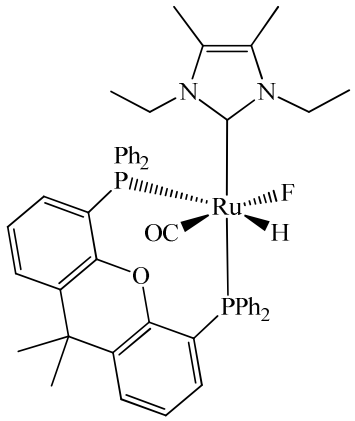

A C_6D_6 solution of [Ru(xantphos)(IEt_2Me_2)(CO)H_2] (**11**) (0.009 g, 0.01 mmol) was prepared in an NMR tube fitted with a resealable J. Young's PTFE valve and $Et_3N{\cdot}3HF$ (3.6 μL, 0.022 mmol) added via syringe. Excess CsF (0.050 g, 0.33 mmol) was added, and the tube left to stand for 2 h at room temperature. As for [Ru(xantphos)(ICy)(CO)HF] (**18**), attempts to synthesise **19** on a preparative scale for elemental analysis proved unsuccessful as the product continually oiled out on attempted recrystallisation. Selected NMR data: ^{19}F NMR ([D_8]-toluene, 470 MHz, 230 K) (both isomers): δ -315.4 (br s), -337.8 (br s); Selected low temperature NMR data for **isomer a**: ^{1}H NMR ([D_8]-toluene, 400 MHz, 217 K): δ -5.51 (dd, $^{2}J_{HP}$ = 130.9 Hz, $^{2}J_{HP}$ = 22.1 Hz, 1H, Ru*H*); $^{31}P\{^{1}H\}$ NMR ([D_8]-toluene, 162 MHz, 217 K): δ 31.8 (br s), 7.0 (br s); Selected low temperature NMR data for **isomer b**: ^{1}H NMR ([D_8]-toluene, 400 MHz, 217 K): δ -6.99 (dd, $^{2}J_{HP}$ = 129.4 Hz, $^{2}J_{HP}$ = 23.5 Hz, 1H, Ru*H*); $^{31}P\{^{1}H\}$ NMR ([D_8]-toluene, 162 MHz, 217 K): δ 41.7 (br s), 19.5 (br s); IR (nujol, cm^{-1}): ν(CO) = 1895 (s), 1883 (s); ESI-TOF MS: $[M-H]^{+}$ *m/z* = 879.2212 (theoretical 879.2226).

5.4.11 Synthesis of [Ru(dppf)(ICy)(CO)H_2] (21)

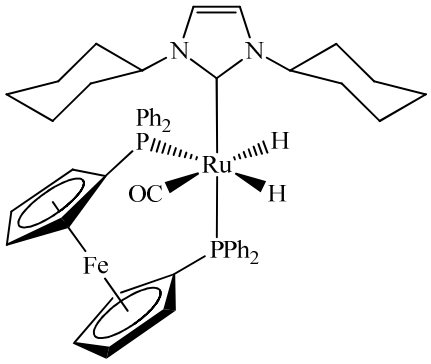

[Ru(dppf)(PPh_3)(CO)H_2] (**20**) (0.204 g, 0.22 mmol) and ICy (0.150 g, 0.65 mmol) were charged to an ampoule fitted with a J. Young's PTFE valve, dissolved in toluene (10 mL) and stirred at 393 K for 2 h. After cooling, the solvent was removed under vacuum to leave a light yellow solid, which was recrystallised from C_6H_6/hexane. Yield: 0.105 g (53 % yield). Selected ^{1}H NMR (C_6D_6, 400 MHz, 298 K) δ -5.66 (ddd, $^2J_{HP}$ = 87.9 Hz, $^2J_{HP}$ = 34.0 Hz, $^2J_{HH}$ = 2.1 Hz, 1H, Ru*H*), -8.13 (dd, $^2J_{HP}$ = 42.1 Hz, $^2J_{HP}$ = 22.4 Hz, 1H, Ru*H*); ^{31}P{^{1}H} NMR (C_6D_6, 162 MHz, 298 K): δ 57.7 (d, $^2J_{PP}$ = 19.0 Hz), 39.3 (d, $^2J_{PP}$ = 19.0 Hz); Selected ^{13}C NMR (C_6D_6, 100 MHz, 298 K): δ 207.8 (dd, $^2J_{CP}$ = 12.0 Hz, $^2J_{CP}$ = 5.8 Hz, *C*O), 188.6 (dd, $^2J_{CP}$ = 79.7 Hz, $^2J_{CP}$ = 8.9 Hz, N*C*N); IR (nujol, cm^{-1}): ν(CO/RuH) = 1923 (s), 1907 (s) and 1854 (s); Elemental analysis calcd for $C_{50}FeH_{54}N_2OP_2Ru$ (917.86): C 65.40, H 5.93, N 3.05; found: C 65.60, H 6.07, N 3.12.

5.4.12 Synthesis of [Ru(dppf)(ICy)(CO)HF] (22)

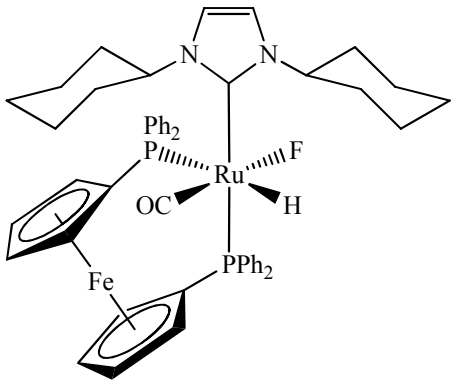

To a solution of [Ru(dppf)(ICy)(CO)H_2] (**21**) (0.197 g, 0.22 mmol) in C_6H_6 (10 mL) was added $Et_3N{\cdot}3HF$ (72 μL, 0.44 mmol) via syringe. The solution was added to a Schlenk tube containing an excess of CsF (0.150 g, 0.098 mmol), stirred for 1 h and the CsF then removed by

filtration. The volume of the solution was reduced by approximately half, before layering with hexane to give orange crystals (0.076 g, 39% yield). Selected ^{1}H NMR ([D_8]-toluene, 400 MHz, 320 K): δ -6.69 (ddd, $^{2}J_{HP}$ = 128.5 Hz, $^{2}J_{HP}$ = 31.5 Hz, $^{2}J_{HF}$ = 8.4 Hz, 1H, Ru*H*); ^{31}P{^{1}H} NMR ([D_8]-toluene, 162 MHz, 320 K): δ 31.7 (dd, $^{2}J_{PP}$ = 19.0 Hz, $^{2}J_{PF}$ = 14.8 Hz), 18.7 (dd, $^{2}J_{PF}$ = 79.5 Hz, $^{2}J_{PP}$ = 19.0 Hz); ^{19}F NMR ([D_8]-toluene, 376 MHz, 320 K): δ -347.4 (br s); ^{19}F NMR ([D_8]-toluene, 376 MHz, 213 K): δ -322.1 (br s), -351.9 (br s); ^{13}C{^{1}H} NMR ([D_8]-toluene, 125 MHz, 298 K): δ 207.0 (ddd, $^{2}J_{CF}$ = 69.9 Hz, $^{2}J_{CP}$ = 22.9 Hz, $^{2}J_{CP}$ = 8.0 Hz, *C*O), 182.7 (br d, $^{2}J_{CP}$ = 105.2 Hz, N*C*N); Selected low temperature NMR data for **isomer a**: ^{1}H NMR ([D_8]-toluene, 400 MHz, 217 K): δ -6.06 (br d, $^{2}J_{HP}$ = 129 Hz, 1H, Ru*H*); ^{31}P{^{1}H} NMR ([D_8]-toluene, 162 MHz, 213 K): δ 30.3 (br s), 20.5 (dd, $^{2}J_{PF}$ = 79.7 Hz, $^{2}J_{PP}$ = 18.6 Hz); Selected low temperature NMR data for **isomer b**: ^{1}H NMR ([D_8]-toluene, 400 MHz, 217 K): δ -6.13 (br d, $^{2}J_{HP}$ = 128 Hz, 1H, Ru*H*); ^{31}P{^{1}H} NMR ([D_8]-toluene, 162 MHz, 213 K): δ 32.6 (br s), 19.2 (dd, $^{2}J_{PF}$ = 81.8 Hz, $^{2}J_{PP}$ = 18.5 Hz); IR (nujol, cm^{-1}): ν(CO/RuH) = 1894 (s), 1883 (s) and 1869 (s); Elemental analysis calcd for $C_{50}FeH_{53}N_2OP_2F_1Ru$ (935.85): C 64.17, H 5.71, N 2.99; found: C 64.27, H 5.72, N 2.84.

5.5 CHAPTER 3

[$Ru(PPh_3)_3HCl$] (**23**) was prepared according to literature methods.[12]

5.5.1 Synthesis of $(Ph_2PCH_2CH_2)_2O$ (c)

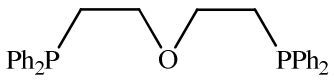

Synthesis of this ligand was adapted from the literature.[13] 2-chloroethyl ether, $(ClCH_2CH_2)_2O$ (1.47 mL, 12.5 mmol) was dissolved in dry THF (15 mL), and added dropwise to a 0.5 M solution of potassium diphenylphosphide, $(C_6H_5)_2P{\cdot}K$, in THF (50 mL, 25 mmol) over 15 min. The reaction mixture changed colour from a clear red to an opaque orange, with some heat generated, before being refluxed for 1 h. The resulting pale orange solution was filtered to remove the white precipitate, leaving a clear yellow solution. The solvent was then removed *in vacuo* to yield a cream wax (3.24 g, 59% yield). Selected ^{1}H NMR (C_6D_6, 500 MHz, 298 K): δ 2.24 (t, $^{3}J_{HH}$ = 7.6 Hz, 4H, C*H*$_2$PPh$_2$), 3.41 (app. q, J_{HH} = 7.6 Hz, 4H, C*H*$_2$O), 7.00-7.91 (m, 20H, P*Ph*$_2$); ^{31}P{^{1}H} NMR (C_6D_6, 162 MHz, 298 K): δ -20.2 (broad s, PPh_2).

5.5.2 Synthesis of [Ru(xantphos)(PPh_3)HCl] (24a)

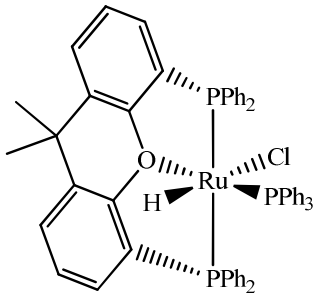

[$Ru(PPh_3)_3HCl$] (**23**) (0.092 g, 0.1 mmol) and xantphos (0.069 g, 0.12 mmol) were refluxed together in dry THF (10 mL) for 3 h to give a bright orange solution. After removal of the solvent, the product was washed with hexane (3 x 10 mL) and recrystallised from C_6H_6/hexane to give **24a** as orange needle-like crystals (0.086 g, 88% yield). Selected ^{1}H NMR (C_6D_6, 400 MHz, 298 K): δ = -16.22 (dt, $^2J_{HP}$ = 27.2 Hz, $^2J_{HP}$ = 23.9 Hz, 1H, Ru*H*); $^{31}P\{^1H\}$ NMR (C_6D_6, 162 MHz, 298 K): δ = 75.2 (t, $^2J_{PP}$ = 32.8 Hz, PPh_3), 46.7 (d, $^2J_{PP}$ = 32.8 Hz, P_{transP}); Elemental analysis calcd (%) for $C_{57}H_{48}OP_3ClRu.2C_6H_6$ (1134.66): C 73.04, H 5.33; found: C 72.63, H 5.41.

5.5.3 Synthesis of [Ru(DPEphos)(PPh_3)HCl] (24b)

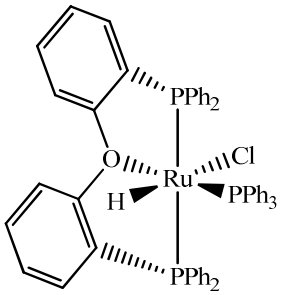

[$Ru(PPh_3)_3HCl$] (**23**) (0.092 g, 0.1 mmol) and DPEphos (0.162 g, 0.3 mmol) were refluxed together in dry THF (10 mL) for 1.5 h to give a bright orange solution. After removal of the solvent, the product was washed with hexane (3 x 10 mL) and recrystallised from CH_2Cl_2/hexane to give **24b** as orange needle-like crystals (0.061 g, 65% yield). Selected ^{1}H NMR (CD_2Cl_2, 400 MHz, 298 K): δ = -16.34 (dt, $^2J_{HP}$ = 27.6 Hz, $^2J_{HP}$ = 23.6 Hz, 1H, Ru*H*); $^{31}P\{^1H\}$ NMR (CD_2Cl_2, 162 MHz, 298 K): δ = 75.3 (t, $^2J_{PP}$ = 30.9 Hz, PPh_3), 46.7 (broad, P_{transP}); Selected low temperature NMR data: $^{31}P\{^1H\}$ NMR (CD_2Cl_2, 162 MHz, 233 K): δ = 75.0 (t, $^2J_{PP}$ = 30.8 Hz, PPh_3), 39.7 (dd, roofed, $^2J_{PP}$ = 284.6 Hz, $^2J_{PP}$ = 31.2 Hz, P_{transP}), 30.8 (dd, roofed, $^2J_{PP}$ = 284.6 Hz, $^2J_{PP}$ = 31.2 Hz,

P_{transP}); Elemental analysis calcd (%) for $C_{54}H_{44}OP_3ClRu.0.5CH_2Cl_2$ (885.79): C 66.74, H 4.62; found: C 66.77, H 4.82.

5.5.4 Synthesis of [Ru((Ph$_2$PCH$_2$CH$_2$)$_2$O)(PPh$_3$)HCl] (24c)

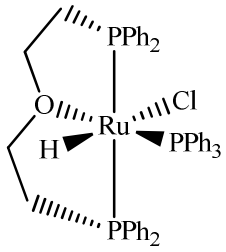

[Ru(PPh$_3$)$_3$HCl] (**23**) (0.092 g, 0.10 mmol) and (Ph$_2$PCH$_2$CH$_2$)$_2$O, (0.049 g, 0.12 mmol) were charged to an ampoule fitted with a J. Young's PTFE tap and then refluxed together in THF (10 mL) for 0.5 h. The solvent was removed and the resulting solid washed twice with hexane (10 mL) before being recrystallised from CH_2Cl_2/hexane to afford **24c** as orange crystals (0.051 g, 60% yield). Selected ^{1}H NMR (CD_2Cl_2, 500 MHz, 298 K): δ -17.54 (dt, $^2J_{HP}$ = 28.5 Hz, $^2J_{HP}$ = 21.7 Hz, 1H, Ru*H*), 2.48 (m, 2H, PC*H*H), 2.72 (m, 2H, PCH*H*), 3.37 (m, 2H, OC*H*H), 4.11 (m, 2H, OCH*H*); ^{31}P{^{1}H} NMR (CD_2Cl_2, 202 MHz, 298 K): δ 71.0 (t, $^2J_{PP}$ = 32.3 Hz, PPh$_3$), 42.3 (d, $^2J_{PP}$ = 32.3 Hz, P_{transP}); Selected ^{13}C{^{1}H} NMR (CD_2Cl_2, 125 MHz, 298 K): δ 72.6 (broad, O*C*H$_2$), 37.5 (vt, J_{CP} = 10.6 Hz, P*C*H$_2$); Elemental analysis calcd (%) for $C_{46}H_{44}OP_3ClRu.0.75CH_2Cl_2$ (906.00): C 61.98, H 5.06; found: C 61.98, H 5.24.

5.5.5 Synthesis of [Ru(xantphos)(PPh$_3$)(OH$_2$)H]BAr$_4^F$ / OTf ([25a]BAr$_4^F$ / [25a]OTf)

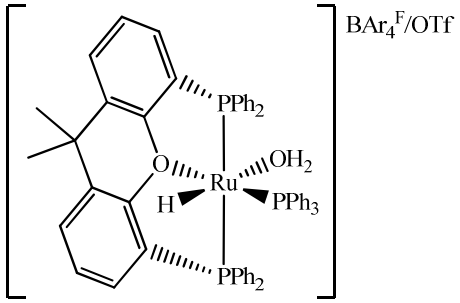

A CD_2Cl_2 solution of [Ru(xantphos)(PPh$_3$)HCl] (**24a**) (0.010 g, 0.01 mmol) and NaBAr$_4^F$ (0.009 g, 0.011 mmol) was left to stand in an NMR tube fitted with a resealable J. Young's PTFE valve at room temperature for 15 h to afford **[25a]BAr$_4^F$**. Selected ^{1}H NMR (CD_2Cl_2, 400 MHz,

298 K): δ -19.67 (dt, $^{2}J_{HP}$ = 29.4 Hz, $^{2}J_{HP}$ = 18.6 Hz, 1H, Ru*H*); $^{31}P\{^{1}H\}$ NMR (CD_2Cl_2, 162 MHz, 298 K): δ 73.2 (t, $^{2}J_{PP}$ = 28.4 Hz), 46.9 (d, $^{2}J_{PP}$ = 28.4 Hz); ESI-TOF MS: $[M\text{-}H_2O]^+$ *m/z* = 943.1993 (theoretical 943.1972).

The corresponding triflate salt [Ru(xantphos)(PPh_3)(OH_2)H]OTf (**[25a]OTf**) was prepared by stirring **24a** (0.098 g, 0.10 mmol) with AgOTf (0.043 g, 0.11 mmol) in CH_2Cl_2 (10 mL) for 15 h. After filtration to remove AgCl, degassed H_2O (0.027 mL, 0.001 mol) was added and the suspension stirred for 30 min. The volume of solvent was removed by half and a layer of hexane added. This afforded yellow crystals, at least some of which corresponded to **[25a]OTf** on the basis of X-ray diffraction. NMR analysis of the crystalline material as a whole showed it to consist of both the aqua complex (0.045 g, 41% yield) and [Ru(xantphos)(PPh_3)(η^2-O_2)H]OTf (0.011 g, 10% yield). The latter species was always formed as a side-product in varying amounts and could not be separated. This excluded the possibility of determining CHN analysis of the aqua complex.

5.5.6 Synthesis of [Ru(DPEphos)(PPh_3)(OH_2)H]BAr_4^F (25b)

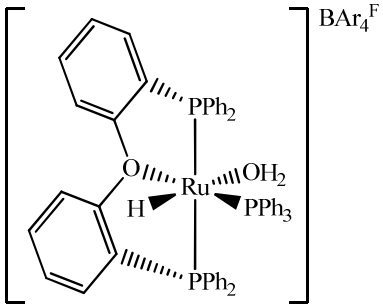

A CD_2Cl_2 solution of [Ru(DPEphos)(PPh_3)HCl] (**24b**) (0.009 g, 0.01 mmol) and $NaBAr_4^F$ (0.009 g, 0.011 mmol) was left to stand in an NMR tube fitted with a resealable J. Young's PTFE valve at room temperature for 15 h to afford **25b**. Selected ^{1}H NMR (CD_2Cl_2, 400 MHz, 298 K): δ -18.67 (dt, $^{2}J_{HP}$ = 31.4 Hz, $^{2}J_{HP}$ = 20.2 Hz, 1H, Ru*H*); $^{31}P\{^{1}H\}$ NMR (CD_2Cl_2, 162 MHz, 298 K): δ 72.0 (br s), 45.1 (br s).

5.5.7 Synthesis of [Ru((Ph$_2$CH$_2$CH$_2$)$_2$O)(PPh$_3$)(OH$_2$)H]BAr$_4^F$ (25c)

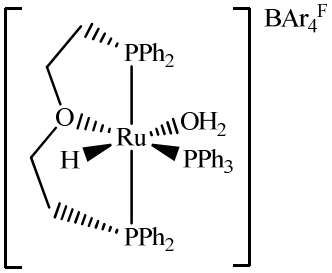

A CD_2Cl_2 solution of [Ru((Ph$_2$CH$_2$CH$_2$)$_2$O)(PPh$_3$)HCl] (**24c**) (0.008 g, 0.01 mmol) and NaBAr$_4^F$ (0.009 g, 0.011 mmol) was left to stand in an NMR tube fitted with a resealable J. Young's PTFE valve at room temperature for 15 h to afford **25c**. Selected ^{1}H NMR (CD_2Cl_2, 400 MHz, 298 K): δ -21.05 (dt, $^2J_{HP}$ = 30.3 Hz, $^2J_{HP}$ = 18.1 Hz, 1H, Ru*H*); ^{31}P{^{1}H} NMR (CD_2Cl_2, 162 MHz, 298 K): δ 72.4 (t, $^2J_{PP}$ = 28.9 Hz), 47.8 (d, $^2J_{PP}$ = 28.9 Hz).

5.5.8 Synthesis of [Ru(xantphos)(PPh$_3$)(OTf)H] (26a)

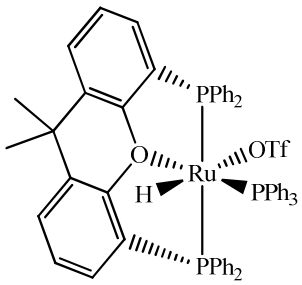

A CH_2Cl_2 solution (10 mL) of **24a** (0.200 g, 0.20 mmol) and AgOTf (0.086 g, 0.22 mmol) was stirred in an ampoule fitted with a resealable J. Young's PTFE valve at room temperature for 15 h and then filtered to remove a grey precipitate of AgCl. The solvent was reduced by half and layered with hexane to afford yellow crystals of **26a** (0.132 g, 59% yield). Selected ^{1}H NMR (CD_2Cl_2, 400 MHz, 315 K): δ -22.27 (dt, $^2J_{HP}$ = 31.0 Hz, $^2J_{HP}$ = 22.6 Hz, 1H, Ru*H*); ^{31}P{^{1}H} NMR (CD_2Cl_2, 162 MHz, 315 K): δ 68.9 (t, $^2J_{PP}$ = 30.8 Hz), 44.9 (d, $^2J_{PP}$ = 30.8 Hz); ^{19}F NMR (CD_2Cl_2, 376 MHz, 298 K): δ -78.8 (s, OTf); Elemental analysis calcd (%) for $C_{58}H_{48}O_4P_3SF_3Ru$ (1092.07): C 63.79, H 4.43; found: C 63.66, H 4.30.

5.5.9 Synthesis of [Ru(xantphos)(PPh_3)(MeCN)H]BAr_4^F/OTf (27a)

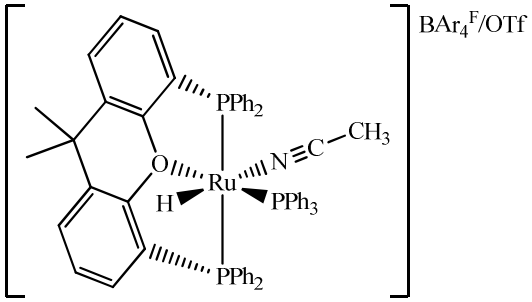

A CD_2Cl_2 solution of **24a** (0.010 g, 0.01 mmol) and $NaBAr_4^F$ (0.009 g, 0.011 mmol) was left to stand in an NMR tube fitted with a resealable J. Young's PTFE valve at room temperature for 15 h. MeCN (0.003 mL, 0.05 mmol) was then added to the solution via syringe. The product, **27a**, was spectroscopically characterised. Selected ^1H NMR (CD_2Cl_2, 500 MHz, 298 K): δ -13.39 (dt, $^2J_{HP}$ = 27.0 Hz, $^2J_{HP}$ = 19.1 Hz, 1H, Ru*H*), 1.36 (s, 3H, NC-C*H*$_3$); $^{31}P\{^1H\}$ NMR (CD_2Cl_2, 202 MHz, 298 K): δ 75.8 (br), 51.2 (d, $^2J_{PP}$ = 30.1 Hz); Selected $^{13}C\{^1H\}$ NMR (CD_2Cl_2, 126 MHz, 298 K): δ 121.8 (s, N*C*-CH$_3$), 2.9 (s, NC-*C*H$_3$); IR (nujol, cm^{-1}): ν(CN) = 2241 (s). Comparable spectroscopic data was recorded for the corresponding triflate salt, which was prepared by addition of MeCN (0.003 mL, 0.05 mmol) to a CD_2Cl_2 solution of **26a** (0.011 g, 0.01 mmol) in a J. Young's NMR tube. Selected ^1H NMR (CD_2Cl_2, 500 MHz, 298 K): -13.42 (dt, $^2J_{HP}$ = 27.0 Hz, $^2J_{HP}$ = 19.1 Hz, 1H, Ru*H*), 1.42 (s, 3H, NC-CH$_3$); $^{31}P\{^1H\}$ NMR (CD_2Cl_2, 202 MHz, 298 K): 76.1 (br), 51.4 (d, $^2J_{PP}$ = 30.1 Hz).

5.5.10 Synthesis of [Ru(xantphos)(PPh_3)(O_2)H]BAr_4^F (28a)

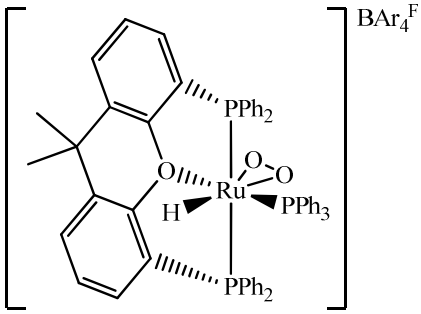

[Ru(xantphos)(PPh_3)HCl] (**24a**) (0.120 mg, 0.12 mmol) and $NaBAr_4^F$ (0.110 mg, 0.14 mmol) were charged to an ampoule fitted with a J. Young's PTFE tap, dissolved in dry CH_2Cl_2 (10 mL), and then left to stir at room temperature for 15 h. The solution was filtered to remove a white

precipitate of NaCl. The filtrate was then opened to air and left stirring for 10 min. before the solvent was removed *in vacuo*. The resulting solid was then washed once with hexane (10 mL) before being recrystallised from CH_2Cl_2/hexane to afford brown crystals of **28a** (0.109 mg, 49% yield). Selected ^{1}H NMR (CD_2Cl_2, 400 MHz, 298 K): δ -1.48 (dt, $^2J_{HP}$ = 29.4 Hz, $^2J_{HP}$ = 27.2 Hz, 1H, Ru*H*); ^{31}P{^{1}H} NMR (CD_2Cl_2, 162 MHz, 298 K): δ 48.2 (t, $^2J_{PP}$ = 19.2 Hz, PPh_3), 44.4 (d, $^2J_{PP}$ = 19.2 Hz, P_{transP}); ESI-TOF MS: $[M]^+$ *m/z* = 975.1931 (theoretical 975.1870); Elemental analysis calcd (%) for $C_{89}H_{60}BO_3F_{24}P_3Ru$ (1838.17): C 58.15, H 3.29; found: C 57.98, H 3.10.

5.5.11 Synthesis of [Ru(DPEphos)(PPh_3)(O_2)H]BAr_4^F (28b)

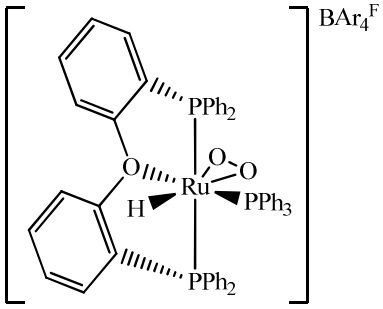

[Ru(DPEphos)(PPh_3)HCl] (**24b**) (0.100 mg, 0.11 mmol) and $NaBAr_4^F$ (0.095 mg, 0.12 mmol) were charged to an ampoule fitted with a J. Young's PTFE tap, dissolved in dry CH_2Cl_2 (10 mL), and then left to stir at room temperature for 15 h. The solution was filtered to remove a white precipitate of NaCl. The filtrate was then opened to air and left stirring for 10 min. before the solvent was removed *in vacuo*. The resulting solid was then washed twice with hexane (10 mL) and sonicated before being dried overnight under vacuum (0.090 mg, 48% yield). Larger scale recrystallisations proved difficult due to the rapid over-oxidation of the complex in solution, although a crystal suitable for X-ray analysis was obtained serendipitously. Selected ^{1}H NMR (CD_2Cl_2, 400 MHz, 298 K): δ -2.01 (dt, $^2J_{HP}$ = 32.0 Hz, $^2J_{HP}$ = 30.4 Hz, 1H, Ru*H*); ^{31}P{^{1}H} NMR (CD_2Cl_2, 162 MHz, 298 K): δ 41.4 (t, $^2J_{PP}$ = 18.6 Hz, PPh_3), 36.2 (d, $^2J_{PP}$ = 18.6 Hz, P_{transP}); ESI-TOF MS: $[M]^+$ *m/z* = 935.1600 (theoretical 935.1556).

5.5.12 Synthesis of [Ru((Ph$_2$PCH$_2$CH$_2$)$_2$O)(PPh$_3$)(η^2-O$_2$)H]BAr$_4^F$ (28c)

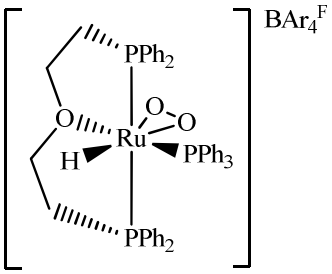

A CD_2Cl_2 solution of [Ru((Ph$_2$PCH$_2$CH$_2$)$_2$O)(PPh$_3$)HCl] (**24c**) (0.008 g, 0.01 mmol) and NaBAr$_4^F$ (0.009 g, 0.011 mmol) was prepared at room temperature in a resealable J. Young's NMR tube. The solution was left for 15 h and then exposed to air, which resulted in an instantaneous color change from yellow to yellow-green. NMR spectra of **28c** were run immediately to minimize the degradation of the complex. Selected ^{1}H NMR (CD_2Cl_2, 400 MHz, 298 K): δ -2.88 (dt, $^2J_{HP}$ = 29.6 Hz, $^2J_{HP}$ = 25.9 Hz, 1H, Ru*H*), 2.42-2.61 (m, 4H, PCH_2), 3.48 (m, 2H, OCH_2), 3.74 (m, 2H, OCH_2); ^{31}P{^{1}H} (CD_2Cl_2, 162 MHz, 298 K): δ 48.2 (t, $^2J_{PP}$ = 19.2 Hz, PPh$_3$), 45.8 (d, $^2J_{PP}$ = 19.2 Hz, P$_{transP}$).

5.5.13 Synthesis of [Ru(xantphos)(PPh$_3$)(η^2-H$_2$)H]BAr$_4^F$ (29a)

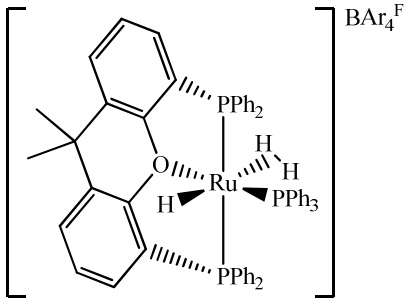

A CD_2Cl_2 solution of [Ru(xantphos)(PPh$_3$)HCl] (**24a**) (0.010 g, 0.01 mmol) and NaBAr$_4^F$ (0.009 g, 0.011 mmol) was left to stand in an NMR tube fitted with a resealable J. Young's PTFE valve at room temperature for 15 h. The solution was freeze-pump-thaw degassed (x 3) and placed under 1 atm. of H_2 to give a mixture of **29a** and unreacted [Ru(xantphos)(PPh$_3$)(OH$_2$)H]BAr$_4^F$ (**25a**) in a ratio of 3.8:1 at 180 K. Selected ^{1}H NMR (CD_2Cl_2, 400 MHz, 180 K): δ -8.79 (dt, $^2J_{HP}$ = 22.4 Hz, $^2J_{HP}$ = 19.1 Hz, 1H, Ru*H*), -0.95 (broad s, 2H**,** η^2-*H*$_2$); ^{31}P{^{1}H} (CD_2Cl_2, 162 MHz, 180 K): δ 67.6 (t, $^2J_{PP}$ = 27.8 Hz, PPh$_3$), 51.9 (d, $^2J_{PP}$ = 27.8 Hz, P$_{transP}$).

5.5.14 Synthesis of [Ru(DPEphos)(PPh_3)(η^2-H_2)H]BAr_4^F (29b)

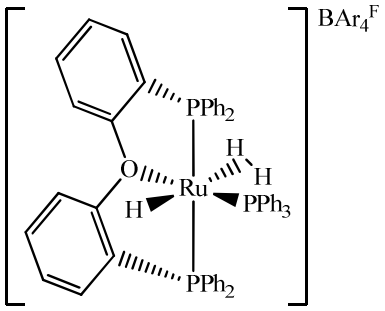

A CD_2Cl_2 solution of [Ru(DPEphos)(PPh_3)HCl] (**24b**) (0.009 g, 0.01 mmol) and $NaBAr_4^F$ (0.009 g, 0.011 mmol) was left to stand in an NMR tube fitted with a resealable J. Young's PTFE valve at room temperature for 15 h. The solution was freeze-pump-thaw degassed (x 3) and placed under 1 atm. of H_2 to afford a mixture of **29b** and unreacted [Ru(DPEphos)(PPh_3)(OH_2)H]BAr_4^F (**25b**) in a ratio of 6.1:1 at 195 K. Selected ^{1}H NMR (CD_2Cl_2, 400 MHz, 195 K): δ -7.95 (dt, $^2J_{HP}$ = 22.8 Hz, $^2J_{HP}$ = 19.4 Hz, 1H, Ru*H*), -0.25 (broad s, 2H**,** η^2-H_2); $^{31}P\{^1H\}$ (CD_2Cl_2, 162 MHz, 195 K): δ 69.2 (t, $^2J_{PP}$ = 26.0 Hz, PPh_3), 47.1 (dd, $^2J_{PP}$ = 225.5 Hz, $^2J_{PP}$ = 26.0 Hz, P_{transP}), 46.2 (dd, $^2J_{PP}$ = 225.5 Hz, $^2J_{PP}$ = 26.0 Hz, P_{transP}).

5.5.15 Synthesis of [Ru(($Ph_2PCH_2CH_2)_2O$)(PPh_3)(η^2-H_2)H]BAr_4^F (29c)

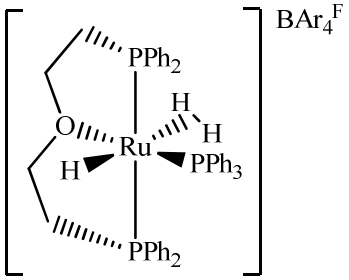

A CD_2Cl_2 solution of [Ru(($Ph_2PCH_2CH_2)_2O$)(PPh_3)HCl] (**24c**) (0.008 g, 0.01 mmol) and $NaBAr_4^F$ (0.009 g, 0.011 mmol) was left to stand in an NMR tube fitted with a resealable J. Young's PTFE valve at room temperature for 15 h. The solution was freeze-pump-thaw degassed (x 3) and placed under 1 atm. of H_2 to afford a mixture of **29c** and unreacted [Ru(($Ph_2PCH_2CH_2)_2O$)(PPh_3)(OH_2)H]BAr_4^F (**25c**) in a ratio of 4.4:1 at 195 K. Selected ^{1}H NMR (CD_2Cl_2, 400 MHz, 195 K): δ -9.16 (dt, $^2J_{HP}$ = 23.6 Hz, $^2J_{HP}$ = 16.2 Hz, 1H, Ru*H*), -1.91 (broad s, 2H**,** η^2-H_2), 2.35 (m, 2H, PCH_2), 2.60 (m, 2H, PCH_2), 3.17 (m, 2H, OCH_2), 3.71 (m, 2H, OCH_2). $^{31}P\{^1H\}$ (CD_2Cl_2, 162 MHz, 195 K): δ 66.9 (t, $^2J_{PP}$ = 26.7 Hz, PPh_3), 56.2 (d, $^2J_{PP}$ = 26.7 Hz, P_{transP}).

5.5.16 Synthesis of [Ru(xantphos)(PPh_3)(N_2)H]BAr_4^F (30a)

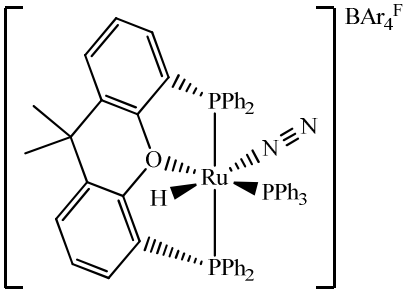

A CD_2Cl_2 solution of [Ru(xantphos)(PPh_3)HCl] (**24a**) (0.010 g, 0.01 mmol) and $NaBAr_4^F$ (0.009 g, 0.011 mmol) was left to stand in an NMR tube fitted with a resealable J. Young's PTFE valve at room temperature for 15 h. The solution was freeze-pump-thaw degassed (x 3) and placed under 1 atm. of N_2 to give a mixture of **30a** and unreacted [Ru(xantphos)(PPh_3)(OH_2)H]BAr_4^F (**25a**) in a ratio of 6.7:1 at 180 K. Selected ^{1}H NMR (CD_2Cl_2, 400 MHz, 180 K): δ -11.72 (dt, $^2J_{HP}$ = 26.0 Hz, $^2J_{HP}$ = 16.5 Hz, 1H, Ru*H*); $^1H\{^{31}P\}$ NMR spectrum recorded with ^{15}N labelling: δ -11.76 (d, $^2J_{HN}$ = 17.9 Hz, Ru*H*); $^{31}P\{^1H\}$ (CD_2Cl_2, 162 MHz, 180 K): δ 68.2 (t, $^2J_{PP}$ = 27.1 Hz, PPh_3), 47.8 (d, $^2J_{PP}$ = 27.1 Hz, P_{transP}); $^{15}N\{^1H\}$ (CD_2Cl_2, 41 MHz, 180 K): δ -88.7 (s, α-*N*), -57.6 (s, β-*N*).

5.5.17 Synthesis of [Ru(DPEphos)(PPh_3)(N_2)H]BAr_4^F (30b)

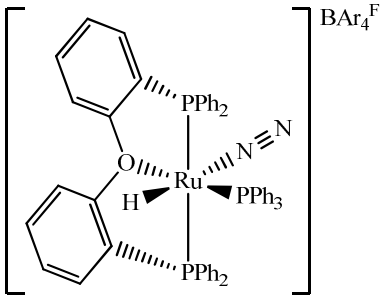

A CD_2Cl_2 solution of [Ru(DPEphos)(PPh_3)HCl] (**24b**) (0.009 g, 0.01 mmol) and $NaBAr_4^F$ (0.009 g, 0.011 mmol) was left to stand in an NMR tube fitted with a resealable J. Young's PTFE valve at room temperature for 15 h. The solution was freeze-pump-thaw degassed (x 3) and placed under 1 atm. of N_2 to give a mixture of **30b** and unreacted [Ru(DPEphos)(PPh_3)(OH_2)H]BAr_4^F (**25b**) in a ratio of 4.5:1 at 180 K. Selected ^{1}H NMR (CD_2Cl_2, 400 MHz, 180 K): δ -11.04 (dt, $^2J_{HP}$ = 26.7 Hz, $^2J_{HP}$ = 20.0 Hz, 1H, Ru*H*); $^1H\{^{31}P\}$ NMR spectrum recorded with ^{15}N labelling: δ -11.06 (d, $^2J_{HN}$ = 16.9 Hz, Ru*H*); $^{31}P\{^1H\}$ (CD_2Cl_2, 162 MHz, 180 K): δ 65.4 (t, $^2J_{PP}$ = 26.9 Hz, PPh_3), 43.1

(dd, $^2J_{PP}$ = 241.3 Hz, $^2J_{PP}$ = 25.1 Hz, P_{transP}), 41.7 (dd, $^2J_{PP}$ = 241.3 Hz, $^2J_{PP}$ = 27.8 Hz, P_{transP}); $^{15}N\{^1H\}$ (CD_2Cl_2, 41 MHz, 180 K): δ -82.6 (s, α-*N*), -51.8 (s, β-*N*).

5.5.18 Synthesis of [Ru((Ph$_2$PCH$_2$CH$_2$)$_2$O)(PPh$_3$)(N$_2$)H]BAr$_4^F$ (30c)

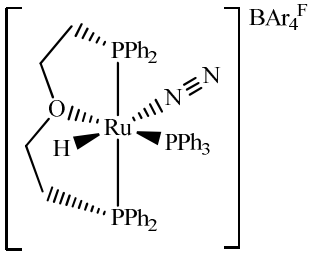

A CD_2Cl_2 solution of [Ru((Ph$_2$PCH$_2$CH$_2$)$_2$O)(PPh$_3$)HCl] (**24c**) (0.008 g, 0.01 mmol) and $NaBAr_4^F$ (0.009 g, 0.011 mmol) was left to stand in an NMR tube fitted with a resealable J. Young's PTFE valve at room temperature for 15 h. The solution was freeze-pump-thaw degassed (x 3) and placed under 1 atm. of N_2 to afford a mixture of **30c** and unreacted [Ru((Ph$_2$PCH$_2$CH$_2$)$_2$O)(PPh$_3$)(OH$_2$)H]BAr$_4^F$ (**25c**) in a ratio of 2.4:1 at 195 K. Selected ^1H NMR data: (CD_2Cl_2, 400 MHz, 195 K): δ -12.06 (dt, $^2J_{HP}$ = 25.3 Hz, $^2J_{HP}$ = 16.6 Hz, 1H, Ru*H*); $^1H\{^{31}P\}$ NMR spectrum recorded with ^{15}N labelling: δ -12.08 (d, $^2J_{HN}$ = 18.1 Hz, Ru*H*), 2.11 (m, 2H, P-C*H*H), 2.70 (m, 2H, P-CH*H*), 3.28 (m, 2H, O-C*H*H), 3.87 (m, 2H, O-CH*H*); $^{31}P\{^1H\}$ (CD_2Cl_2, 162 MHz, 195 K): δ 67.2 (t, $^2J_{PP}$ = 27.0 Hz, PPh$_3$), 51.1 (d, $^2J_{PP}$ = 27.0 Hz, P_{transP}); $^{15}N\{^1H\}$ (CD_2Cl_2, 41 MHz, 195 K): δ -86.2 (s, α-*N*), -59.1 (s, β-*N*).

5.5.19 Synthesis of [Ru(dppf)(PPh$_3$)HCl] (31)

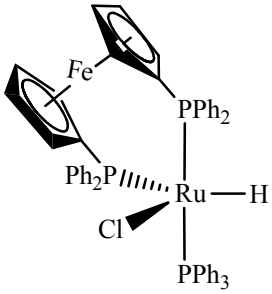

[Ru(PPh$_3$)$_3$HCl] (**23**) (0.092 g, 0.10 mmol) and dppf (0.055 g, 0.12 mmol) were charged to an ampoule fitted with a J. Young's PTFE tap and then refluxed together in THF (10 mL) for 0.5 h. The solvent was removed and the resulting solid washed twice with hexane (10 mL) before being

recrystallised from THF/hexane to afford orange crystals (0.046 g, 48% yield). Selected ^{1}H NMR ([D$_8$]-THF, 500 MHz, 298 K): δ -19.99 (dt, $^{2}J_{HP}$ = 29.9 Hz, $^{2}J_{HP}$ = 19.9 Hz, 1H, Ru*H*), 4.16 (s, 2H, dppf), 4.27 (s, 2H, dppf), 4.30 (s, 2H, dppf), 4.51 (s, 2H, dppf); Selected ^{31}P{^{1}H} NMR ([D$_8$]-THF, 162 MHz, 298 K): δ 64.9 (broad), 41.4 (t, $^{2}J_{PP}$ = 134.1 Hz); Selected low temperature NMR data: ^{31}P{^{1}H} NMR ([D$_8$]-THF, 162 MHz, 213 K): δ = 83.1 (broad, PPh$_3$), 48.4 (dd, roofed, $^{2}J_{PP}$ = 299.2 Hz, $^{2}J_{PP}$ = 29.9 Hz, P$_{transP}$), 41.5 (dd, roofed, $^{2}J_{PP}$ = 294.2 Hz, $^{2}J_{PP}$ = 24.9 Hz, P$_{transP}$); Elemental analysis calcd (%) for $C_{52}H_{44}P_3ClRuFe.3C_4H_8O$ (1170.54): C 65.67, H 5.86; found: C 65.56, H 6.11.

5.5.20 Synthesis of [Ru(dppf)({η^6-C$_6$H$_5$}PPh$_2$)H]BAr$_4^F$ (32)

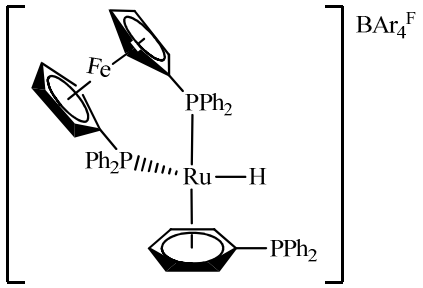

[Ru(dppf)(PPh$_3$)HCl] (**31**) (0.095 mg, 0.10 mmol) and NaBAr$_4^F$ (0.089 mg, 0.11 mmol) were charged to an ampoule fitted with a J. Young's PTFE tap, dissolved in CH_2Cl_2 (10 mL) and stirred at room temperature for 15 h. The suspension was filtered by cannula to remove NaCl, and the filtrate reduced to dryness. The resulting orange solid was washed with hexane (2 x 10 mL) and recrystallized from CH_2Cl_2/hexane (0.178 mg, 52% yield). Selected ^{1}H NMR (CD_2Cl_2, 400 MHz, 298 K): δ -9.32 (dt, $^{2}J_{HP}$ = 38.8 Hz, J_{HP} = 7.0 Hz, 1H, Ru*H*), 4.20 (s, 2H, dppf), 4.32 (s, 2H, dppf), 4.36 (s, 4H, dppf), 4.72 (m, 2H, {η^6-C$_6$*H*$_5$}PPh$_2$), 4.84 (m, 2H, {η^6-C$_6$*H*$_5$}PPh$_2$), 6.02 (m, 1H, ({η^6-C$_6$*H*$_5$}PPh$_2$); ^{31}P{^{1}H} (CD_2Cl_2, 162 MHz, 298 K): δ 50.2 (s, P$_{dppf}$), -8.1 (s, {η^6-C$_6$H$_5$}PPh$_2$); Selected ^{13}C{^{1}H} (CD_2Cl_2, 100 MHz, 298 K): δ 73.9 (m, dppf), 75.6 (m, dppf), 76.0 (m, dppf), 94.6 (dt, J_{CP} = 15.7 Hz, J_{CP} = 3.1 Hz, {η^6-*C*$_6$H$_5$}PPh$_2$), 97.1 (m, {η^6-*C*$_6$H$_5$}PPh$_2$), 96.3 (s, {η^6-*C*$_6$H$_5$}PPh$_2$), 109.7 (dt, J_{CP} = 27.4 Hz, J_{CP} = 2.1 Hz, {η^6-*C*$_6$H$_5$}PPh$_2$); Elemental analysis calcd (%) for $C_{84}H_{44}BF_{24}P_3FeRu.CH_2Cl_2$ (1781.98): C 54.69, H 3.13; found: C 54.77, H 2.91.

5.5.21 Synthesis of [Ru(dppf)(PPh_3)$(CO)_2$H]BAr_4^F (33)

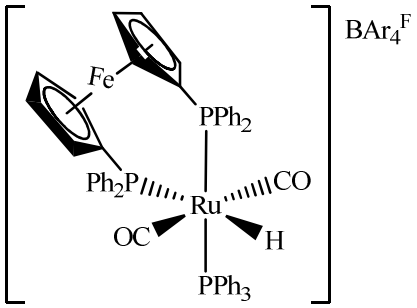

A solution of [Ru(dppf)({η^6-C_6H_5}PPh_2)H]BAr_4^F (**32**) (0.100 g, 0.057 mmol) in CH_2Cl_2 (10 mL) in an ampoule fitted with a J. Young's PTFE valve was freeze-pump-thaw degassed three times, placed under 1 atm. CO and heated at reflux for 15 h. After cooling, the solvent was removed and the resulting orange solid washed with hexane (2 x 10 mL) to give **33** as a yellow solid (0.058 g, 56% yield). Selected ^{1}H NMR (CD_2Cl_2, 400 MHz, 298 K): δ -8.56 (ddd, $^2J_{HP}$ = 62.2 Hz, $^2J_{HP}$ = 24.3 Hz, $^2J_{HP}$ = 19.3 Hz, 1H, Ru*H*); ^{1}H{^{31}P} NMR spectrum recorded with ^{13}CO labelling: δ -8.56 (t, $^2J_{HC}$ = 5.6 Hz, Ru*H*), 4.25 (s, 2H, dppf), 4.49 (s, 2H, dppf), 4.52 (s, 2H, dppf), 4.62 (m, 2H, dppf); ^{31}P{^{1}H} (CD_2Cl_2, 162 MHz, 298 K): δ 36.8 (dd, $^2J_{PP}$ = 178.3 Hz, $^2J_{PP}$ = 13.1 Hz, P_{transP}), 32.3 (dd, $^2J_{PP}$ = 178.3 Hz, $^2J_{PP}$ = 17.0 Hz, P_{transP}), 20.4 (dd, $^2J_{PP}$ = 17.0 Hz, $^2J_{PP}$ = 13.1 Hz, P_{transH}); Selected ^{13}C{^{1}H} (CD_2Cl_2, 100 MHz, 298 K): δ 200.2 (dt, $^2J_{CP}$ = 14.1 Hz, $^2J_{CP}$ = 11.1 Hz, *C*O); IR (CH_2Cl_2, cm^{-1}): ν(CO) = 2001 (s); ESI-TOF MS: $[M]^+$ *m/z* = 975.0980 (theoretical 975.0958).

5.5.22 Synthesis of [Ru(PMe_3)$_5$H]BAr_4^F (34)

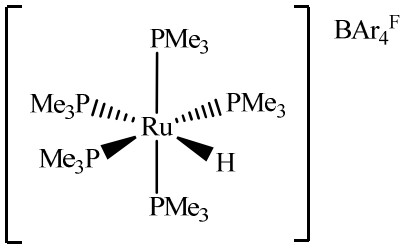

Excess PMe_3 (0.077 mL, 0.75 mmol) was added by syringe to a THF (10 mL) solution of [Ru(dppf)({η^6-C_6H_5}PPh_2)H]BAr_4^F (**32**) (0.267 g, 0.15 mmol) in an ampoule fitted with a J. Young's PTFE valve, and the reaction mixture heated at reflux for 3 h. After cooling, the solvent was removed and the resulting pale yellow solid washed with benzene (2 x 10 mL) and recrystallised from THF/hexane to afford **34** as clear needle-like crystals (0.100 g, 50%). ^{1}H NMR

([D_8]-THF, 500 MHz, 298 K): δ -11.35 (dquin, $^2J_{HP}$ = 74.4 Hz, $^2J_{HP}$ = 25.3 Hz, 1H, Ru*H*), 1.38 (d, 9H, $^2J_{HP}$ = 5.9 Hz, P*Me*$_3$), 1.54 (br s, 36H, P*Me*$_3$); $^{31}P\{^1H\}$ ([D_8]-THF, 201 MHz, 298 K): δ -23.2 (quint, $^2J_{PP}$ = 26.1 Hz, P_{transH}), -9.9 (d, $^2J_{PP}$ = 26.1 Hz, P_{transP}); Elemental analysis calcd (%) for $C_{47}H_{58}BF_{24}P_5Ru$ (1345.69): C 41.95, H 4.34; found: C 41.86, H 4.28.

5.6 CHAPTER 4

The N-heterocyclic carbene IAd was prepared according to the literature procedure.[14]

5.6.1 Synthesis of [Ru(xantphos)(PPh_3)($H_3B{\cdot}NH_2{}^tBu$)H]$BAr_4{}^F$ (35)

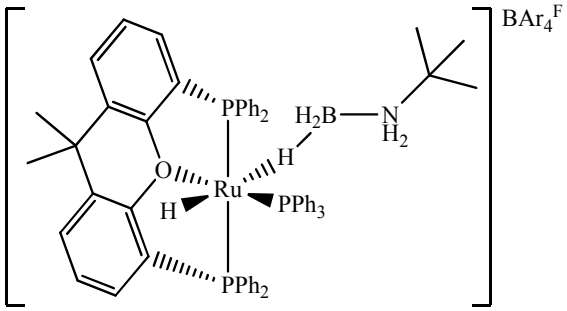

[Ru(xantphos)(PPh_3)HCl] (**24a**) (0.196 g, 0.2 mmol) and $NaBAr_4{}^F$ (0.178 g, 0.22 mmol) were charged to an ampoule fitted with a J. Young's resealable PTFE valve, dissolved in dry CH_2Cl_2 (10 mL), and stirred at ambient temperature for 15 h. The resulting orange solution of [Ru(xantphos)(PPh_3)(OH_2)H]$BAr_4{}^F$ (**25a**) was filtered by cannula into an ampoule charged with $H_3B{\cdot}NH_2{}^tBu$ (0.017 g, 0.2 mmol) and the mixture stirred for 1 h. The solvent was reduced by half and layered with hexane to afford **35** as a yellow crystalline solid (0.247 g, 65% yield). Selected ^1H NMR (400 MHz, CD_2Cl_2, 298 K): δ = -14.50 (dt, $^2J_{HP}$ = 26.7 Hz, $^2J_{HP}$ = 19.3 Hz, 1H, Ru*H*), -1.63 (br s, 3H, BH_3), 0.69 (s, 9H, C(CH_3)$_3$), 1.12 (s, 1H, N*H*), 1.27 (s, 1H, N*H*); $^{31}P\{^1H\}$ NMR (162 MHz, CD_2Cl_2, 298 K): δ = 50.9 (d, $^2J_{PP}$ = 30.0 Hz), 72.9 (t, $^2J_{PP}$ = 30.0 Hz); Selected $^{11}B\{^1H\}$ NMR (CD_2Cl_2, 138 MHz, 303 K): δ = -21.5 (br s, *B*H_3); Selected $^{13}C\{^1H\}$ NMR (CD_2Cl_2, 125 MHz, 250 K): δ = 27.3 (s, ^{t}Bu-*C*H_3), 54.2 (s, ^{t}Bu-*C*); IR (KBr, cm^{-1}): ν(NH) = 3276 (m) and 3241 (m), ν(BH) = 2480 (m) and 2452 (m), ν(Ru-H-BH_2) = 2120 (w); Elemental analysis calcd (%) for $C_{93}H_{74}B_2F_{24}NOP_3Ru$: (1893.20) C 59.00, H 3.94, N 0.74; found C 58.85, H 3.86, N 0.76.

5.6.2 Synthesis of [Ru(xantphos)(PPh_3)($H_3B{\cdot}NHMe_2$)H]BAr_4^F (36)

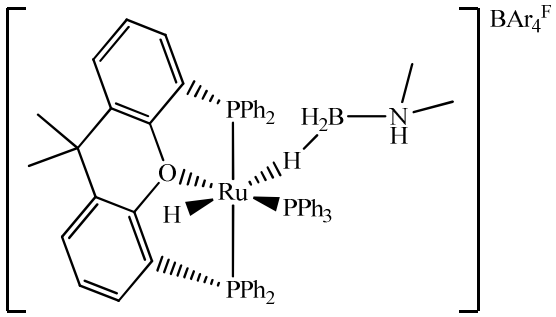

[Ru(xantphos)(PPh_3)HCl] (**24a**) (0.020 g, 0.02 mmol) and $NaBAr_4^F$ (0.018 g, 0.022 mmol) were dissolved in CD_2Cl_2 in a J. Young's resealable NMR tube and left at ambient temperature for 15 h. The solution was then filtered into a second J. Young's NMR tube charged with $H_3B{\cdot}NHMe_2$ (0.002 g, 0.04 mmol). Selected ^1H NMR (CD_2Cl_2, 400 MHz, 298 K): δ = -15.22 (dt, $^2J_{HP}$ = 26.1 Hz, $^2J_{HP}$ = 21.0 Hz, 1H, Ru*H*), -0.80 (broad s, 3H, BH_3), 1.19 (br, 1H, N*H*(CH_3)$_2$), 1.79 (d, $^3J_{HH}$ = 5.3 Hz, 6H, NH(CH_3)$_2$); $^{31}P\{^1H\}$ NMR (CD_2Cl_2,162 MHz, 298 K): δ = 46.1 (d, $^2J_{PP}$ = 30.4 Hz), 73.0 (t, $^2J_{PP}$ = 30.4 Hz).

5.6.3 Synthesis of [Ru(xantphos)(PPh_3)($H_3B{\cdot}HN\{CH_2CH_2\}_2O$)H]$BAr_4^F$ (37)

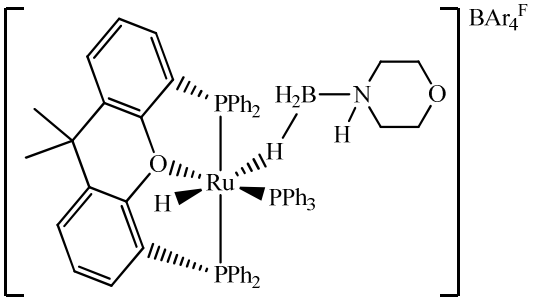

A CD_2Cl_2 solution of [Ru(xantphos)(PPh_3)HCl] (**24a**) (0.020 g, 0.02 mmol) and $NaBAr_4^F$ (0.018 g, 0.022 mmol) was left to stand in an NMR tube fitted with a resealable J. Young's PTFE valve at 298 K for 15 h. The solution was then filtered into a second NMR tube fitted with a resealable J. Young's PTFE valve charged with $H_3B{\cdot}HN\{CH_2CH_2\}_2O$ (0.004 g, 0.04 mmol) to form the product. Selected ^1H NMR (CD_2Cl_2, 500 MHz, 250 K): δ -15.35 (dt, $^2J_{HP}$ = 26.5 Hz, $^2J_{HP}$ = 21.5 Hz 1H, Ru*H*), -0.67 (broad s, 3H, BH_3), 1.38 (broad s, 1H, N*H*), 2.18 (m, 2H, N(C*H*H)$_2$), 2.46 (broad m, 2H, N(CH*H*)$_2$), 2.91 (m, 2H, O(C*H*H)$_2$), 3.60 (broad m, 2H, O(CH*H*)$_2$); $^{31}P\{^1H\}$ NMR (CD_2Cl_2, 202 MHz, 250 K): δ 48.1 (d, $^2J_{PP}$ = 30.5 Hz), 74.4 (t, $^2J_{PP}$ = 30.5 Hz).

5.6.4 Synthesis of [Ru(xantphos)(PPh_3)($H_3B{\cdot}NH_3$)H]BPh_4 (38)

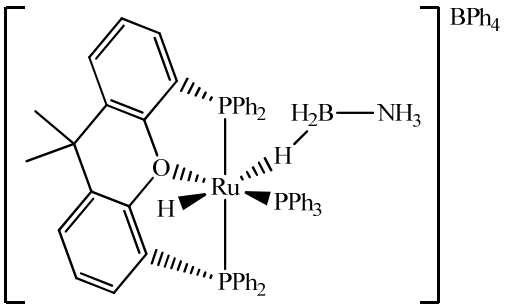

[Ru(xantphos)(PPh_3)HCl] (**24a**) (0.196 g, 0.2 mmol) and $NaBPh_4$ (0.075 g, 0.22 mmol) were charged to an ampoule fitted with a J. Young's resealable PTFE valve, dissolved in dry CH_2Cl_2 (10 mL), and stirred at ambient temperature for 15 h. The resulting orange solution of [Ru(xantphos)(PPh_3)(OH_2)H]BAr_4^F (**25a**) was filtered by cannula into an ampoule charged with $H_3B{\cdot}NH_3$ (12 mg, 0.2 mmol). After stirring for 1.5 h, the solvent was removed and the resulting yellow waxy solid washed with Et_2O (2 x 10 mL) and then recrystallised from CH_2Cl_2/Et_2O to afford **38** (0.052 g, 20% yield). Selected ^{1}H NMR (CD_2Cl_2, 500 MHz, 298 K): δ = -14.60 (dt, $^2J_{HP}$ = 26.9 Hz, $^2J_{HP}$ = 19.5 Hz, 1H, Ru*H*), -1.65 (br s, 3H, BH_3), 0.62 (br s, 3H, NH_3); $^{31}P\{^1H\}$ NMR (CD_2Cl_2, 202 MHz, 298 K): δ = 51.9 (d, $^2J_{PP}$ = 30.1 Hz), 75.4 (t, $^2J_{PP}$ = 30.1 Hz); $^{11}B\{^1H\}$ NMR (CD_2Cl_2, 160 MHz, 308 K): δ = -20.5 (br s, *B*H_3), -6.6 (s, *B*Ph_4); IR (KBr, cm^{-1}): νNH = 3318 (m), 3290 (m) and 3231 (m), ν(BH) = 2461 (m) and 2426 (m), ν(Ru-H-BH_2) = 2117 (w), ν(RuH) = 1950 (m); Elemental analysis calcd (%) for $C_{81}H_{74}B_2NOP_3Ru$: (1282.29) C 75.87, H 5.82, N 1.09; found C 75.68, H 5.71, N 1.09.

5.6.5 Synthesis of [Ru(xantphos)(PPh_3)(NH_3)H]BPh_4 (39)

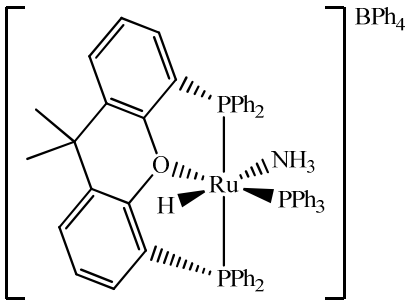

[Ru(xantphos)(PPh_3)HCl] (**24a**) (0.196 g, 0.2 mmol) and $NaBPh_4$ (0.075 g, 0.22 mmol) were charged to an ampoule fitted with a J. Young's PTFE valve, dissolved in dry CH_2Cl_2 (10 mL), and stirred at 298 K for 15 h. An atmosphere of NH_3 was introduced to the ampoule, and the

resulting light yellow solution stirred for 1 h. The resulting yellow solution was reduced to dryness, and washed with Et_2O (1 x 10 mL). Recrystallisation from THF:Et_2O afforded **39** as extremely fine yellow crystals (0.161 g, 63%). Selected ^{1}H NMR (CD_2Cl_2, 500 MHz, 272 K): δ -13.92 (dt, $^2J_{HP}$ = 27.5 Hz, $^2J_{HP}$ = 18.2 Hz, 1H, Ru*H*), 0.15 (broad s, 3H, N*H*$_3$); ^{31}P{^{1}H} (CD_2Cl_2, 202 MHz, 298 K): δ 80.0 (t, $^2J_{PP}$ = 29.7 Hz), 54.2 (d, $^2J_{PP}$ = 29.7 Hz); IR (KBr, cm^{-1}): ν(NH$_{s,as}$) = 3350, 3333 and 3260 (s), ν(RuH) = 1967 (s); Elemental analysis calcd (%) for $C_{81}H_{71}N_1O_1P_3Ru$ (1268.46): C 76.70, H 5.64, N 1.10; found: C 76.53, H 5.48, N 1.11.

5.6.6 [Ru(xantphos)(PPh$_3$)(PPh$_2$H)H]BAr$_4^F$ (40)

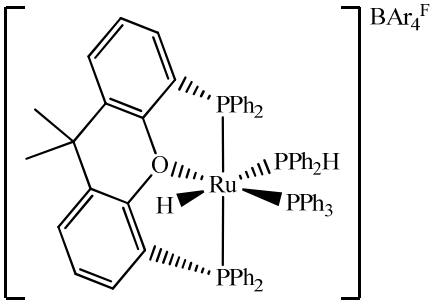

Intermediate observed on reaction of a pre-formed CD_2Cl_2 solution of [Ru(xantphos)(PPh$_3$)(OH$_2$)H]BAr$_4^F$ (**25a**) (0.02 mmol) with $H_3B{\cdot}PHPh_2$ (0.008 g, 0.04 mmol). Selected ^{1}H NMR (CD_2Cl_2, 400 MHz, 298 K): δ -7.51 (dq, $^2J_{HP}$ = 82.2 Hz, $^2J_{HP}$ = 24.6 Hz, 1H, Ru*H*); ^{31}P{^{1}H} (CD_2Cl_2, 162 MHz, 298 K): δ 65.7 (td, $^2J_{PP}$ = 28.9 Hz, $^2J_{PP}$ = 14.4 Hz), 45.3 (dd, $^2J_{PP}$ = 28.9 Hz, $^2J_{PP}$ = 17.4 Hz), 10.0 (dt, $^2J_{PP}$ = 17.4 Hz, $^2J_{PP}$ = 14.4 Hz).

5.6.7 Synthesis of [Ru(xantphos)(PHPh$_2$)$_2$H]BPh$_4$ (41)

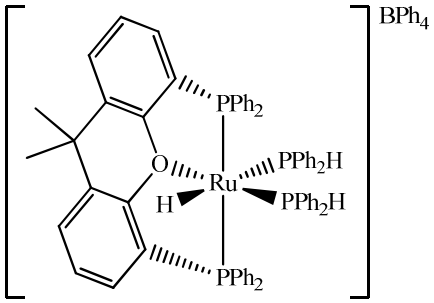

[Ru(xantphos)(PPh$_3$)HCl] (**24a**) (0.196 g, 0.2 mmol) and NaBPh$_4$ (0.075 g, 0.22 mmol) were charged to an ampoule fitted with a J. Young's resealable PTFE valve, dissolved in dry

CH_2Cl_2 (10 mL), and stirred at ambient temperature for 15 h. The resulting orange solution of [Ru(xantphos)(PPh_3)(OH_2)H]BAr_4^F (**25a**) was filtered by cannula into an ampoule charged with $H_3B{\cdot}PHPh_2$ (0.080 g, 0.4 mmol) and the mixture stirred for 2 h at room temperature to generate a bright yellow solution. Removal of the solvent under vacuum afforded a waxy solid, which was washed with Et_2O (2 x 10 mL) and recrystallised from THF/Et_2O to afford **41** (0.117 g, 43% yield) as a yellow microcrystalline solid. Selected ^{1}H NMR (CD_2Cl_2, 500 MHz, 298 K): δ = -6.47 (ddt, $^2J_{HP}$ = 81.3 Hz, $^2J_{HP}$ = 23.2 Hz, $^2J_{HP}$ = 20.3 Hz, 1H, Ru*H*), 5.07 (dt, $^1J_{HP}$ = 337.6 Hz, $^3J_{HP}$ = 11.4 Hz, 1H, P*H*), 5.92 (ddt, $^1J_{HP}$ = 361.4 Hz, $^3J_{HP}$ = 16.0 Hz, $^3J_{HP}$ = 3.2 Hz, 1H, P*H*); ^{31}P{^{1}H} NMR (162 MHz, CD_2Cl_2, 298 K): δ = 57.8 (td, $^2J_{PP}$ = 30.7 Hz, $^2J_{PP}$ = 15.6 Hz), 52.4 (dd, $^2J_{PP}$ = 30.7 Hz, $^2J_{PP}$ = 15.6 Hz), 15.4 (q, $^2J_{PP}$ = 15.6 Hz); Elemental analysis calcd (%) for $C_{87}H_{75}BOP_4Ru$: (1372.33) C 76.14, H 5.51; found C 76.18, H 5.59.

5.6.8 [Ru(xantphos)(PPh_3)($H_3B{\cdot}PPh_2H$)H]BAr_4^F (42)

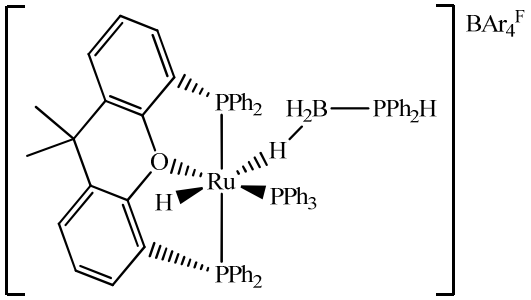

Intermediate observed on reaction of a pre-formed CD_2Cl_2 solution of [Ru(xantphos)(PPh_3)(OH_2)H]BAr_4^F (**25a**) (0.02 mmol) with $H_3B{\cdot}PHPh_2$ (0.008 g, 0.04 mmol). Selected ^{1}H NMR (CD_2Cl_2, 400 MHz, 218 K): δ -13.91 (dt, $^2J_{HP}$ = 22.4 Hz, $^2J_{HP}$ = 19.4 Hz, 1H, Ru*H*). -1.89 (broad s, 3H, BH_3); ^{31}P{^{1}H} (CD_2Cl_2, 162 MHz, 218 K): δ 55.5 (t, $^2J_{PP}$ = 32.0 Hz), 53.7 (d, $^2J_{PP}$ = 32.0 Hz), -5.6 (broad s, PPh_2H); Selected ^{31}P NMR (CD_2Cl_2, 162 MHz, 218 K): δ -5.6 (broad d, $^1J_{PH}$ = 405 Hz, PPh_2H).

5.6.9 Synthesis of [Ru(dppf)(ICy)HCl] (43)

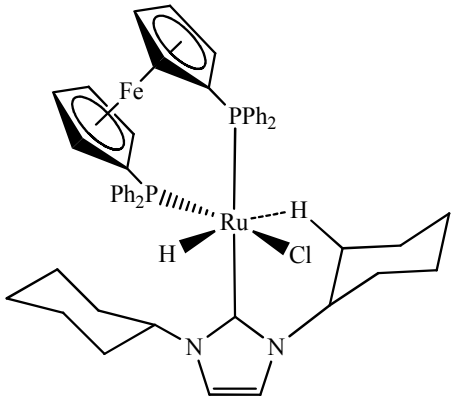

[Ru(dppf)(PPh_3)HCl] (**31**) (0.095 g, 0.1 mmol) and ICy (0.047 g, 0.2 mmol) were charged to an ampoule fitted with a J. Young's resealable PTFE valve, dissolved in THF (10 mL), and stirred at room temperature for 15 h to afford an orange solution. After removal of the solvent, the residue was dissolved in benzene (10 mL) and filtered.[15] The solution was concentrated to half volume and layered with hexane to afford **43** as dark orange crystals (0.042 g, 45% yield). ^{1}H NMR (C_6D_6, 500 MHz, 298 K): δ = -25.63 (br m, 1H, Ru*H*), 0.65 (m, 1H, Cy-CH$H_{agostic}$), 0.94-1.16 (m, 4H, Cy-CH_2), 1.19-1.34 (m, 4H, Cy-CH_2), 1.40-1.55 (m, 4H, Cy-CH_2), 1.56-1.73 (m, 4H, Cy-CH_2), 1.79-1.92 (m, 1H, Cy-C*H*H), 1.93-2.01 (m, 1H, Cy-CH*H*), 3.42 (m, 1H, NC*H*(CH_2)CH_2), 3.52 (m, 1H, Cy-C*H*$H_{agostic}$), 3.67 (s, 1H, dppf), 3.74 (s, 1H, dppf), 3.79 (s, 1H, dppf), 3.89 (s, 1H, dppf), 3.96 (s, 1H, dppf), 4.22 (s, 1H, dppf), 4.37 (s, 1H, dppf), 4.69 (m, 1H, NC*H*(CH_2)CH_2), 5.31 (s, 1H, dppf), 6.29 (s, 1H, NC*H*=CHN), 6.38 (s 1H, NCH=C*H*N); ^{13}C{^{1}H} NMR (C_6D_6, 125 MHz, 298 K): δ = 25.8 (s, Cy-*C*H_2), 25.9 (s, Cy-*C*H_2), 26.6 (s, Cy-*C*H_2), 26.8 (s, Cy-*C*H_2), 27.1 (s, Cy-*C*H_2), 31.6 (s, Cy-*C*H_2), 31.8 (s, Cy-*C*H$H_{agostic}$), 31.9 (s, Cy-*C*H_2), 33.3 (s, Cy-*C*H_2), 36.1 (s, Cy-*C*H_2), 59.5 (s, N*C*H(CH_2)CH_2), 61.1 (s, N*C*H(CH_2)CH_2), 70.0 (s, dppf), 71.8 (d, J_{CP} = 4 Hz, dppf), 72.0 (d, J_{CP} = 4 Hz, dppf), 73.6 (d, J_{CP} = 7 Hz, dppf), 74.4 (s, dppf), 74.5 (d, J_{CP} = 9 Hz, dppf), 75.7 (d, J_{CP} = 5 Hz, dppf), 77.3 (d, J_{CP} = 17 Hz, dppf), 85.3 (dd, J_{CP} = 38 Hz, J_{CP} = 2 Hz, dppf), 85.4 (dd, J_{CP} = 51 Hz, J_{CP} = 3 Hz, dppf), 116.4 (s, N*C*H=CHN), 116.7 (s, NCH=*C*HN), 194.7 (dd, $^2J_{CP}$ = 100.2 Hz, $^2J_{CP}$ = 14.2 Hz, N*C*N); ^{31}P{^{1}H} NMR (C_6D_6, 162 MHz, 298 K): δ = 42.9 (d, $^2J_{PP}$ = 29.4 Hz), 66.4 (d, $^2J_{PP}$ = 29.4 Hz); Elemental analysis calcd (%) for $C_{49}H_{53}N_2P_2ClFeRu$: (924.29) C 63.67, H 5.78, N 3.03; found C 63.33, H 5.73, N 3.29.

5.6.10 Synthesis of [Ru(dppf)(IAd)HCl] (44)

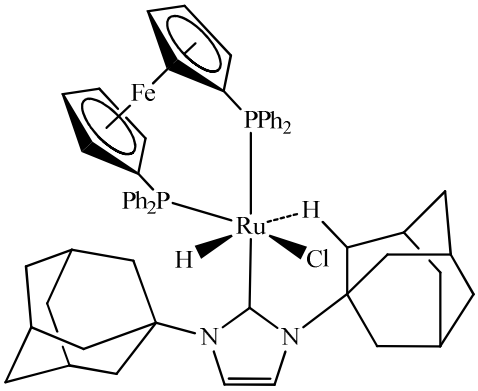

{Ru(dppf)(PPh_3)HCl) (**31**) (0.095 g, 0.1 mmol) and IAd (0.067 g, 0.2 mmol) were charged to an ampoule fitted with a J. Young's resealable PTFE valve, dissolved in THF (10 mL), and stirred at ambient temperature for 15 h to give a bright orange solution. Removal of the solvent under vacuum gave an orange solid which was washed with hexane (2 x 10 mL) and recrystallised from C_6H_6/hexane to afford **44** as an orange crystalline solid (0.049 g, 48% yield). Selected NMR data for **isomer a**: ^{1}H NMR (C_6D_6, 500 MHz, 298 K): δ = -21.60 (dd, $^2J_{HP}$ = 34.0 Hz, $^2J_{HP}$ = 27.7 Hz, 1H, Ru*H*), 0.95 (br m, 1H, CH$H_{agostic}$), 1.42-2.41 (br m, 20H, 7 x Ad-CH_2, 6 x Ad-C*H*), 2.42-2.72 (m, 9H, 4 x Ad-CH_2, C*H*$H_{agostic}$), 3.56 (s, 1H, dppf), 3.72 (s, 1H, dppf), 3.76 (s, 1H, dppf), 3.78 (s, 1H, dppf), 3.93 (s, 1H, dppf), 4.23 (s, 1H, dppf), 4.56 (s, 1H, dppf), 5.37 (s, 1H, dppf), 6.68 (s, 1H, NC*H*=CHN), 6.78 (s, 1H, NCH=C*H*N); ^{13}C{^{1}H} NMR (C_6D_6, 125 MHz, 298 K): δ = 29.5 (s, 3 x Ad-*C*H), 30.6 (s, 3 x Ad-*C*H), 36.0 (s, 4 x Ad-*C*H_2), 36.5 (s, 3 x Ad-*C*H_2), 37.7 (br s, *C*H$H_{agostic}$), 42.7 (s, 4 x Ad-*C*H_2), 59.9 (s, *C*NAd), 69.3 (d, J_{CP} = 4 Hz, dppf), 71.1 (d, J_{CP} = 4 Hz, dppf), 71.4 (d, J_{CP} = 4 Hz, dppf), 73.5 (d, J_{CP} = 8 Hz, dppf), 74.2 (br s, dppf), 74.3 (d, J_{CP} = 8 Hz, dppf), 75.4 (d, J_{CP} = 18 Hz, dppf), 76.1 (d, J_{CP} = 4 Hz, dppf), 84.0 (dd, J_{CP} = 37 Hz, J_{CP} = 2 Hz, dppf), 84.8 (dd, J_{CP} = 53 Hz, J_{CP} = 3 Hz, dppf), 114.3 (br s, N*C*H=CHN), 118.2 (br s, NCH=*C*HN), 190.6 (dd, $^2J_{CP}$ = 99.0 Hz, $^2J_{CP}$ = 14.4 Hz, N*C*N); ^{31}P{^{1}H} NMR (C_6D_6, 162 MHz, 298 K): δ = 44.4 (d, $^2J_{PP}$ = 30.0 Hz), 65.0 (d, $^2J_{PP}$ = 30.0 Hz); Selected NMR data for **isomer b**: ^{1}H NMR (C_6D_6, 500 MHz, 298 K): δ = -20.59 (t, $^2J_{HP}$ = 31.4 Hz, 1H, Ru*H*), 1.22-1.33 (br m, 2H, Ad-C*H*$H_{agostic}$), 1.42-2.41 (br m, 22H, 8 x Ad-CH_2, 6 x Ad-C*H*), 2.75 – 2.99 (m, 6H, 3 x Ad-CH_2), 3.58 (s, 1H, dppf), 3.75 (s, 1H, dppf), 3.91 (s, 1H, dppf), 3.97 (s, 1H, dppf), 4.09 (s, 1H, dppf), 4.44 (s, 1H, dppf), 4.53 (s, 1H, dppf), 5.01 (s, 1H, dppf), 6.51 (s, 1H, NC*H*=CHN), 6.94 (s, 1H, NCH=C*H*N); ^{13}C{^{1}H} NMR (C_6D_6, 125 MHz, 298 K): δ = 22.8 (s, *C*H$H_{agostic}$), 30.2 (s, 3 x Ad-*C*H), 30.5 (s, 3 x Ad-*C*H), 36.1 (s, 8 x Ad-*C*H_2), 43.1 (s, 3 x Ad-*C*H_2), 57.9 (s, N*C*Ad), 60.1 (s, N*C*Ad), 69.4 (d, J_{CP} = 3 Hz, dppf), 70.4 (d, J_{CP} = 3 Hz, dppf), 71.9 (d, J_{CP} = 5 Hz, dppf), 73.6 (d, J_{CP} = 8 Hz, dppf), 73.8 (d, J_{CP} = 11 Hz, dppf), 74.5 (br s, dppf), 74.6 (d, J_{CP} = 3 Hz, dppf), 75.5 (d, J_{CP} = 17 Hz, dppf), 83.8 (d, J_{CP} = 33 Hz, dppf), 87.3 (d,

J_{CP} = 39 Hz, dppf), 115.3 (br s, N*C*H=CHN), 117.6 (br s, NCH=*C*HN), 191.1 (dd, $^2J_{CP}$ = 107.9 Hz, $^2J_{CP}$ = 10.2 Hz, N*C*N); $^{31}P\{^1H\}$ NMR (C_6D_6, 162 MHz, 298 K): δ = 41.3 (d, $^2J_{PP}$ = 29.0 Hz), 66.2 (d, $^2J_{PP}$ = 29.0 Hz); Elemental analysis calcd (%) for $C_{57}H_{61}N_2P_2ClFeRu$ (1028.44): C 66.57, H 5.98, N 2.72; found: C 66.49, H 6.10, N 2.89.

5.6.11 Large scale catalytic amine-borane dehydrogenation

[Ru(dppf)(ICy)HCl] (**43**) (0.018 g, 0.019 mmol) was charged to an ampoule fitted with a J. Young's PTFE valve, dissolved in dry toluene (3 mL), and left to stir for 1 h at room temperature. $H_3B{\cdot}NMe_2H$ (0.038 g, 0.64 mmol) was charged to a 3-necked round-bottomed flask stoppered with a rubber septum. Dry toluene (3 mL) was then syringed into the flask and the vessel connected to an upturned, water-filled graduated burette by a thin metal cannula. This was left to stand for 10 min to ensure that the pressure between the flask and the burette equalised. The catalyst solution (2.5 mL, 0.016 mmol, 2.5 mol%) was then syringed into the flask, and the volume of H_2 gas evolved recorded at minute intervals.

In the reaction performed with Hg, the catalytic procedure was repeated as above but with Hg (0.384 g, 0.002 mol) added to the $H_3B{\cdot}NMe_2H$ solution, which was then stirred vigorously for 0.5 h prior to the addition of the catalyst solution.

References

1. Sheldrick, G. M. *Acta Crystallogr. Sect. A* **1990**, *46,* 467-473.
2. Ahmad, N., Levison, J. J., Robinson, S. D., Uttley, M. F. *Inorg. Synth.* **1974**, *15,* 48.
3. Jung, C. W.; Garrou, P. E. *Organometallics* **1982**, *1,* 658-666.
4. Levison, J. J.; Robinson, S. D. *J. Chem. Soc. (A)* **1970**, 2947-2954.
5. Previously obtained by Dr P. A. Slatford.
6. Reade, S. P.; Acton, A. L.; Mahon, M. F.; Martin, T. A.; Whittlesey, M. K. *Eur. J. Inorg. Chem.* **2009**, 1774-1785.
7. Reade, S. P.; Nama, D.; Mahon, M. F.; Pregosin, P. S.; Whittlesey, M. K. *Organometallics* **2007**, *26,* 3484-3491.
8. Kawano, H.; Tanaka, R.; Fujikawa, T.; Hiraki, K.; Onishi, M. *Chem. Lett.* **1999**, 401-402.
9. Kuhn, N.; Kratz, T. *Synthesis-Stuttgart* **1993**, 561-562.
10. Arduengo, A. J.; Krafczyk, R.; Schmutzler, R.; Craig, H. A.; Goerlich, J. R.; Marshall, W. J.; Unverzagt, M. *Tetrahedron* **1999**, *55,* 14523-14534.
11. Nolan, S. P.; Private communication
12. Schunn, R. A., Wonchoba, E. R., Wilkinson, G. *Inorg. Synth.* **1971**, *13,* 131-134.
13. (a) Bolzati, C.; Boschi, A.; Uccelli, L.; Tisato, F.; Refosco, F.; Cagnolini, A.; Duatti, A.; Prakash, S.; Bandoli, G.; Vittadini, A. *J. Am. Chem. Soc.* **2002**, *124,* 11468-11479; (b) Sacconi, L.; Gelsomin.J *Inorg. Chem.* **1968**, *7,* 291-294; (c) Thewissen, D. H. M. W.; Timmer, K.; Noltes, J. G.; Marsman, J. W.; Laine, R. M. *Inorg. Chim. Acta* **1985**, *97,* 143-150.
14. Arduengo, A. J.; Harlow, R. L.; Kline, M. *J. Am. Chem. Soc.* **1991**, *113,* 361-363.
15. This filtration was necessary to remove traces of a purple solid formed during the reaction, believed to be $[Ru(ICy)_4H]^+$ on comparison with previous work: Burling S.; Häller, L. J. L.; Mas-Marzá, E.; Moreno, A.; Macgragor S. A.; Mahon, M. F.; Pregosin, P. S.; Whittlesey, M. K. *Chem. Eur. J.* **2009**, *15*, 10912-10923.

APPENDIX 1: Crystallographic data

Compound	[Ru(xantphos)(PPh_3)($CO)H_2$] (**2**)	[Ru(xantphos)($CO)_2H_2$] (**4**)	[Ru(xantphos)($CO)_3$] (**6**)
Empirical formula	C58 H49 O2 P3 Ru	C41 H34 O3 P2 Ru	C48 H38 O4 P2 Ru
Formula weight	971.95	737.69	841.79
Temperature	150(2) K	150(2) K	150(2) K
Wavelength	0.71073 Å	0.71073 Å	0.71073 Å
Crystal system	Triclinic	Triclinic	Monoclinic
Space group	P-1	P-1	P21/c
Unit cell dimensions	a = 11.0940(1)Å α = 92.599(1)˚	a = 10.0620(2)Å α = 73.413(1)˚	a = 10.7330(1)Å α = 90˚
	b = 12.9620(1)Å β = 92.909(1)˚	b = 10.6710(2)Å β = 73.881(1)˚	b = 28.5420(2)Å β = 96.661(1)˚
	c = 18.1840(2)Å γ = 113.854(1)˚	c = 18.1510(4)Å γ = 73.441(1)˚	c = 13.0640(1)Å γ = 90˚
Volume	2382.20(4) $Å^3$	1749.00(6) $Å^3$	3975.03(6) $Å^3$
Z	2	2	4
Density (calculated)	1.355 Mg/m^3	1.401 Mg/m^3	1.407 Mg/m^3
Absorption coefficient	0.473 mm^{-1}	0.577 mm^{-1}	0.520 mm^{-1}
F(000)	1004	756	1728
Crystal size	0.20 x 0.12 x 0.07 mm	0.08 x 0.08 x 0.06 mm	0.25 x 0.25 x 0.10 mm
Theta range for data collection	3.55 to 27.44˚	4.07 to 27.46˚	3.55 to 27.50˚
Index ranges	-14<=h<=14; -16<=k<=16; -23<=l<=23	-13<=h<=13; -13<=k<=13; -23<=l<=23	-13<=h<=12; -36<=k<=37; -16<=l<=16
Reflections collected	44250	25664	57366
Independent reflections	10813 [R(int) = 0.0523]	7924 [R(int) = 0.0703]	9072 [R(int) = 0.0489]
Reflections observed (>2σ)	9114	5643	7068
Data Completeness	0.993	0.991	0.995
Absorption correction	Semi-empirical from equivalents	Semi-empirical from equivalents	Semi-empirical from equivalents
Max. and min. transmission	0.95 and 0.92	0.92 and 0.91	0.91 and 0.85
Refinement method	Full-matrix least-squares on F2	Full-matrix least-squares on F2	Full-matrix least-squares on F2
Data / restraints / parameters	10813 / 0 / 632	7924 / 2 / 435	9072 / 0 / 499
Goodness-of-fit on F2	1.047	1.009	1.027
Final R indices [I>2σ(I)]	R1 = 0.0399 wR2 = 0.0766	R1 = 0.0478 wR2 = 0.0800	R1 = 0.0344 wR2 = 0.0840
R indices (all data)	R1 = 0.0549 wR2 = 0.0809	R1 = 0.0841 wR2 = 0.0909	R1 = 0.0540 wR2 = 0.0917
Largest diff. peak and hole	0.466 and -0.579 $eÅ^{-3}$	0.510 and -1.125 $eÅ^{-3}$	0.454 and -0.506 $eÅ^{-3}$

Compound	[Ru(xantphos)($I^iPr_2Me_2$)'(CO)H] (**9**)	[Ru(xantphos)(ICy)(CO)H_2] (**12**)	[Ru(xantphos)(ICy)'(CO)H] (**13**)
Empirical formula	C51 H52 N2 O2 P2 Ru	C55 H58 N2 O2 P2 Ru	C58 H63 N2 O2 P2 Ru
Formula weight	887.96	942.04	983.11
Temperature	150(2) K	150(2) K	150(2) K
Wavelength	0.71073 Å	0.71073 Å	0.71073 Å
Crystal system	Triclinic	Triclinic	Triclinic
Space group	P-1	P-1	P-1
Unit cell dimensions	a = 12.2910(3)Å α = 86.559(1)˚ b = 13.4770(3)Å β = 89.898(2)˚ c = 13.7930(3)Å γ = 71.091(1)˚	a = 10.8270(1)Å α = 81.022(1)˚ b = 11.6570(2)Å β = 85.197(1)˚ c = 20.7780(4)Å γ = 65.431(1)˚	a = 11.5450(2)Å α = 103.174(1)˚ b = 12.4830(2)Å β = 95.791(1)˚ c = 19.4880(3)Å γ = 114.276(1)˚
Volume	2157.18(9) $Å^3$	2355.23(6) $Å^3$	2432.16(7) $Å^3$
Z	2	2	2
Density (calculated)	1.367 Mg/m^3	1.328 Mg/m^3	1.342 Mg/m^3
Absorption coefficient	0.481 mm^{-1}	0.444 mm^{-1}	0.433 mm^{-1}
F(000)	924	984	1030
Crystal size	0.25 x 0.25 x 0.15 mm	0.13 x 0.13 x 0.06 mm	0.13 x 0.13 x 0.05 mm
Theta range for data collection	3.61 to 27.45˚	3.55 to 27.45˚	3.55 to 27.54˚
Index ranges	-15<=h<=15; -17<=k<=17; -17<=l<=17	-14<=h<=14; -15<=k<=15; -26<=l<=26	-14<=h<=14; -16<=k<=16; -24<=l<=25
Reflections collected	42117	46023	49059
Independent reflections	9787 [R(int) = 0.0480]	10691 [R(int) = 0.0956]	11115 [R(int) = 0.0982]
Reflections observed (>2σ)	7945	7679	7952
Data Completeness	0.994	0.995	0.992
Absorption correction	Semi-empirical from equivalents	Semi-empirical from equivalents	Semi-empirical from equivalents
Max. and min. transmission	0.93 and 0.88	0.96 and 0.88	0.92 and 0.85
Refinement method	Full-matrix least-squares on F2	Full-matrix least-squares on F2	Full-matrix least-squares on F2
Data / restraints / parameters	9787 / 5 / 550	10691 / 3 / 570	11115 / 3 / 600
Goodness-of-fit on F2	1.058	1.053	1.053
Final R indices [I>2σ(I)]	R1 = 0.0369 wR2 = 0.0789	R1 = 0.0505 wR2 = 0.1123	R1 = 0.0484 wR2 = 0.0853
R indices (all data)	R1 = 0.0541 wR2 = 0.0853	R1 = 0.0878 wR2 = 0.1281	R1 = 0.0868 wR2 = 0.0984
Largest diff. peak and hole	0.583 and -0.675 $eÅ^{-3}$	0.943 and -0.947 $eÅ^{-3}$	0.641 and -0.742 $eÅ^{-3}$

Compound	[Ru(DPEphos)(PPh_3)$(CO)H_2$] (**14**)	[Ru(xantphos)(PPh_3)(CO)HF] (**17**)	[Ru(dppf)(ICy)$(CO)H_2$] (**21**)
Empirical formula	C56 H47 Cl2 O2 P3 Ru	C62 H56 F O3 P3 Ru	C50 H54 Fe N2 O P2 Ru
Formula weight	1016.82	1062.05	917.81
Temperature	150(2) K	150(2) K	150(2) K
Wavelength	0.71073 Å	0.71073 Å	0.71073 Å
Crystal system	Triclinic	Triclinic	Triclinic
Space group	P-1	P-1	P-1
Unit cell dimensions	a = 10.4940(2)Å α = 71.9740(10)°	a = 11.9970(2)Å α = 75.428(1)°	a = 13.7320(1)Å α = 114.46°
	b = 12.3400(2)Å β = 82.1580(10)°	b = 12.9300(2)Å β = 81.523(1)°	b = 18.4300(1)Å β = 98.14°
	c = 19.1250(3)Å γ = 89.6640(10)°	c = 19.4470(5)Å γ = 62.665(1)°	c = 19.2370(1)Å γ = 96.03°
Volume	2331.29(7) $Å^3$	2591.81(9) $Å^3$	4313.90(5) $Å^3$
Z	2	2	4
Density (calculated)	1.449 Mg/m^3	1.361 Mg/m^3	1.413 Mg/m^3
Absorption coefficient	0.597 mm^{-1}	0.445 mm^{-1}	0.800 mm^{-1}
F(000)	1044	1100	1904
Crystal size	0.43 x 0.20 x 0.15 mm	0.18 x 0.13 x 0.07 mm	0.20 x 0.20 x 0.15 mm
Theta range for data collection	3.59 to 27.57°	3.66 to 27.48°	3.55 to 30.09°
Index ranges	-13<=h<=13; -16<=k<=16; -24<=l<=24	-15<=h<=15; -16<=k<=16; -25<=l<=25	-19<=h<=19; -25<=k<=23; -27<=l<=27
Reflections collected	28901	38188	101778
Independent reflections	10584 [R(int) = 0.0263]	11787 [R(int) = 0.0798]	25200 [R(int) = 0.0524]
Reflections observed (>2σ)	9312	7221	20209
Data Completeness	0.983	0.99	0.994
Absorption correction	Semi-empirical from equivalents	Semi-empirical from equivalents	Semi-empirical from equivalents
Max. and min. transmission	0.901 and 0.876	0.97 and 0.91	0.890 and 0.801
Refinement method	Full-matrix least-squares on F2	Full-matrix least-squares on F2	Full-matrix least-squares on F2
Data / restraints / parameters	10584 / 2 / 582	11787 / 29 / 637	25200 / 4 / 1043
Goodness-of-fit on F2	1.032	1.027	1.039
Final R indices [I>2σ(I)]	R1 = 0.0321 wR2 = 0.0767	R1 = 0.0586 wR2 = 0.1319	R1 = 0.0351 wR2 = 0.0767
R indices (all data)	R1 = 0.0391 wR2 = 0.0808	R1 = 0.1169 wR2 = 0.1535	R1 = 0.0517 wR2 = 0.0845
Largest diff. peak and hole	1.201 and -1.173 $eÅ^{-3}$	1.128 and -0.734 $eÅ^{-3}$	0.572 and -1.075 $eÅ^{-3}$

Compound	[Ru(dppf)(ICy)(CO)HF] (**22**)	[Ru(xantphos)(PPh_3)HCl] (**24a**)	[Ru(DPEphos)(PPh_3)HCl] (**24b**)
Empirical formula	C50 H54 F2 Fe N2 O P2 Ru	C69 H60 Cl O P3 Ru	C56 H48 Cl5 O P3 Ru
Formula weight	955.81	1134.6	1108.17
Temperature	150(2) K	150(2) K	150(2) K
Wavelength	0.71073 Å	0.71073 Å	0.71073 Å
Crystal system	Monoclinic	Monoclinic	Monoclinic
Space group	P21/a	P21/n	P21/a
Unit cell dimensions	a = 18.4130(3)Å α = 90° b = 12.9800(2)Å β = 107.671(1)° c = 19.0140(3)Å γ = 90°	a = 13.3340(1)Å α = 90° b = 30.1610(3)Å β = 96.471(1)° c = 14.0980(2)Å γ = 90°	a = 12.0690(1)Å α = 90° b = 36.7400(3)Å β = 109.006(1)° c = 12.1330(1)Å γ = 90°
Volume	4329.93(12) $Å^3$	5633.62(11) $Å^3$	5086.66(7) $Å^3$
Z	4	4	4
Density (calculated)	1.466 Mg/m^3	1.338 Mg/m^3	1.447 Mg/m^3
Absorption coefficient	0.807 mm^{-1}	0.455 mm^{-1}	0.705 mm^{-1}
F(000)	1976	2352	2264
Crystal size	0.20 x 0.20 x 0.10 mm	0.45 x 0.40 x 0.25 mm	0.32 x 0.20 x 0.12 mm
Theta range for data collection	3.67 to 27.51°	3.52 to 30.07°	3.55 to 27.48°
Index ranges	-23<=h<=23; -16<=k<=16; -24<=l<=24	-18<=h<=18; -42<=k<=42; -19<=l<=19	-15<=h<=15; -47<=k<=47; -15<=l<=15
Reflections collected	68475	70022	50533
Independent reflections	9907 [R(int) = 0.0629]	16368 [R(int) = 0.1263]	11498 [R(int) = 0.0656]
Reflections observed (>2σ)	7901	9135	9373
Data Completeness	0.995	0.99	0.986
Absorption correction	Semi-empirical from equivalents	Semi-empirical from equivalents	Semi-empirical from equivalents
Max. and min. transmission	0.924 and 0.729	0.90 and 0.78	0.94 and 0.88
Refinement method	Full-matrix least-squares on F2	Full-matrix least-squares on F2	Full-matrix least-squares on F2
Data / restraints / parameters	9907 / 6 / 540	16368 / 4 / 682	11498 / 1 / 614
Goodness-of-fit on F2	1.054	1.004	1.018
Final R indices [I>2σ(I)]	R1 = 0.0387 wR2 = 0.0891	R1 = 0.0564 wR2 = 0.1048	R1 = 0.0432 wR2 = 0.1038
R indices (all data)	R1 = 0.0566 wR2 = 0.0965	R1 = 0.1363 wR2 = 0.1295	R1 = 0.0588 wR2 = 0.1126
Largest diff. peak and hole	0.780 and -0.818 $eÅ^{-3}$	1.471 and -0.540 $eÅ^{-3}$	1.624 and -1.343 $eÅ^{-3}$

Compound	[Ru((Ph$_2$CH$_2$CH$_2$)$_2$O)(PPh$_3$)HCl].0.75CH$_2$Cl$_2$ (**24c**)	[Ru(xantphos)(PPh$_3$)(OH$_2$)H]BAr$_4^F$ .3.6C (**[25a]BAr$_4^F$**)	[Ru(xantphos)(PPh$_3$)(OH$_2$)H]OTf (**[25a]OTf**)
Empirical formula	C46.75 H45.50 Cl2.50 O P3 Ru	C92.60 H62 B F24 O2 P3 Ru	C60 H54 Cl4 F3 O5 P3 Ru S
Formula weight	905.94	1867.41	1279.87
Temperature	150(2) K	150(2) K	150(2) K
Wavelength	0.71073 Å	0.71073 Å	0.71073 Å
Crystal system	Monoclinic	Monoclinic	Monoclinic
Space group	P21/n	P21/a	P21/n
Unit cell dimensions	a = 9.8590(1)Å α = 90° b = 26.7330(4)Å β = 103.583(1)° c = 16.7610(3)Å γ = 90°	a = 18.4540(2)Å α = 90° b = 20.4010(3)Å β = 94.3870(10)° c = 22.4910(3)Å γ = 90°	a = 12.0500(1)Å α = 90° b = 18.0250(1)Å β = 90° c = 26.3230(2)Å γ = 90°
Volume	4293.98(11) Å^3	8442.60(19) Å^3	5717.39(7) Å^3
Z	4	4	4
Density (calculated)	1.401 Mg/m^3	1.469 Mg/m^3	1.487 Mg/m^3
Absorption coefficient	0.667 mm^{-1}	0.345 mm^{-1}	0.640 mm^{-1}
F(000)	1862	3774	2616
Crystal size	0.25 x 0.07 x 0.07 mm	0.25 x 0.15 x 0.07 mm	0.30 x 0.20 x 0.20 mm
Theta range for data collection	3.72 to 27.49°	3.52 to 25.03°	3.53 to 30.03°
Index ranges	-12<=h<=12; -34<=k<=34; -21<=l<=21	-21<=h<=21; -24<=k<=24; -26<=l<=26	-16<=h<=16; -24<=k<=25; -37<=l<=37
Reflections collected	67435	119161	119674
Independent reflections	9827 [R(int) = 0.0538]	14858 [R(int) = 0.1470]	16683 [R(int) = 0.0931]
Reflections observed (>2σ)	8020	11104	12832
Data Completeness	0.996	0.997	0.997
Absorption correction	Semi-empirical from equivalents	Semi-empirical from equivalents	Semi-empirical from equivalents
Max. and min. transmission	0.894 and 0.829	0.987 and 0.559	0.864 and 0.754
Refinement method	Full-matrix least-squares on F2	Full-matrix least-squares on F2	Full-matrix least-squares on F2
Data / restraints / parameters	9827 / 1 / 501	14858 / 131 / 1210	16683 / 4 / 708
Goodness-of-fit on F2	1.099	1.053	1.024
Final R indices [I>2σ(I)]	R1 = 0.0442 wR2 = 0.1039	R1 = 0.0502 wR2 = 0.1184	R1 = 0.0440 wR2 = 0.0850
R indices (all data)	R1 = 0.0605 wR2 = 0.1109	R1 = 0.0761 wR2 = 0.1382	R1 = 0.0743 wR2 = 0.0955
Largest diff. peak and hole	1.417 and -0.474 eÅ^{-3}	0.684 and -0.521 eÅ^{-3}	0.760 and -0.632 eÅ^{-3}
Absolute structure parameter	-	-	-0.027(18)

Compound	[Ru(xantphos)(PPh_3)(OTf)H].0.7CH_2Cl_2 (**26a**)	[Ru(xantphos)(PPh_3)(η^2-O_2)H]BAr_4^F .0.5CH_2Cl_2(**28a**)	[Ru(DPEphos)(PPh_3)(η^2-O_2)H]BAr_4^F (**28b**)
Empirical formula	C60.70 H53.40 Cl5.40 F3 O4 P3 Ru S	C89.50 H61 B Cl F24 O3 P3 Ru	C86 H56 B F24 O3 P3 Ru
Formula weight	1321.3	1880.62	1798.1
Temperature	150(2) K	150(2) K	150(2) K
Wavelength	0.71073 Å	0.71073 Å	0.71073 Å
Crystal system	Triclinic	Monoclinic	Triclinic
Space group	P-1	P21/a	P-1
Unit cell dimensions	a = 12.97300(10)Å α = 86.63° b = 14.88500(10)Å β = 84.02° c = 15.5800(2)Å γ = 80.9540(10)°	a = 13.2770(1)Å α = 90° b = 40.2040(4)Å β = 97.14° c = 17.2050(2)Å γ = 90°	a = 12.9450(3)Å α = 101.010(2)° b = 15.8550(4)Å β = 91.365(1)° c = 19.7860(5)Å γ = 90.110(1)°
Volume	2952.21(5) $Å^3$	9112.55(16) $Å^3$	3984.97(17) $Å^3$
Z	2	4	2
Density (calculated)	1.486 Mg/m^3	1.371 Mg/m^3	1.499 Mg/m^3
Absorption coefficient	0.683 mm^{-1}	0.349 mm^{-1}	0.363 mm^{-1}
F(000)	1347	3796	1812
Crystal size	0.30 x 0.25 x 0.25 mm	0.30 x 0.15 x 0.05 mm	0.20 x 0.20 x 0.12 mm
Theta range for data collection	3.55 to 30.00°	3.52 to 25.00°	3.55 to 27.47°
Index ranges	-18<=h<=18; -20<=k<=20; -21<=l<=21	-15<=h<=15; -47<=k<=47; -20<=l<=20	-16<=h<=16; -18<=k<=19; -22<=l<=25
Reflections collected	67721	126839	22391
Independent reflections	17100 [R(int) = 0.0424]	15997 [R(int) = 0.1394]	15058 [R(int) = 0.0389]
Reflections observed (>2σ)	14227	10693	11363
Data Completeness	0.995	0.996	0.824
Absorption correction	Semi-empirical from equivalents	Semi-empirical from equivalents	Semi-empirical from equivalents
Max. and min. transmission	0.900 and 0.801	0.973 and 0.868	0.927 and 0.895
Refinement method	Full-matrix least-squares on F2	Full-matrix least-squares on F2	Full-matrix least-squares on F2
Data / restraints / parameters	17100 / 6 / 730	15997 / 199 / 1172	15058 / 151 / 1115
Goodness-of-fit on F2	1.028	1.11	1.047
Final R indices [I>2σ(I)]	R1 = 0.0433 wR2 = 0.1108	R1 = 0.0963 wR2 = 0.2347	R1 = 0.0696 wR2 = 0.1555
R indices (all data)	R1 = 0.0560 wR2 = 0.1195	R1 = 0.1470 wR2 = 0.2625	R1 = 0.0985 wR2 = 0.1696
Largest diff. peak and hole	1.626 and -1.329 $eÅ^{-3}$	0.854 and -0.704 $eÅ^{-3}$	1.278 and -0.667 $eÅ^{-3}$

Compound	[Ru(dppf)(PPh_3)HCl] (**31**)	[Ru(dppf)({η^6-C_6H_5}PPh_2)H]BAr_4^F (**32**)	[Ru(PMe_3)$_5$H]BAr_4^F (**34**)
Empirical formula	C64 H68 Cl Fe O3 P3 Ru	C84 H56 B F24 Fe P3 Ru	C62.75 H80.50 B1.25 F30 O P6.25 Ru1.25
Formula weight	1170.46	1781.93	1754.18
Temperature	150(2) K	150(2) K	100(2) K
Wavelength	0.71073 Å	0.71073 Å	0.7107 Å
Crystal system	Triclinic	Monoclinic	Tetragonal
Space group	P-1	P21/c	P42/n
Unit cell dimensions	a = 11.4620(1)Å α = 100.190(1)° b = 15.0460(2)Å β = 93.125(1)° c = 16.2070(2)Å γ = 97.346(1)°	a = 10.4940(1)Å α = 90° b = 39.4160(5)Å β = 100.025(1)° c = 19.0500(2)Å γ = 90°	a = 29.3244(2)Å α = 90° b = 29.3244(2)Å β = 90° c = 17.9383(2)Å γ = 90°
Volume	2719.82(5) $Å^3$	7759.37(15) $Å^3$	15425.5(2) $Å^3$
Z	2	4	8
Density (calculated)	1.429 Mg/m^3	1.525 Mg/m^3	1.511 Mg/m^3
Absorption coefficient	0.729 mm^{-1}	0.547 mm^{-1}	0.491 mm^{-1}
F(000)	1216	3584	7120
Crystal size	0.25 x 0.20 x 0.20 mm	0.15 x 0.15 x 0.12 mm	0.35 x 0.35 x 0.24 mm
Theta range for data collection	3.51 to 27.52°	3.61 to 27.53°	2.75 to 27.48°
Index ranges	-14<=h<=14; -19<=k<=19; -20<=l<=21	-13<=h<=13; -51<=k<=51; -24<=l<=24	-38<=h<=38; -38<=k<=38; -23<=l<=23
Reflections collected	55440	98604	253414
Independent reflections	12442 [R(int) = 0.0580]	17766 [R(int) = 0.0633]	17670 [R(int) = 0.0412]
Reflections observed (>2σ)	9843	12706	12713
Data Completeness	0.995	0.994	0.999
Absorption correction	Semi-empirical from equivalents	Semi-empirical from equivalents	Semi-empirical from equivalents
Max. and min. transmission	0.870 and 0.821	0.901 and 0.829	1.00000 and 0.94386
Refinement method	Full-matrix least-squares on F2	Full-matrix least-squares on F2	Full-matrix least-squares on F2
Data / restraints / parameters	12442 / 1 / 662	17766 / 121 / 1099	17670 / 139 / 898
Goodness-of-fit on F2	1.053	1.027	1.094
Final R indices [I>2σ(I)]	R1 = 0.0423 wR2 = 0.1023	R1 = 0.0540 wR2 = 0.1195	R1 = 0.0675 wR2 = 0.2011
R indices (all data)	R1 = 0.0625 wR2 = 0.1127	R1 = 0.0857 wR2 = 0.1344	R1 = 0.0875 wR2 = 0.2115
Largest diff. peak and hole	1.030 and -1.008 $eÅ^{-3}$	0.826 and -0.637 $eÅ^{-3}$	1.907 and -0.767 $eÅ^{-3}$

Compound	[Ru(xantphos)(PPh_3)($H_3B{\cdot}NH_2{}^tBu$)H]BAr_4^F .0.65CH_2Cl_2(**35**)	[Ru(xantphos)(PPh_3)($H_3B{\cdot}NH_3$)H]BPh_4 (**38**)	[Ru(xantphos)(PPh_2H)$_2$H]BPh_4 (**41**)
Empirical formula	C93.65 H75.30 B2 Cl1.30 F24 N O P3 Ru	C82 H76 B2 Cl2 N O P3 Ru	C91 H84 B O2 P4 Ru
Formula weight	1948.33	1377.94	1445.34
Temperature	150(2) K	150(2) K	150(2) K
Wavelength	1.54184 Å	0.71073 Å	0.71073 Å
Crystal system	Monoclinic	Triclinic	Triclinic
Space group	P21/n	P-1	P-1
Unit cell dimensions	a = 12.5054(1)Å α = 90° b = 16.3210(1)Å β = 96.421(1)° c = 43.6884(4)Å γ = 90°	a = 13.3493(2)Å α = 90.027(2)° b = 14.2123(3)Å β = 110.229(2)° c = 19.1411(4)Å γ = 91.479(2)°	a = 14.2280(2)Å α = 92.730(1)° b = 17.3940(2)Å β = 90.021(1)° c = 17.4800(2)Å γ = 110.220(1)°
Volume	8860.89(12) $Å^3$	3406.22(11) $Å^3$	4054.12(9) $Å^3$
Z	4	2	2
Density (calculated)	1.460 Mg/m^3	1.343 Mg/m^3	1.184 Mg/m^3
Absorption coefficient	3.170 mm^{-1}	0.428 mm^{-1}	0.318 mm^{-1}
F(000)	3957	1432	1510
Crystal size	0.40 x 0.26 x 0.19 mm	0.15 x 0.12 x 0.10 mm	0.20 x 0.20 x 0.05 mm
Theta range for data collection	3.39 to 62.25°	2.69 to 27.48°	3.88 to 27.50°
Index ranges	-14<=h<=14; -18<=k<=17; -42<=l<=49	-15<=h<=17; -16<=k<=18; -24<=l<=24	-18<=h<=18; -22<=k<=22; -22<=l<=22
Reflections collected	44539	34586	72110
Independent reflections	13866 [R(int) = 0.0242]	15575 [R(int) = 0.0247]	18474 [R(int) = 0.0552]
Reflections observed (>2σ)	12406	13222	14565
Data Completeness	0.987	0.998	0.991
Absorption correction	Semi-empirical from equivalents	Semi-empirical from equivalents	Semi-empirical from equivalents
Max. and min. transmission	1.00000 and 0.68067	1.00000 and 0.96006	0.990 and 0.890
Refinement method	Full-matrix least-squares on F2	Full-matrix least-squares on F2	Full-matrix least-squares on F2
Data / restraints / parameters	13866 / 176 / 1252	15575 / 4 / 846	18474 / 32 / 906
Goodness-of-fit on F2	1.036	1.037	1.048
Final R indices [I>2σ(I)]	R1 = 0.0429 wR2 = 0.1100	R1 = 0.0336 wR2 = 0.0727	R1 = 0.0472 wR2 = 0.1251
R indices (all data)	R1 = 0.0487 wR2 = 0.1139	R1 = 0.0448 wR2 = 0.0774	R1 = 0.0653 wR2 = 0.1335
Largest diff. peak and hole	1.406 and -0.548 $eÅ^{-3}$	0.654 and -0.493 $eÅ^{-3}$	1.222 and -0.624 $eÅ^{-3}$

Compound	[Ru(dppf)(ICy)HCl] (**43**)	[Ru(dppf)(IAd)HCl] (**44**)
Empirical formula	C49 H53 Cl Fe N2 P2 Ru	C57 H61 Cl Fe N2 P2 Ru
Formula weight	924.24	1028.39
Temperature	150(2) K	150(2) K
Wavelength	0.71073 Å	0.71073 Å
Crystal system	Monoclinic	Monoclinic
Space group	P21/c	P21/c
Unit cell dimensions	a = 12.3990(2)Å α = 90° b = 18.4170(3)Å β = 102.378(1)° c = 19.0450(2)Å γ = 90°	a = 13.0180(4)Å α = 90° b = 18.4470(5)Å β = 101.029(1)° c = 20.2060(6)Å γ = 90°
Volume	4247.88(11) $Å^3$	4762.7(2) $Å^3$
Z	4	4
Density (calculated)	1.445 Mg/m^3	1.434 Mg/m^3
Absorption coefficient	0.872 mm^{-1}	0.786 mm^{-1}
F(000)	1912	2136
Crystal size	0.20 x 0.10 x 0.10 mm	0.30 x 0.25 x 0.20 mm
Theta range for data collection	3.53 to 27.49o	3.59 to 27.52o
Index ranges	-16<=h<=16; -23<=k<=23; -24<=l<=24	-16<=h<=16; -23<=k<=23; -26<=l<=26
Reflections collected	70926	72220
Independent reflections	9709 [R(int) = 0.0497]	10898 [R(int) = 0.1209]
Reflections observed (>2σ)	7970	6929
Data Completeness	0.996	0.995
Absorption correction	Semi-empirical from equivalents	Semi-empirical from equivalents
Max. and min. transmission	0.883 and 0.749	0.935 and 0.705
Refinement method	Full-matrix least-squares on F2	Full-matrix least-squares on F2
Data / restraints / parameters	9709 / 15 / 565	10898 / 1 / 584
Goodness-of-fit on F2	1.052	1.094
Final R indices [I>2σ(I)]	R1 = 0.0277 wR2 = 0.0638	R1 = 0.0718 wR2 = 0.1546
R indices (all data)	R1 = 0.0407 wR2 = 0.0703	R1 = 0.1301 wR2 = 0.1701
Largest diff. peak and hole	0.389 and -0.489 $eÅ^{-3}$	2.029 and -0.898 $eÅ^{-3}$

APPENDIX 2: T_1(min) Data & Calculations

[Ru(xantphos)(PPh$_3$)(η^2-H$_2$)H]BAr$_4^F$ (29a) T_1(min) (η^2-H$_2$ signal):

T / K	T_1 / ms
258.8	10.21
245.3	9.45
238.6	9.22
217.7	10.47
194.3	18.74

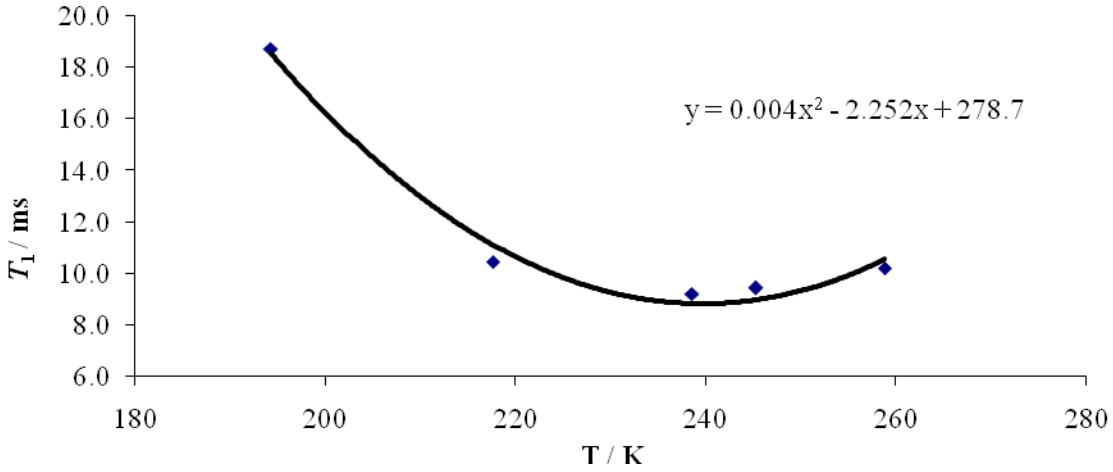

[Ru(DPEphos)(PPh$_3$)(η^2-H$_2$)H]BAr$_4^F$ (29b) T_1(min) (η^2-H$_2$ signal):

T / K	T_1 / ms
252.1	9.56
238.6	9.11
228.2	9.32
217.7	9.90
194.3	15.01

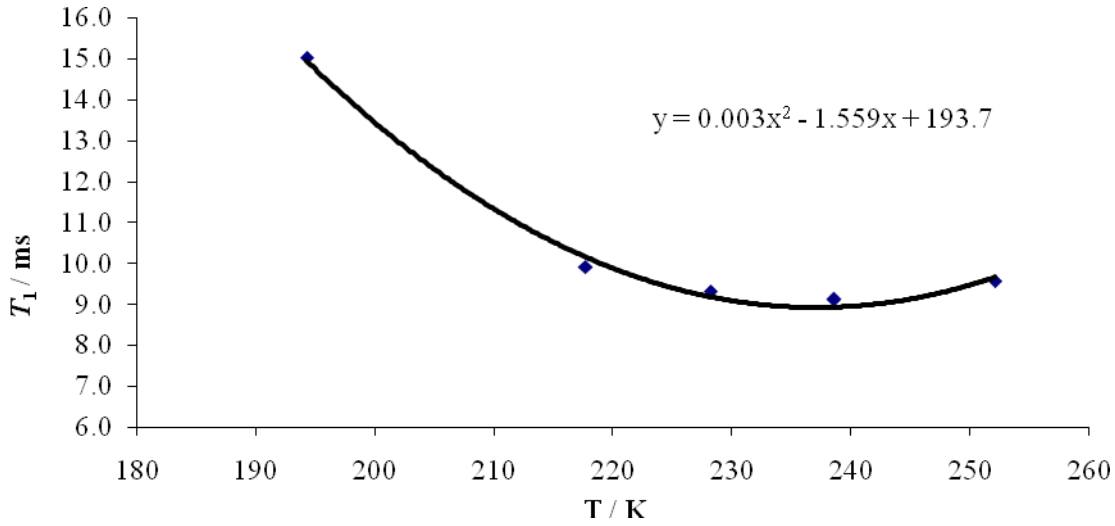

[Ru((Ph$_2$CH$_2$CH$_2$)$_2$O)(PPh$_3$)(η^2-H$_2$)H]BAr$_4^F$ (29c) T_1(min) (η^2-H$_2$ signal):

T / K	T_1 / ms
194.3	10.63
206.0	8.69
217.7	8.06
228.2	8.07
238.6	8.45

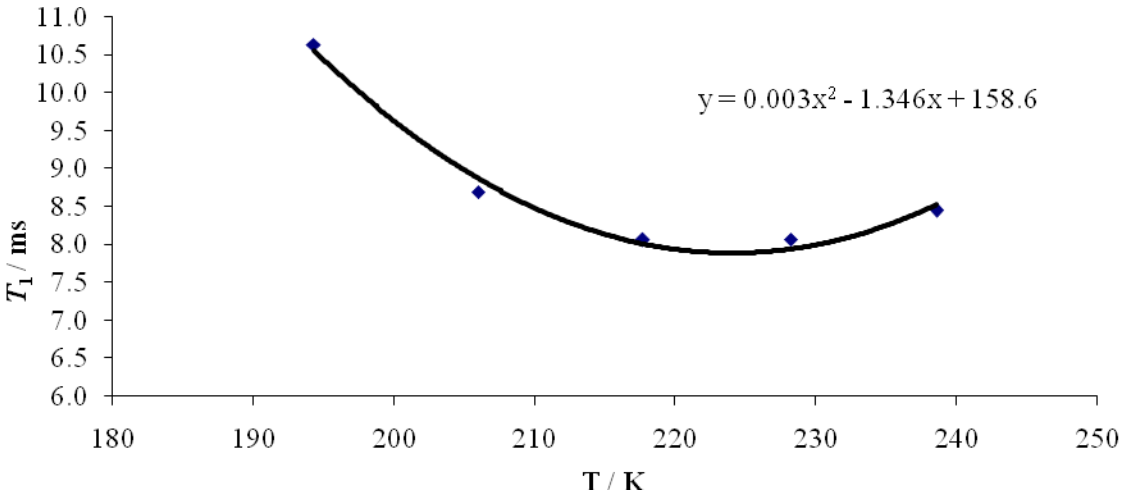

APPENDIX 3: X-ray Crystal Structure of [Ru(IMe$_4$)$_4$HCl]

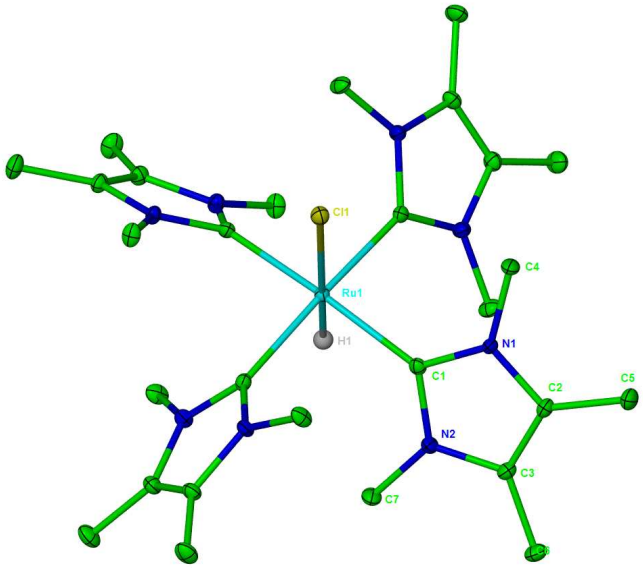

Bond lengths [Å] and angles [°] for [Ru(IMe$_4$)$_4$HCl]	
Ru-C1	2.0873(14)
Ru-C1#1	2.0873(14)
Ru-C1#2	2.0873(14)
Ru-C1#3	2.0873(14)
Ru-H	1.600(5)
Ru-Cl	2.7672(10)
C1-Ru-C1#1	89.755(7)
C1-Ru-C1#2	172.51(11)
C1-Ru-Cl	93.75(5)
C1-Ru-H	86.25(5)
Cl-Ru-H	180.000(1)

C1#1, C1#2 AND C1#3 generated by symmetry transformations

Crystallographic data for $[Ru(IMe_4)_4HCl]$	
Empirical formula	C28 H49 Cl N8 Ru
Formula weight	634.27
Temperature	150(2) K
Wavelength	0.71073 Å
Crystal system	Tetragonal
Space group	P4nc
Unit cell dimensions	a = 11.7730(2)Å α = 90°
	b = 11.7730(2)Å β = 90°
	c = 11.2000(2)Å γ = 90°
Volume	1552.36(5) $Å^3$
Z	2
Density (calculated)	1.357 Mg/m^3
Absorption coefficient	0.622 mm^{-1}
F(000)	668
Crystal size	0.20 x 0.20 x 0.18 mm
Theta range for data collection	3.64 to 27.47°
Index ranges	-15<=h<=15; -15<=k<=15; -14<=l<=14
Reflections collected	24764
Independent reflections	1778 [R(int) = 0.0348]
Reflections observed (>2σ)	1655
Data Completeness	0.996
Absorption correction	Semi-empirical from equivalents
Max. and min. transmission	0.886 and 0.846
Refinement method	Full-matrix least-squares on F2
Data / restraints / parameters	1778 / 2 / 95
Goodness-of-fit on F2	1.092
Final R indices [I>2σ(I)]	R1 = 0.0196 wR2 = 0.0509
R indices (all data)	R1 = 0.0227 wR2 = 0.0528
Absolute structure parameter	0.00(3)
Largest diff. peak and hole	0.727 and -0.376 $eÅ^{-3}$

APPENDIX 4: Large scale catalytic dehydrocoupling of $H_3B{\cdot}NMe_2H$

Volumetric results for the dehydrogenation of $H_3B{\cdot}NMe_2H$ (0.6 mmol) with 2.5 mol% [Ru(dppf)(ICy)HCl] (**43**)

	Run 1		Run 2		Average
t / s	Volume H_2 / mL	nH_2 / nAB_0	Volume H_2 / mL	nH_2 / nAB_0	nH_2 / nAB_0
0	0	0	0	0	0
60	0	0	0	0	0
120	0.04	0.002570737	0	0	0.001285369
180	0.11	0.007069527	0	0	0.003534763
240	0.18	0.011568317	0	0	0.005784158
300	0.35	0.022493949	0.05	0.003213421	0.012853685
360	0.57	0.036633003	0.12	0.007712211	0.022172607
420	0.89	0.057198899	0.49	0.031491529	0.044345214
480	1.36	0.087405059	1.06	0.068124532	0.077764796
540	1.93	0.124038062	1.53	0.098330692	0.111184377
600	2.4	0.154244223	1.95	0.125323431	0.139783827
660	2.87	0.184450383	2.27	0.145889327	0.165169855
720	3.24	0.2082297	2.64	0.169668645	0.188949173
780	3.56	0.228795597	2.91	0.18702112	0.207908358
840	3.83	0.246148072	3.23	0.207587016	0.226867544
900	4.1	0.263500547	3.5	0.224939491	0.244220019
960	4.42	0.284066443	3.82	0.245505388	0.264785915
1020	4.74	0.30463234	4.09	0.262857863	0.283745101
1080	5.06	0.325198236	4.36	0.280210338	0.302704287
1140	5.28	0.33933729	4.68	0.300776234	0.320056762
1200	5.5	0.353476343	4.95	0.318128709	0.335802526
1260	5.72	0.367615397	5.27	0.338694605	0.353155001
1320	5.99	0.384967872	5.54	0.35604708	0.370507476
1380	6.26	0.402320347	5.81	0.373399556	0.387859951
1440	6.58	0.422886244	6.08	0.390752031	0.406819137
1500	6.9	0.44345214	6.35	0.408104506	0.425778323
1560	7.17	0.460804615	6.62	0.425456981	0.443130798
1620	7.39	0.474943669	6.89	0.442809456	0.458876562
1680	7.61	0.489082722	7.11	0.456948509	0.473015616
1740	7.83	0.503221776	7.33	0.471087563	0.48715467
1800	8.1	0.520574251	7.55	0.485226617	0.502900434
1860	8.32	0.534713305	7.82	0.502579092	0.518646198
1920	8.54	0.548852359	8.04	0.516718146	0.532785252
1980	8.71	0.559777991	8.26	0.530857199	0.545317595
2040	8.88	0.570703624	8.53	0.548209674	0.559456649
2100	9.05	0.581629256	8.75	0.562348728	0.571988992
2160	9.22	0.592554888	8.97	0.576487782	0.584521335
2220	9.44	0.606693942	9.19	0.590626836	0.598660389
2280	9.66	0.620832996	9.41	0.604765889	0.612799443
2340	9.88	0.63497205	9.63	0.618904943	0.626938496
2400	10.1	0.649111103	9.8	0.629830576	0.639470839
2460	10.27	0.660036736	9.97	0.640756208	0.650396472
2520	10.44	0.670962368	10.14	0.65168184	0.661322104
2580	10.61	0.681888001	10.36	0.665820894	0.673854447
2640	10.78	0.692813633	10.53	0.676746527	0.68478008

2700	10.95	0.703739266	10.75	0.69088558	0.697312423
2760	11.12	0.714664898	10.92	0.701811213	0.708238055
2820	11.29	0.72559053	11.09	0.712736845	0.719163688
2880	11.46	0.736516163	11.26	0.723662478	0.73008932
2940	11.63	0.747441795	11.43	0.73458811	0.741014953
3000	11.8	0.758367428	11.6	0.745513743	0.751940585
3300	12.35	0.793715062	12.15	0.780861377	0.787288219
3600	12.8	0.822635854	12.6	0.809782169	0.816209011
3900	13.25	0.851556646	12.95	0.832276118	0.841916382
4200	13.6	0.874050595	13.3	0.854770067	0.864410331
4500	13.85	0.890117701	13.55	0.870837173	0.880477437
4800	14.1	0.906184808	13.75	0.883690859	0.894937833
5400	14.5	0.931892178	14.1	0.906184808	0.919038493
6000	14.6	0.938319021			

Volumetric results for the dehydrogenation of $H_3B{\cdot}NMe_2H$ (0.6 mmol) with 5 mol% [Ru(dppf)(ICy)HCl] (**43**)

	Run 1		Run 2		Average
t / s	Volume H_2 / mL	nH_2 / nAB_0	Volume H_2 / mL	nH_2 / nAB_0	nH_2 / nAB_0
0	0	0	0	0	0
60	0	0	0.065	0.004177448	0.002088724
120	0.02	3144.654088	0.18	0.011568317	0.006426843
180	0.18	4716.981132	0.345	0.022172607	0.016870462
240	0.34	6289.308176	0.56	0.035990319	0.028920792
300	0.7	7861.63522	1.025	0.065875137	0.055431517
360	1.36	9433.962264	1.49	0.095759955	0.091582507
420	2.12	11006.28931	2.055	0.132071616	0.134160339
480	2.98	12578.61635	2.62	0.168383276	0.179951593
540	3.54	14150.9434	3.385	0.217548622	0.222529425
600	4.1	15723.27044	4.15	0.266713968	0.265107258
660	4.66	17295.59748	4.815	0.309452472	0.304471669
720	5.12	18867.92453	5.38	0.345764132	0.337409237
780	5.58	20440.25157	5.945	0.382075793	0.370346805
840	5.94	22012.57862	6.51	0.418387454	0.400070952
900	6.3	23584.90566	7.075	0.454699115	0.429795099
960	6.71	25157.2327	7.59	0.487797354	0.459519246
1020	7.12	26729.55975	8.105	0.520895593	0.489243394
1080	7.48	28301.88679	8.62	0.553993833	0.51736083
1140	7.84	29874.21384	9.135	0.587092072	0.545478266
1200	8.2	31446.54088	9.6	0.61697689	0.571988992
1260	8.56	33018.86792	10.065	0.646861708	0.598499718
1320	8.92	34591.19497	10.53	0.676746527	0.625010444
1380	9.28	36163.52201	10.895	0.700204502	0.648307748
1440	9.64	37735.84906	11.26	0.723662478	0.671605053
1500	9.95	39308.1761	11.625	0.747120453	0.693295646
1560	10.26	40880.50314	11.99	0.770578429	0.71498624
1620	10.52	42452.83019	12.305	0.790822983	0.733463413
1680	10.78	44025.15723	12.62	0.811067537	0.751940585
1740	11.04	45597.48428	12.885	0.82809867	0.768811047

1800	11.3	47169.81132	13.1	0.841916382	0.784074798
1860	11.56	48742.13836	13.315	0.855734093	0.799338549
1920	11.77	50314.46541	13.53	0.869551805	0.81299559
1980	11.98	51886.79245	13.745	0.883369516	0.82665263
2040	12.19	53459.1195	13.91	0.893973807	0.83870296
2100	12.4	55031.44654	14.075	0.904578097	0.85075329
2160	12.56	56603.77358			
2220	12.72	58176.10063			
2280	12.88	59748.42767			
2340	12.99	61320.75472			
2400	13.1	62893.08176	14.7	0.944745863	0.893331122
2460	13.21	64465.40881			
2520	13.32	66037.73585			
2580	13.43	67610.06289			
2640	13.54	69182.38994			
2700	13.6	70754.71698	14.825	0.952779417	0.913415006
2760	13.66	72327.04403			
2820	13.72	73899.37107			
2880	13.78	75471.69811			
2940	13.84	77044.02516			
3000	13.9	78616.3522	14.95	0.96081297	0.927072046
3600	14.4	94339.62264	15	0.964026391	0.944745863

Volumetric results for the dehydrogenation of $H_3B{\cdot}NMe_2H$ (0.6 mmol) with 7.5 mol% [Ru(dppf)(ICy)HCl] (**43**)

	Run 1		Run 2		Average
t / s	Volume H_2 / mL	nH_2 / nAB_0	Volume H_2 / mL	nH_2 / nAB_0	nH_2 / nAB_0
0	0	0	0	0	0
60	0	0	0	0	0
120	0.83	0.053342794	0	0	0.0266714
180	1.845	0.118575246	0.1	0.0064268	0.062501
240	3.26	0.209515069	0.2	0.0128537	0.1111844
300	4.675	0.300454892	0.5	0.0321342	0.1662946
360	5.89	0.37854103	0.85	0.0546282	0.2165846
420	6.905	0.443773482	1.25	0.0803355	0.2620545
480	7.67	0.492938828	1.7	0.1092563	0.3010976
540	8.535	0.548531017	2.3	0.1478174	0.3481742
600	9.35	0.600909784	3	0.1928053	0.3968575
660	10.065	0.646861708	3.7	0.2377932	0.4423274
720	10.68	0.686386791	4.4	0.2827811	0.4845839
780	11.195	0.71948503	5.1	0.327769	0.523627
840	11.71	0.752583269	5.7	0.36633	0.5594566
900	12.175	0.782468088	6.3	0.4048911	0.5936796
960	12.54	0.805926063	6.9	0.4434521	0.6246891
1020	12.855	0.826170617	7.4	0.4755864	0.6508785
1080	13.12	0.84320175	7.9	0.5077206	0.6754612
1140	13.385	0.860232883	8.4	0.5398548	0.7000438
1200	13.6	0.874050595	8.9	0.571989	0.7230198
1260	13.765	0.884654885	9.4	0.6041232	0.744389

1320	13.88	0.892045754	9.9	0.6362574	0.7641516
1380	13.995	0.899436623	10.3	0.6619648	0.7807007
1440	14.11	0.906827492	10.7	0.6876722	0.7972498
1500	14.225	0.914218361	11.05	0.7101661	0.8121922
1800	14.65	0.941532442	12.5	0.8033553	0.8724439
2100	15.025	0.965633102	13.1	0.8419164	0.9037747
2400	15.4	0.989733762	13.6	0.8740506	0.9318922
2700	15.675	1.007407579	13.9	0.8933311	0.9503694
3000	15.8	1.015441132	14.1	0.9061848	0.960813
3300	15.825	1.017047843	14.3	0.9190385	0.9680432
3900	15.825	1.017047843	14.5	0.9318922	0.97447

Volumetric results for the dehydrogenation of $H_3B{\cdot}NMe_2H$ (0.6 mmol) with 2.5 mol% [Ru(dppf)(ICy)HCl] (**43**) with and without addition of Hg

	2.5 mol% + Hg		2.5 mol% (higher stir rate)	
t / s	Volume H_2 / mL	nH_2 / nAB_0	Volume H_2 / mL	nH_2 / nAB_0
0	0	0	0	0
60	0	0	0	0
120	0.2	0.012853685	0.07	0.00449879
180	0.4	0.02570737	0.155	0.009961606
240	0.6	0.038561056	0.34	0.021851265
300	0.8	0.051414741	0.525	0.033740924
360	1.2	0.077122111	0.91	0.058484268
420	1.9	0.12211001	1.595	0.10250814
480	2.55	0.163884487	2.08	0.133678326
540	3	0.192805278	2.615	0.168061934
600	3.4	0.218512649	3.15	0.202445542
660	3.8	0.244220019	3.635	0.233615729
720	4.2	0.26992739	4.12	0.264785915
780	4.6	0.29563476	4.605	0.295956102
840	5	0.32134213	4.99	0.320699446
900	5.4	0.347049501	5.375	0.34544279
960	5.7	0.366330029	5.76	0.370186134
1020	6	0.385610556	6.245	0.401356321
1080	6.25	0.401677663	6.68	0.429313086
1140	6.5	0.41774477	7.115	0.457269852
1200	6.75	0.433811876	7.5	0.482013196
1260	7.05	0.453092404	7.885	0.50675654
1320	7.35	0.472372932	8.27	0.531499884
1380	7.65	0.49165346	8.655	0.556243228
1440	7.95	0.510933987	9.04	0.580986572
1500	8.25	0.530214515	9.425	0.605729916
1560	8.5	0.546281622	9.81	0.63047326
1620	8.75	0.562348728	10.195	0.655216604
1680	9	0.578415835	10.48	0.673533105
1740	9.25	0.594482941	10.815	0.695063028
1800	9.5	0.610550048	11.15	0.716592951
1860	9.75	0.626617154	11.435	0.734909452

1920	10	0.642684261	11.72	0.753225954
1980	10.2	0.655537946	11.955	0.768329034
2040	10.4	0.668391631	12.19	0.783432114
2100	10.65	0.684458738	12.425	0.798535194
2160	10.9	0.700525844	12.66	0.813638274
2220	11.1	0.713379529	12.895	0.828741354
2280	11.3	0.726233215	13.13	0.843844434
2340	11.5	0.7390869	13.315	0.855734093
2400	11.7	0.751940585	13.5	0.867623752
2460	11.9	0.76479427		
2520	12.1	0.777647956		
2580	12.25	0.787288219		
2640	12.4	0.796928483		
2700	12.55	0.806568747	14.225	0.914218361
2760	12.7	0.816209011		
2820	12.85	0.825849275		
2880	13	0.835489539		
2940	13.1	0.841916382		
3000	13.2	0.848343224	14.55	0.935105599
3060				
3120				
3180				
3240				
3300	13.65	0.877264016	14.625	0.939925731
3360				
3420				
3480				
3540				
3600	14.05	0.902971386	14.65	0.941532442
3660				
3720				
3780				
3840				
3900	14.4	0.925465336		
3960				
4020				
4080				
4140				
4200	14.4	0.925465336		